INCORPORATION OF HYDROGEN BONDING FOR HIGH PERFORMANCE WATERBORNE COATINGS

NEREA JIMÉNEZ IRURZUN | 2022

eman ta zabal zazu

Universidad del País Vasco
Euskal Herriko Unibertsitatea

(cc) 2022 Nerea Jiménez Irurzun (cc by-nc-nd 4.0)

INCORPORATION OF HYDROGEN BONDING FOR HIGH PERFORMANCE WATERBORNE COATINGS

Nerea Jiménez Irurzun

Supervisors:

Dr. Nicholas Ballard and Prof. José M. Asua

Chemical Engineering Group

University of the Basque Country UPV/EHU

Donostia – San Sebastian

2022

POLYMAT

eman ta zabal zazu

Universidad del País Vasco Euskal Herriko Unibertsitatea

Acknowledgements

First, I would like to thank my supervisors Dr. Nicholas Ballard and Prof. José M. Asua for giving me the opportunity to do this PhD. Thank you for the guidance and support. You have been excellent role models to me.

In addition, I would like to thank all the professors of the group for the discussions, suggestions and help. Specially, I would like to thank Maria and Gordana for being my mentors in my first contact with the lab and for introducing me to research with patience and enthusiasm. I also thank Ines for her kindness, patience and support.

Thanks to the Spanish Ministry of Education, Culture and Sport for the predoctoral FPU fellowship received to carry out the PhD. Thank you also to the Industrial Liaison Program "Polymerization in Dispersed Media" for the financial support.

I would like to express my gratitude to Dr. Bernd Reck, Dr. Arnold Leidner and BASF for giving me the opportunity to join BASF for an internship.

Thanks to the Sgiker Services of the Basque Country for the support, Maite and Ana for the TEM images, Fernando Ruipérez for the DFT calculations and Estibaliz González de San Román for the MALDI-TOF analysis.

Thank you to all the members of the polymerization processes group and other groups in POLYMAT. I can tell with all my heart that THE BEST PART WAS KNOWING YOU. I will never forget the moments we shared inside and outside the lab. Remember you have a friend in Atarrabia (Pamplona) whenever you need. Thank you also to Gordana, Miki, Samane, Ehsan and Goran for hosting me as a little family during my stay in Germany. I will always remember your kindness.

Eta ze garrantzitsuak diren lagunak. Mila esker kuadrilako, bandako, unibertsitateko, pintxopoteetako eta baita Naitec-eko etapa berri honetan ezagutzen ari ditudan lagun berriei! Mila esker zuen laguntza eta animoengatik, baina batez ere barrea eragin didazuen aldi bakoitzarengatik!! Eta pertsonarik berezienari, Fermin. Mila esker urte hauetan konpartitutako maitasun, algara, konfidantza eta babesarengatik. Ezin dut bidai hau imajinatu zu gabe.

Dejo para el final lo más importante: la familia. Muchas gracias por apoyarme siempre. Elisa, Oskar eta Enara opari bat izan da Donostian zuekin bizitzea. Ama, aita siempre habéis creído y creéis en mí, y no hay nada más valioso que eso. Todo lo que he conseguido ha sido gracias a vuestro apoyo incondicional y cariño.

Contents

Chapter 1. Introduction

1.1. Polymer coatings **1**

1.2. Polymerization in dispersed media **3**

1.2.1. Emulsion polymerization 3

1.2.1.1. Batch emulsion polymerization 5

1.2.1.2. Semibatch emulsion polymerization 9

1.2.2. Miniemulsion polymerization 9

1.3. Film formation **12**

1.3.1. Analysis of film formation 14

1.4. Approaches to overcome the film formation dilemma **18**

1.4.1. Diffusion promotors 18

1.4.2. Structural reinforcement 20

1.4.3. Crosslinking of the polymer chains 23

1.4.3.1. Development of the mechanical strength of the films 24

1.4.3.2. Chemical crosslinking 28

1.4.3.2.1. Chemical crosslinking of hydroxyl functional polymer particles 28

1.4.3.2.2. Chemistries involving carboxylic groups 31

1.4.3.2.3. Oxirane/amine crosslinking 33

1.4.3.2.4. Diketo/diamine crosslinking 34

1.4.3.2.5. Unsaturated groups 36

1.4.3.2.6. Self-condensation 38

1.4.3.2.7. Challenges and limitations of the chemical crosslinking technologies 39

1.4.3.3. Physical crosslinking 40
1.4.3.3.1. Ionic interactions 41
1.4.3.3.2. H-bonding 42
1.4.3.4. Classification of the crosslinking systems depending on the position of the functional groups 51
1.5. Motivation and outline **54**
1.6. References **56**

Chapter 2. Functional polymer dispersions with H-bonding groups: pyrrolidone – hydroxyl and uracil – adenine complexation

2.1. Introduction **83**
2.2. Experimental part **87**
2.2.1. Materials 87
2.2.2. Synthesis of polymer dispersions with pyrrolidone and hydroxyl groups 88
2.2.3. Synthesis of uracil acrylate (UrA) and adenine acrylate (AdA) 90
2.2.4. Synthesis of polymer dispersions with uracil and adenine groups 94
2.2.5. High temperature solution polymerizations 96
2.2.6. Blending and film casting 97
2.2.7. Characterization 98
2.3. Results and discussion **100**
2.3.1. Pyrrolidone-hydroxyl complexation 100
2.3.1.1. Synthesis of polymer dispersions with pyrrolidone and hydroxyl groups 100
2.3.1.2. Tensile properties 102
2.3.2. Uracil-adenine complexation 108

2.3.2.1. Synthesis of polymer dispersions with uracil and adenine groups 108
2.3.2.2. Tensile properties 110
2.3.3. Rheological behavior of functional low molar mass polymers 112
2.3.3.1. High temperature solution polymerizations 112
2.3.3.2. Rheological behavior 115
2.3.4. Fundamental considerations for physically crosslinked waterborne polymer dispersions 118
2.4. Conclusions **128**
2.5. References **129**

Chapter 3. H-bonding complexation of polyvinyl alcohol (PVOH) stabilized polymer dispersions and water-soluble species

3.1. Introduction **133**
3.2. Experimental part **136**
3.2.1. Materials 136
3.2.2. Synthesis of polymer dispersions 136
3.2.3. Blending and film casting 138
3.2.4. Characterization 138
3.3. Results and discussion **139**
3.3.1. Synthesis of polymer dispersions 139
3.3.2. Film appearance 141
3.3.3. Tensile properties 143
3.3.4. Water sensitivity 146
3.4. Conclusions **153**

3.5. References **154**

Chapter 4. N-vinyl pyrrolidone (NVP) and tannic acid complexation for coatings applications

4.1. Introduction **159**

4.2. Experimental part **161**

4.2.1. Materials 161

4.2.2. Synthesis of polymer dispersions 162

4.2.3. Blending and film casting 165

4.2.4. Formulation of white paints 165

4.2.5. Characterization 166

4.3. Results and discussion **168**

4.3.1. Synthesis of polymer dispersions 168

4.3.2. Tensile properties 171

4.3.3. Film morphology 173

4.3.4. Dynamic mechanical properties 179

4.3.5. Fourier Transform Infrared Spectroscopy (FTIR) 181

4.3.6. Influence of microstructuring 183

4.3.7. Water sensitivity 186

4.3.8. Investigation of industrially interesting variables 194

4.3.9. Application tests 199

4.4. Conclusions **202**

4.5. References **203**

Chapter 5. N-vinyl pyrrolidone (NVP) and tannic acid complexation for Pressure Sensitive Adhesives (PSAs)

5.1. Introduction **207**

5.2. Experimental part **211**

5.2.1. Materials 211

5.2.2. Synthesis of polymer dispersions 211

5.2.3. Blending and film casting 213

5.2.4. Characterization 214

5.3. Results and discussion **217**

5.3.1. Synthesis of polymer dispersions 217

5.3.2. Film morphology 220

5.3.3. Glass transition temperature (T_g) 222

5.3.4. Adhesive properties: Probe tack, 180° peel and shear adhesion tests 223

5.3.5. Tensile properties 229

5.3.6. Water sensitivity 232

5.3.7. Investigation of industrially interesting variables 234

5.4. Conclusions **238**

5.5. References **239**

Chapter 6. Fundamental insights into free radical polymerization in the presence of catechols and catechol functionalized monomers

6.1. Introduction **245**

6.2. Experimental part **250**

6.2.1. Materials 250

6.2.2. Synthetic procedures 251

6.2.3. Isolation of polymers 256

6.2.4. Characterization 257

6.2.4.1. Monomer conversion 257

6.2.4.2. Molar mass distribution 257

6.2.4.3. Matrix-assisted laser desorption/ionization time of flight mass spectrometry (MALDI-TOF-MS) 258

6.2.5. Computational work 259

6.3. Results and discussion **259**

6.3.1. Polymerizations in presence of pyrocatechol 259

6.3.2. Determination of chain transfer constants with pyrocatechol 268

6.3.3. Theoretical calculations 270

6.3.4. Copolymerization of catechol containing monomers 272

6.3.4.1. Effect of the solvent 273

6.3.4.2. Effect of the nature of the main monomer 274

6.3.4.3. Effect of the nature of the catechol monomer 282

6.4. Conclusions **287**

6.5. References **289**

Chapter 7. Catechol-containing copolymers as water-soluble H-bond donors

7.1. Introduction **297**

7.2. Experimental part **302**

7.2.1. Materials 302

7.2.2. Synthesis of polymer dispersions 302

7.2.3. Synthesis of catechol-containing water-soluble copolymers 303

7.2.4. Isolation of the copolymers 305

7.2.5. Blending and film casting 305

7.2.6. Characterization 305

7.3. Results and discussion **307**

7.3.1. Synthesis of polymer dispersions 307

7.3.2. Synthesis of catechol-containing water-soluble copolymers 308

7.3.3. Film appearance 310

7.3.4. Tensile properties and morphology of the films 313

7.3.5. Water sensitivity 320

7.4. Conclusions **322**

7.5. References **324**

Chapter 8. Conclusions **331**

Resumen y conclusiones **339**

Appendix I. General characterization methods

I.1. Latex characterization **347**

I.1.1. Solids content and monomer conversion 347

I.1.2. Particle size 348

I.1.3. Gel content 349

I.1.4. Molecular weight distribution 350

I.2. Film properties **351**

I.2.1. Glass trasition temperature (T_g) 351

I.2.2. Morphology 351

I.2.3. Mechanical properties 352

I.2.4. Water sensitivity 352

I.3. References **355**

Appendix II. Supporting information for Chapter 6

II.1. Synthesis of dopamine methacrylamide (DMA) **357**

II.2. Synthesis of vinyl catechol (VC) **359**

II.3. Reaction mechanism **361**

II.4. MALDI-TOF-MS spectra **363**

II.5. Individual monomer conversions in Runs 1-11 of set 4 of experiments **367**

II.6. Time evolution of the molecular weight distributions in Runs 1-7- of set 4 of experiments **369**

II.7. References **372**

Appendix III. List of acronyms, abbreviations and symbols 375

List of publications, conference presentations and awards 381

Chapter 1. Introduction

1.1. Polymer coatings

Polymer coatings are thin polymer layers employed for the decoration and protection of substrates.[1] They find applications in many sectors such as architectural, automotive or marine coatings, and their use as protective layers extends the lifetime of many products, saving millions of dollars per year in the replacement of damaged goods. Accordingly, the global market size of coatings was USD 146.54 billion in 2018 and it is predicted to reach USD 236.11 billion by 2026.[2]

The basic formulation of a coating includes a binder solution/dispersion, pigments to provide colour and enhance the opacity of the films, fillers to improve the mechanical performance and reduce the cost of the coating, rheology modifiers and other additives.[3] The binder (the polymer) is the film-forming element of the formulation. As described by its name, it binds the rest of the components but also determines other important features such as the adhesion to the substrate, durability and gloss. A wide variety of polymer resins such as acrylic, epoxy, polyurethane or alkyds are used as binders. For the application, the binder and the rest of the components are dispersed/dissolved in a continuous liquid phase. They are applied as liquid dispersions and they become solid during the drying through the evaporation of the liquid dispersant. Traditionally, organic solvents have been employed as continuous phase, but due to the growing awareness about the negative impact of Volatile Organic Compounds (VOC) in the environment, water is increasingly being employed as continuous medium.[4] Nevertheless, the mechanical properties of waterborne coatings are typically not as good as those of solventborne coatings because of differences in the film formation process, which leads to poor cohesion in

films cast from waterborne systems. Thus, solventborne coatings still dominate the market in applications that require mechanical strength. Therefore, in order to complete the replacement from solventborne to waterborne products, the production of high performance waterborne coatings is required.

The film formation process of waterborne coatings has been widely studied as a critical transition for the production of cohesive materials and several approaches have been proposed for the preparation of mechanically strong films. These approaches include the use of diffusion promotors, structural reinforcing agents or the crosslinking of the polymer chains. In this PhD Thesis, the use of hydrogen bonds is proposed to physically crosslink the polymer chains and enhance the mechanical performance of the films cast from waterborne polymer dispersions.

In this introductory chapter, the processes of emulsion and miniemulsion polymerization, which are two of the most relevant techniques for the production of aqueous polymer dispersions, are first explained. Then, the film formation process of waterborne dispersions and the main parameters affecting it are discussed. Finally, the main approaches employed for the improvement of mechanical properties of films cast from waterborne dispersions are summarized.

1.2. Polymerization in dispersed media

1.2.1. Emulsion polymerization

Emulsion polymerization is the main technique to produce waterborne polymer dispersions for coatings. In this technique, monomers with limited water solubility are polymerized mainly by free radical polymerization (FRP) dispersed in water. The resulting product is a colloidal dispersion of polymer particles in water with particle sizes ranging between 50 and 1000 nm, more commonly from 80 to 300 nm. This product is commonly called latex.[5]

Compared to solution polymerization, the polymerization in aqueous medium presents several advantages. In the first place, the process is more environmentally friendly because the toxic organic solvents are replaced by water. In the second place, the polymerization process is safer because combustive solvents are removed from the formulation. In addition, the viscosity of the dispersion is lower which allows the easier stirring of the system and facilitates heat removal. The high specific heat of water also contributes to the temperature control of the system and decreases the possibility of a thermal runaway. Finally, emulsion polymerization presents a unique feature attributed to the isolation of the growing radicals within the polymer particles. The growing radicals confined in different polymer particles are not able to terminate between them and therefore, they are allowed to grow for longer times (in the absence of chain transfer reactions, until a second radical enters to the polymer particle). As result, very high molecular weight polymer chains (typically on the order of 10^6 g/mol) are produced.[6] In addition, the decrease of the chain termination events results in an increase in the total radical concentration and, consequently, the polymerization rate. Therefore, radical compartmentalization allows the simultaneous increase in the polymerization rate and the molecular weights.

Nevertheless, colloidal dispersions are thermodynamically unstable and require surfactants to achieve kinetic stability. Surfactants are amphiphilic molecules that are preferentially located at the oil-water interface and prevent the aggregation of the polymer particles by steric or electrostatic repulsions.[7] Electrostatic stabilization is also achieved by incorporating functional monomers such as (meth)acrylic acid to the formulation.[8] One of the main drawbacks of the emulsion polymers is that the surfactants and stabilizing groups remain in the final products increasing their water sensitivity.[9,10]

The basic formulation for emulsion FRP includes at least one vinyl monomer, a radical initiator, surfactant and water. In addition, chain transfer agents (CTA) or crosslinkers can be employed to decrease and increase the molecular weight of the polymer, respectively. Usually, more than one monomer is copolymerized to achieve a product with the desired properties. For example, it is well known that the glass transition temperature (T_g) of a copolymer depends on the nature and ratio of the monomers employed.[11–14] The main monomers polymerized with this technique are vinyl acetate, styrene-butadiene, styrene-acrylics, and (meth)acrylic copolymers.

Emulsion polymerizations are usually performed in semicontinuous mode where a fraction of the reactants is gradually added to the reactor because this allows control over both the heat generation rate and many design variables such as the copolymer composition, particle morphology, or particle size distribution. Nevertheless, for the understanding of the polymerization technique, it is often convenient to analyze the batch emulsion polymerization first.

1.2.1.1. Batch emulsion polymerization

The batch emulsion polymerization process is illustrated in Figure 1.1.[15,16] Before initiation, the system is composed of water, monomer and surfactant. A small fraction of the monomer dissolves in the aqueous phase (e.g. 2.5g VAc/100g H_20 and 0.045g S/100g H_20) and the rest accumulates in the monomer droplets. The surfactant adsorbs on the surface of the monomer droplets stabilizing them but also covers the water/air surface, and dissolves in water. When the concentration of the surfactant in water is above the saturation concentration, also known as critical micelle concentration (CMC), it forms aggregates. These aggregates are called micelles and they are swollen with monomer. It is important to highlight that the concentration of monomer and surfactant in each phase is at thermodynamic equilibrium and that the monomer and surfactant molecules will continuously diffuse during the polymerization across the different phases to maintain the equilibrium. The polymerization is initiated by the addition of the initiator. The initiators employed usually are water-soluble and they decompose into water-soluble radicals when they are heated or undergo redox reactions. Common thermal initiators include persulfates, peroxides and azo compounds. From this point, the batch emulsion polymerization process is divided into 3 periods or intervals.

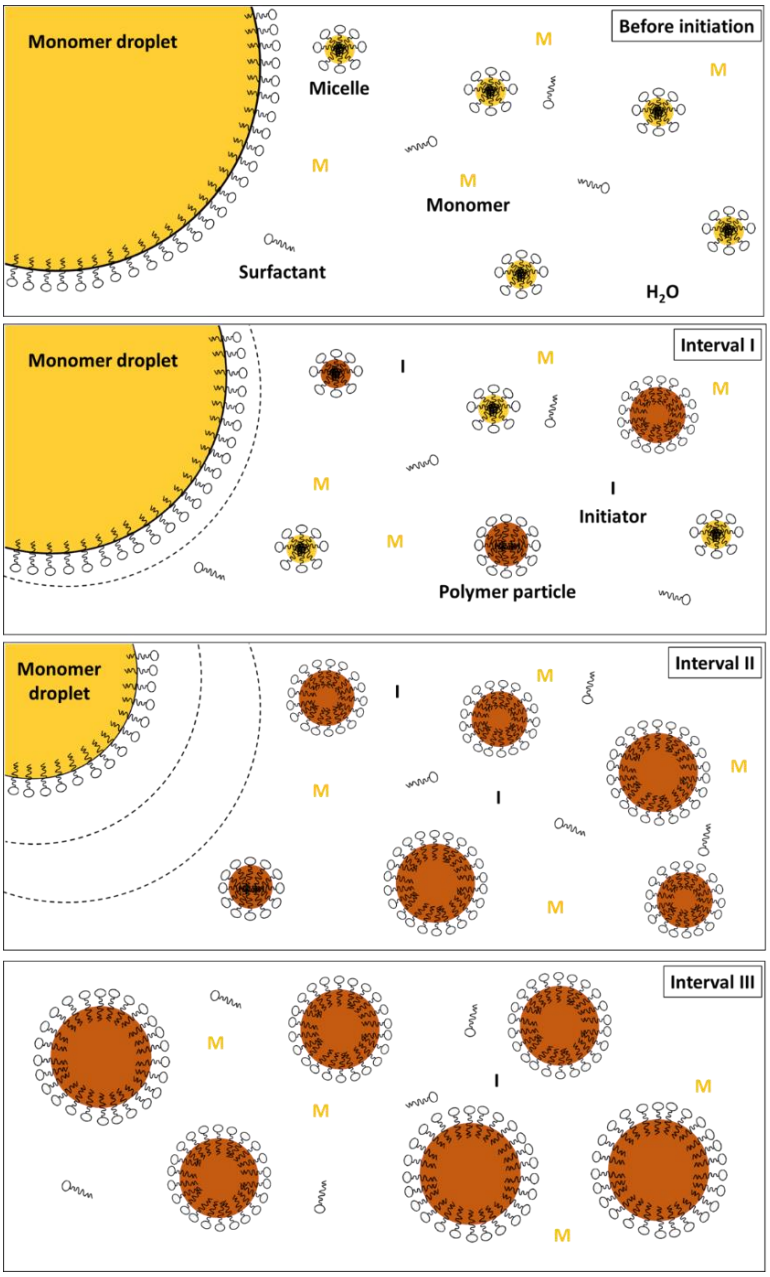

Figure 1.1. Representation of a batch emulsion polymerization before initiation and during intervals I-III. Reproduced and modified with permission from John Wiley and Sons.[16]

Interval I

In interval I, polymer particles are generated in a process called particle nucleation. There are two main mechanisms of particle nucleation: Heterogeneous nucleation and homogeneous nucleation.

In heterogeneous nucleation, a polymer particle is formed when a radical enters to a micelle.[17–19] The radicals created from the initiator are too hydrophilic to enter directly to the organic phase and they need to react with the monomer dissolved in the aqueous phase to achieve a critical chain length and become hydrophobic enough to enter to the organic phase. The hydrophobic oligoradicals can enter micelles or monomer droplets but the probability of this last event is low since the surface area of the monomer droplets is roughly 3 orders of magnitude smaller than the surface area of the micelles. In homogeneous nucleation, the water-soluble radical grows until it becomes insoluble and precipitates.[20–22] The surfactant molecules dissolved in the aqueous phase migrate and adsorb on the surface of the precipitated oligoradical to stabilize it and form a polymer particle. In some polymerization systems, both nucleation mechanisms can coexist. Nevertheless, it is known that homogeneous nucleation prevails with relatively water-soluble monomers such as vinyl acetate[23] or at surfactant concentrations below the CMC[20] and that heterogeneous nucleation is favoured with more hydrophobic monomers such as styrene and high surfactant concentrations.

The newly formed polymer particles become the main polymerization loci and the monomer from the monomer droplets diffuses continuously through the aqueous phase to the polymer particles to equilibrate the monomer consumed in the polymerization. Usually, the diffusion rate of the monomers is faster than the monomer consumption rate and the emulsion polymerizations proceed under thermodynamic equilibrium.[24] As a result of the polymerization and the continuous monomer diffusion to the polymerization loci, the polymer particles grow and

surfactant molecules diffuse through the aqueous phase to stabilize the newly formed surface area. The majority of the surfactant is in the form of micelles, and therefore, some micelles are consumed for the stabilization of the growing polymer particles. In addition, in the newly formed growing particles, the surface area generation rate is huge and the surfactant molecules might not be able to diffuse and adsorb fast enough to cover it.[25,26] In this case, the small polymer particles (known as precursor particles) coagulate leading to bigger and stable particles. The process in which stable polymer particles are generated from particle precursors is called coagulative nucleation.[27–29]

During interval I, the number of particles increases and the number of micelles decreases until all the micelles are consumed. This event marks the end of interval I. From this point, unless coagulation occurs, the number of particles in the system remains constant.

Interval II

During interval II, the system is composed of growing polymer particles and monomer droplets. The polymerization occurs inside the polymer particles and the monomer needed for the polymerization is continuously provided by the monomer droplets. During this interval, the monomer concentration in the particles and, thus, the polymerization rate is roughly constant and usually maximum (the polymerization rate is proportional to the concentration of monomer in the polymer particles).[24] The disappearance of the monomer droplets marks the end of interval II.

Interval III

In the last interval, the monomer remaining in the polymer particles and dissolved in the aqueous phase is consumed. In this interval, in general, the polymerization rate gradually decreases as the concentration of monomer in the particles decreases until all the monomer is

consumed. The occurrence of gel effect may result in an increase of the polymerization rate during this period.

1.2.1.2. Semibatch emulsion polymerization

In a semibatch polymerization, a fraction of the monomers is gradually added to the reaction medium. The nucleation step is the most variable event in emulsion polymerization and it is often circumvented by initiating the polymerization from pre-synthetized small polymer particles. This is called seeded semibatch emulsion polymerization. The polymer seed is initially charged to the reactor and after the initiation of the system, the rest of the ingredients are fed into the reactor. After the feeding stage, the system is usually allowed to react for an additional time to ensure complete monomer consumption.

Compared to the batch mode, the semibatch process is safer because the monomer concentration in the system at any time is low. In addition, due to the low monomer concentration, the monomers react as they enter to the reactor and this allows the preparation of copolymers with homogeneous composition from monomers with different reactivity ratios.[30–32] Finally, the correct design of the process allows the preparation of more complex particle morphologies such as core-shell particles.[33–35]

1.2.2. Miniemulsion polymerization

Miniemulsion polymerization is a polymerization technique utilized to produce aqueous polymer dispersions with particle sizes in the range 50 – 500 nm.[36,37] The main difference with emulsion polymerization is that the nucleation of particles takes place primarily in the monomer droplets.[38–40] This is achieved by applying mechanical energy to break the big monomer droplets and decrease their size. The surfactant molecules aggregated in the micelles migrate to cover

the newly formed water/droplet interface generated in the breakage. As a result of this process, the micelles disappear and the number of monomer droplets increases significantly. The final monomer droplet size achieved during the miniemulsification is a result of two consecutive processes;[41,42] Droplet break-up determined by the energy applied in relation with the viscoelasticity of the droplets, and coagulation of newly formed droplets insufficiently covered by emulsifier. The final droplet size is determined by the mechanism that gives the largest droplet size. In systems with low viscosity of the organic phase, the final droplet size is determined by the surfactant available. Polymeric surfactants such as polyvinyl alcohol (PVOH) have low desorption rates from oil-water interphases[26] and therefore, in emulsion polymerization they are less efficient covering the newly formed particles leading to a greater number of coagulation processes and bigger particle sizes. On the other hand, PVOH can be efficiently used to form miniemulsions because during miniemulsification it is well distributed among droplets and it does not need to move during polymerization.[43] Miniemulsification is the bottleneck for industrialization of miniemulsion polymerization.[44]

The initiation of the polymerization can be carried out with both water-soluble and oil-soluble initiators. Oil-soluble initiators reduce the likelihood of secondary nucleation. Nucleation will take place directly in the monomer droplets and the monomer in each droplet is converted into polymer as represented in Figure 1.2, with no need of monomer diffusion. This feature allows the polymerization in aqueous media of monomers with negligible water-solubility such as stearyl acrylate (SA)[45,46] or the incorporation of inorganic nanoparticles for development of novel hybrid materials.[47–51] One mechanistic phenomenon that has to be considered in miniemulsion polymerization is the diffusional degradation of the smaller monomer droplets, known as Ostwald ripening.[52,53] The chemical potential of the monomer in the small droplets is higher than in the big ones and thus, the monomer in the smaller particles diffuses through the aqueous phase to

the big ones leading to the disappearance of the smaller particles. This issue can be circunvented adding costabilizers, which are low molecular weight hydrophobic compounds such as hexadecane[42,54] or stearyl acrylate (SA).[42,55] Due to their low water-solubility, they do not diffuse across the aqueous phase and prevent the disappearance of the smallest droplets.[56–59]

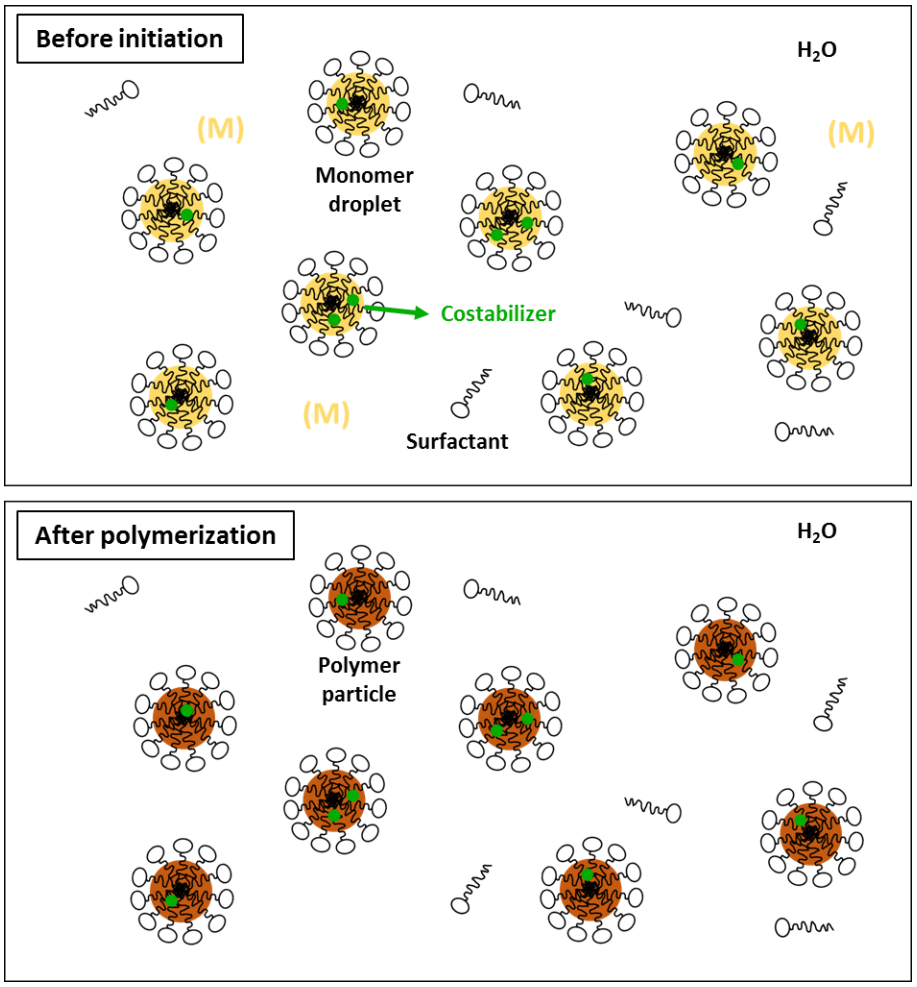

Figure 1.2. Representation of a miniemulsion polymerization before and after polymerization.

1.3. Film formation

As explained in Section 1.1, polymer coatings are thin polymer layers employed for the protection and decoration of substrates. In waterborne systems, polymers are produced as water dispersions but they need to be dried for the application. The process where a polymer dispersion becomes a polymer film is called film formation and it is a crucial step for obtaining good quality cohesive films. Therefore, it is important to analyze the different stages the system goes through and understand the main parameters affecting them for the development of high performance materials.

The film formation process of a waterborne polymer dispersion is shown in Figure 1.3.[60,61] At the beginning of the process, the polymer particles are dispersed in water (stage I). As the water evaporates, the particles get closer to each other until they form a close-packed structure (stage II). In the next step, the spherical particles deform to form a dodecahedral structure (stage III). The driving force for the deformation is the reduction of the surface free energy of the particles. This point can be recognized visually because the film becomes optically transparent due to the disappearance of the voids between particles. Nevertheless, this transition only occurs at temperatures above the Minimum Film Formation Temperature (MFFT) of the dispersions which is defined as the lowest temperature at which the polymer particles are soft enough to deform and form a crack-free transparent film. In the last step, the polymer chains diffuse through the polymer particle boundaries and mix with the polymer chains in the neighbouring particles. In this process, the polymer particles fuse together and lose their particle identity leading to a homogeneous film. This last step is particularly important for the development of cohesive materials since full mechanical strength is only achieved when the diffusion distance of the polymer chains is comparable to their radius of gyration (R_g).[62,63] However, the diffusion of the polymer chains and coalescence only take place when the polymer chains have enough mobility,

and therefore occurs at temperatures higher than the effective T_g of the (co)polymer. The deformation and coalescence steps make challenging to obtain mechanically stiff films at room temperature because chain mobility (low T_g) and hardness (high T_g) are required at the same time. This is known as the film formation dilemma. In the solventborne counterparts, the polymer chains are not confined in individual polymer particles and the omission of the deformation and coalescence steps allows the film formation of high T_g polymer solutions at room temperature. Due to the differences in the film formation process, solventborne products continue to dominate the market in the applications that require mechanical strength. However, as described in Section 1.4, the fundamental understanding of the film formation process of the waterborne dispersions, especially during the deformation, coalescence and interpenetration steps, has allowed the development of high performance materials. The main techniques employed to follow these last stages of the film formation process and the effect of the main variables are described in the next section.

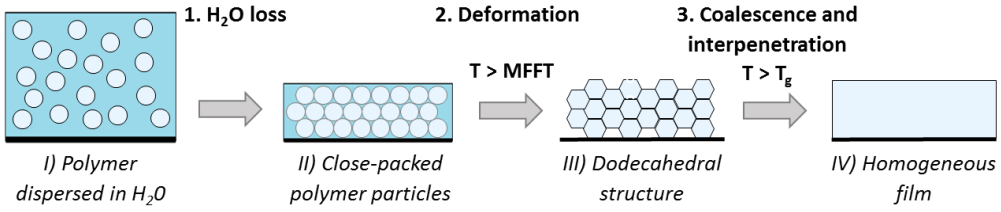

Figure 1.3. Film formation process from a waterborne dispersion. Figure reproduced and modified with permission from Springer Nature.[61]

1.3.1. Analysis of film formation

The last two stages of the film formation where the polymer particles deform and coalesce are crucial for the production of homogeneous and cohesive films. Accordingly, several techniques have been developed to follow these transitions and analyze the effect of the different parameters on the film formation process and the development of the mechanical strength of the films.

Industrially, the MFFT is used as an indicator of the film formation ability of the latexes because it shows the minimum temperature at which the polymer particles are able to deform into a honey-comb structure and become a clear film.[1,64] The MFFT is determined by casting a thin film on a metal substrate with a temperature gradient and analyzing the minimum temperature at which a crack-free clear film is obtained. The main parameter affecting the MFFT of the dispersions is the T_g of the (co)polymer, since the hardness of the polymer particles is what mainly determines their deformation ability. However, it has been shown by different authors that the MFFT of the dispersion also depends on the particle size: Smaller particle size dispersions have higher surface area, and because the driving force for the deformation of the particles is the reduction of the surface energy, they present slightly lower MFFT-s.[14,65]

Spectroscopic techniques such as Scanning Electron Microscopy (SEM) Transmission Electron Microscopy (TEM) or Atomic Force Microscopy (AFM) have also been employed for tracking the film formation process.[66–70] With these techniques, it is possible to observe the morphology of the films at the nano-scale and analyze its evolution during the film formation process. For example, Meincken *et al* prepared P(S/BA/MAA) particles with a T_g of about 19.8 ºC and analyzed the evolution of the coalescence of the particles at ambient temperature with time by AFM.[67] Figure 1.4 shows how the particles underwent coalescence with time.

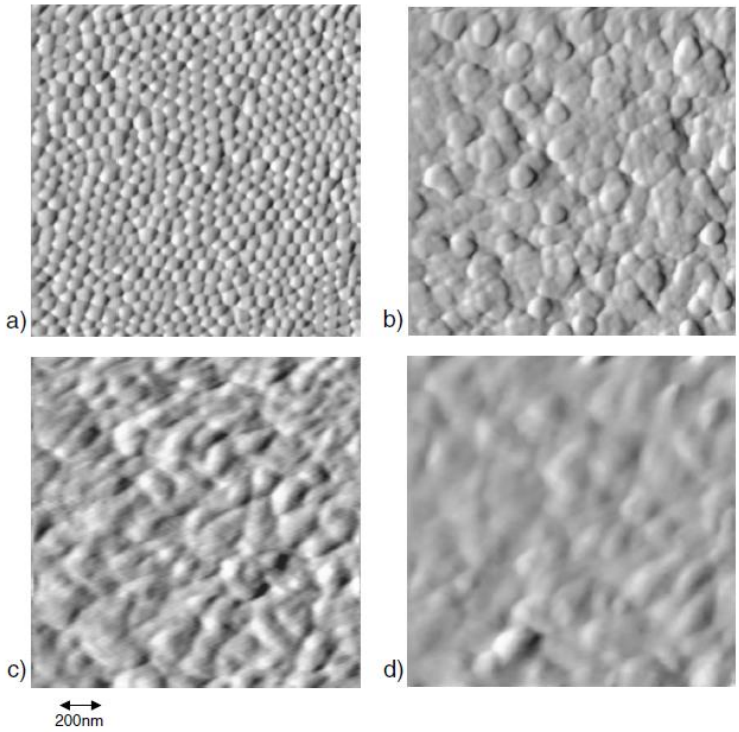

Figure 1.4. AFM images of P(S/BA/MAA) polymer films acquired 30, 240, 660 and 1440 minutes after film casting at ambient conditions.[67] Reproduced with permission from Elsevier.

TEM and SEM techniques are not appropriate for the analysis of wet samples since they require high vacuum and water would evaporate during the measurement. This issue impedes the visualization of the system in most of the cases during the deformation stage since small amounts of water are still present in the film. Alternatively, cryogenic analysis of the samples can be carried out in which the wet samples are frozen and examined at cryogenic temperatures.[71] In addition, techniques that do not require vacuum such as environmental-SEM have also been developed.[72,73]

Although the coalescence of the particles can be visualized by spectroscopic techniques, from the images it is not possible to determine the extent of interdiffusion across the particle boundaries. As mentioned, the interpenetration step is crucial for the development of the mechanical strength of the films and, therefore, a clear understanding of the influence of different parameters on this process is required for the production of high performance materials. Two main methods have been developed to evaluate the rate and extent of diffusion of the polymer chains across the polymer particle boundaries: Small Angle Neutron Scattering (SANS)[74–76] and Fluorescence Resonance Emission Transfer (FRET).[77–87] In both methods, some polymer particles are labelled and the diffusion of the polymer chains is followed over time.

In SANS experiments, deuterium is used as labelling agent and the contrast is provided by the difference in scattering between protons and deuterium. Experimentally, a small fraction of deuterated polymer particles is added to the main dispersion and the distribution and size of the deuterated particles is analyzed. Before the coalescence, the deuterated particles have a certain R_g, but as the deuterated polymer chains diffuse through the boundaries, the R_g increases until the chains become randomized in the matrix. This process is represented schematically in Figure 1.5.

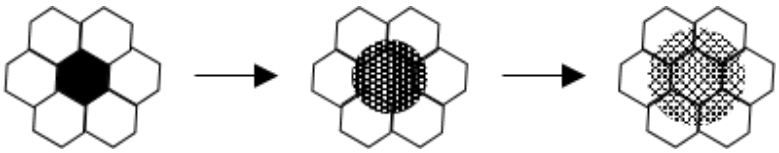

Figure 1.5. Physical description of a SANS experiment: The radius of the deuterated particle (in black) increases with time due to the diffusion of the polymer chains. Reproduced and modified with permission from American Chemical Society.[81]

In FRET experiments, a fraction of the particles (typically half) is labelled with a fluorescent donor dye such as phenantrene and the other half is labelled with a fluorescent acceptor dye like anthracene. During the experiment, the donor dyes are excited and their relaxation decay is analyzed. At the beginning of the process, the donor and acceptor groups are confined in individual particles and the relaxation decay of the donor is slow. However, as interpenetration takes place, the two dyes get closer and the relaxation of the donor group becomes faster. Therefore, the interdiffusion process can be followed monitoring the relaxation decay over time. The physical description of the FRET experiment is shown in Figure 1.6.

Figure 1.6. Physical description of a FRET experiment: The fluorescence donor and acceptor dyes mix upon time due to polymer chain diffusion. Reproduced and modified with permission from American Chemical Society.[81]

These two techniques have been widely employed for studying the influence of different factors such as the drying T - T_g difference, particle size or crosslinking degree on the diffusion of the polymer chains.

In the first place, as in the case of the MFFT, the main parameter affecting the diffusion of the polymer chains is the difference between the drying temperature and the T_g of the polymer. With low T_g polymers or at high drying temperatures, the diffusion of the polymer chains is relatively fast and high interpenetration degrees are achieved in short times.[77,84,85] The use of smaller polymer particles also facilitates the diffusion because the interfacial area for

interpenetration is larger.[77] Regarding the molecular weight of the polymer chains, different works show that the diffusion of the polymer chains is faster decreasing the molecular weight.[68,79,81,84,86] In the work carried out by Tomba *et al*, different molecular weight polymer particles with the same composition were blended and the diffusion of the polymer chains was studied by FRET. According to the results, the low molecular weight polymer chains not only presented higher diffusion rates but also promoted the movement of the high molecular weight chains.[87] This plasticising effect was attributed to an increase in the free volume caused by the short polymer chains. Similarly, it has been demonstrated that the incorporation of small organic molecules enhances significantly the diffusion of the polymer chains.[88–90] On the contrary, the crosslinking of the polymer chains exponentially reduces their diffusion ability.[78,80,83]

The basic understanding of the effect of different factors on the film formation process is necessary to develop high performance materials that present good formation ability at room temperature and high mechanical strength. The main approaches employed for the development of mechanically strong waterborne coatings are discussed in the following section. Ideally, the desired product is a non-toxic, environmentally-friendly, ambient curing waterborne dispersion with high mechanical strength.

1.4. Approaches to overcome the film formation dilemma

1.4.1. Diffusion promotors

The easiest approach and the one that has been widely employed by industry to solve the film formation dilemma, is the incorporation of coalescing aids to the formulation. Coalescing aids are small organic molecules that plasticise the polymer chains and decrease their T_g during film formation, promoting their diffusion across the polymer particle boundaries. Eventually, the

coalescing aids evaporate and the polymer film recovers its mechanical strength. Therefore, the addition of coalescing aids allows the formation of films from hard polymer particles at ambient temperature.[64,88–92] In addition to coalescing aids, it is known that the incorporation of hydrophilic functional groups such as carboxylic acids to the polymer particles also decreases the MFFT of the dispersions. In this case, the water molecules of the continuous phase interact via hydrogen bonding with the hydrophilic functional groups, increasing the free volume and enhancing the mobility of the polymer chains. This phenomenon is known as hydroplasticization.[93]

The decrease in the T_g caused by these phenomena has been investigated by Differential Scanning Calorimetry (DSC) by comparing the data obtained in the wet and dry states.[92,94,95] In addition, information about the film formation process in the presence of plasticisers or hydroplasticising groups can be obtained by FRET.[88,91,96] As shown by Juhué and co-workers, the evaporation rate of the coalescing compound strongly influences its plasticising efficiency. The evaporation rate of the coalescing aid should be low enough to ensure the plasticization of the polymer chains during the deformation and interdiffusion stages.[89] On the other hand, the prolonged retention of solvents limits the mechanical strength of the films.[90]

However, the ultimate evaporation of the plasticising compound brings back the environmental concerns about the VOC emissions. As an alternative, the VOC content of the formulations can be decreased by using reactive plasticisers: They provide chain mobility during film formation but they finally react with the polymer chains instead of evaporating.[78,97–99] For example, Lahtinen *et al* described the synthesis of five reactive coalescing agents with glycidyl functionalities and their application in a carboxylic acid functional latex. The functional coalescing agents decreased efficiently the MFFT of the dispersion and, at the end of the process, the reaction between the epoxy groups in the coalescing agent and the carboxylic acid groups in the polymer backbone prevented the evaporation of the plasticizers. The films presented a pendulum

hardness and gloss comparable to the materials prepared with a commercial non-reactive coalescing agent validating the reactive coalescing agent approach for the production of low-VOC strong waterborne coatings.[100]

A second alternative is to employ higher molar mass plasticizing agents which do not evaporate during film formation. Typically, low molecular weight polymer chains, commonly called oligomers, are employed as non-volatile coalescing aids.[101–103] As discussed in the film formation section, low molecular weight polymer chains can act as efficient plasticisers during film formation.[79,84,87] In the work carried out by Fasano *et al,* the incorporation of oligomers allowed the preparation of VOC-free strong polymer films. The system was composed of soft polymer particles and hard polymer particles loaded with oligomers. Initially, the oligomers plasticized the hard polymer chains promoting their film formation and finally, the oligomers diffused preferably to the soft phase allowing the recovery of the mechanical strength of the hard phase. The coating prepared employing this approach presented better gloss and a hardness comparable to the coating prepared with a commercial volatile coalescing agent.[68] Nevertheless, although oligomer plasticization leads to strong films in many cases, the effect of the oligomers in the final mechanical performance of the materials should be considered in each system, since a small fraction of oligomers can drastically decrease the T_g of the polymer[104] and compromise the mechanical strength of the coating.[105,106]

1.4.2. Structural reinforcement

As an alternative to coalescing aids, it is possible to prepare VOC-free strong polymer films using soft-hard multiphase systems. The soft component allows film formation whilst the hard component acts as structural reinforcement agent and enhances the mechanical strength of the materials.

Typically, the soft component is a polymer dispersion with a T_g low enough to form a homogeneous film and two different types of hard components can be employed: high T_g polymers or inorganic fillers. Multiphase polymer systems containing soft and hard polymers have been prepared blending low and high T_g polymer particles[14,107–114] or combining both components in core-shell structured nanoparticles. It is worth mentioning that two main types of structured particles are distinguished depending on the position of the hard phase within the particles: *hard core*-soft shell particles[108,115,116] and soft core-*hard shell* particles.[34,35,117–119] Compared to the polymer blends, the use of structured nanoparticles promotes the homogeneous distribution of the hard and soft components along the film and avoids stratification.[112,114,120] Regarding the inorganic fillers, they can be added to the dispersions by encapsulation during the synthesis (surface modified CeO_2[50,121] or silica nanoparticles[122,123]), by physical mixing after the synthesis of the latexes ($CaCO_3$,[124–126] TiO_2,[124,127] clay,[124] carbon black,[128] silica,[123,128] carbon nanotubes,[129] nanocellulose,[130] etc.) or as stabilizers for the synthesis (silica,[131,132] clay,[133,134] TiO_2,[135] nanocellulose,[136–138] etc).

When hard components are employed as structural reinforcing agents, two main morphologies can be obtained. In the first scenario, the hard domains are evenly dispersed in the soft matrix. This morphology can be achieved blending a small fraction of inorganic fillers[128,139] or hard polymer particles[107,110,112] with the soft particles dispersion (Figure 1.7.I), or encapsulating the hard domains within the polymer particles[50,108,121,124] (Figure 1.7.IV for hard core-soft shell polymer particles). In such systems, the inclusion of hard domains in the soft matrix increases the Young's Modulus of the material. The hardening of the material is proportional to the volume fraction of the hard phase (films with higher hard phase volume fraction are shown in Figures 1.7.II and 1.7.V). In addition, for the same hard phase volume fraction, smaller hard particles have a greater stiffening effect.[126] The hard core-soft shell

approach was successfully applied by Juhué *et al* to produce low VOC ambient curing dispersions. As they demonstrated, the use of coalescing agents can be avoided by covering the hard particles with a thin soft polymer layer since the materials prepared from the structured nanoparticles and employing coalescing agents showed very similar mechanical performance.[33]

In the second scenario, the hard phase forms a connected network throughout the film. This morphology is obtained with high volume fractions of the hard phase in blends[109,111,140] (Figure 1.7.III), in soft core-hard shell structured particles[34,35,118,119] (Figure 1.7.VI) and in dispersions stabilized with inorganic particles.[131,133–135,137] In general, the hardness of the material increases with the volume fraction of the hard phase (Figure 1.7.VII). In multiphase blends, the transition from the first to the second morphology occurs at a critical hard phase volume fraction characteristic for each R_{soft}/R_{hard} ratio (relative particle sizes of the components).[14,109,113,123,127] Above this critical concentration also called percolating threshold, the MFFT of the dispersion, the hardness and the blocking resistance of the material increase sharply. In addition, it has been shown by different authors that the formation of a hard honeycomb microstructure around the soft polymer particles is an efficient way to enhance the mechanical strength of the films because it provides hardness and extensibility simultaneously. The hard honeycomb increases the elastic modulus of the material whilst the soft domains contribute to the dissipation of the deformation energy and increase the toughness.[140] This behaviour has been observed in polymer particle blends,[140] soft core-hard shell particles[35,118] and particle-inorganic filler composites.[132] In the last case, it should be noted that the use of inorganic fillers above the percolating threshold can also lead to brittle materials because of the weak points formed between hard inorganic particles.[126,137]

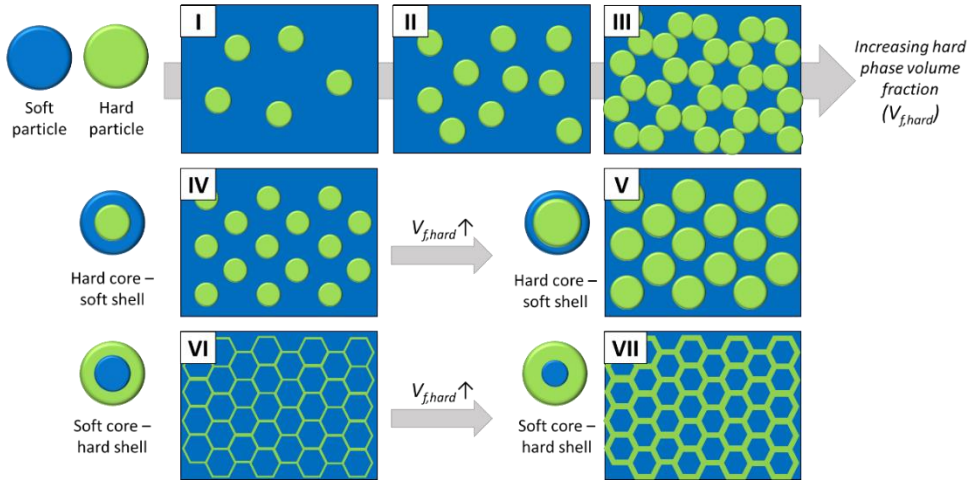

Figure 1.7. Film morphologies developed from blends of soft and hard polymer particles increasing the hard phase volume fraction from (I) to (III), hard core-soft shell polymer particles increasing the shell thickness from (IV) to (V) and soft core-hard shell polymer particles increasing the shell thickness from (VI) to (VII). Note that in parts VI and VII the percolating hard network is represented as a continuous phase for simplification, but film formation will only take place if the hard phase is not continuous.

1.4.3. Crosslinking of the polymer chains

The third approach to improve the performance of waterborne coatings is to crosslink the polymer chains. Typically, a film forming low T_g latex is functionalized with moieties that are able to interact with other functional groups and form new bonds. The use of a low T_g latex ensures the completion of the film formation process while the incorporation of functional groups enables the crosslinking of the polymer chains. The formation of a 3D polymer network enhances the solvent resistance, thermal stability, mechanical performance and durability of the materials.[141] The systems reinforced through crosslinking can be classified as physical or chemical depending on the nature of the bond formed. In physically crosslinked systems, physical bonds such as ionic interactions, host-guest interactions, metal complexation or hydrogen bonds are employed

to reinforce the materials. In chemically crosslinked systems, new covalent bonds are formed as a result of the reactions between functional groups.

1.4.3.1. Development of the mechanical strength of the films

In waterborne crosslinkable systems, an efficient crosslinking reaction between the functional groups does not ensure the formation of a cohesive film. In such systems, relative rates of diffusion and crosslinking during film formation play a crucial role for the development of the mechanical strength of the film.[82,83] The different scenarios are represented in Figure 1.8. When crosslinking is faster than diffusion, the movement of the polymer chains is constrained before they are able to diffuse through the polymer particle boundaries and mix with the polymer chains in the neighbouring particles. At the end of the process, the individual polymer particles are highly crosslinked but the lack of bridging between different particles results in a non-cohesive polymer film. In the second case, when crosslinking and diffusion rates are comparable, the polymer chains are able to diffuse through the polymer particles boundaries up to some extent before their movement is restricted. This results in interfacial crosslinking between polymer particles. In this case, the materials present higher cohesion as the weak points between polymer particles are reinforced by newly formed bonds. In the last case, when diffusion is faster than crosslinking, first polymer diffusion is fully developed and then crosslinking occurs homogeneously throughout the film. This is the ideal case, where highly cohesive films are produced. However, the development of the mechanical strength may take some time. The compatibility between the components also influences the final microstructure and performance of the films. If the components are not compatible, their mixing across the polymer particle boundaries and the final strength of the film will be limited. On the contrary, the high compatibility of the components enhances their homogeneous distribution along the film and facilitates the development of a cohesive material.[142–145]

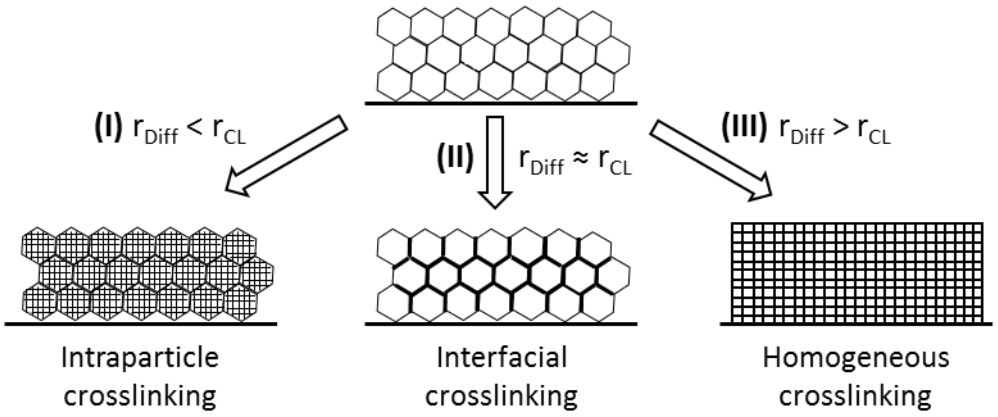

Figure 1.8. Film development depending on the relative diffusion (r_{Diff}) and crosslinking (r_{CL}) rates. Reproduced and modified with permission from Springer Nature.[82]

The development of the mechanical strength of the films during the interpenetration step and the effect of crosslinking in such process has been studied by different authors. In the works carried out by Zosel and Klein, the mechanical strength of the films was followed as a function of the interpenetration depth across the particle boundaries measured by FRET and SANS.[75,76,146,147] In the case of un-crosslinked polymer films, the tensile strength and the fracture energy of the films increased with the interpenetration depth up to a point where the mechanical strength remained constant. This maximum strength was achieved when the interpenetration depth was comparable to the radius of gyration of the polymer chains. On the contrary, increasing the crosslinking degree of films, the movement of the polymer chains was gradually hindered and the materials presented lower fracture energies. The same behaviour was reported by Ghazaly *et al*, who attributed the bad solvent resistance and brittleness of the PBMA-EGDMA films to the tight network formed within the polymer particles during the synthesis, which impeded the diffusion of the polymer chains across the boundaries during film formation.[148] Other authors have also studied the effect of the crosslinking degree of the polymer particles on the diffusion

of the polymer chains.[80,149] However, in contrast to the work of Ghazaly, the highly crosslinked materials prepared in these works did not show brittle behaviour. This was attributed to the movement of dangling chain ends which were able to cross the particle boundaries and heal the interface up to some extent. However, the lack of crosslinking between the particles resulted in poor solvent resistance.

Joshi and coworkers compared two systems crosslinked before and after the coalescence (adding a crosslinker during the synthesis and employing diacetone acrylamide/dihydrazide crosslinking technology respectively). Similar to previous works, the system crosslinked before coalescence showed poor hardness, chemical resistance and adhesion. On the contrary, the system crosslinked after coalescence showed improved hardness and chemical resistance.[150] Therefore, in agreement with the theory explained above, coalescence and interpenetration should precede crosslinking to obtain high performance materials. This principle was followed in the work carried out by Mazuel *et al* who employed acetal self-concensation for the crosslinking of poly(2-ethylhexyl methacrylate) based latexes.[151] In their work, the diffusion and reaction rates were comparable, and considerable extents of interpenetration were obtained before the movement or the polymer chains was constrained by the crosslinks. As shown in Figure 1.9, the tensile behaviour of the materials depended on the concentration of the self-condensing motif, and thus, the crosslinking degree: Increasing the acetal concentration, the materials presented higher elastic modulus, yield stress, tensile strength and lower ultimate strain.

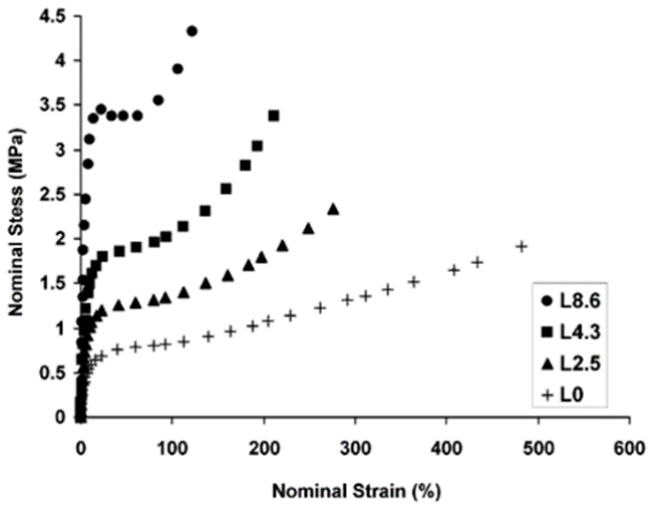

Figure 1.9. Stress-strain plots of PEHMA films with 0, 2.5, 4.3 and 8.6 mol% self-crosslinking acetal functionality. Reprinted with permission from American Chemical Society.[151]

Therefore, as shown in Figure 1.9, the formation of a crosslinked polymer network alters remarkably the mechanical response of the material. On the one hand, crosslinks act as constraints for deformation, and therefore, crosslinked materials oppose higher resistance to deformation, which manifests in higher elastic modulus, yield stress and tensile strength values. On the other hand, the plastic deformation of a polymer material is a result of the movement and orientation of the polymer chains in the direction of the stress. This reorientation process is the main energy dissipation mechanism during the stretching of the materials. In crosslinked systems, the freedom of the polymer chains to move is constrained impeding their reorientation and this leads to low fracture strains and materials with low energy dissipation capabilities (low toughness). Hence, the gradual stiffening observed in Figure 1.9 attributed to the molecular movement constrains caused by the crosslinks is the typical mechanical behaviour of crosslinked polymers.[145–149,152,153]

1.4.3.2. Chemical crosslinking

Chemical crosslinking of polymer chains is an efficient route to improve the mechanical and thermal performance, solvent resistance and durability of polymer materials. The chemistry of polymer crosslinking has been widely studied in the last century trying to understand and control the crosslinking processes, and be able to produce more resistant materials.[141,154] In the field of waterborne coatings, this knowledge has been applied for the production of high performance products in which the film formation dilemma is overcome by hardening the materials in the last stage of the film formation process through chemical crosslinking.[155,156] The ideal crosslinking system would be comprised of a non-toxic and stable polymer dispersion able to cure efficiently at ambient conditions. In the following pages, the main crosslinking chemistries and strategies employed for the chemical crosslinking of the waterborne dispersions will be described and their main advantages and drawbacks will be highlighted. It is worth mentioning that this short literature review is mostly focused in acrylic aqueous dispersions, since the nature of the polymers employed throughout this work is acrylic.

1.4.3.2.1. Chemical crosslinking of hydroxyl functional polymer particles

The pioneering chemical crosslinking technologies combined hydroxyl-functional particles with water-soluble/dispersible crosslinkers. The hydroxyl functional groups are commonly incorporated to the acrylic polymer particles employing in the formulation of the latex functional monomers such as 2-hydroxyethyl methacrylate (HEMA) and they are subsequently crosslinked using melamine type crosslinkers or polyisocyanates (Figures 1.10.A1 and 1.10.B, respectively).

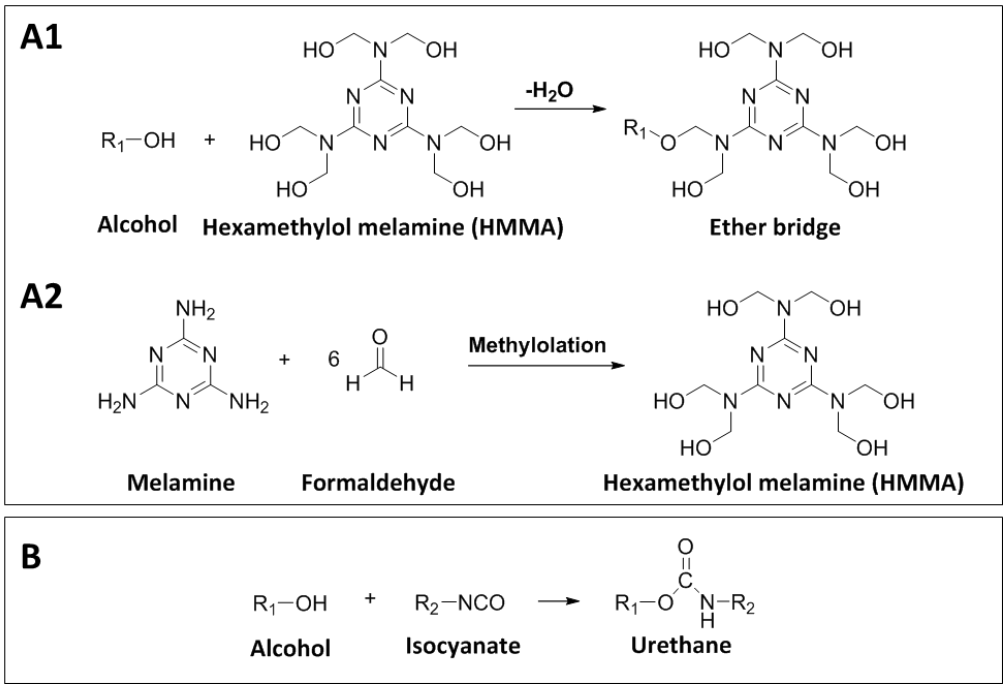

Figure 1.10. Chemical reaction between an alcohol and (A1) a methylol melamine unit and (B) an isocyanate. A2 shows the formation of hexamethylol melamine from melamine and formaldehyde.

The hydroxyl/melamine crosslinking reaction was the first crosslinking technology applied to waterborne systems.[78,145,157–160] It was first reported in the late 1950s for the crosslinking of an automotive basecoat and safer versions of this technology are still used today. This technology provides enhanced chemical resistance and good balance between flexibility and hardness. One drawback of this crosslinking technology is the high temperatures and long times required for the curing.[161] The curing temperature can be reduced by the addition of an acid catalyst such as p-TSA but the product pot-life decreases as a result of the hydrolysis of the functional groups in acid conditions. Nevertheless, the main drawback of this chemistry relies on the use of formaldehyde for the synthesis of hexamethylol melamine (HMMA, Figure 1.10.A2), which can eventually be released as a degradation product during the application of the coating.

Formaldehyde is classified as toxic and carginogenic.[162] In the 1970s, the awareness of the negative effect of using formaldehyde and the creation of the Environmental Protection Agency (EPA) promoted the search for crosslinking technologies that avoided the use of formaldehyde and required lower curing temperatures.

Isocyanates have also been widely used for the chemical crosslinking of hydroxyl functional dispersions.[163–168] Unlike the melamine type crosslinking, the reaction of hydroxyl groups and isocyanates proceeds at room temperature and it is efficiently catalysed by organic metal salts or tertiary amines.[169] Nevertheless, the high sensitivity of isocyanates towards moisture and other nucleophiles limits the pot-life of the products. Commercially, this is overcome by using blocked polyisocyanates resulting from the adduct between the isocyanate and other H-active groups such as alcohols, oximes or amines.[170] However, similar to the melamine type crosslinkers, the main drawback of this technology relies on the high toxicity of the isocyanate group.[171] As alternative, significant progress has been made in recent years in the development of synthetic paths for the synthesis of polyurethanes from isocyanate-free sources.[172,173] One of the most explored and promising synthetic pathways for non-isocyanate polyurethanes (NIPUs) is the reaction between 5 or 6 member cyclic carbonates with amines.[174] Compared to the conventional isocyanate-hydroxyl coupling, this reaction is insensitive to moisture and avoids the formation of bubbles resulting from the side reactions of isocyanates.[175] Nevertheless, the reaction is slow at room temperature[176] and catalysts[177,178] or annealing[179] are required to achieve high reaction yields in reasonable times. In addition, the NIPUs produced in such reactions present low molar masses, which limits their practical application. This is attributed to the high stability of the carbonate group compared to the isocyanate. The toxicity of the functionalities is often related to their reactivity and, therefore, it is challenging to produce non-toxic and ambient curing technologies.

1.4.3.2.2. Chemistries involving carboxylic groups

Although melamine formaldehyde-type and isocyanate-alcohol crosslinking technologies are highly efficient approaches for the mechanical reinforcement of films cast from waterborne dispersions, the awareness about the negative environmental and biological effects of formaldehyde and isocyanates has led to the development of less hazardous crosslinking chemistries that can proceed at low temperatures. Some of these technologies involve the carboxylic acid functionality. Carboxylic acids are very often used in waterborne coating formulations to provide stability to the polymer particles. However, the presence of these groups increases the water sensitivity of the polymer films due to their hydrophilicity. Therefore, the use of these functional groups for the chemical crosslinking of the waterborne coatings has a double function: On the one hand, crosslinking takes place from these moieties without the need of incorporating extra functionalities to the dispersions; and on the other hand, the disappearance of the CO_2H groups due to crosslinking decreases the water sensitivity of the films. The main functional groups employed for the crosslinking of carboxylates are aziridines, carbodiimides and oxiranes. The general chemical structures of the crosslinkers and crosslinking mechanisms are shown in Figure 1.11. These three functionalities have different reactivities and this determines their toxicity, crosslinking efficiency and pot-stability of the dispersions.

Among the three functionalities, aziridines are the most reactive ones and they readily react with ammonium carboxylates at room temperature.[180,181] However, the high reactivity of the aziridine functionality reduces the shelf-life of the mixed components to few hours, which is even shorter than the shelf-life of waterborne isocyanate dispersions.[182] In addition, aziridines are classified as highly toxic and they produce severe allergic reactions when they are in contact with the skin.[180,183]

Carbodiimides (CDI) are a safer alternative to aziridines. The chemical structure of carbodiimides is similar to the structure of isocyanates but they present lower sensitivity toward moisture. Therefore, the products prepared using the carbodiimide technology present longer pot-lifes than aziridine or isocyanate based products. Polycarbodiimide-type water-soluble crosslinkers have been widely employed to crosslink polymer dispersions functionalized with carboxylates.[184–187] In addition, functional monomers such as tert-butylcarbodiimidoethyl methacrylate (tBCEMA) or cyclohexylcarbodiimidoethyl methacrylate (CCEMA) have been used to functionalize polymer particles and prepare blends of dispersions with carbodiimide and carboxylate groups.[188–190]

In the last place, carboxylates react with epoxides leading to epoxy ester groups as shown in Figure 1.11.C. The reaction between carboxylates and epoxides is the slowest at room temperature due to the relative stability of the oxirane groups, and, therefore, epoxides are preferably used in combination with polyamines as described in next section.

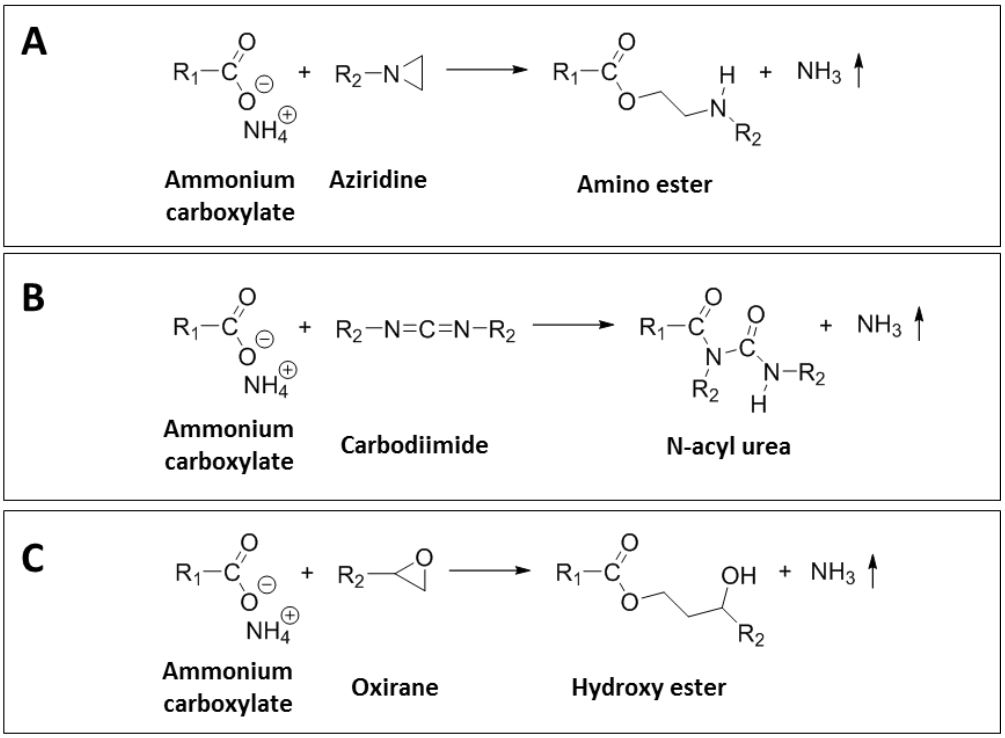

Figure 1.11. Crosslinking mechanisms of carboxylic acids with (A) aziridines, (B) carbodiimides and (C) oxiranes.

1.4.3.2.3. Oxirane/amine crosslinking

The epoxide/amine crosslinking technology, is one of the most promising alternatives due to the low toxicity and long pot-stability of the products. The reaction between an oxirane and an amine is shown in Figure 1.12.A. Usually, the epoxide moieties are incorporated to the acrylic polymer particles by including glycidyl methacrylate (GMA, Figure 1.12.B) in the formulation. The epoxy group of GMA is prone to suffer hydrolysis and subsequent side reactions but it is stable enough to be polymerized in emulsion polymerization. Then, the epoxy functional polymer

particles are combined with either water-soluble/dispersible polyamine crosslinkers[83,142,191,192] or amine-functional polymer particles.[193]

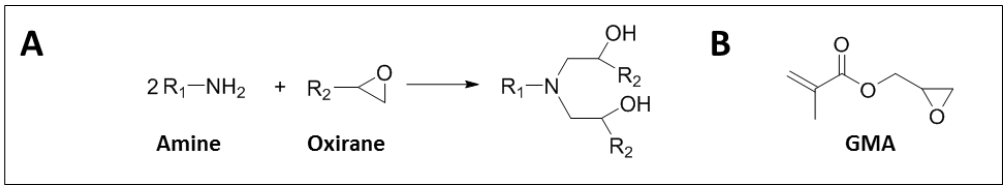

Figure 1.12. (A) Crosslinking mechanism between an amine and an oxirane and (B) chemical structure of glycidyl methacrylate (GMA).

1.4.3.2.4. Diketo/diamine crosslinking

Functional groups containing diketo moieties such as acetoacetoxy, acetoacetamide or diacetones react rapidly at room temperature with amines or hydrazides.[144,194] As in the epoxy/amine system, the low relative toxicity of the functional groups makes this crosslinking technology particularly interesting.

Usually, the diketo functionalities are incorporated to the polymer particles copolymerizing acetoacetoxyethyl methacrylate (AAEMA, Figure 1.13.A1), acetetoacetamido methacrylate (AAMMA, Figure 1.13.A2) or diacetone acrylamide (DAAM, Figure 1.13.A3) and they are subsequently crosslinked employing water-soluble polyamines or polyhydrazides (Figures 1.13.B1 and 1.13.C).[195–200] The main drawback the acetoacetoxy chemistry is the water sensitivity of this functionality, which decomposes in humid conditions to form a hydroxyethyl moiety, acetone and CO_2 (Figure 1.13.B2).[201] This issue can be largely avoided by reversibly protecting the acetoacetoxy groups with ammonium after the synthesis (Figure 1.13.B3). The use of acetoacetamido monomers such as AAMMA has also been suggested as alternative to acetoacetoxy monomers due to their slower hydrolysis rates.[202,203] Nevertheless, the functional

group presenting the highest resistance against hydrolysis is the “diacetone” moiety.[204] In the work carried out by Liu *et al,* the diacetone/dihydrazide crosslinking technology (Figure 1.13.C) was conveniently combined with soft core-hard shell structured particles to produce high performance materials with improved mechanical properties and solvent resistance.[205]

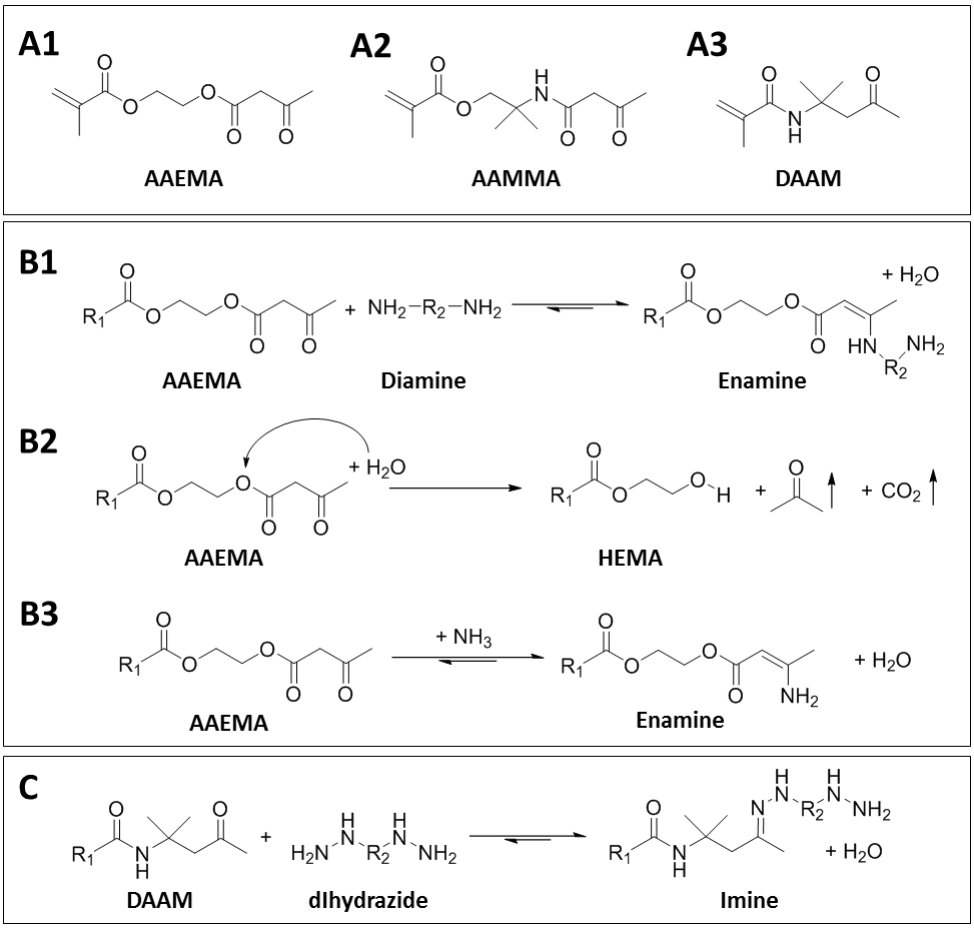

Figure 1.13. (A) Main monomers employed for the diamino/diketo crosslinking technology, (B) reactions involving acetoacetoxy groups and (C) reaction between diacetone diacrylamide and dihydrazide.

1.4.3.2.5. Unsaturated groups

A different approach employed for the chemical crosslinking the waterborne dispersions is the incorporation of unsaturated groups to the latex.

The most widely studied strategy to incorporate unsaturation to the acrylic systems is the addition of an alkyd resin to prepare acrylic-alkyd hybrids.[206–211] Alkyd resins are polyesters modified with unsaturated fatty acids that can undergo oxidative crosslinking.[212] However, the crosslinking of the alkyds is slow at room temperature and requires catalysts to achieve reasonable crosslinking rates.[213–216] One advantage of this technology is that crosslinking is not initiated until the material is exposed to the air during film drying, which ensures long shelf-lifes for the deoxygenated products. The main drawback of this technology is the evolution of the alkyd oxidative curing process after film formation which results in yellowing of the films and continuous release of volatile ketones, aldehydes or alcohols.[217]

Another way to incorporate unsaturation to the acrylic latexes is the copolymerization of functional monomers containing unsaturated double bonds such as allyl methacrylate (ALMA, Figure 1.14.A). The limitation of this approach is that a fraction of the allyl moieties is consumed during polymerization due to the reactivity of these functional groups with radicals.[218–220] One way to avoid the undesired polymerization of the allyl moieties during the polymerization, is to incorporate them to the polymer particles after the synthesis using coupling agents.[221–223] Afterwards, the allyl containing dispersions can crosslink via oxidative curing like alkyds[218,219] or via UV photopolymerization in the presence of UV sensitive initiators.[221] The post-addition of (meth)acrylate units using the carboxylic acid reactive functionalities and their subsequent photopolymerization has also been reported.[224]

Finally, the crosslinking of alkyne groups has also been carried out via 1,3-dipolar azide-alkyne cycloaddition (Figure 1.14.B1). This click reaction is insensitive to water or oxygen and can be carried out at room temperature. However, it requires the presence of a copper catalyst. For example, Hu *et al* prepared a two component system copolymerizing 4-azidomethyl styrene (AMS, Figure 1.14.B2) and propargyl acrylate (PrA, Figure 1.14.B3) via emulsion polymerization in two different set of particles. The materials cast from the blends presented better mechanical performance and water resistance.[225,226]

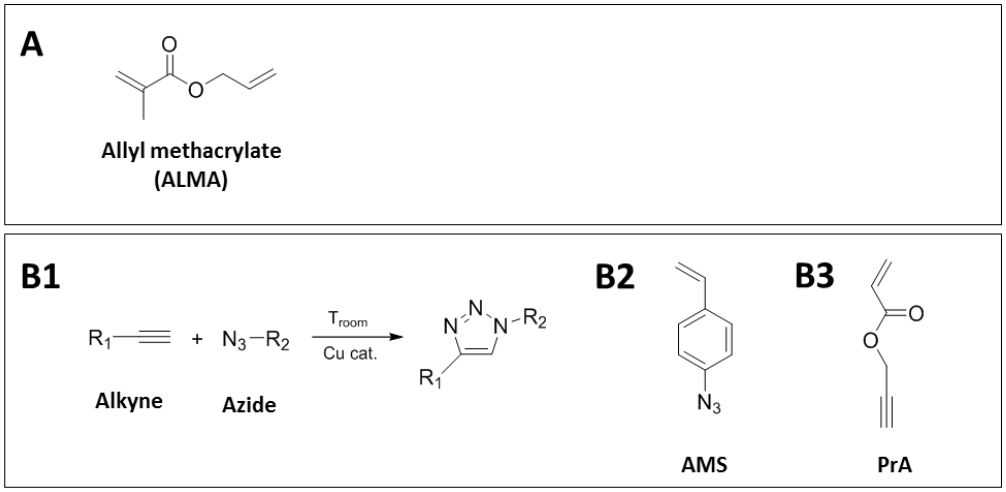

Figure 1.14. Functional groups with unsaturated groups. (A) Chemical structure of allyl methacrylate, (B1) 1,3-dipolar azide-alkyne cycloaddition click reaction, (B2) chemical structure of 4-azidomethyl styrene (AMS) and (B3) chemical structure of propargyl acrylate (PrA).

1.4.3.2.6. Self-condensation

The use of dispersions that undergo self-crosslinking is very interesting from the industrial point of view since they only imply the synthesis of one latex. One way to obtain such systems, is the functionalization of the polymer particles with self-reactive moieties.[156] Two of the most widely employed self-reactive groups are alkoxysilanes[227,228] and N-methylol acrylamide type monomers.[229–232] The crosslinking mechanisms are shown in Figures 1.15.A and 1.15.B, respectively.

On the one hand, the crosslinking between alkoxysilanes occurs at room temperature in two steps: the hydrolysis of the alkoxysilanes to form silanol groups and their posterior condensation to form siloxane units.[233,234] Presumably, the condensation step will only occur in the last stage of film formation when most of the water has evaporated allowing chain diffusion to occur before crosslinking and promoting the formation of cohesive films. In particular, this crosslinking technology is efficient decreasing the water absorption of the materials due to the hydrophobicity of the siloxane linkages.[235,236]

On the other hand, N-methylol acrylamide units (NMA, Figure 1.15.B1) are able to self-condensate in a mechanism very similar to the melamine-formaldehyde type crosslinking reaction explained section 1.4.3.2.1 (Figure 1.15.B2). However, the release of formaldehyde brings back the concerns about the use and release of toxic reagents. As alternative, N-isobutoxy methacrylamide (IBMA, Figure 1.15.C1) has been employed for the synthesis of self-crosslinkable dispersions.[237,238] IBMA self-condensates releasing isobutanol instead of formaldehyde (Figure 1.15.C2).

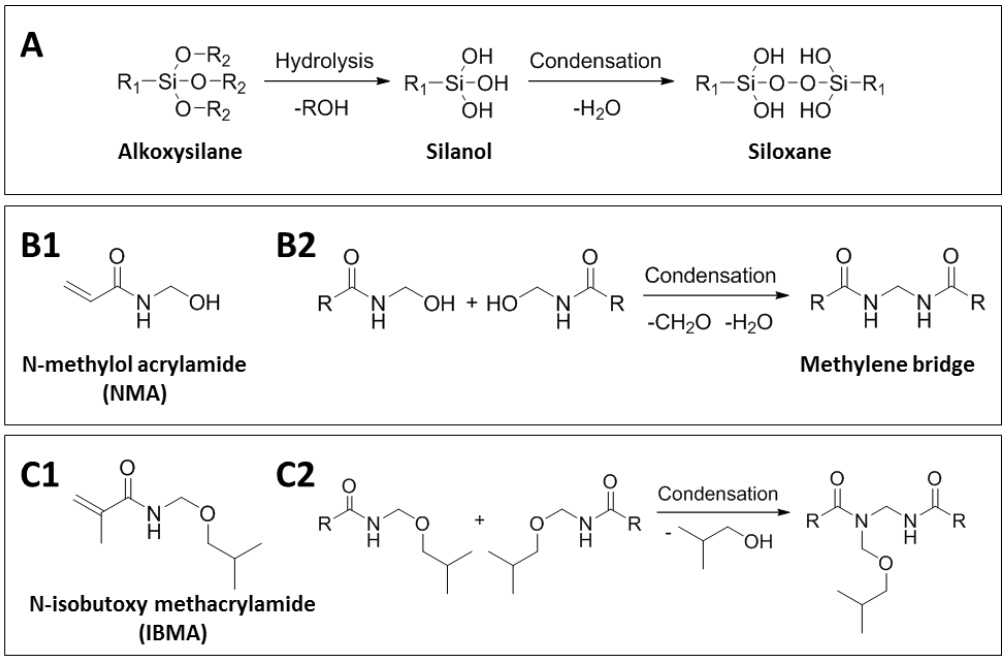

Figure 1.15. Condensation reactions between (A) alkoxysilanes, (B) N-methylol acrylamide groups and (C) N-isobutoxy methacrylamide groups.

The main drawback of such self-condensing chemistries is the short pot-life caused by the premature condensation of the functional groups in the wet state.[236,238,239] As explained at the beginning of section 1.4.3.1, premature crosslinking hinders the polymer diffusion across the polymer particle boundaries and leads to films with little cohesion.

1.4.3.2.7. Challenges and limitations of the chemical crosslinking technologies

From the comparison of all technologies that employ chemical crosslinking it is hard to find a crosslinking system that cures readily at room temperature, avoids the use or release of toxic chemicals and presents considerable product life-time. Usually, ambient temperature curing is achieved by employing highly reactive functional groups at the expense of pot-stability. In

addition, the current crosslinking reagents are increasingly being restricted because of concerns about their toxicity. In this context, physical interactions offer a potential alternative since they avoid the use of toxic chemicals while still generating a network structure. The crosslinking technologies that employ physical interactions will be discussed in Section 1.4.3.3.

1.4.3.3. Physical crosslinking

Physical bonds such as ionic interactions, host-guest interactions, coordination interactions or hydrogen bonds can be used as alternative for the covalent chemistries to crosslinking the polymer chains. In general, physical bonds present lower bonding energies than chemical bonds (≈350 kJ mol^{-1} for a covalent C-C linkage vs 5-250 kJ mol^{-1} energies for physical bonds depending on the nature of the interaction[240]). In addition, unlike covalent bonds, physical interactions are dynamic and reversible. Such chemistries have been widely applied for the synthesis of supramolecular polymers and inter-polymer complexes[241–247] with stimuli-responsive and self-healing properties.[248–252]

The use of physical interactions to crosslink the polymer chains presents some advantages compared to the chemical crosslinking technologies. On the one hand, the functional groups involved in physical interactions typically present lower toxicities and reactivities than the functional groups employed for chemical crosslinking. This reduces the environmental concerns related to the employment of toxic chemicals and ensures the pot-stability of the products. On the other hand, physical bonds readily form at room temperature, which eliminates the annealing step for crosslinking. In addition, their dynamic nature can result very convenient for film formation since the physically crosslinked polymer chains will preserve some mobility compared to the chemically crosslinked chains. As consequence, the dynamic systems will be able to evolve during and after film formation and this will contribute to the formation of a homogeneously

crosslinked polymer network. Nevertheless, as mentioned, physical interactions are weaker than covalent bonds and this could limit their contribution to the mechanical reinforcement of the materials. The drawback is that the low strength of physical linkages could lead to poorly reinforced materials even in the optimal regime shown in part III of Figure 1.8 where diffusion occurs prior to crosslinking. In this context, ionic interactions or hydrogen bonds seem to be the most promising physical interactions for the preparation of ambient curing and non-toxic waterborne dispersions because of their high relative strength.

1.4.3.3.1. Ionic interactions

Ionic interactions are physical bonds resulting from the electrostatic attraction between oppositely charged groups. These interactions are the strongest physical interactions with bonding energies ranging from 50 to 250 kJ mol^{-1}.[240,253] The use of ionic interactions for the crosslinking of waterborne dispersions was first reported in 1967 by S. C. Johnson & Son.[254,255] They described the crosslinking of anionic carboxylate groups with different metal cations such as Zn^{2+}, Cu^{2+}, Cd^{2+}, Ni^{2+} or Zr^{2+}. The carboxylic acid latex – metal ion blends were stable in the wet state and underwent crosslinking during film formation leading to harder materials with improved solvent resistance. In addition, these coatings presented controlled removability by ion complexing agents in alkaline medium. In recent years, the crosslinking of carboxylic acid groups by Zn^{2+} ions has been employed by different authors for the preparation of mechanically reinforced and water resistant materials.[256–258]

The film formation process of carboxylic acid containing polymer particles in the presence of different metal salts was analyzed in 1995 by Kim and co-workers by FRET.[96] They observed that the strong ionic interactions between the metal cations and the carboxylic groups hindered the diffusion of the polymer chains resulting in the interfacial crosslinking of the polymer particles.

In a different approach described recently by Wahdat and co-workers, complete interdiffusion followed by ionic crosslinking was achieved employing aluminium acetylacetonate ($Al(acac)_3$) as crosslinker.[259] The aluminium crosslinker reacted in a nucleophilic substitution with the carboxylic acid groups releasing acetylacetone (Figure 1.16). The equilibrium nature of this crosslinking reaction allows crosslinking to happen only in the last stages of film formation when the equilibrium is shifted to the right through the evaporation of acetylacetone. However, it implies the release acetylacetone, bringing back the environmental concern about the release of VOCs.

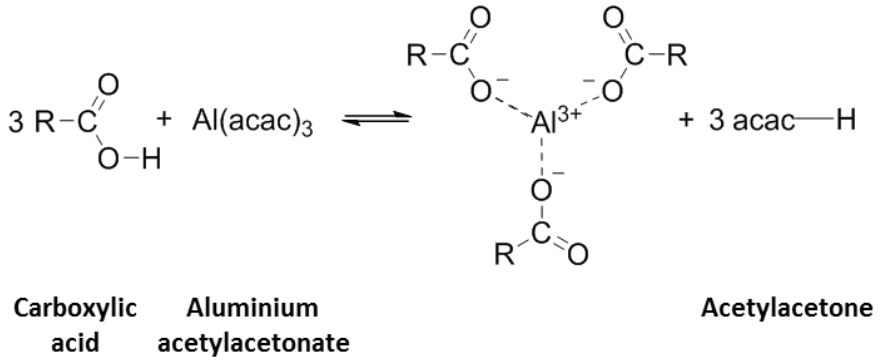

Figure 1.16. Reaction between carboxylic acids and aluminium acetylacetonate to produce Al-carboxylic acid complexes and acetylacetone.[259]

1.4.3.3.2. Hydrogen bonding

Hydrogen bonding is the electrostatic attraction between a partially positively charged hydrogen atom attached to a highly electronegative atom (H-bond donor) and a nearby lone-pair carrier electronegative atom (H-bond acceptor).[244,260] The general structure of a H-bond is shown in Figure 1.17. In the scheme, “D-H” refers to the H-bond donor also known as electron acceptor and “A” represents the H-bond acceptor also called electron donor.

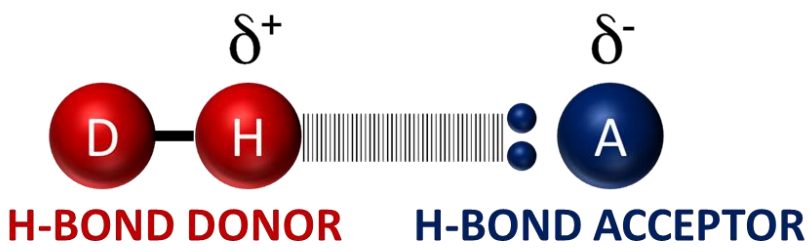

Figure 1.17. General structure of a H-bond.

Among physical interactions, hydrogen bonds are relatively strong and directional with bonding energies ranging from 1.7 to 167 kJ mol^{-1}.[260] H-bonds are reversible and their nature is described by the association/dissociation equilibrium shown in Figure 1.18. The parameter that expresses the complexation state of the functional groups in equilibrium is the equilibrium association constant (K_a) which is defined as the ratio between the concentration of the dimer and the product of the concentrations of the free H-bonding motifs in equilibrium. The association constant is proportional to the binding strength, and thus, it is a widely employed way to define and compare the strength of the physical linkages.[261]

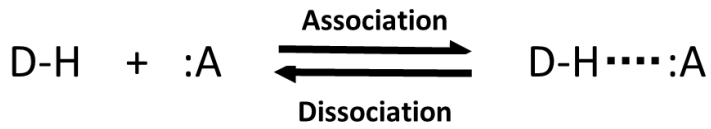

Figure 1.18. H-bonding complex formation equilibrium.

There are several factors affecting the K_a and strength of the H-bonds. In the first place, the strength of the H-bond depends on the acidity and basicity of the H-bond donor and acceptor groups respectively: The higher the acidity of the H-bond donor and the basicity of the H-bond acceptor, the stronger the resulting H-bond.[262,263] The strongest H-bond acceptors are oxygen

and nitrogen due to their high electronegativity and polarizability and the best H-bond donors are “O-H” and “N-H” groups. The functional groups attached to the H-bond donor/acceptors can also contribute to the acidity/basicity of the H-bond donor/acceptors and increase final strength of the H-bond. For example, in hydroxyl groups attached to a benzene ring, the greater polarization of the “O-H” bond will lead to H-bonds one order of magnitude stronger than in H-bonds involving aliphatic hydroxyls, where the “O-H” bond is less polarized (the hydrogen bonds between pyridine and ethanol or phenol and the corresponding association constants are shown in Figures 1.19.A and 1.19.B)[264,265].

In addition to the acidity and basicity of the functional groups, the number of bonds strongly influences the strength of the linkage. In general, the higher the number of H-bonds the stronger is the resulting complex.[266] Single H-bonds present the lowest association constants and then, the K_a increases in a nonlinear way with the number of H-bonds in the array. Some examples of H-bonds with different number of linkages are shown in Figure 1.19: The single H-bonds between pyridine and alcohols have K_a values equal or below 40 M^{-1},[264,265] the complementary double H-bond between adenine and thymine nucleotides has a K_a of the order 10^2 M^{-1},[266] the triple H-bond between guanine and cytosine has a K_a of 10^4-10^5 M^{-1} [266] and the ureido pyrimidinone (UPy) functional group with four complementary H-bonds presents a self-association constant higher than 10^6 M^{-1}.[266]

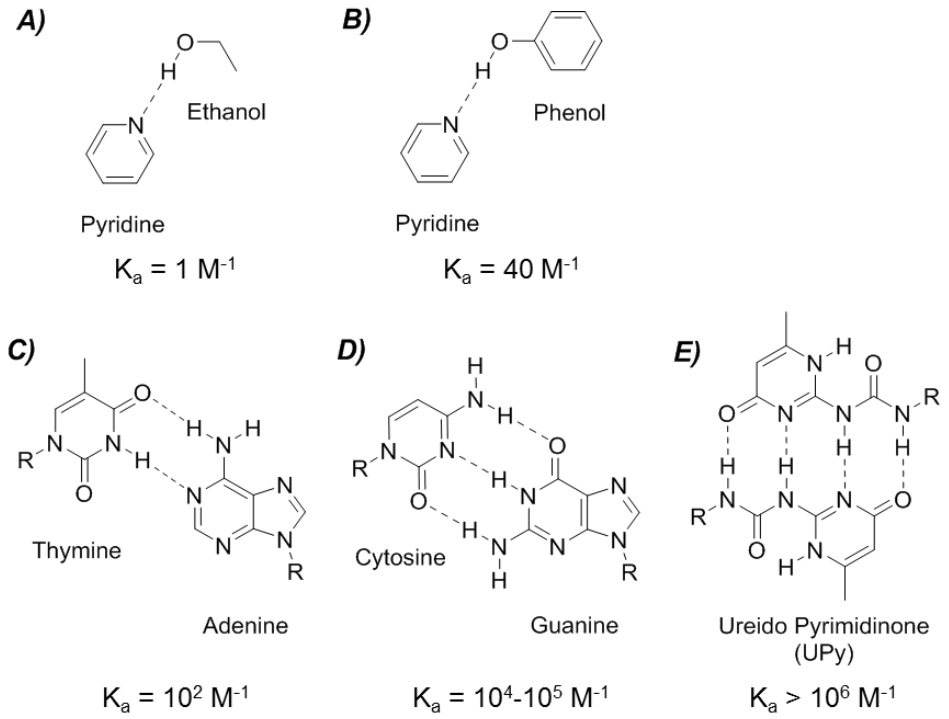

Figure 1.19. Association constants of H-bonds with different number of linkages: (A) pyridine-ethanol[264], (B) pyridine-phenol,[265] (C) thymine-adenine,[266] (D) cytosine-guanine[266] and (E) UPy-UPy[266] complexes.

In addition to the number of linkages, the strength of the arrays also depends on the sequence of the donor and acceptor groups due to the secondary interactions (S) formed between the functionalities in diagonal positions. Donor-acceptor interactions in diagonal positions are attractive and lead to stronger complexes. Sartorius and co-workers calculated the association energies (ΔG) and association constants (K_a) for a series of H-bond arrays taking into account the contribution of secondary interactions.[267] The results obtained for the quadruple H-bonds are shown in Figure 1.20.

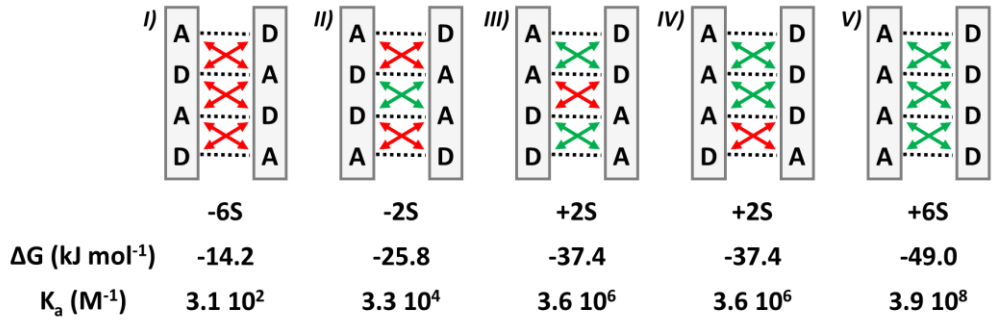

Figure 1.20. Association energies (ΔG) and association constants (K_a) of quadruple H-bonding arrays depending on the secondary interactions. H-bonds are represented with dotted lines, attractive secondary interactions are depicted in green and repulsive secondary interactions in red. Reproduced and modified with permission from John Wiley and Sons.[267]

Figure 1.20 shows how the association energy and association constant of the complexes increase with the number of secondary attractive interactions. Maximum binding strength is achieved when the all acceptor and donor groups are separated in the two parts of the array (e.g. AAAA + DDDD).[268–271] In the case of self-complementary arrays, where the only possibilities are $(ADAD)_2$ and $(AADD)_2$ (Figures 1.20 I and III), maximum strength is achieved with the $(AADD)_2$ geometry due to the higher number of attractive secondary interactions. This is the case of the UPy functionality, which presents a particularly high association constant due to the high number of attractive secondary interactions in the array.[272]

Hydrogen bonds are extensively utilized by nature to create unique supramolecular structures like those of proteins or DNA. In fact, the combination of toughness, strength and extensibility presented by many natural materials such as silk or muscle is directly related to multiple hydrogen bonds in their structure.[273] Similarly, synthetic polymers with H-bonding motifs such Kevlar® and nylon also present outstanding mechanical properties as result of the

hydrogen bonds between polymer chains. Besides polyamides, there is a wide portfolio of monomers and polymers that contain hydrogen bonding donors and acceptors in their structure such as hydroxyl groups, amines, amides, carboxylic acids or arrays formed thereof. Such polymers/monomers are able to interact via hydrogen bonding and have been employed in the development of two new types of materials: supramolecular polymers[274–279] and interpolymer complexes.[280–282] The formation of supramolecular polymers and interpolymer complexes is schematically illustrated in Figures 1.21.A and 1.21.B, respectively.

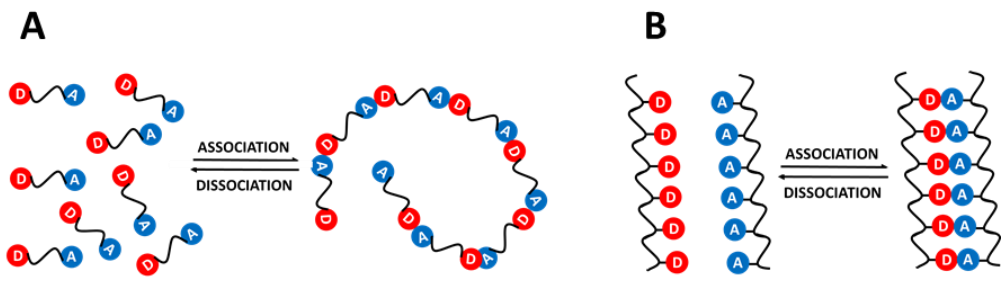

Figure 1.21. (A) Polymerization equilibrium in supramolecular polymers and (B) reversible formation of an interpolymer complex from complementary H-bonding polymers.

On the one hand, supramolecular polymers are a kind of polymer where the monomer units are held together by non-covalent interactions.[276] Compared to conventional covalent polymers, the linkages between monomer units are reversible and the polymerization degree depends on the equilibrium shown in Figure 1.21.A. The main parameters affecting the polymerization degree of supramolecular polymers at room temperature are the monomer concentration and the association constant (K_a) of the H-bond. In general, the polymerization degree increases with the monomer concentration and the K_a of the complex. Typically, single hydrogen bonds with low K_a values are not able to form reasonable chain length polymers and, thus, H-bond arrays with high K_a values are employed for the synthesis of supramolecular

polymers.[275,278,283] In addition, similar to step growth polymerization mechanism, high polymerization degrees are only achieved when stoichiometric amounts of the complementary functional groups are employed. This last issue can be circumvented by using self-complementary moieties. In this context, the ureido pyridimidinone (UPy) self-complementary functionality is a great candidate to be employed for the synthesis of supramolecular polymers because of its high binding constant.[272,274,277,284,285] For example, Folmer *et al* prepared supramolecular polymers from telechelic oligomers functionalized with UPy terminal groups. As a result of the dimerization of the UPy groups, the liquid oligomers transformed into elastic solid films. At elevated temperatures, the H-bonds broke, and the high virtual molecular weight supramolecular polymer returned to the oligomer state. The materials presented a strong temperature dependency of the melt viscosity providing to the supramolecular polymers excellent processability compared to their covalent analogues.[286]

Unlike supramolecular polymers, interpolymer complexes are the products formed from the non-covalent interactions between two polymers.[287] When the non-covalent interactions are H-bonds, two different types of polymer chains with H-bond donor and acceptor groups respectively interact and form a complex which has very different characteristics compared to the initial un-complexed polymers.

The first interpolymer complexes were reported by Bailey and Smith who described the complexation of poly(acrylic acid) (PAA) with poly(alkylene oxide)-s (PEO-s).[288,289] Both polymers were soluble in aqueous medium, but when they were mixed together, immediate precipitation occurred as result of the H-bonds between the “O-H” groups of the carboxylic acid in PAA and the oxide groups of PEO. The complexation depended on different parameters such as the salt concentration in water, molecular weight of the polymers, PAA/PEO ratio, pH or temperature. Besides PEO, the complexation of PAA with different H-bond acceptor polymers

has been widely studied.[290–295] For example, Swift *et al* analyzed the complexation of PAA with different non-ionic H-bond acceptor polymers employing Fluorescence Anisotropy. The formation of the complex strongly depended on the pH and the ionization degree of the PAA. In addition, for each polymer couple, there was a critical maximum pH for the formation of the complex. This critical pH depended on the association constant of the H-bonds and the solvation energies of the individual polymers.[296]

Hydrogen bonds have been employed to crosslink the polymers and form supramolecular networks.[279,285,297,298] The materials crosslinked with hydrogen bonds normally present tunable high strength, large extensibility, improved thermostability and healable capability.[273,299,300] In addition, in many systems physical and chemical crosslinking are combined to achieve a great balance of properties.[301–304]

For example, H-bonds have been used for the synthesis of supramolecular hydrogels.[300,305,306] Physical hydrogels are physical polymer networks able to absorb great amounts of water and their softness, inherent reversibility, dynamism, adaptability and stimuli-responsiveness make them particularly interesting for medical applications such as cell culture, tissue engineering, on-demand controlled release of therapeutics or molecular sensing.[247,307]

In addition, hydrogen bonds have been utilized for the synthesis of supramolecular adhesives.[308–310] For example, Feldstein and co-workers prepared pressure sensitive adhesives (PSAs) based on stoichiometric complexes of high molecular weight H-bond accepting polymers such as polyvinyl pyrrolidone (PVP) and hydroxyl terminated polyethylene glycol oligomers (OH-PEG) as H-bond donor crosslinkers. The PVP-PEG blends at 8-9% degree of hydration presented higher elastic modulus and tensile strength and lower break elongation with the PEG

content Maximum toughness was achieved when 36 wt% of PEG was employed. In addition, the adhesives presented thermo-switchable adhesive properties.[311–313]

In the field of waterborne coatings, hydrogen bonds have been employed to reinforce the mechanical properties of the films cast from aqueous dispersions. For example, Richard and Maquet demonstrated that the presence of carboxylic acids in a polystyrene/butadiene latex led to the formation of reinforced particle-particle interface because of H-bond interactions.[314] In addition, it has been shown that hydrophilic polyacrylic acid blocks on the shell of the polymer particles can form a percolating network of acrylic acid units that increases the Young's modulus of the materials because of physical crosslinking.[315–318] However, the main drawback of such systems relies in their high water sensitivity. When the films are put into contact with water, the water molecules disrupt the relatively weak H-bonds between carboxylic acids and the films lose the mechanical coherence gained due to the acrylic acid percolating network.[319,320] One way to address this issue is to increase the strength of the H-bonds by employing H-bonding arrays instead of single or double H-bonds. For example, Chen *et al* incorporated an ureido pyrimidinone (Upy) self-associating functional monomer to an aqueous acrylic formulation. The dried film exhibited polyhedral-type structure where the particle-particle interface was reinforced by the quadruple hydrogen bonding interactions. These films presented improved mechanical performance and solvent resistance. Nevertheless, >100% weight based on monomers of chloroform was utilized in the synthesis to solubilize the Upy monomer.[321] In a different example, Karikari *et al.* employed a functional Upy monomer to produce physically crosslinked metal-free aqueous floor coatings with improved durability.[322]

1.4.3.4. Classification of the crosslinking systems depending on the position of the functional groups

Another practical way to classify the crosslinking systems is depending on the position of the functional groups in the dispersion. The possible different geometries are summarized in Figure 1.22. The first approach is the two component two pot system shown in Figure 1.22.A where functional polymer particles are crosslinked by water-soluble/dispersible crosslinkers. Some examples of this approach are melamine/formaldehyde,[78,205] hydroxyl/isocyanate,[164–166] carboxylic acid/aziridine,[180,181] carboxylic acid/carbodiimides,[185,186] carboxilate/cation,[254–258] acetoacetoxy/amine[195–200] or epoxy/amine[142,192,323] crosslinking technologies. In this approach, the high reactivity of the functional groups typically causes the premature crosslinking of the polymer chains in the wet state and therefore, the components must be stored separately and mixed just before the application. Industrially, the pot-life of the products can be extended by “blocking” the functional groups of the crosslinker. The blocked species are unreactive adducts formed from the reaction between the reactive moiety of the crosslinker with another functionality. The blocked crosslinkers stay latent in the wet state but they become active during the film formation when the adduct is broken at high temperatures.[142,163,166,167,170] In these systems, the pot-life is extended at the expense of higher curing temperatures and an increase in the VOC content in the formulation, since the small molecules released from the adduct will eventually evaporate.

Another way to prevent the premature crosslinking of the functional groups and expand the shelf-life of the dispersions is to locate the crosslinking functionality in a second set of polymer particles. This scenario is illustrated in Figure 1.22.B. In this case, the reaction between the functional groups is avoided by steric or anionic repulsions between the polymer particles and crosslinking only takes place when the functional groups are brought into intimate contact during

film formation. Since the two components can co-exist in the same dispersion, these systems are referred as two component one pot products. Some examples are epoxy/amine,[193] carboxylic acid/carbodiimide[188,189] or acetoacetoxy/amine[144,324,325] functional polymer particle blends. Compared to the two component two pot systems, the absence of the mixing step provides several advantages to the one-pot products such as higher crosslinking reproducibility and easier manipulation for the user.

The last system is the one component one pot product shown in Figures 1.22.C and 1.22.D where one self-curing dispersion is employed. The first option to achieve self-curing dispersions is to incorporate the two functional groups needed for the crosslinking reaction in the same dispersion (see Figure 1.22.C). However, the lack of examples in the literature for these systems suggests that the double functionalization of the polymer particles leads to the premature crosslinking of the polymer particles limiting their practical use. The second option shown in Figure 1.22.D comprises the use of polymer dispersions with self-interacting functional groups. Some examples of this approach are alkoxysilane,[156,228] N-methylol methacrylamide[231,232] or Upy[321,322,326] containing functional particles. The main advantage of this approach is the production of one sole functional dispersion. The two component two pot stable systems composed of functional polymer particles and water-soluble crosslinkers may also be included in this group since it only implies the synthesis of one latex.

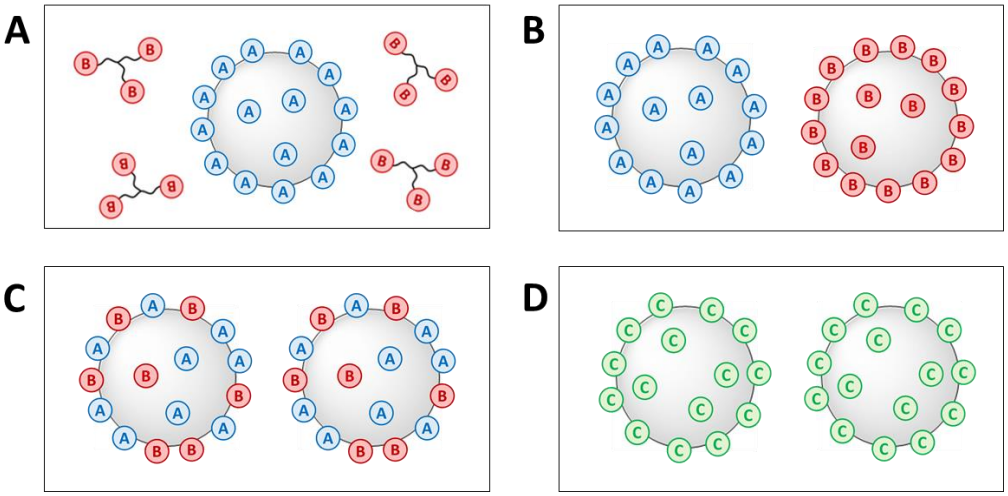

Figure 1.22. Different dispositions of the functional groups in the crosslinking dispersions: (A) Functional polymer particles with water-soluble crosslinkers, (B) blends of complementary functional particles, (C) doubly functionalized polymer particles and (D) functional polymer particles with self-interacting functional groups. The blue "A" moieties and red "B" moieties represent complementary functional groups that are able to interact between them and the "C" green moieties represent self-interacting functional groups.

In addition, the position of the functional groups within the polymer particles also varies according to the hydrophilicity of the functionalities employed in each system. In Figure 1.22, the functional groups are represented preferably on the surface of the polymer particles due to the hydrophilic nature of most reactive groups, but their position should be considered in each case.

The position of the crosslinkers (Figure 1.22 A) in the system also depends on their hydrophilicity. For example, polyamines are hydrophilic and water-soluble whilst polyisocyanates or carbodiimides are hydrophobic and need to be pre-emulsified in order to be incorporated to the system. In some systems, the hydrophilicity of the crosslinkers is tuned by attaching different pendant groups to their structure. For example, hydrophilic pendant groups such as polyethers, polyesters or carboxylic groups containing alkyl chains are attached to hydrophobic crosslinkers

to make them surface-active and water-dispersible. After the chemical modification, the surface-active crosslinkers can be added self-dispersed in water without the incorporation of additional surfactants.[142,165,168,185,186]

1.5. Motivation and outline

High performance waterborne dispersions are required for the complete replacement of solventborne products by their waterborne counterparts. Industrially, coalescing agents are used to temporarily plasticize high T_g polymer chains and enable film formation of hard polymer dispersions that lead to stiff polymer films. However, the need for a volatile plasticizer brings back the environmental concerns related to the release of VOCs to the atmosphere. Another widely employed way to improve the mechanical performance of the films cast from aqueous dispersions is the crosslinking of the polymer chains after film formation. The aim of this PhD thesis is to explore the use of hydrogen bonding for the physical crosslinking of waterborne polymer dispersions and the mechanical reinforcement of the materials cast from those dispersions. The use of H-bonds as crosslinks is presented as an alternative to the conventional covalent crosslinking chemistries that often employ toxic chemicals and require annealing. The knowledge gained in this work aims to contribute to the progress towards the production of mechanically strong polymer films cast from non-toxic, stable and ambient curable waterborne dispersions for the complete replacement of solvent-based products.

Chapter 2 is dedicated to the investigation of systems composed of blends of functional particles with H-bond and acceptor groups and doubly functionalized polymer particles. Two types of H-bonds were utilized: The single H-bond between a pyrrolidone and an aliphatic hydroxyl group and the double H-bond between uracil and adenine groups. The influence of such

hydrogen bonds on the mechanical performance of the polymer films cast from the dispersions is analyzed.

Chapters 3-5 are devoted to the analysis of systems composed of functional polymer particles and water-soluble species. In **Chapter 3**, polyvinyl alcohol (PVOH) stabilized polymer particles were combined with water-soluble H-bond acceptor species such as polyvinyl pyrrolidone, tannic acid or gallic acid. In **Chapters 4** and **5**, functional polymer dispersions with pyrrolidone moieties were blended with aqueous solutions of tannic acid. **Chapter 4** is dedicated to materials for coating applications and **Chapter 5** to pressure sensitive adhesives. The influence of the H-bonds on the microstructure, mechanical performance and water sensitivity of the materials is discussed in each chapter.

In **Chapter 6**, the free radical polymerization of various monomer families in presence of catechols and catechol-containing monomers is studied. The knowledge gained in this fundamental study was utilized in **Chapter 7** for the synthesis of catechol-based water-soluble polymers. The catechol-polymers were subsequently combined with pyrrolidone functionalized polymer dispersions and the effect of the pyrrolidone-catechol H-bonds on the performance of the materials was analyzed.

1.6. References

(1) Tracton, A. A. *Coatings Technology Handbook*; Taylor & Francis: Boca Raton, Florida, 2006.

(2) Businesswire. *Water Borne Coatings Global Market Report 2020*; Dublin, 2020.

(3) de With, G.; Esteves, A. C. C.; van der Ven, L. G. J.; van Benthem, R. A. T. M.; Laven, J.; Tuinier, R. *Polymer Coatings: A Guide to Chemistry, Characterization and Selected Application*; Wiley-VCH: Weinheim, Germany, 2018.

(4) Sherman, J.; Chin, B.; Huibers, P. D. T.; Hatton, T. A. Solvent Replacement for Green Processing *Environ. Health Perspect.* **1998**, *106(suppl)*, 253–271.

(5) Asua, J. M. *Polymer Reaction Engineering*; Blackwell Publishing, 2007.

(6) Gardon, J. L. Emulsion Polymerization. II. Review of Experimental Data in the Context of the Revised Smith-Ewart Theory *J. Polym. Sci. Part A.1* **1968**, *6*, 643–664.

(7) Myers, D. *Surfaces, interfaces, and colloids*; John Wiley & Sons, 1999.

(8) Reynhout, X. E. E.; Beckers, M.; Meuldijk, J. A. N.; Drinkenburg, B. A. H. Electrosteric Stability of Styrene / Acrylic Acid Copolymer Latices under Emulsion Polymerization Reaction Conditions *J. Polym. Sci. Part A Polym. Chem.* **2005**, *43*, 726–732.

(9) Aguirreurreta, Z.; Dimmer, J.-A.; Willerich, I.; de la Cal, J. C.; Leiza, J. R. Water Whitening Reduction in Waterborne Pressure-Sensitive Adhesives Produced with Polymerizable Surfactants *Macromol. Mater. Eng.* **2015**, *9*, 925–936.

(10) Aguirreurreta, Z.; de la Cal, J. C.; Leiza, J. R. Preparation of high solids content waterborne acrylic coatings using polymerizable surfactants to improve water sensitivity *Prog. Org. Coatings* **2017**, *112*, 200–209.

(11) Barton, J. M. Relation of glass transition temperature to molecular structure of addition copolymers *J. Polym. Sci. Part C Polym. Symp.* **1970**, *30*, 573–597.

(12) Keddie, J. L.; Meredith, P.; Jones, R. A. L.; Donald, A. M. Film Formation of Acrylic Latices with Varying Concentrations of Non-Film-Forming Latex Particles *Langmuir* **1996**, *12*, 3793–3801.

(13) Schneider, H. A.; Rieger, J.; Penzel, E. The glass transition temperature of random copolymers: 2. Extension of the Gordon-Taylor equation for asymmetric Tg vs composition curves *Polymer* **1997**, *38*, 1323–1337.

(14) Colombini, D.; Hassander, H.; Karlsson, O. J.; Maurer, F. H. J. Influence of the particle size and particle size ratio on the morphology and viscoelastic properties of bimodal hard/soft latex blends *Macromolecules* **2004**, *37*, 6865–6873.

(15) Asua, J. M. *Polymeric Dispersions: Principles and applications*; 1997; Vol. 335.

(16) Meyer, T.; Keurentjes, J. *Handbook of Polymer Reaction Engineering*; Wiley-VCH Verlag GmbH & Co.KGaA: Weinheim, Germany, 2005.

(17) Harkins, W. D. A General Theory of the Mechanism of Emulsion Polymerization *J. Am. Chem. Soc.* **1946**, *69*, 1428–1444.

(18) Smith, W. V.; Ewart, R. H. Kinetics of Emulsion Polymerization Kinetics of Emulsion Polymerization *J. Chem. Phys.* **1948**, *16*, 592–597.

(19) Nomura, M. Emulsion Polymerization: Kinetic and Mechanistic Aspects *Adv. Polym. Sci.* **2005**, *175*, 1–128.

(20) Fitch, R. M.; Tsai, C. J. Polymer colloids: particle formation in nonmicellar systems *J. Polym. Sci. Part B Polym. Lett.* **1970**, *8*, 703–710.

(21) Fitch, R. M.; Tsai, C. H. Particle formation in polymer colloids, III: Prediction of the number of partiles by a homogeneous nucleation theory *Polym. colloids* **1971**, 73–102.

(22) Hansen, F. K.; Ugelstad, J. Particle Nucleation in Emulsion Polymerization. I. A Theory for Homogeneous Nucleation *J. Polym. Sci. Polym. Chem. Ed.* **1978**, *16*, 1953–1979.

(23) Sayer, C.; Palma, M.; Giudici, R. Modeling Continuous Vinyl Acetate Emulsion Polymerization Reactions in a Pulsed Sieve Plate Column *Ind. Eng. Chem. Res.* **2002**, *41*, 1733–1744.

(24) Morton, M.; Kaizerman, S.; Altier, M. W. Swelling of latex particles *J. Colloid Sci.* **1954**, *9*, 300–312.

(25) Dunn, A. S. Kinetics of Emulsifier Adsorption and Nucleation of Latex Particles *Polym. Int.* **1993**, *30*, 547–550.

(26) Ballard, N.; Urrutia, J.; Eizagirre, S.; Schäfer, T.; Diaconu, G.; de la Cal, J. C.; Asua, J. M. Surfactant Kinetics and Their Importance in Nucleation Events in (Mini)emulsion Polymerization Revealed by Quartz Crystal Microbalance with Dissipation Monitoring *Langmuir* **2014**, *30*, 9053–9062.

(27) Lichti, G.; Gilbert, R. G.; Napper, D. H. The Mechanisms of Latex Particle Formation and Growth in the Emulsion Polymerization of Styrene Using the Surfactant Sodium Dodecyl Sulfate *J. Polym. Sci. Polym. Chem. Ed.* **1983**, *21*, 269–291.

(28) Herrera-Ordonez, J.; Olayo, R.; Carro, S. The Kinetics of Emulsion Polymerization: Some Controversial Aspects *J. Macromol. Sci. Part C* **2004**, *44*, 207–229.

(29) Thickett, S. C.; Gilbert, R. G. Emulsion polymerization: State of the art in kinetics and mechanisms *Polymer* **2007**, *48*, 6965–6991.

(30) Arzamendi, G.; Asua, J. M. Monomer Addition Policies for Copolymer Composition Control in Semicontinuous Emulsion Copolymerization *J. Appl. Polym. Sci.* **1989**, *38*, 2019–2036.

(31) Urretabizkaia, A.; Leiza, J. R.; Asua, J. M. On-line terpolymer composition control in semicontinuous emulsion polymerization *AIChE J.* **1994**, *40*, 1850–1864.

(32) Othman, N.; Févotte, G.; McKenna, T. F. Nonlinear state estimation and control of a semibatch terpolymerisation reactor *IFAC Proc. Vol.* **2000**, *33*, 515–520.

(33) Juhué, D.; Lang, J. Film Formation from Dispersion of Core-Shell Latex Particles *Macromolecules* **1995**, *28*, 1306–1308.

(34) Domingues Dos Santos, F.; Fabre, P.; Drujon, X.; Meunier, G.; Leibler, L. Films from Soft-Core/Hard-Shell Hydrophobic Latexes: Structure and Thermomechanical Properties *J. Polym. Sci. Part B Polym. Phys.* **2000**, *38*, 2989–3000.

(35) Limousin, E.; Ballard, N.; Asua, J. M. Soft core–hard shell latex particles for mechanically strong VOC-free polymer films *J. Appl. Polym. Sci.* **2019**, *136*, 47608.

(36) Asua, J. M. Miniemulsion polymerization *Prog. Polym. Sci.* **2002**, *27*, 1283–1346.

(37) Schork, F. J.; Luo, Y.; Smulders, W.; Russum, J. P.; Butté, A.; Fontenot, K. Miniemulsion Polymerization *Adv. Polym. Sci.* **2005**, *175*, 129–255.

(38) Ugelstad, J.; El-Aasser, M. S.; Vanderhoff, J. W. Emulsion polymerization: Initiation of polymerization in monomer droplets *J. Polym. Sci. Polym. Lett.* **1973**, *11*, 503–513.

(39) Hansen, F. K.; Ugelstad, J. Particle nucleation in emulsion polymerization. IV. Nucleation in monomer droplets *J. Polym. Sci. Polym. Chem. Ed.* **1979**, *17*, 3069–3082.

(40) Rodriguez, R.; Barandiaran, M. J.; Asua, J. M. Particle Nucleation in High Solids Miniemulsion Polymerization *Macromolecules* **2007**, *40*, 5735–5742.

(41) Manea, M.; Chemtob, A.; Paulis, M.; de la Cal, J. C.; Barandiaran, M. J.; Asua, J. M. Miniemulsification in High-Pressure Homogenizers *Am. Inst. Chem. Eng.* **2007**, *54*, 289–297.

(42) Lopez, A.; Chemtob, A.; Milton, J. L.; Manea, M.; Paulis, M.; Barandiaran, M. J.;

Theisinger, S.; Landfester, K.; Hergeth, W. D.; Udagama, R.; Mckenna, T.; Asua, J. M. Miniemulsification of Monomer-Resin Hybrid Systems *Ind. Eng. Chem. Res.* **2008**, *47*, 6289–6297.

(43) Bohorquez, S. J.; Asua, J. M. Particle Nucleation in High Solids Batch Miniemulsion Polymerization Stabilized with a Polymeric Surfactant *J. Polym. Sci. Part A Polym. Chem.* **2008**, *46*, 6407–6414.

(44) Asua, J. M. Challenges for industrialization of miniemulsion polymerization *Prog. Polym. Sci.* **2014**, *39*, 1797–1826.

(45) Mehravar, E.; Leiza, J. R.; Asua, J. M. Synthesis and characterization of comb-like acrylic-based polymer latexes containing nano-sized crystallizable domains *Polymer* **2016**, *84*, 167–177.

(46) Siljanovska, G.; Auschra, C.; Paulis, M. Confinement driven crystallization of ABA crystalline-soft-crystalline block copolymers synthesized via RAFT mediated miniemulsion polymerization *Polymer* **2018**, *158*, 327–337.

(47) Zhang, M.; Gao, G.; Li, C. Q.; Liu, F. Q. Titania-Coated Polystyrene Hybrid Microballs Prepared with Miniemulsion Polymerization *Langmuir* **2004**, *20*, 1420–1424.

(48) Landfester, K. Miniemulsion Polymerization and the Structure of Polymer and Hybrid Nanoparticles *Angew. Chemie Int. Ed.* **2009**, *48*, 4488–4507.

(49) Crespy, D.; Landfester, K. Miniemulsion polymerization as a versatile tool for the synthesis of functionalized polymers *Beilstein J. Org. Chem.* **2010**, *6*, 1132–1148.

(50) Aguirre, M.; Paulis, M.; Leiza, J. R. UV screening clear coats based on encapsulated CeO2 hybrid latexes *J. Mater. Chem. A* **2013**, *1*, 3155–3162.

(51) Gonzalez, E.; Stuhr, R.; Vega, J. M.; García-Lecina, E.; Grande, H.-J.; Leiza, J. R.; Paulis, M. Assessing the Effect of CeO2 Nanoparticles as Corrosion Inhibitor in Hybrid Biobased Waterborne Acrylic Direct to Metal Coating Binders *Polymers (Basel).* **2021**, *13*, 1–13.

(52) Higuchi, W. I.; Misra, J. Physical Degradation of Emulsions Via the Molecular Diffusion Route and the Possible Prevention Thereof *J. Pharm. Sci.* **1962**, *51*, 459–466.

(53) Asua, J. M. Ostwald ripening of reactive costabilizers in miniemulsion polymerization *Eur. Polym. J.* **2018**, *106*, 30–41.

(54) Wang, S.; Schork, F. J. Miniemulsion Polymerization of Vinyl Acetate with Nonionic Surfactant *J. Appl. Polym. Sci.* **1994**, *58*, 2157–2164.

(55) Bohórquez, S. J.; Asua, J. M. Poly(vinyl alcohol) Grafting in Miniemulsion Polymerization *Macromolecules* **2008**, *41*, 8597–8602.

(56) Chern, C. S.; Chen, T. J. Effect of Ostwald ripening on styrene miniemulsion stabilized by reactive cosurfactants *Colloids and Surfaces* **1998**, *138*, 65–74.

(57) Chern, C.-S.; Liou, Y.-C. Kinetics of styrene miniemulsion polymerization stabilized by nonionic surfactant / alkyl methacrylate *Polymer* **1999**, *40*, 3763–3772.

(58) Rodríguez, R.; de las Heras Alarcón, C.; Ekanayake, P.; Mcdonald, P. J.; Keddie, J. L.; Barandiaran, M. J.; Asua, J. M. Correlation of Silicone Incorporation into Hybrid Acrylic Coatings with the Resulting Hydrophobic and Thermal Properties *Macromolecules* **2008**, *41*, 8537–8546.

(59) Meliana, Y.; Lin, C. T.; Suprianti, L.; Huang, Y. J.; Chern, C. S. Characterization of Costabilizers in Retarding Ostwald Ripening of Monomer Miniemulsions *J. Dispers. Sci. Technol.* **2012**, *33*, 1346–1353.

(60) Steward, P. A.; Hearn, J.; Wilkinson, M. C. An overview of polymer latex film formation and properties *Adv. Colloid Interface Sci.* **2000**, *86*, 195–267.

(61) Keddie, J. L.; Routh, A. F. *Fundamentals of Latex Film Formation: Processes and Properties*; Springer: Bristol, UK, 2010.

(62) Zhang, H.; Wool, R. P. Concentration Profile for a Polymer-Polymer Interface. 1. Identical Chemical Composition and Molecular Weight *Macromolecules* **1989**, *22*, 3018–3021.

(63) Kim, K. D.; Sperling, L. H. Reptation Time, Temperature, and Cosurfactant Effects on the Molecular Interdiffusion Rate during Polystyrene Latex Film Formation *Macromolecules* **1994**, *27*, 6841–6850.

(64) Yi, W.; Zhonghua, C.; Fei, Y. Coalescing Aid Influences on Acrylic Latexes Property and Film Formation Process *Indian J. Mater. Sci.* **2016**, *2016*, 1–8.

(65) Jensen, D. P.; Morgan, W. Particle Size as it Relates to the Minimum Film Formation Temperature of Latices *J. Appl. Polym. Sci.* **1991**, *42*, 2845–2849.

(66) Mallégol, J.; Bennett, G.; Mcdonald, P. J.; Keddie, J. K.; Dupont, O. Skin Development during the Film Formation of Waterborne Acrylic Pressure- Sensitive Adhesives Containing Tackifying Resin *J. Adhes.* **2006**, *82*, 217–238.

(67) Meincken, M.; Sanderson, R. D. Determination of the influence of the polymer structure and particle size on the film formation process of polymers by atomic force microscopy *Polymer* **2002**, *43*, 4947–4955.

(68) Fasano, D. M.; Fitzwater, S. J.; Lau, W.; Sheppard, A. C. Diffusion of oligomers in latex systems — A route to low volatile organic compound (VOC) coatings *Can. J. Chem.* **2010**, *88*, 500–513.

(69) Yang, Z.; Craig, D. Q. M. Monitoring film coalescence from aqueous polymeric dispersions using atomic force microscopy: surface topographic and nano-adhesion studies *Asian J. Pharm. Sci.* **2018**, *15*, 104–111.

(70) Rharbi, Y.; Boué, F.; Joanicot, M.; Cabane, B. Deformation of cellular polymeric films *Macromolecules* **1996**, *29*, 4346–4359.

(71) Ma, Y.; Davis, H. T.; Scriven, L. E. Microstructure development in drying latex coatings *Prog. Org. Coatings* **2005**, *52*, 46–62.

(72) Gonzalez, E.; Tollan, C.; Chuvilin, A.; Barandiaran, M. J.; Paulis, M. Determination of the Coalescence Temperature of Latexes by Environmental Scanning Electron Microscopy *Appl. Mater. Interfaces* **2012**, *4*, 4276−4282.

(73) Donald, A. M.; He, C.; Royall, C. P.; Sferrazza, M.; Stelmashenko, N. A.; Thiel, B. L. Applications of environmental scanning electron microscopy to colloidal aggregation and film formation *Colloids and Surfaces* **2000**, *174*, 37–53.

(74) Hahn, K.; Ley, G.; Schuller, H.; Oberthür, R. On particle coalescence in latex films *Colloid Polym. Sci.* **1986**, *264*, 1092–1096.

(75) Yoo, J. N.; Sperling, L. H.; Glinka, C. J.; Klein, A. Characterization of Film Formation from Polystyrene Latex Particles via SANS. 1. Moderate Molecular Weight *Macromolecules* **1990**, *23*, 3962–3967.

(76) Linné, M. A.; Klein, A.; Miller, G. A.; Wignall, G. D. Film formation from latex: Hindered initial interdiffusion of constrained polystyrene chains characterized by small-angle neutron scattering *J. Macromol. Sci. Part B Phys.* **1988**, *27*, 217–231.

(77) Boczar, E. M.; Dionne, B. C.; Fu, Z.; Kirk, A. B.; Lesko, P. M.; Koller, A. D. Spectroscopic Studies of Polymer Interdiffusion during Film Formation *Macromolecules* **1993**, *26*, 5772–5781.

(78) Winnik, M. A.; Pinenq, P.; Krüger, C.; Zhang, J.; Yaneff, P. V. Crosslinking vs. interdiffusion rates in melamine-formaldehyde cured latex coatings: A model for waterborne automotive basecoat *J. Coatings Technol.* **1999**, *71*, 47–60.

(79) Soleimani, M.; Khan, S.; Mendenhall, D.; Lau, W.; Winnik, M. A. Effect of molecular weight distribution on polymer diffusion during film formation of two-component high-/low-molecular weight latex particles *Polymer* **2012**, *53*, 2652–2663.

(80) Pinenq, P.; Toronto, W. Polymer Diffusion and Mechanical Properties of Films Prepared from Crosslinked Latex Particles *J. Coatings Technol.* **2000**, *72*, 45–61.

(81) Odrobina, E.; Winnik, M. A. Influence of Entanglements on the Time Dependence of Mixing in Nonradiative Energy Transfer Studies of Polymer Diffusion in Latex Films *Macromolecules* **2001**, *34*, 6029–6038.

(82) Winnik, M. A. Interdiffusion and Crosslinking in Thermoset Latex Films *J. Coatings Technol.* **2002**, *74*, 49–63.

(83) Tronc, F.; Chen, W.; Winnik, M. A.; Eckersley, S. T.; Rose, G. D.; Weishuhn, J. M.; Meunier, D. M. Epoxy-Functionalized, Low-Glass-Transition-Temperature Latex. II. Interdiffusion versus Crosslinking in the Presence of a Diamine *J. Polym. Sci. Part A Polym. Chem.* **2002**, *40*, 4098–4116.

(84) Oh, J. K.; Yang, J.; Tomba, J. P.; Rademacher, J.; Farwaha, R.; Winnik, M. A. Molar Mass Effect on the Rate of Polymer Diffusion in Poly(vinyl acetate-co-butyl acrylate) Latex Films *Macromolecules* **2003**, *36*, 8836–8845.

(85) Oh, J. K.; Tomba, P.; Ye, X.; Eley, R.; Rademacher, J.; Farwaha, R.; Winnik, M. A. Film Formation and Polymer Diffusion in Poly(vinyl acetate-co-butyl acrylate) Latex Films. Temperature Dependence *Macromolecules* **2003**, *36*, 5804–5814.

(86) Tomba, J. P.; Ye, X.; Li, F.; Winnik, M. A.; Lau, W. Polymer blend latex films: Miscibility and polymer diffusion studied by energy transfer *Polymer* **2008**, *49*, 2055–2064.

(87) Tomba, J. P.; Portinha, D.; Schroeder, W. F.; Winnik, M. A.; Lau, W. Polymer diffusion in high-M/low-M hard-soft latex blends *Colloid Polym. Sci.* **2009**, *287*, 367–378.

(88) Juhué, D.; Wangb, Y.; Winnik, M. A.; Haley, F. Influence of a coalescing aid on polymer diffusion in poly(butyl methacrylate) latex films *Macromol. Rapid Commun.* **1993**, *14*, 345–349.

(89) Juhué, D.; Lang, J. Latex Film Formation in the Presence of Organic Solvents *Macromolecules* **1994**, *27*, 695–701.

(90) Berce, P.; Skale, S.; Razborsek, T.; Slemnik, M. Influence of coalescing aids on the latex properties and film formation of waterborne coatings *J. Appl. Polym. Sci.* **2017**, *134*, 45142.

(91) Wang, Y.; Winnik, M. A. Effect of a Coalescing Aid on Polymer Diffusion in Latex Films *Macromolecules* **1990**, *23*, 4731–4732.

(92) Toussaint, A.; de Wilde, M.; Molenaar, F.; Mulvihill, J. Calculation of Tg and MFFT depression due to added coalescing agents *Prog. Org. Coatings* **1997**, *30*, 179–184.

(93) Voogt, B.; Huinink, H. P.; Erich, S. J. F.; Scheerder, J.; Venema, P.; Keddie, J. L.; Adan, O. C. G. Film Formation of High Tg Latex Using Hydroplasticization: Explanations from NMR Relaxometry *Langmuir* **2019**, *35*, 12418–12427.

(94) Jiang, B.; Tsavalas, J.; Sundberg, D. Measuring the Glass Transition of Latex-Based Polymers in the Hydroplasticized State via Differential Scanning Calorimetry *Langmuir* **2010**, *26*, 9408–9415.

(95) Lee, D. I.; Walker, L. C.; Kan, C. S. The thermal behaviors of latexes: Wet latex glass transition temperatures *Macromol. Symp.* **1997**, *118*, 267–273.

(96) Kim, H.-B.; Winnik, M. A. Factors Affecting Interdiffusion Rates in Films Prepared from Latex Particles with a Surface Rich in Acid Groups and Their Salts *Macromolecules* **1995**, *28*, 2033–2041.

(97) Buckmann, A. J. P.; Martin, E.; Overbeek, G. C.; Van Hilst, J. L. M.; Scheerder, J.; Steenwinkel, P.; Tennebrock, R. Polymeric Aqueous Coating Compositions. US 7217758 B2, 2007.

(98) Piçarra, S.; Fidalgo, A.; Fedorov, A.; Martinho, J. M. G.; Farinha, J. P. S. Smart Polymer Nanoparticles for High-Performance Water-Borne Coatings *Langmuir* **2014**, *30*, 12345−12353.

(99) Barbosa, J. V.; Moniz, J.; Mendes, A.; Magalhaes, F. D.; Bastos, M. M. S. M. Incorporation of an acrylic fatty acid derivative as comonomer for oxidative cure in acrylic latex *J. Coatings Technol. Res.* **2014**, *11*, 765–773.

(100) Lahtinen, M.; Glad, E.; Koskimies, S.; Sundholm, F.; Rissanen, K. Synthesis of Novel Reactive Coalescing Agents and Their Application in a Latex Coating *J. Appl. Polym. Sci.* **2003**, *87*, 610–615.

(101) Ueberreiter, K.; Kanig, G. Self-plasticization of polymers *J. Colloid Sci.* **1952**, *6*, 569–583.

(102) Farinha, J. P. S.; Martinho, J. M. G.; Kawaguchi, S.; Yekta, A.; Winnik, M. A. Latex Film Formation Probed by Nonradiative Energy Transfer: Effect of Grafted and Free Poly(ethylene oxide) on a Poly(n-butyl methacrylate) Latex *J. Phys. Chem.* **1996**, *100*, 12552–12558.

(103) Yu, Y.; Cheng, Y.; Ren, J.; Cao, E.; Fu, X.; Guo, W. Plasticizing effect of poly (ethylene glycol)s with different molecular weights in poly(lactic acid)/starch blends *J. Appl. Polym. Sci.* **2015**, *132*, 41808.

(104) Blanchard, L.-P.; Hesse, J.; Malhotra, S. L. Effect of Molecular Weight on Glass Transition by Differential Scanning Calorimetry *Can. J. Chem.* **1974**, *52*, 3170–3175.

(105) Wypych, G. In *Handbook of Plasticizers*; ChemTec Publishing, 2002.

(106) Lim, H.; Hoag, S. W. Plasticizer Effects on Physical – Mechanical Properties of Solvent Cast Soluplus ® Films *AAPS PharmSciTech* **2013**, *14*, 903–910.

(107) Feng, J.; Winnik, M. A.; Shivers, R. R.; Clubb, B. Polymer Blend Latex Films: Morphology and Transparency *Macromolecules* **1995**, *28*, 7671–7682.

(108) Hagen, R.; Salmen, L.; Karlsson, O.; Wesslen, B. Viscoelastic Properties and Film Morphology of Heterogeneous Styrene-Butadiene Latexes *J. Appl. Polym. Sci.* **1996**, *62*, 1067–1078.

(109) Eckersley, S. T.; Helmer, B. J. Mechanistic Considerations of Particle Size Effects on Film Properties of Hard/Soft Latex Blends *J. Coatings Technol.* **1997**, *69*, 97–107.

(110) Feng, J.; Odrobina, E.; Winnik, M. A. Effect of Hard Polymer Filler Particles on Polymer Diffusion in a Low-Tg Latex Film *Macromolecules* **1998**, *31*, 5290–5299.

(111) Tzitzinou, A.; Keddie, J. L. Film Formation of Latex Blends with Bimodal Particle Size Distributions: Consideration of Particle Deformability and Continuity of the Dispersed Phase *Macromolecules* **2000**, *33*, 2695–2708.

(112) Ugur, S.; Elaissari, A.; Holl, Y. Film Formation From Polystyrene – Poly (butyl acrylate-co-methyl methacrylate) Latex Blends *Polym. Compos.* **2006**, *27*, 431–442.

(113) Singh, K. B.; Deoghare, G.; Tirumkudulu, M. S. Cracking in Soft-Hard Latex Blends: Theory and Experiments *Langmuir* **2009**, *25*, 751–760.

(114) Ugur, Z.; Sunay, S.; Önder, P. Film Formation of Nano-Sized Hard Latex (PS) in Soft Polymer Matrix (PBA): An Excimer Study *Polym. Compos.* **2010**, *31*, 1611–1619.

(115) Sundberg, D. C.; Casassa, A. P.; Pantazopoulos, J.; Muscato, M. R. Morphology Development of Polymeric Microparticles in Aqueous Dispersions. I. Thermodynamic Considerations *J. Appl. Polym. Sci.* **1990**, *41*, 1425–1442.

(116) Hasanzadeh, I.; Mahdavian, A. R.; Salehi-mobarakeh, H. Particle size and shell composition as effective parameters on MFFT for acrylic core – shell particles prepared via seeded emulsion polymerization *Prog. Org. Coatings* **2014**, *77*, 1874–1882.

(117) Devon, M. J.; Gardon, J. L.; Roberts, G.; Rudin, A. Effects of Core-Shell Latex Morphology on Film Forming Behavior *J. Appl. Polym. Sci.* **1990**, *39*, 2119–2128.

(118) Domingues Dos Santos, F.; Leibler, L. Large deformation of films from soft-core/hard-shell hydrophobic lattices *J. Polym. Sci. Part B Polym. Phys.* **2003**, *41*, 224–234.

(119) Price, K.; Wu, W.; Wood, K.; Kong, S.; McCormick, A.; Francis, L. Stress development and film formation in multiphase composite latexes *J. Coatings Technol. Res.* **2014**, *11*, 827–839.

(120) Limousin, E.; Ballard, N.; Asua, J. M. The influence of particle morphology on the structure and mechanical properties of films cast from hybrid latexes *Prog. Org. Coatings* **2019**, *129*, 69–76.

(121) Aguirre, M.; Paulis, M.; Leiza, J. R. Particle nucleation and growth in seeded semibatch miniemulsion polymerization of hybrid CeO2/acrylic latexes *Polymer* **2014**, *55*, 752–761.

(122) Bourgeat-Lami, E.; Lang, J. Encapsulation of Inorganic Particles by Dispersion Polymerization in Polar Media. 1. Silica Nanoparticles Encapsulated by Polystyrene *J. Colloid Interface Sci.* **1998**, *197*, 293–308.

(123) Chabert, E.; Bornert, M.; Bourgeat-lami, E.; Cavaillé, J.-Y.; Dendievel, R.; Gauthier, C.; Putaux, J.-L.; Zaoui, A.; Chabert, E.; Bornert, M.; Bourgeat-lami, E.; Cavaillé, J.; Dendievel, R. Filler-filler interactions and viscoelastic behavior of polymer nanocomposites *Mater. Sci. Eng. A* **2004**, *381*, 320–330.

(124) Hagan, E. W. S.; Charalambides, M. N.; Young, C. R. T.; Learner, T. J. S.; Hackney, S. Influence of the inorganic phase concentration and geometry on the viscoelastic properties of latex coatings through the glass-transition *Polymer* **2011**, *52*, 1662–1673.

(125) Alvarez, V.; Paulis, M. Effect of acrylic binder type and calcium carbonate filler amount on the properties of paint-like blends *Prog. Org. Coatings* **2017**, *112*, 210–218.

(126) Makepeace, D. K.; Locatelli, P.; Lindsay, C.; Adams, J. M.; Keddie, J. L. Colloidal polymer composites: Are nano-fillers always better for improving mechanical properties? *J. Colloid Interface Sci.* **2018**, *523*, 45–55.

(127) Ugur, S.; Sunay, M. S.; Pekcan, Ö. Study of Film Formation From PS Latex/TiO2 Nanocomposites; Effect of Latex Size and TiO2 content *Polym. Compos.* **2014**, *35*, 2376–2389.

(128) Robertson, C. G.; Lin, C. J.; Rackaitis, M.; Roland, C. M. Influence of Particle Size and Polymer - Filler Coupling on Viscoelastic Glass Transition of Particle-Reinforced Polymers *Macromolecules* **2008**, *41*, 2727–2731.

(129) Wang, T.; Dalton, A. B.; Keddie, J. L. Importance of Molecular Friction in a Soft Polymer - Nanotube Nanocomposite *Macromol. Symp.* **2008**, *41*, 7656–7661.

(130) Vatansever, A.; Dogan, H.; Inan, T.; Sezer, S.; Sirkecioglu, A. Properties of Na-Montmorillonite and Cellulose Nanocrystal Reinforced Poly(butyl acrylate-co-methyl methacrylate) Nanocomposites *Polym. Eng. Sci.* **2015**, *55*, 2922–2928.

(131) Schmid, A.; Tonnar, J.; Armes, S. P. A New Highly Efficient Route to Polymer-Silica Colloidal Nanocomposite Particles *Adv. Mater.* **2008**, *20*, 3331–3336.

(132) Gonzalez-Matheus, K.; Leal, G. P.; Asua, J. M. Film formation from Pickering stabilized waterborne polymer dispersions *Polymer* **2015**, *69*, 73–82.

(133) Bon, S. A. F.; Colver, P. J. Pickering Miniemulsion Polymerization Using Laponite Clay as a Stabilizer *Langmuir* **2007**, *23*, 8316–8322.

(134) Ruggerone, R.; Plummer, C. J. G.; Herrera, N. N.; Bourgeat-lami, E.; Månson, J.-A. E. Fracture mechanisms in polystyrene/laponite nanocomposites prepared by emulsion polymerization *Eng. Fract. Mech.* **2009**, *76*, 2846–2855.

(135) González, E.; Bonnefond, A.; Barrado, M.; Barrasa, A. M. C.; Asua, J. M.; Leiza, J. R. Photoactive Self-cleaning Polymer Coatings by TiO2 nanoparticle Pickering Miniemulsion Polymerization *Chem. Eng. J.* **2015**, *281*, 209–217.

(136) Zhang, Y.; Karimkhani, V.; Makowski, B. T.; Samaranayake, G.; Rowan, S. J. Nanoemulsions and Nanolatexes Stabilized by Hydrophobically Functionalized Cellulose Nanocrystals *Macromolecules* **2017**, *50*, 6032–6042.

(137) Limousin, E.; Ballard, N.; Asua, J. M. Synthesis of cellulose nanocrystal armored latex particles for mechanically strong nanocomposite films *Polym. Chem.* **2019**, *10*, 1823–1831.

(138) Zhang, Y.; Yang, H.; Naren, N.; Rowan, S. J. Surfactant-Free Latex Nanocomposites Stabilized and Reinforced by Hydrophobically Functionalized Cellulose Nanocrystals *Appl. Polym. Mater.* **2020**, *2*, 2291–2302.

(139) Touaiti, F.; Pahlevan, M.; Nilsson, R.; Alam, P.; Toivakka, M.; Ansell, M. P.; Wilen, C. E. Impact of functionalised dispersing agents on the mechanical and viscoelastic properties of pigment coating *Prog. Org. Coatings* **2013**, *76*, 101–106.

(140) Geurts, J.; Bouman, J.; Overbeek, A. New waterborne acrylic binders for zero VOC paints *J. Coatings Technol. Res.* **2008**, *5*, 57–63.

(141) Ooka, M.; Ozawa, H. Recent developments in crosslinking technology for coating resins *Prog. Org. Coatings* **1994**, *23*, 325–338.

(142) Galgoci, E. C.; Komar, P. C.; Elmore, J. D. High Performance Waterborne Coatings and an Amine-Functional Curing Agent *J. Coatings Technol.* **1999**, *71*, 45–52.

(143) Aradian, A.; Raphae, E.; de Gennes, P.-G. Strengthening of a Polymer Interface: Interdiffusion and Cross-Linking *Macromolecules* **2000**, *33*, 9444–9451.

(144) González, I.; Asua, J. M.; Leiza, J. R. Crosslinking in Acetoacetoxy Functional Waterborne Crosslinkable Latexes *Macromol. Symp.* **2006**, *243*, 53–62.

(145) Córdoba, C. A.; Collins, S. E.; Passeggi, M. C. G.; Vaillard, S. E.; Gugliotta, L. M.; Minari, R. J. Crosslinkable acrylic-melamine latex produced by miniemulsion polymerization *Prog. Org. Coatings* **2018**, *118*, 82–90.

(146) Zosel, A.; Ley, G. Influence of crosslinking on Structure, Mechanical Properties, and Strength of Latex Films *Macromolecules* **1993**, *26*, 2222–2227.

(147) Zosel, A. Mechanical Properties of Films from Polymer Latices *Polym. Adv. Technol.* **1995**, *6*, 263–269.

(148) Ghazaly, H. M.; Daniels, E. S.; Dimonie, V. L.; Klein, A.; Sperling, L. H.; El-Aasser, M. S. Properties of n-Butyl Methacrylate Copolymer Latex Films Derived from Crosslinked Latex Particles *J. Polym. Sci.* **2003**, *88*, 42–49.

(149) Tamai, T.; Pinenq, P.; Winnik, M. A. Effect of Cross-Linking on Polymer Diffusion in Poly(butyl methacrylate-co-butyl acrylate) Latex Films *Macromolecules* **1999**, *32*, 6102–6110.

(150) Joshi, R. G.; Provder, T.; Ziemer, P.; Mao, W.; Shen, W.; Jones, F. N. Investigation of the effect of precoalescence or postcoalescence crosslinking on film formation, properties, and latex morphology *J. Coat. Technol. Res.* **2009**, *6*, 47–65.

(151) Mazuel, F.; Bui, C.; Charleux, B.; Cabet-deliry, E.; Winnik, M. A. Interdiffusion and Self-Cross-Linking in Acetal-Functionalized Latex Films *Macromolecules* **2004**, *37*, 6141–6152.

(152) Wang, R.; Ma, J.; Zhou, X.; Wang, Z.; Kang, H.; Zhang, L.; Hua, K.; Kulig, J. Design and Preparation of a Novel Cross-Linkable, High Molecular Weight, and Bio-Based Elastomer by Emulsion Polymerization *Macromolecules* **2012**, *45*, 6830–6839.

(153) Wang, T.; De Las Heras Alarcón, C.; Goikoetxea, M.; Beristain, I.; Paulis, M.; Barandiaran, M. J.; Asua, J. M.; Keddie, J. L. Cross-linked network development in compatibilized Alkyd/acrylic hybrid latex films for the creation of hard coatings *Langmuir* **2010**, *26*, 14323–14333.

(154) Tillet, G.; Boutevin, B.; Ameduri, B. Chemical reactions of polymer crosslinking and post-crosslinking at room and medium temperature *Prog. Polym. Sci.* **2011**, *36*, 191–217.

(155) Taylor, J. W.; Winnik, M. A. Functional latex and thermoset latex films *JCT Res.* **2004**, *1*, 163–190.

(156) Parvate, S.; Mahanwar, P. Advances in self-crosslinking of acrylic emulsion: what we

know and what we would like to know *J. Dispers. Sci. Technol.* **2018**, *40*, 1–18.

(157) Huang, Y.; Jones, F. N. Synthesis of crosslinkable acrylic latexes by emulsion polymerization the presence of etherified melamine-formaldehyde (MF) resins *Prog. Org. Coatings* **1996**, *28*, 133–141.

(158) Liu, X.; Fan, X.; Tang, M.; Nie, Y. Synthesis and Characterization of Core-Shell Acrylate Based Latex and Study of Its Reactive Blends *Int. J. Mol. Sci.* **2008**, *9*, 342–354.

(159) Córdoba, C. A.; Ronco, L. I.; Barrios, C. E.; Gugliotta, L. M.; Minari, R. J. High Solid Acrylic–Melamine Latexes with Tunable Crosslinking Capability *Macromol. React. Eng.* **2018**, *1800063*, 1–9.

(160) Córdoba, C. A.; Ronco, L. I.; Passeggi, M. C. G.; Minari, R. J.; Gugliotta, L. M. Waterborne acrylic-melamine latexes with controlled film microstructure *Prog. Org. Coatings* **2019**, *136*, 105239.

(161) Merline, D. J.; Vukusic, S.; Abdala, A. A. Melamine formaldehyde: curing studies and reaction mechanism *Polym. J.* **2012**, *45*, 413–419.

(162) Fischer, M. H. M. D. The toxic effects of formaldehyde and formalin *J. Exp. Med.* **1905**, *VI*, 487–518.

(163) Lu, S.-P.; Xiao, H.; Frisch, K. C.; Witte, F. M.; Van de Ploeg, A. F. M. J. Acrylic based powder paint. WO 94/10221 A1, 1994.

(164) Nabuurs, T.; Pears, D.; Overbeek, A. Defect free coatings from two-pack isocyanate curable acrylic dispersions *Prog. Org. Coatings* **1999**, *35*, 129–140.

(165) Flori, D. E. Low VOC, isocyanate based aqueous curable compositions. US 6316543 B1, 2001.

(166) Taylor, J. W.; Renner, S. L. Isocyanate crosslinked waterborne coatings. US 2002/0151651 A1, 2002.

(167) Zhou, X.; Tu, W.; Hu, J. Preparation and Characterization of Two-component Waterborne Poly- urethane Comprised of Water-soluble Acrylic Resin and HDI Biuret *Chinese J. Chem. Eng.* **2006**, *14*, 99–104.

(168) Nabuurs, T.; Soer, W.-J.; Peters, R. Isocyanate crosslinking in two component waterborne coatings *Polym. Int.* **2018**, *68*.

(169) Noomen, A. The chemistry and physics of low-emission coatings part 2. waterborne two-pack coatings *Prog. Org. Coatings* **1989**, *17*, 27–39.

(170) Rolph, M. S.; Markowska, A. L. J.; Warriner, C. N.; O'Reilly, R. K. Blocked Isocyanates: from Analytical and Experimental Considerations to Non-Polyurethane Applications *Polym. Chem.* **2016**, *7*, 7351–7364.

(171) Peters, J. M. M. D.; Raymond, L. H.; Murphy, M. D. Pulmonary Toxicity of Isocyanates *Ann. Intern. Med.* **1970**, *73*, 654–655.

(172) Rokicki, G.; Parzuchowski, P. G.; Mazurek, M. Non-isocyanate polyurethanes: synthesis, properties, and applications *Polym.* **2015**, *26*, 707–761.

(173) Bizet, B.; Grau, É.; Cramail, H.; Asua, J. M. Water-based Non-Isocyanate Polyurethanes-Polyureas (NIPUUs) *Polym. Chem.* **2020**, *11*, 3786–3799.

(174) Gomez-lopez, A.; Elizalde, F.; Calvo, I.; Sardon, H. Trends in non-isocyanate polyurethane (NIPU) development *Chem. Commun.* **2021**, *57*, 12254–12265.

(175) Kathalewar, M. S.; Joshi, P. B.; Sabnis, A. S.; Malshe, V. C. Non-isocyanate polyurethanes: from chemistry to applications *RSC Adv.* **2013**, *3*, 4110.

(176) Cornille, A.; Blain, M.; Auvergne, R.; Andrioletti, B.; Boutevin, B.; Caillol, S. A study of cyclic carbonate aminolysis at room temperature: effect of cyclic carbonate structures and solvents on polyhydroxyurethane synthesis *Polym. Chem.* **2016**, *8*, 592–604.

(177) Blain, M.; Jean-Gérard, L.; Auvergne, R.; Benazet, D.; Caillol, S.; Andrioletti, B. Rational investigations in the ring opening of cyclic carbonates by amines *Green Chem.* **2014**, *16*, 4286–4291.

(178) Lombardo, V.; Scheidt, K.; Leitsch, E.; Torquelson, J.; Dhulst, E.; Heath, W. H.; Wilmot, N. Catalyst for non-isocyanate based polyurethane. US 2015/0247004 A1, 2015.

(179) Levina, M. A.; Krasheninnikov, V. G.; Zabalov, M. V.; Tiger, R. P. Nonisocyanate Polyurethanes from Amines and Cyclic Carbonates: Kinetics and Mechanism of a Model Reaction *Polym. Sci. Ser. B* **2014**, *56*, 139–147.

(180) Roesler, R. R.; Danielmeier, K. Tris-3-(1-aziridino) propionates and their use in formulated products *Prog. Org. Coatings* **2004**, *50*, 1–27.

(181) Mistry, J. K.; Van De Mark, M. R. Aziridine cure of acrylic colloidal unimolecular polymers (CUPs) *J. Coatings Technol. Res.* **2013**, *10*, 453–463.

(182) Czech, Z. New generation of crosslinking agents based on multifunctional methylaziridines *Int. J. Adhes. Adhes.* **2007**, *27*, 49–58.

(183) Cofield, B. G.; Storrs, F. J.; Strawn, C. B. Contact Allergy to Aziridine Paint Hardener *Arch. Dermatol.* **1985**, *121*, 373–376.

(184) Watson, S. L. Low temperature crosslinking of water-borne resins. US 4997219, 1990.

(185) Taylor, J. W. Surface active polycarbodiimides and their dispersions. US 5108653, 1992.

(186) Brown, W. T. Effect of Crosslinker Reaction Rate on Film Properties for Thermoset Coatings *J. Chem. Eng. Process Technol.* **2000**, *72*, 63–70.

(187) Taylor, J. W. Surface active polycarbodiimides and their dispersions. US5108653A, 1992.

(188) Pham, H. H.; Winnik, M. A. Synthesis, Characterization, and Stability of Carbodiimide Groups in Carbodiimide-Functionalized Latex Dispersions and Films *J. Polym. Sci. Part A Polym. Chem.* **2000**, *38*, 855–869.

(189) Pham, H. H.; Winnik, M. A. Polymer Interdiffusion vs Cross-Linking in Carboxylic Acid-Carbodiimide Latex Films. Effect of Annealing Temperature, Reactive Group Concentration, and Carbodiimide Substituent *Macromolecules* **2006**, *39*, 1425–1435.

(190) Pham, H. H.; Farinha, J. P. S.; Winnik, M. A. Cross-Linking, Miscibility, and Interface Structure in Blends of Poly(2-ethylhexyl methacrylate) Copolymers. An Energy Transfer Study *Macromolecules* **2000**, *33*, 5850–5862.

(191) Papalos, J. G.; Grinstein, R. H.; Shah, S.; Mulvey, J. L.; Jewell, B. G. Self-Dispersing Curable Epoxy Resins and Coatings. WO 95/01387, 1995.

(192) Das, S. K.; Olson, Kurt, G.; Claar, J. A. Water-based coating compositions comprising epoxy-containing acrylic polymers an polyfunctional water-soluble amines. US 4748167, 1988.

(193) Geurts, J. M.; van Es, J. J. G. S.; German, A. L. Latexes with intrinsic crosslink activity *Prog. Org. Coatings* **1996**, *29*, 107–115.

(194) Kessel, N.; Illsley, D. R.; Keddie, J. L. The diacetone acrylamide crosslinking reaction and its influence on the film formation of an acrylic latex *J. Coatings Technol. Res.* **2008**, *5*, 285–297.

(195) Overbeek, G. C.; Heuts, M. P. J. Aqueous coating compositions. US 4998762, 1991.

(196) Geurink, P. J. A.; Van Dalen, L.; Van Der Ven, L. G. J.; Lamping, R. R. Analytical aspects and film properties of two-pack functional latexes acetoacetate *Prog. Org. Coatings* **1996**, *27*, 73–78.

(197) Feng, J.; Pham, H.; Macdonald, P.; Winnik, M. A. Formation and Crosslinking of Latex Films through the Reaction of Acetoacetoxy Groups with Diamines under Ambient Conditions *J. Coatings Technol.* **1998**, *70*, 57–68.

(198) González, I.; Arzamendi, G.; Asua, J. M.; Leiza, J. R. Unexpected crosslinking during acetoacetoxy group protection on waterborne crosslinkable latexes *Macromol. Mater. Eng.* **2006**, *291*, 1185–1193.

(199) Lu, J.; Easteal, A. J.; Edmonds, N. R. Crosslinkable poly(vinyl acetate) emulsions for wood adhesive *Pigment Resin Technol.* **2011**, *40*, 161–168.

(200) Pi, P.; Wang, W.; Wen, X.; Xu, S.; Cheng, J. Synthesis and characterization of low-temperature self-crosslinkable acrylic emulsion for PE film ink *Prog. Org. Coatings* **2015**, *81*, 66–71.

(201) Beshah, K.; Devonport, W. A study of acetoacetoxyethyl methacrylate hydrolysis in acrylic latex polymers as a function of pH *J. Coatings Technol. Res.* **2013**, *10*, 821–828.

(202) Blasko, J. E.; Calhoun, G. C.; Esser, R. J.; Karabetsos, R. E.; Krawczak, D. T.; Giddings, C. S.; Trumbo, D. L. Waterborne Polymers for Use in Thermoset Coatings: A New Hydrolysis Resistant Monomer as a Replacement for Acetoacetoxyethyl Methacrylate *J. Coatings Technol.* **2002**, *74*, 83–87.

(203) Park, Y.-J.; Kim, J. H. The Use of ATR - FTIR to Determine the Effects of Functional Groups on Interfacial Crosslinking of Reactive Nanoparticles *J. Dispers. Sci. Technol.* **2003**, *24*, 537–541.

(204) Koukiotis, C.; Sideridou, I. D. Synthesis and characterization of latexes based on copolymers BA\MMA\DAAM and BA\MMA\VEOVA-10\DAAM and the corresponding 1K crosslinkable binder using the adipic acid dihydrazide as crosslinking agent *Prog. Org. Coatings* **2010**, *69*, 504–509.

(205) Liu, X.; Zhang, C.; Xiong, T.; Chen, D.; Zhong, A. Rheological and Curing Behavior of Aqueous Ambient Self-Crosslinkable Polyacrylate Emulsion *J. Appl. Polym. Sci.* **2007**, *106*, 1448–1455.

(206) Heuts, M. P. J.; Fêbre, R. A.; van Hilst, J. L. M.; Overbeek, G. C. In *Film Formation in Waterborne Coatings*; 1996; pp. 271–285.

(207) Wu, X. Q.; Schork, F. J.; Gooch, J. W. Hybrid Miniemulsion Polymerization of Acrylic/Alkyd Systems and Characterization of the Resulting Polymers *J. Polym. Sci. Part A Polym. Chem.* **1999**, *37*, 4159–4168.

(208) Wang, T.; De las Heras Alarcón, C.; Goikoetxea, M.; Beristain, I.; Paulis, M.; Barandiaran, M. J.; Asua, J. M.; Keddie, J. L. Cross-Linked Network Development in Compatibilized Alkyd/Acrylic Hybrid Latex Films for the Creation of Hard Coatings *Langmuir* **2010**, *26*, 14323–14333.

(209) Udagama, R.; de las Heras Alarcón, C.; Keddie, J. L.; Tsavalas, J. G.; Bourgeat-lami, E.; Mckenna, T. F. L. Acrylic–Alkyd Hybrids: Secondary Nucleation, Particle Morphology,

and Limiting Conversions *Macromol. React. Eng.* **2014**, *8*, 622–638.

(210) Limousin, E.; Martinez-Tong, D. E.; Ballard, N.; Asua, J. M. Cure-Dependent Morphology of Acrylic/Alkyd Hybrid Latex Films via Nanomechanical Mapping *Appl. Polym. Mater.* **2019**, *1*, 2213–2223.

(211) Limousin, E.; González, E.; Martínez-Tong, D. E.; Ballard, N.; Asua, J. M. Modelling the dynamic development of the curing process and film morphology of films cast from waterborne acrylic-alkyd hybrids **2020**, *400*.

(212) Soucek, M. D.; Khattab, T.; Wu, J. Progress in Organic Coatings Review of autoxidation and driers *Prog. Org. Coatings* **2012**, *73*, 435–454.

(213) Liu, Z.; Kooijman, H.; Spek, A. L.; Bouwman, E. New manganese-based catalyst systems for alkyd paint drying *Prog. Org. Coatings* **2007**, *60*, 343–349.

(214) Pirs, B.; Znoj, B.; Skale, S.; Zabret, J.; Godnjavec, J.; Venturini, P. Iron as an alternative drier for curing of high-solid alkyd coatings *J. Coatings Technol. Res.* **2015**, *12*, 965–974.

(215) Erich, S. J. F.; Gezici-Koç, Ö.; Michel, M.-E. B.; Thomas, C. A. A. M.; Van Der Ven, L. G. J.; Huinink, H. P.; Flapper, J.; Duivenvoorde, F. L.; Adan, O. C. G. The influence of calcium and zirconium based secondary driers on drying solvent borne alkyd coatings *Polymer* **2017**, *121*, 262–273.

(216) Dubrulle, L.; Lebeuf, R.; Thomas, L.; Fressancourt-Collinet, M.; Nardello-Rataj, V. Catalytic activity of primary and secondary driers towards the oxidation and hydroperoxide decomposition steps for the chemical drying of alkyd resin *Prog. Org. Coatings* **2017**, *104*, 141–151.

(217) Mallégol, J.; Barry, A. M.; Ciampi, E.; Glover, P. M.; McDonald, P. J.; Keddie, J. L. Influence of Drier Combination on Through-Drying in Waterborne Alkyd Emulsion Coatings Observed with Magnetic Resonance Profiling *J. Coatings Technol.* **2002**, *74*, 113–124.

(218) Tillson, H. C. Coating composition comprising a terpolymer of an alkyl acrylate, an alkyl methacrylate and an ester of a b-g-unsaturated alcohol with methacrylic acid. US 3219610, 1965.

(219) Taylor, J. W.; Collins, M. J.; Clark, M. D. Waterborne polymers having pendant allyl groups. US 5539073, 1996.

(220) Matsumoto, A.; Kodama, K.; Aota, H.; Capek, I. Kinetics of emulsion crosslinking polymerization and copolymerization of allyl methacrylate *Eur. Polym. J.* **1999**, *35*, 1509–1517.

(221) Mcginniss, V. D.; Seidewand, R. J.; Erickson, J. R. Ultraviolet curable latexes. US 4107013, 1978.

(222) Mylonakis, S. G. Air curable latex. US 4244850, 1981.

(223) Wolfersberger, M. H.; Schindler, F. J.; Beckley, R. S.; Novak, R. W. Functionalized multistage polymer. US 5306744, 1994.

(224) Taylor, J. W.; Collins, M. J.; Bassett, D. R. A study on the chemistry of alkylcarbodiimide ethylmethacrylates as reactive monomers for acrylic and vinyl ester-based latexes *Prog. Org. Coatings* **1999**, *35*, 215–221.

(225) Hu, J.; Peng, K.; Guo, J.; Shan, D.; Kim, G. B.; Li, Q.; Zhu, L.; Gerhard, E.; Zhu, L.; Tu, W.; Lv, W.; Hickner, M. A.; Yang, J. Click crosslinking improved waterborne polymers for environment-friendly coatings and adhesives *ACS Appl. Mater. Interfaces* **2016**, *8*, 499–510.

(226) Yang, J.; Hu, J.; Guo, J. Clickable waterborne polymers and click-crosslinked waterborne polymers, clickable functional compounds, click functionalized waterborne polymers, and uses thereof. US 2019/0211148 A1, 2019.

(227) Kan, C.; Yuan, Q.; Wang, M.; Kong, X. Synthesis of Silicone-Acrylate Copolymer Latexes and their Film Properties *Polym. Adv. Technol.* **1996**, *7*, 95–97.

(228) Chen, M.; Osterholtz, F. D. Aqueous curable silane/polymer compositions. EP 000853645 B1, 1996.

(229) Hutton, T. W.; Novak, R. W. Low-formaldehyde self-crosslinking polymer latex composition. EP 0488605 A2, 1992.

(230) Volfova, P.; Chrastova, V.; Cernakova, L.; Mrenica, J.; Kozankova, J. Properties of Polystyrene/Poly(butyl acrylate) Core/Shell Polymers Modified with N-Methylol Acrylamide *Macromol. Symp.* **2001**, *170*, 283–290.

(231) Fourdrin, S.; Rochery, M.; Lewandowski, M.; Ferreira, M.; Bourbigot, S. Rheological and Thermogravimetric Studies of the Crosslinking Process of Functionalized Acrylic Latexes *J. Appl. Polym. Sci.* **2006**, *99*, 1117–1123.

(232) Aguilar, J.; Rabelero, M.; Mendizábal, E.; Nuño-Donlucas, S. M.; Arellano, M.; Puig, J. E. Tensile Properties of Self-Crosslinkable Poly(n-butyl methacrylate-co-N-methylolacrylamide) Films Prepared by Emulsion and Microemulsion Latexes *Macromol. Symp.* **2009**, *283–284*, 223–229.

(233) Witucki, G. L. A Silane Primer: Chemistry and Applications of Alkoxy Silanes *J. Coatings Technol.* **1993**, *65*, 57−60.

(234) Osterholtz, F. D.; Pohl, E. R. Kinetics of the hydrolysis and condensation of organofunctional alkoxysilanes: a review *J. Adhes. Sci. Technol.* **2012**, *6*, 127–149.

(235) Sun, Z.-G.; Fan, D.-Q.; Huang, S.-Q. Preparation and Properties of Alkoxysilane/Butyl Acrylate/Methyl Methacrylate Copolymer Latices *J. Appl. Polym. Sci.* **2009**, *111*, 185–188.

(236) Barquero, A.; Agirre, A.; Barandiaran, M. J.; Leiza, J. R. Monitoring the evolution of the microstructure of vinyl silane monomer containing poly (vinyl acetate) based copolymer latexes during storage *Eur. Polym. J.* **2019**, *121*, 109299.

(237) Liu, R.; Winnik, M. A.; Di Stefano, F.; Vanketessan, J. Interdiffusion vs cross-linking rates in isobutoxyacrylamide-containing latex coatings *Macromolecules* **2001**, *34*, 7306–7314.

(238) Aguilar, J.; Mendizábal, E.; Nuño-Donlucas, S. M.; Arellano, M.; Puig, J. E.; Rabelero, M. The Effect of Synthesis Methods on the Mechanical Properties of Self-Crosslinkable Poly(n -butyl methacrylate-co-N-methylolacrylamide) Films *J. Appl. Polym. Sci.* **2011**, *121*, 1669–1674.

(239) Cernáková, L.; Chrástová, V.; Volfová, P. Nanosized Polystyrene/Poly(Butyl Acrylate) Core-Shell Latex Particles Functionalized with Acrylamides Nanosized Polystyrene/Poly(Butyl Acrylate) Core-Shell Latex Particles *J. Macromol. Sci. Part A Pure Appl. Chem.* **2005**, *42*, 427–439.

(240) Faul, C. F. J.; Antonietti, M. Ionic Self-Assembly: Facile Synthesis of Supramolecular Materials *Adv. Mater.* **2003**, *15*, 673–683.

(241) Appel, E. A.; del Barrio, J.; Loh, X. J.; Scherman, O. A. Supramolecular polymeric hydrogels *Chem. Soc. Rev.* **2012**, *41*, 6195–6214.

(242) Aida, T.; Meijer, E. W.; Stupp, S. I. Functional Supramolecular Polymers *Science* **2012**, *335*, 813–817.

(243) Yang, L.; Tan, X.; Wang, Z.; Zhang, X. Supramolecular Polymers: Historical Development, Preparation, Characterization, and Functions *Chem. Rev.* **2015**, *115*, 7196–7239.

(244) Li, Z.-T.; Wu, L.-Z. *Hydrogen Bonded Supramolecular Structures*; Springer: Beijing (China), 2015; Vol. 88.

(245) Voorhaar, L.; Hoogenboom, R. Supramolecular polymer networks: Hydrogels and bulk materials *Chem. Soc. Rev.* **2016**, *45*, 4013–4031.

(246) Myung, D.; Water, D.; Wiseman, M.; Duhamel, P.-E.; Noolandi, J.; Ta, C. N.; Frank, C. W. Progress in the development of interpenetrating polymer network hydrogels *Polym.*

Adv. Technol. **2018**, *19*, 647–657.

(247) Lim, J. Y. C.; Lin, Q.; Xue, K.; Loh, X. J. Recent advances in supramolecular hydrogels for biomedical applications *Mater. Today Adv.* **2019**, *3*, 100021.

(248) Yan, X.; Wang, F.; Zheng, B.; Huang, F. Stimuli-responsive supramolecular polymeric materials *Chem. Soc. Rev.* **2012**, *41*, 6042.

(249) Yang, Y.; Urban, M. W. Self-healing polymeric materials *Chem. Soc. Rev.* **2013**, *42*, 7446–7467.

(250) Yang, Y.; Ding, X.; Urban, M. W. Chemical and physical aspects of self-healing materials *Prog. Polym. Sci.* **2015**, *49–50*, 34–59.

(251) Huynh, T.-P.; Sonar, P.; Haick, H. Advanced Materials for Use in Soft Self-Healing Devices *Adv. Mater.* **2017**, *29*, 1604973.

(252) Campanella, A.; Döhler, D.; Binder, W. H. Self-Healing in Supramolecular Polymers *Macromol. Rapid Commun.* **2018**, *1700739*, 1–19.

(253) Bhagavan, N. V.; Ha, C.-E. *Three-Dimensional Structure of Proteins and Disorders of Protein Misfolding*; 2015; Vol. second edi.

(254) Rogers, J. R.; Sesso, L. M. Coating compositions. US 3308078, 1967.

(255) Rogers, J. R. Coating composition comprising a terpolymer, an alkali soluble resin, and a zirconyl-fugitive ligand compound. US 3320196, 1967.

(256) Pinprayoon, O.; Groves, R.; Lovell, P. A.; Tungchaiwattana, S.; Saunders, B. R. Polymer films prepared using ionically crosslinked soft core – shell nanoparticles: a new class of nanostructured ionomers *Soft Matter* **2011**, *7*, 247–257.

(257) Tungchaiwattana, S.; Groves, R.; Lovell, P. A.; Pinprayoon, O.; Saunders, B. R. Tuning the mechanical properties of nanostructured ionomer films by controlling the extents of covalent crosslinking in core-shell nanoparticles *J. Mater. Chem.* **2012**, *22*, 5840–5847.

(258) Musa, M. S.; Milani, A. H.; Shaw, P.; Simpson, G.; Lovell, P. A.; Eaves, E.; Hodson, N.; Saunders, B. R. Tuning the modulus of nanostructured ionomer films of core–shell nanoparticles based on poly(n-butyl acrylate) *Soft Matter* **2016**, *12*, 8112–8123.

(259) Wahdat, H.; Gerst, M.; Ru, M.; Mo, S.; Adams, J. Influence of Delayed, Ionic Polymer Cross-Linking on Film Formation Kinetics of Waterborne Adhesives *Macromolecules* **2019**, *52*, 271–280.

(260) Gilli, G.; Gilli, P. *The Nature of the Hydrogen Bond*; Oxford University Press Inc: New

York, 2009.

(261) Anthamatten, M. *Supramolecular Polymer Networks and Gels*; 2015; Vol. 268.

(262) Green, A.; Popelier, P. L. A. Theoretical Prediction of Hydrogen Bond Basicity pKBHX Using Quantum Chemical Topology Descriptors Theoretic *J. Chem. Inf. Model.* **2014**, *54*, 553–561.

(263) Cacelli, I.; Campanile, S.; Giolitti, A.; Molin, D. Theoretical Prediction of the Abraham Hydrogen Bond Acidity and Basicity Factors from a Reaction Field Method *J. Chem. Inf. Model.* **2005**, *45*, 327–333.

(264) Lomas, J. S.; François, M. Water and alcohol(s): what's the difference? A proton NMR and DFT study of hetero-association with pyridine *J. Phys. Org. Chem.* **2008**, *21*, 464–471.

(265) Mullens, J.; Yperman, J.; François, J. P.; Van Poucke, I. C. Simultaneous Calorimetric Determination of Equillibrium Constant and Enthalpy Change of Hydrogen-bond Complexes in Dillute Solutions of Phenol with Pyridine in Carbon Tetrachloride *J. Phys. Chem.* **1985**, *89*, 2937–2941.

(266) Wilson, A. J. Non-covalent polymer assembly using arrays of hydrogen-bonds *Soft Matter* **2007**, *3*, 409–425.

(267) Sartorius, J.; Schneider, H.-J. A General Scheme Based on Empirical Increments for the Prediction of Hydrogen-Bond Associations of Nucleobases and of Synthetic Host - Guest Complexes *Chem. - A Eur. J.* **1996**, *2*, 1446–1452.

(268) Pranata, J.; Wierschke, S. G.; Jorgensen, W. L. OPLS Potential Functions for Nucleotide Bases. Relative Association Constants of Hydrogen-Bonded Base Pairs in Chloroform *J. Am. Chem. Soc.* **1991**, *113*, 2810–2819.

(269) Armstrong, G.; Buggy, M. Hydrogen-bonded supramolecular polymers: A literature review *J. Mater. Sci.* **2005**, *40*, 547–559.

(270) Sijbesma, R. P.; Meijer, E. W. Quadruple hydrogen bonded systems *Chem. Commun.* **2003**, 5–16.

(271) Leigh, D. A.; Robertson, C. C.; Slawin, A. M. Z.; Thomson, P. I. T. AAAA-DDDD Quadruple Hydrogen-Bond Arrays Featuring NH···N and CH···N Hydrogen Bonds *J. Am. Chem. Soc.* **2013**, *135*, 9939–9943.

(272) Beijer, F. H.; Sijbesma, R. P.; Kooijman, H.; Spek, A. L.; Meijer, E. W. Strong Dimerization of Ureidopyrimidones via Quadruple Hydrogen Bonding *J. Am. Chem. Soc.* **1998**, *120*, 6761–6769.

(273) Song, P.; Wang, H. High-Performance Polymeric Materials through Hydrogen-Bond Cross-Linking *Adv. Mater.* **2019**, *1901244*, 1–12.

(274) Sijbesma, R. P.; Beijer, F. H.; Brunsveld, L.; Folmer, B. J. B.; Hirschberg, J. H. K. K.; Lange, R. F. M.; Lowe, J. K. L.; Meijer, E. W. Reversible Polymers Formed from Self-Complementary Monomers Using Quadruple Hydrogen Bonding *Science* **1997**, *278*, 1–4.

(275) Bertrand, A.; Chen, S.; Ladavi, C.; Fleury, E.; Bernard, J. Straightforward Preparation of Telechelic H-bonding Polymers From Difunctional Trithiocarbonates and Supramolecular Block Copolymers Thereof *Macromolecules* **2011**, *44*, 3694–3704.

(276) Shimizu, L. S. Perspectives on main-chain hydrogen bonded supramolecular polymers *Polym. Int.* **2007**, *56*, 444–452.

(277) Yamauchi, K.; Lizotte, J. R.; Long, T. E. Thermoreversible poly(alkyl acrylates) consisting of self-complementary multiple hydrogen bonding *Macromolecules* **2003**, *36*, 1083–1088.

(278) Schmuck, C.; Wienand, W. Self-complementary quadruple hydrogen-bonding motifs as a functional principle: From dimeric supramolecules to supramolecular Polymers *Angew. Chemie - Int. Ed.* **2001**, *40*, 4363–4369.

(279) Cordier, P.; Tournilhac, F.; Soulié-Ziakovic, C.; Leibler, L. Self-healing and thermoreversible rubber from supramolecular assembly *Nature* **2008**, *451*, 977–980.

(280) Byun, J.; Lee, Y. M.; Cho, C. S. Swelling of thermosensitive interpenetrating polymer networks composed of poly(vinyl alcohol) and poly(acrylic acid) *J. Appl. Polym. Sci.* **1996**, *61*, 697–702.

(281) Das, S.; Joseph, M. T.; Sarkar, D. Hydrogen bonding interpolymer complex formation and study of its host-guest interaction with cyclodextrin and its application as an active delivery vehicle *Langmuir* **2013**, *29*, 1818–1830.

(282) Erel-Unal, I.; Sukhishvili, S. A. Hydrogen-bonded multilayers of a neutral polymer and a polyphenol *Macromolecules* **2008**, *41*, 3962–3970.

(283) Yang, K.; Zimmerman, S. C. Hydrogen Bonding Modules for Use in Supramolecular Polymers *Isr. J. Chem.* **2013**, *53*, 511–520.

(284) Janssen, H. M.; van Gemert, G. M. L.; Cate, A. T. Ten; Van Beek, D. J. M.; Pieter, S. R.; Meijer, E. W.; Bosman, A. W. Preparation of Supramolecular Polymers By Copolymerization of Monomers Containing Quadruple Hydrogen Bonding Units With Regular Monomers. US 6803447 B2, 2004.

(285) Lange, R. F. M.; Van Gurp, M.; Meijer, E. W. Hydrogen-bonded supramolecular polymer networks *J. Polym. Sci. Part A Polym. Chem.* **1999**, *37*, 3657–3670.

(286) Folmer, B. J. B.; Sijbesma, R. P.; Versteegen, R. M.; van der Rijt, J. A. J.; Meijer, E. W. Supramolecular Polymer Materials: Chain Extension of Telechelic Polymers Using a Reactive Hydrogen-Bonding Synthon *Adv. Mater.* **2000**, *12*, 874–878.

(287) Khutoryanskiy, V. V.; Staikos, G. *Hydrogen-Bonded Interpolymer Complexes: Formation, Structure and Applications*; World Scientific: Singapore, 2009.

(288) Bailey, F. E.; Lukdberg, R. D.; Callard, R. W. Some Factors Meeting the Molecular Association of Poly(ethyene Oxide) and Poly(acrylic Acid) In Aqueous Solution *J. Polym. Sci. Part A* **1964**, *2*, 845–851.

(289) Smith, K. L.; Winslow, A. E.; Petersen, D. E. Association Reactions for Poly(alkylene Oxides) and Polymeric Poly(carboxylic Acids) *Ind. Eng. Chem.* **1959**, *51*, 1361–1364.

(290) Khutoryanskiy, V. V.; Mun, G. A.; Nurkeeva, Z. S.; Dubolazov, A. V. pH and salt effects on interpolymer complexation via hydrogen bonding in aqueous solutions *Polym. Int.* **2004**, *53*, 1382–1387.

(291) Khutoryanskiy, V. V. Hydrogen-bonded interpolymer complexes as materials for pharmaceutical applications *Int. J. Pharm.* **2007**, *334*, 15–26.

(292) Kudaibergenov, S. E.; Bimendina, L. A.; Zhumadilova, G. T. Interpolymer complexes of acrylic acid and vinylbutyl ether copolymers with non-ionic and cationic polymers *Polym. Adv. Technol.* **2000**, *11*, 506–511.

(293) Farahani, B. V.; Rajabi, F. H.; Ahmadi, M. H.; Zenooz, N. Qualitative Investigation on some H-bonded Interpolymer Complexes by Determination of Thermodynamic Parameters *J. Mex. Chem. Soc.* **2012**, *56*, 212–216.

(294) Nurkeeva, Z. S.; Mun, G. A.; Khutoryanskiy, V. V.; Bitekenova, A. B.; Dzhusupbekova, A. B. Polymeric complexes of lidocaine hydrochloride with poly(acrylic acid) and poly(2-hydroxyethyl vinyl ether) *J. Biomater. Sci. Polym. Ed.* **2002**, *13*, 759–768.

(295) Swift, T.; Paul, N.; Swanson, L.; Katsikogianni, M.; Rimmer, S. Förster Resonance Energy Transfer across interpolymer complexes of poly(acrylic acid) and poly(acrylamide) *Polymer* **2017**, *123*, 10–20.

(296) Swift, T.; Seaton, C. C.; Rimmer, S. Poly(acrylic acid) interpolymer complexes *Soft Matter* **2017**, *13*, 8736–8744.

(297) Chen, Y.; Ballard, N.; Gayet, F.; Bon, S. A. F. High internal phase emulsion gels (HIPE-gels) from polymer dispersions reinforced with quadruple hydrogen bond functionality

Chem. Commun. **2012**, *48*, 1117–1119.

(298) Kaitz, J. A.; Possanza, C. M.; Song, Y.; Diesendruck, C. E.; Spiering, A. J. H.; Meijer, E. W.; Moore, J. S. Depolymerizable, adaptive supramolecular polymer nanoparticles and networks *Polym. Chem.* **2014**, *5*, 3788–3794.

(299) Nair, K. P.; Weck, M. Modulating mechanical properties of self-assembled polymer networks by multi-functional complementary hydrogen bonding *Soft Matter* **2011**, *7*, 553–559.

(300) Su, E.; Yurtsever, M.; Okay, O. A Self-Healing and Highly Stretchable Polyelectrolyte Hydrogel via Cooperative Hydrogen Bonding as a Superabsorbent Polymer *Macromolecules* **2019**, *52*, 3257–3267.

(301) Zhang, J.; Wang, N.; Liu, W.; Zhao, X.; Lu, W. Intermolecular hydrogen bonding strategy to fabricate mechanically strong hydrogels with high elasticity an fatigue resistance *Soft Matter* **2013**, *9*, 6331.

(302) Sordo, F.; Mougnier, S.-J.; Loureiro, N.; Tournilhac, F.; Michaud, V. Design of Self-Healing Supramolecular Rubbers with a Tunable Number of Chemical Cross-Links *Macromolecules* **2008**, *48*, 4394–4402.

(303) Montarnal, D.; Tournilhac, O. I. S.; Hidalgo, M.; Leibler, L. Epoxy-Based Networks Combining Chemical and Supramolecular Hydrogen-Bonding Crosslinks *J. Polym. Sci. Part A Polym. Chem.* **2010**, *48*, 1133–1141.

(304) Michael, P.; Diana, D.; Binder, W. H. Improving autonomous self healing via combined chemical/physical principles *Polymer* **2015**, *69*, 216–227.

(305) Chen, Y.-N.; Peng, L.; Liu, T.; Wang, Y.; Shi, S.; Huiliang, W. Poly(vinyl alcohol)-Tannic Acid Hydrogels with Excellent Mechanical Properties and Shape Memory Behaviors *ACS Appl. Mater. Interfaces* **2016**, *8*, 27199–27206.

(306) Euti, E. M.; Wolfel, A.; Picchio, M. L.; Romero, M. R.; Martinelli, M.; Minari, R. J.; Igarzabal, C. I. A. Controlled Thermoreversible Formation of Supramolecular Hydrogels Based on Poly(vinyl alcohol) and Natural Phenolic Compounds *Macromol. Rapid Commun.* **2019**, *0*, 1900217.

(307) Hoque, J.; Sangaj, N.; Varghese, S. Stimuli-Responsive Supramolecular Hydrogels and Their Applications in Regenerative Medicine *Macromol. Biosci.* **2018**, *1800259*, 1–16.

(308) Cheng, S.; Zhang, M.; Dixit, N.; Moore, R. B.; Long, T. E. Nucleobase self-assembly in supramolecular adhesives *Macromolecules* **2012**, *45*, 805–812.

(309) Heinzmann, C.; Weder, C.; De Espinosa, L. M. Supramolecular polymer adhesives:

Advanced materials inspired by nature *Chem. Soc. Rev.* **2016**, *45*, 342–358.

(310) Nam, H. G.; Nam, M. G.; Yoo, P. J.; Kim, J. Hydrogen bonding-based strongly adhesive coacervate hydrogels synthesized using poly(N-vinylpyrrolidone) and tannic acid *Soft Matter* **2019**, *15*, 785–791.

(311) Chalykh, A. A.; Chalykh, A. E.; Novikov, M. B.; Feldstein, M. M. Pressure-sensitive adhesion in the blends of poly(n-vinyl pyrrolidone) and poly(ethylene glycol) of disparate chain lengths *J. Adhes.* **2002**, *78*, 667–694.

(312) Feldstein, M. M.; Bovaldinova, K. A.; Bermesheva, E. V; Moscalets, A. P.; Dormidontova, E. E.; Grinberg, V. Y.; Khokhlov, A. R. Thermo-Switchable Pressure-Sensitive Adhesives Based on Poly(N‐vinyl caprolactam) Non-Covalently Cross-Linked by Poly(ethylene glycol) *Macromolecules* **2014**, *47*, 5759−5767.

(313) Feldstein, M. M.; Dormidontova, E. E.; Khokhlov, A. R. Pressure sensitive adhesives based on interpolymer complexes *Prog. Polym. Sci.* **2015**, *42*, 79–153.

(314) Richard, J.; Maquet, J. Dynamic micromechanical investigations into particle/particle interfaces in latex films *Polymer* **1992**, *33*, 4164–4173.

(315) Chenal, M.; Rieger, J.; Véchambre, C.; Chenal, J.-M.; Chazeau, L.; Creton, C.; Boutleiller, L. Soft Nanostructured Films with an Ultra-Low Volume Fraction of Percolating Hard Phase *Macromol. Rapid Commun.* **2013**, *34*, 1524–1529.

(316) Gurney, R. S.; Morse, A.; Siband, E.; Dupin, D.; Armes, S. P.; Keddie, J. L. Mechanical properties of a waterborne pressure-sensitive adhesive with a percolating poly(acrylic acid)-based diblock copolymer network: Effect of pH *J. Colloid Interface Sci.* **2015**, *448*, 8–16.

(317) Chenal, M.; Véchambre, C.; Chenal, J.-M.; Chazeau, L.; Humblot, V.; Bouteiller, L.; Creton, C.; Rieger, J. Mechanical properties of nanostructured films with an ultralow volume fraction of hard phase *Polymer* **2017**, *109*, 187–196.

(318) Lesage de la Haye, J.; Martin-Fabiani, I.; Schulz, M.; Keddie, J. L.; D'Agosto, F.; Lansalot, M. Hydrophilic MacroRAFT-Mediated Emulsion Polymerization: Synthesis of Latexes for Cross-Linked and Surfactant-Free Films *Macromolecules* **2017**, *50*, 9315–9328.

(319) González, I.; Mestach, D.; Leiza, J. R.; Asua, J. M. Adhesion enhancement in waterborne acrylic latex binders synthesized with phosphate methacrylate monomers *Prog. Org. Coatings* **2008**, *61*, 38–44.

(320) González, E.; Paulis, M.; Barandiaran, M. J. Effect of controlled length acrylic acid-based electrosteric stabilizers on latex film properties *Eur. Polym. J.* **2014**, *59*, 122–128.

(321) Chen, Y.; Jones, S. T.; Hancox, I.; Beanland, R.; Tunnah, E. J.; Bon, S. A. F. Multiple hydrogen-bond array reinforced cellular polymer films from colloidal crystalline assemblies of soft latex particles *ACS Macro Lett.* **2012**, *1*, 603–608.

(322) Karikari, A. S.; Tysak, T. Floor coating compositions containing supramolecular polymers. US 2016/0230035 A1, 2016.

(323) Tronc, F.; Liu, R.; Winnik, M. A.; Eckersley, S. T.; Rose, G. D.; Weishuhn, J. M.; Meunier, D. M. Epoxy-Functionalized, Low Glass-Transition Temperature Latex. I. Synthesis, Characterizations, and Polymer Interdiffusion *J. Polym. Sci. Part A Polym. Chem.* **2002**, *40*, 2609–2625.

(324) Collins, M. J.; Taylor, J. W. Surfactant-containing acetoacetoxy-functional and enamine-functional polymers. US 006028155 A, 2000.

(325) Collins, M. J.; Taylor, J. W. Stable amino-containing polymer latex blends. US 005998543 A, 1999.

(326) Qiu, T.; Wang, X.; Lin, X.; Zhu, Z.; Li, X.; Guo, L. Emulsion Polymerization to Synthesize Self-Healing Films Toward Healing on Fractures: A Feasible Strategy *Polym. Chem.* **2016**, *54*, 3071–3078.

Chapter 2. Functional polymer dispersions with H-bonding groups: pyrrolidone – hydroxyl and uracil – adenine complexation

2.1. Introduction

As highlighted in the introduction of this thesis, physical bonding networks arising from hydrogen bond interactions can be used to significantly improve the mechanical properties of polymer materials. Although more recent work has focused on motifs that lead to multiple hydrogen bond arrays,[1–8] even relatively weak single/double hydrogen bond interactions such as those of pyrrolidone – hydroxyl and uracil – adenine H-bonds (see Figure 2.1) can potentially be used to increase interactions between polymer chains.[9–16]

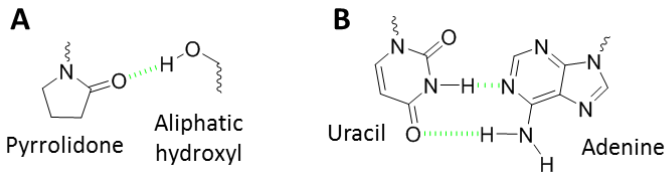

Figure 2.1. (A) Single H-bond between a pyrrolidone and an aliphatic hydroxyl and (B) double H-bond between uracil and adenine.

In this chapter, we look at the potential use of functional acrylic dispersions that contain hydrogen bonding groups within the backbone of the main latex polymer phase to form films that are physically crosslinked. These systems are comparable to many two-pot chemically crosslinked systems where the reactive groups are initially in different particles and later react to form a network in the dried state. We look in detail at two distinct systems. In the first system we explore the use of the pyrrolidone-hydroxyl pair, which interact via H-bonding leading to a complex with an association constant of the order of 1 M^{-1}.[17] Systems in which the pyrrolidone and hydroxyl groups are in different particles and in the same particle are analyzed as shown schematically in Figure 2.2. The second system explores the use of monomers containing uracil and adenine nucleobases which interact forming double complexes with an association constant of 100 M^{-1}.[4] In this second case, the uracil and adenine are in different particles as shown schematically in Figure 2.3.

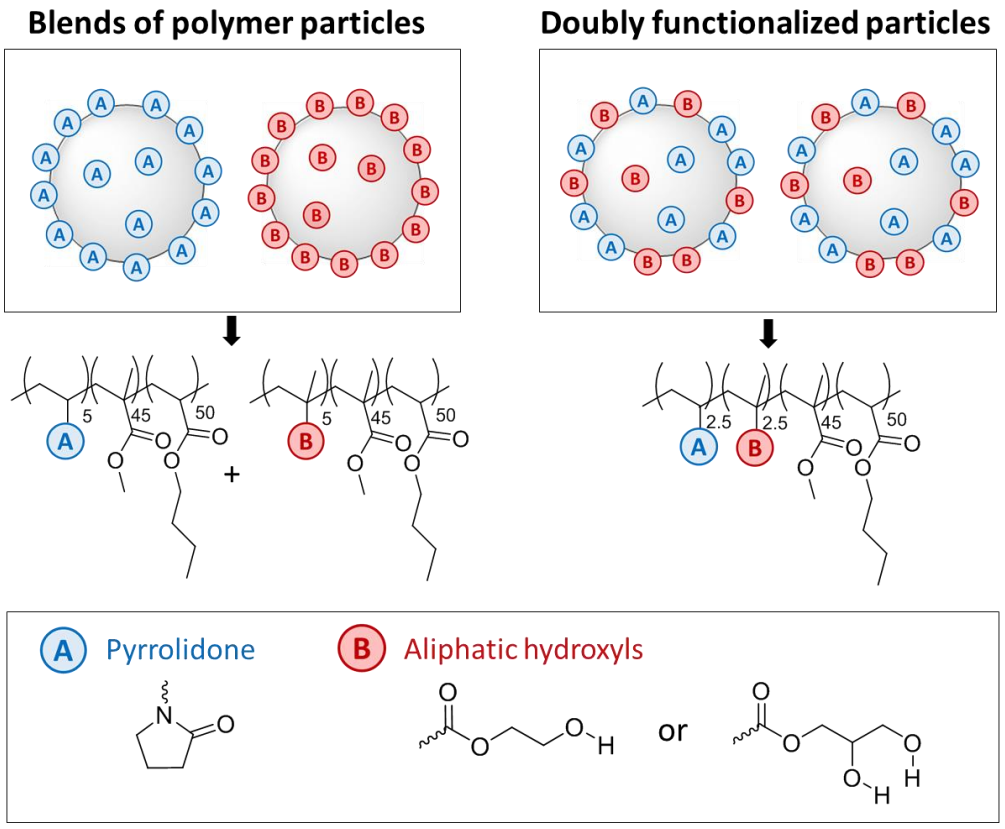

Figure 2.2. Schematic representation of the polymer dispersions and polymer dispersion blends used for the investigation of the influence of pyrrolidone – hydroxyl H-bonds on film properties. In the scheme, the subscripts after the monomer units express the weight % of the monomers used for the synthesis.

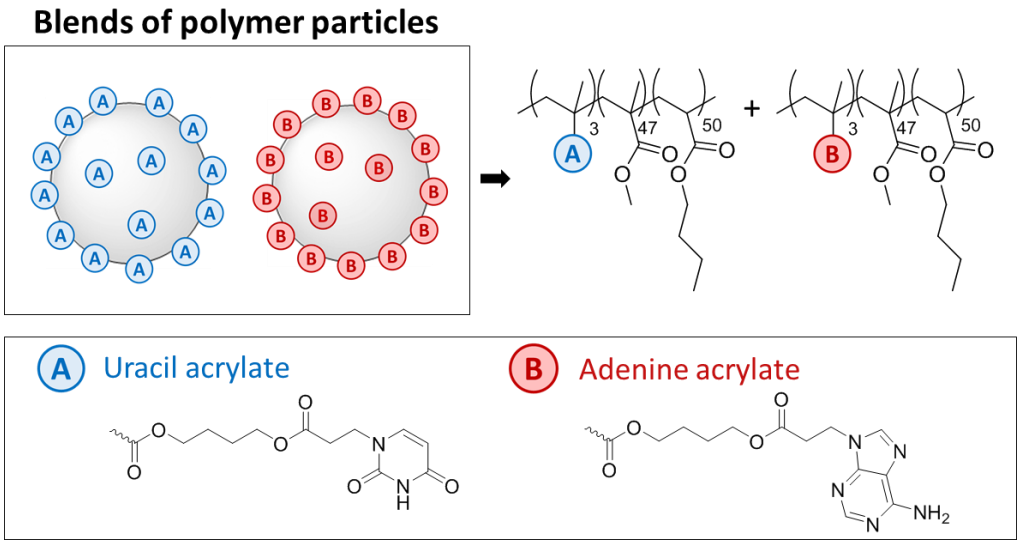

Figure 2.3. Schematic representation of the polymer blends prepared from the polymer dispersions functionalized with uracil and adenine units. In the scheme, the subscripts after the monomer units express the weight % of the monomers used for the synthesis.

Following these results we explore the limitations of the use of hydrogen bonding systems in the development of physically crosslinked films cast from latex dispersions. To do so, the influence of pyrrolidone – hydroxyl and uracil – adenine H-bonds on the rheological behavior of low molar mass polymers is explored.

2.2. Experimental part

2.2.1. Materials

Technical grade monomers methyl methacrylate (MMA, Quimidroga) and n-butyl acrylate (BA, Quimidroga) were used without purification. N-vinyl pyrrolidone (NVP, >99%, Sigma Aldrich), 2-hydroxyethyl methacrylate (HEMA, 97%, Sigma Aldrich), 2,3-dihydroxypropyl methacrylate (DHPMA, 90%, Polysciences), adenine (99%, Alfa Aesar), uracil (99+%, Alfa Aesar), 1,4-butanediol diacrylate (BDDA, 90%, Sigma Aldrich), 2,6-di-tert-butyl-4-methylphenol (BHT, ≥99%, Fluka), ammonium persulfate (APS, ≥98%, Sigma Aldrich), 4,4-azobis(4-cyanovaleric acid) (V-501, >98%, Sigma-Aldrich), dibenzyl peroxide (DBP, 75%, Sigma Aldrich), sodium bicarbonate ($NaHCO_3$, Sigma Aldrich), sodium carbonate (Na_2CO_3, Sigma Aldrich), potassium carbonate (K_2CO_3, ≥99%, anhydrous, Sigma Aldrich), sodium chloride (NaCl, synthesis grade, Fischer), magnesium sulfate ($MgSO_4$, anhydrous, Fischer) triethylamine (TEA, 99%, Sigma Aldrich) and n-dodecanethiol (DSH, ≥97%, Sigma-Aldrich) were used as received. Dimethyl formamide (DMF, ≥99.8%, Sigma Aldrich), dimethyl sulfoxide (DMSO, synthesis grade, Scharlau), m-xylene (for synthesis, Merck), diethyl ether (synthesis grade, Scharlau), n-hexane (96%, Scharlab), tetrahydrofuran (THF, laboratory reagent grade from Fischer and HPLC grade from Scharlab) and dichloromethane (DCM, Pharmpur®, Scharlab) were used without purification. Dowfax 2A1 was kindly supplied by Dow Chemical Company. Deionized water was used as polymerization media.

2.2.2. Synthesis of polymer dispersions with pyrrolidone and hydroxyl groups

The polymer dispersions with pyrrolidone and/or hydroxyl groups were synthesized by seeded semibatch emulsion polymerization according to the procedure proposed by Haddock *et al.*[18] N-vinyl pyrrolidone (NVP) was used as functional monomer (F.M.) to incorporate the pyrrolidone groups to the acrylic dispersions, and 2-hydroxyethyl methacrylate (HEMA) and 2,3-dihydroxypropyl methacrylate (DHPMA) with one and two aliphatic hydroxyl groups in their structure respectively were used to incorporate the hydroxyl functionality into the dispersions. The chemical structures of NVP, HEMA and DHPMA are shown in Figure 2.4.

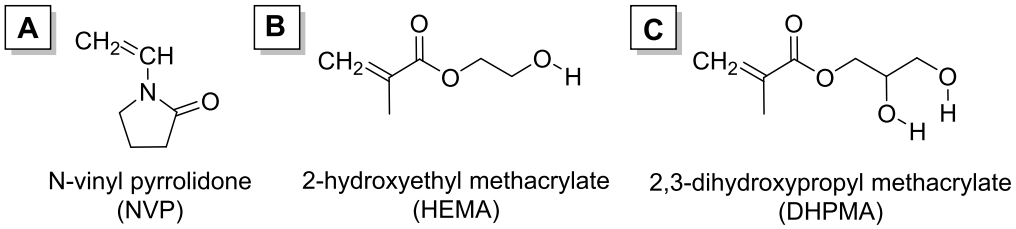

Figure 2.4. Chemical structures of NVP, HEMA and DHPMA.

The formulations used for the polymerizations are presented in Table 2.1. In the reactions, methyl methacrylate (MMA) and n-butyl acrylate (BA) were used as main monomers, sodium bicarbonate ($NaHCO_3$) was used as buffer to control the pH, Dowfax 2A1 was used as surfactant and ammonium persulfate (APS) as thermal initiator. In addition, 0.1 weight based on monomers (wbm) % of n-dodecanethiol (DSH) was used as chain transfer agent (CTA) to limit the crosslinking of the polymer chains and gel formation during the polymerizations.

Table 2.1. Formulations employed for the synthesis of the polymer dispersions with pyrrolidone and hydroxyl functionalities. F.M. refers to functional monomer.

		F.M. (g)	MMA (g)	BA (g)	DSH (g)	H_2O (g)	Dowfax (g)	APS (g)	$NaHCO_3$ (g)
Latex 1 0% F.M.	Seed	-	10	10	-	160	4.28	0.267	1
	F1	-	-	-	-	37.3	2.38	1.333	-
	F2	-	90	90	0.18	-	-	-	-
Latex 2 5% NVP	Seed	NVP 1	9	10	-	160	4.28	0.267	1
	F1	-	-	-	-	37.3	2.38	1.333	-
	F2	NVP 9	81	90	0.18	-	-	-	-
Latex 3 5% HEMA	Seed	HEMA 1	9	10	-	160	4.28	0.267	1
	F1	-	-	-	-	37.3	2.38	1.333	-
	F2	HEMA 9	81	90	0.18	-	-	-	-
Latex 4 5% DHPMA	Seed	DHPMA 1	9	10	-	160	4.28	0.267	1
	F1	-	-	-	-	37.3	2.38	1.333	-
	F2	DHPMA 9	81	90	0.18	-	-	-	-
Latex 5 2.5% NVP +2.5% HEMA	Seed	NVP 0.5 HEMA 0.5	9	10	-	160	4.28	0.267	1
	F1	-	-	-	-	37.3	2.38	1.333	-
	F2	NVP 4.5 HEMA 4.5	81	90	0.18	-	-	-	-
Latex 6 2.5% NVP + 2.5% DHPMA	Seed	NVP 0.5 DHPMA 0.5	9	10	-	160	4.28	0.267	1
	F1	-	-	-	-	37.3	2.38	1.333	-
	F2	NVP 4.5 DHPMA 4.5	81	90	0.18	-	-	-	-

The set up employed to carried out the polymerizations consisted of a glass reactor equipped with a nitrogen inlet, a reflux condenser, an anchor-type mechanic stirrer, a thermocouple and two feeding pumps. The temperature of the reaction medium was controlled using a water jacket connected to a thermostatic bath. The whole system was controlled by an

automatic control system (Camile TG, Biotage). The reactions were carried out under nitrogen atmosphere at 70 °C and a stirring velocity of 200 rpm. First, the ingredients of the seed were charged into the reactor and the system was stirred and purged with N_2 for 20 min. Then, the temperature was increased to 70 °C and the initiator was injected to start the polymerization and create the seed polymer particles. After 30 min of polymerization, the two feeding streams, one containing an aqueous solution of initiator and surfactant (F1) and the other a mixture of monomers with 0.1 % wbm CTA (F2), were added to the reactor for 3 h. At the end of the feeding, the temperature was kept at 70 °C for additional 30 min to ensure high monomer conversion. Samples were withdrawn from the reactor during the course of the reactions to follow the polymerization process.

In total, 6 polymer dispersions were prepared. In Latex 1, no functional monomer was used as reference. In Latexes 2-4, 5 wt% of NVP, HEMA and DHPMA were incorporated, respectively. Latexes 5 and 6 were doubly functionalized polymer dispersions with 2.5 wt% of NVP and 2.5 wt% of either HEMA or DHPMA.

2.2.3. Synthesis of uracil acrylate (UrA) and adenine acrylate (AdA)

The acrylic monomers containing adenine and uracil nucleobases were synthesized by means of the Aza-Michael Addition reaction of adenine and uracil with 1,4-butanediol diacrylate (BDDA) based on the procedure reported by Cheng *et al.*[10] The reaction pathway is shown in Scheme 2.1 and the formulations used for the synthesis of the nucleobase functionalized acrylates are shown in Table 2.2.

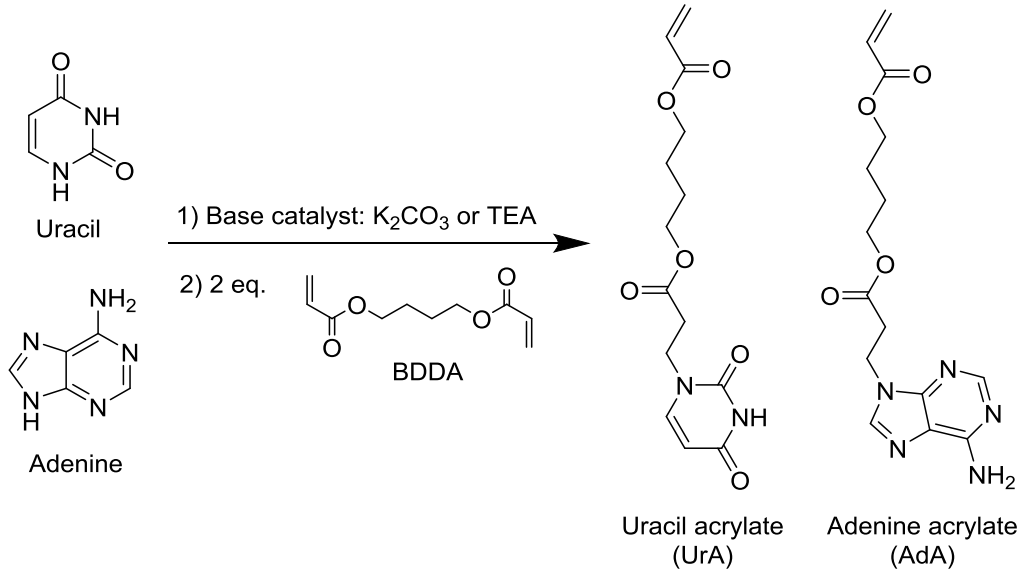

Scheme 2.1. Aza-Michael Addition reaction of adenine and uracil with 1,4-butanediol diacrylate for the synthesis of uracil acrylate (UrA) and adenine acrylate (AdA).

Table 2.2. Formulations used for the synthesis of uracil acrylate (UrA) and adenine acrylate (AdA).

Monomer	Nucleobase (g)	Solvent (mL)	Base (g)	BDDA (mL)	BHT (g)
Uracil acrylate (UrA)	Uracil 5	DMF 100	TEA 4.72	17.45	0.3
Adenine acrylate (AdA)	Adenine 5	DMSO 100	K_2CO_3 0.25	18.70	0.3

First, the nucleobases were dispersed in the continuous media (DMF for uracil and DMSO for adenine) and BHT was added to avoid the polymerization of the acrylic monomers during the synthesis. Then, the base was added as catalyst to the dispersion (1 equivalent of trimethylamine, TEA, in the case of the uracil and catalytic amount of potassium carbonate, K_2CO_3, in the case of adenine) and the mixture was stirred at room temperature for uracil and at

60 °C for adenine. After one hour of stirring the mixtures became transparent indicating the deprotonation of the nucleobases. At this moment, 2 equivalents of 1,4-butanediol diacrylate (BDDA) were added and the mixtures were stirred at 60 °C for 24 h.

The reaction mixture was poured into 1 L of brine (5% NaCl in H_2O) and washed 3 times with 80 mL of hexane to remove the excess of BDDA. Afterwards, the aqueous phase was extracted 3 times with 100 mL of dichloromethane (DCM). The organic extracts were combined and washed 3 times with 500 mL of brine to remove the traces of DMF and DMSO. Then, the organic phase was dried using $MgSO_4$, filtered and concentrated in a vacuum evaporator to remove all the solvents. Finally, the adenine acrylate monomer was washed with diethyl ether to remove the last DMSO traces. In the case of uracil acrylate, the concentrated solution obtained in the vacuum evaporator was extracted with diethyl ether and crystalized in the freezer for 3 days.

For UrA, the yield of the reaction was 39.3 % and the ^{1}H-NMR spectrum after purification is shown in Figure 2.5. ^{1}H NMR (400 MHz, Chloroform-*d*) δ 8.96 ppm (1H, s, -C(O)-N**H**-C(O)-, signal l), 7.41 ppm (1H, d, -C(O)-CH=C**H**-N-, signal j), 6.43 ppm (1H, d, -CH=C**H**H, trans, signal a), 6.14 ppm (1H, dd, -C**H**=CHH, signal b), 5.86 ppm (1H, d, -CH=CH**H**, cis, signal c) 5.69 ppm (1H, d, -C(O)-C**H**=CH-N-, signal k), 4.26 – 4.13 ppm (4H, m, -C(O)-O-C$\mathbf{H_2}$-CH_2-, signals g and d), 4.02 ppm (2H, t, -O-C(O)-CH_2-C$\mathbf{H_2}$-N-, signal i), 2.81 ppm (2H, t, -O-C(O)-C$\mathbf{H_2}$-CH_2-, signal h), 1.76 ppm (4H, p, -C(O)-O-CH_2-C$\mathbf{H_2}$, signals e and f).

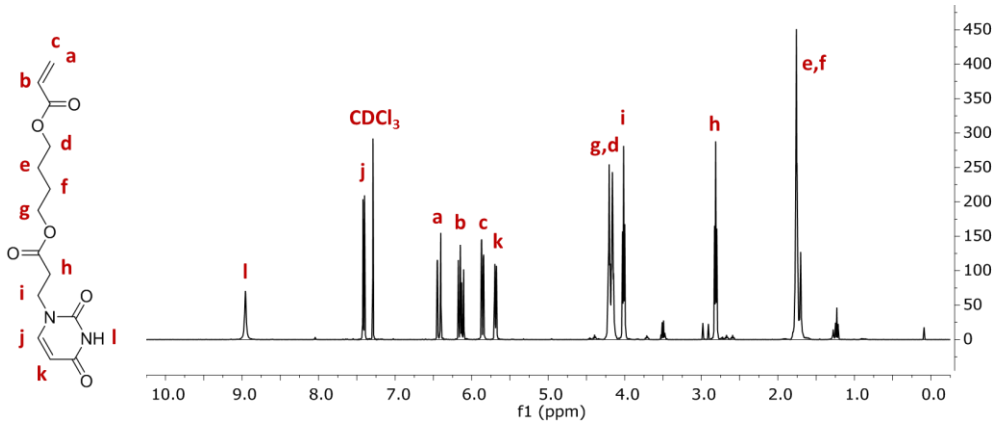

Figure 2.5. ^{1}H-NMR spectrum of uracil acrylate.

For AdA, the yield of the reaction was 17.3 %. The ^{1}H-NMR spectrum of AdA after purification is shown in Figure 2.6. ^{1}H NMR (400 MHz, Chloroform-*d*) δ 8.38 ppm (1H, s, =N-C**H**=N-, signal l), 7.95 ppm (1H, s, -N-C**H**=N-, signal j), 6.42 ppm (1H, d, -CH=C**H**H, trans, signal a), 6.13 ppm (1H, dd, -C**H**=CHH, signal b), 5.82 ppm (1H, d, -CH=CH**H**, cis, signal c), 5.64 ppm (2H, d, =N-C(N**H$_2$**)=, signal k), 4.53 ppm (2H, t, -O-C(O)-CH$_2$-C**H$_2$**-, signal i), 4.23 – 4.07 ppm (4H, m, -C(O)-O-C**H$_2$**-CH$_2$-, signals d and g), 2.97 ppm (2H, t, -O-C(O)-C**H$_2$**-CH$_2$-N, signal h), 1.71 ppm (4H, p, -C(O)-O-CH$_2$-C**H$_2$**-, signals e and f).

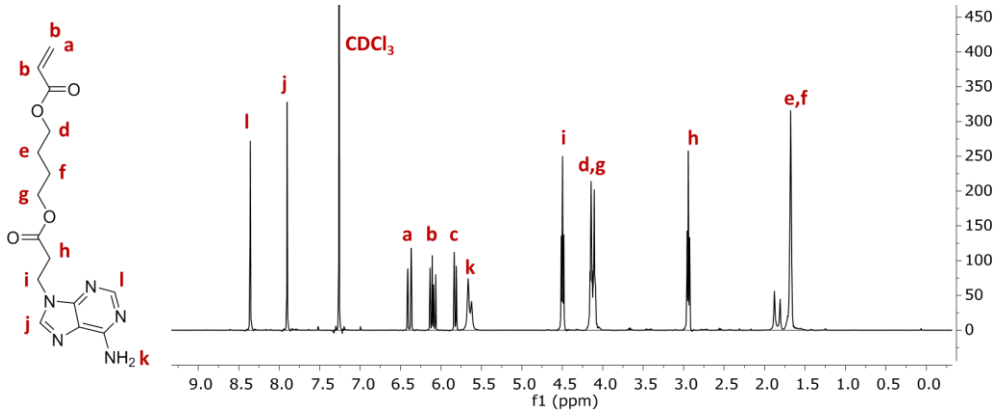

Figure 2.6. ^{1}H-NMR spectrum of adenine acrylate.

2.2.4. Synthesis of polymer dispersions with uracil and adenine groups

Polymer dispersions with uracil or adenine units were produced by batch emulsion polymerization. The formulations used for the synthesis of the acrylic dispersions are shown in Table 2.3. In the polymerizations, MMA and BA were used as main monomers in a ≈ 50 / 50 weight ratio and 3 wt% UrA and AdA were added in runs NB2 and NB3 to incorporate the uracil and adenine groups. The monomer weight ratios were selected to obtain polymers with glass transition temperatures (T_g) near 10 °C. For the emulsion polymerizations 2 % wbm Dowfax 2A1 was used as surfactant and 0.5 % wbm of V501 as thermal initiator.

Table 2.3. Formulations used for the synthesis of the acrylic dispersions with uracil and adenine moieties. NB is the short name of nucleobase.

Run	F.M. (g)	MMA (g)	BA (g)	H_20 (g)	Dowfax (g)	V501 (g)	Na_2CO_3 (g)	$NaHCO_3$ (g)
NB1 – Blank	-	10	10	30	0.4	0.1	0.159	0.126
NB2 – 3 wt% UrA	UrA 0.6	9.8	9.6	30	0.4	0.1	0.159	0.126
NB3 – 3 wt% AdA	AdA 0.6	9.7	9.7	30	0.4	0.1	0.159	0.126

UrA and AdA are solid monomers with very low solubility in the MMA / BA mixture (≈ 1 wt%) and insoluble in water at neutral pH. Therefore, to increase the solubility of the monomers in water, the pH of the aqueous phase was increased to 10.3 using a 1/1 mol ratio $Na_2CO_3/NaHCO_3$ buffer, which allowed the deprotonation of the nucleobases ($pK_{a,uracil} \approx 9.5$ and $pK_{a,adenine} \approx 9.8$)[19] and the solubilization of UrA and AdA monomers in the aqueous phase. Then, the surfactant and the rest of the monomers were added to the aqueous phase to prepare the preemulsion. The preemulsion was transferred to a 100 mL glass reactor equipped with a nitrogen inlet, anchor type stirrer and reflux condenser. The reaction was controlled using a water jacket connected to a thermostatic bath. The system was purged with N_2 and heated to 70 °C. When the temperature was reached, the polymerization was initiated with a shot of V501 dissolved in 2 g of water. Then, the polymerization was conducted for 240 minutes in NB2 and for 150 minutes in NB1 and NB3. The system was stirred mechanically during the synthesis using a stirring velocity 200 rpm.

2.2.5. High temperature solution polymerizations

Low molar mass polymers with pyrrolidone, hydroxyl, uracil and adenine functionalities were produced by high temperature solution polymerization based on a procedure described by Hutchinson *et al*.[20] The copolymerization with NVP and HEMA was carried out using m-xylene as solvent. Due to solubility limitations in m-xylene, the copolymerization with UrA and AdA was conducted in DMF. The formulations used for the copolymerizations are given in Table 2.4. In both cases, 1.5 mol% dibenzyl peroxide (DBP) was used as thermal initiator. The set up used to carry out the reactions consisted of a 250 mL three-neck round bottom flask, a condenser, a syringe pump, a nitrogen inlet and an oil bath to control the temperature. The polymerizations were conducted at 110 °C under nitrogen atmosphere. The reaction medium was stirred with magnetic stirring and a condenser was employed to avoid the evaporation of the volatile components.

Table 2.4. Formulations used for the high temperature copolymerizations of NVP, HEMA, UrA and AdA.

Copolymer	NVP (g)	HEMA (g)	UrA (g)	AdA (g)	MMA (g)	BA (g)	m-xylene (g)	DMF (g)	DBP (g)
SP1 – Blank	-	-	-	-	35	35	100	-	4.5
SP2 – 20 wt% NVP	14	-	-	-	21	35	100	-	4.5
SP3 – 20 wt% HEMA	-	14	-	-	21	35	100	-	4.5
SP4 – 10 wt% NVP + 10 wt% HEMA	7	7	-	-	21	35	100	-	4.5
SP5 – Blank	-	-			5	5	-	100	0.32
SP6 – 20 wt% UrA	-	-	2	-	3	5	-	100	0.32
SP7 – 20 wt% AdA	-	-	-	2	3	5	-	100	0.32

For the polymerizations in m-xylene (SP 1-4), first the solvent was charged into the round bottom flask and the system was purged with N_2 for 30 minutes. Then, the round bottom flask was immersed in the oil bath at 110 °C and 10 minutes after, the remaining ingredients (mixture of monomers and initiator) were fed for 4 hours with a syringe pump. After the completion of the feeding, the system was kept at high temperature for 1 h to ensure high monomer conversion.

In the copolymerizations carried out in DMF (SP 5-7), first the monomers and the initiator were dissolved in the continuous medium. 10 g of the solution were placed inside the round bottom flask and the system was stirred and purged with N_2 for 30 minutes. Then, the system was heated to 110 °C and after 10 minutes, the rest of the solution was fed with a syringe pump for 4 h and 30 min. After the feeding, the system was post-polymerized for 1 h.

2.2.6. Blending and film casting

After the synthesis of the polymer dispersions, Latex 2 (5 wt% NVP) was blended with Latex 3 (5 wt% HEMA) and Latex 4 (5 wt% DHPMA) in a 1 / 1 weight ratio. The blends were stirred for 30 minutes. Then, the blends and the neat latexes (Latex 1-7) were cast into silicone molds and dried for 7 days at 23 ± 2 °C and 55 ± 5% relative humidity. To remove the water traces from the films, the films were dried for two more days at 25 °C and vacuum. The tensile measurements of these films were performed right after the drying under vacuum conditions. For the films cast from solution, the polymers obtained from drying the dispersions were redissolved in THF at a concentration of ≈ 5 wt%, cast from the THF solutions and dried for 5 days at room temperature and 8 days at 65 °C. The dried polymer films were then cut in small pieces and reprocessed using a Collin P 200E hot press at 120 °C using the following method: heat the samples at 120 °C for one minute, increase gradually the pressure to 200 bar in 1 minute, keep the pressure at 200 bar for 1 minute, cool down the system to 30 °C at 200 bar (around 5 minutes)

and release the pressure. The 5%DHPMA and NVP-DHPMA blend materials could not be reprocessed due to the insolubility of the polymer in THF. For the annealing experiments, the films cast from the dispersions were heated to 65 °C for 7 days. The tensile test probes prepared from the annealed films and materials cast from solution were conditioned for at least 1 hour at 23 ± 2 °C and 55 ± 5% relative humidity before the tensile tests.

The latexes with 3 wt% UrA (NB2) and 3 wt% AdA (NB3) were blended in a 1 / 1 weight ratio and magnetically stirred for 30 minutes. Then, the blend and the neat latexes (NB 1-3) were cast into silicone molds and dried for 7 days at 23 ± 2 °C and 55 ± 5% relative humidity.

After the high temperature solution copolymerizations, the polymer solutions obtained in SP2 (20 wt% NVP) and SP3 (20 wt% HEMA) were blended in a 1 / 1 weight ratio. Then, the solutions obtained in SP1-4 and the SP2-SP3 blend were dried at 65 °C until constant weight of the samples was achieved (≈ 8 days). The polymers obtained in SP5-7 were precipitated from 500 mL deionized water. Then, the polymers were redissolved in acetone and the solutions prepared from the copolymers produced in SP6 (20 wt% UrA) and SP7 (20 wt% AdA) were mixed in a 1 / 1 weight ratio. The acetone solutions were dried at 65 °C until constant weight of the samples was achieved (≈ 8 days).

2.2.7. Characterization

During the synthesis of the polymer dispersions, the monomer conversion of the volatile monomers was determined gravimetrically and the particle size was measured using Dynamic Light Scattering (DLS). In the high temperature copolymerizations, the individual monomer conversions were determined by ^{1}H-NMR following the disappearance of the vinyl proton peaks and using the signal at 2.4 ppm of the 2 methyl groups of xylene as internal standard in SP1-4

and the signal at 8.05 ppm of DMF in SP5-7 to normalize the signals of the vinyl protons. For the analysis, around 50 µL samples were taken from the polymerization medium and they were diluted in 500 µL $CDCl_3$ in SP1-4 and in 500 µL d_6-DMSO in SP5-7. The spectra were acquired on a Bruker 400 MHz equipment at room temperature.

The gel content of the polymers was determined with Soxhlet extractions in THF and the molecular weight distributions (MWDs) of the polymers were measured using size exclusion chromatography in THF. More information about the monomer conversion, particle size, gel content and MWD characterization methods is given in Appendix I.1.

The mechanical properties were evaluated by tensile tests at a strain rate of 10 mm/min (see Section I.2.1 of Appendix I for more information). The dynamic mechanical analysis (DMA) measurements were carried out in a Triton 2000 DMA (Triton Technology) equipped with a liquid nitrogen cooling system. The measurements were performed in tension mode at 1 % deformation and a single frequency of 1 Hz. The samples were cooled down to ≈ −50 °C and heated with a rate of 4 °C min^{-1} until ≈ 100 °C. The linear viscoelastic behavior of the low molar mass polymers was analyzed by conducting frequency sweep tests (0.1 – 100 Hz) at constant temperature and applying a strain of 0.1 %. The experiments were carried out on an Anton Paar rheometer, using ≈ 1 mm thick polymer layers and an 8 mm diameter parallel plate geometry. The results obtained at -10, 1, 10 and 25 °C where then superposed using 10 °C as reference temperature.

2.3. Results and discussion

2.3.1. Pyrrolidone – hydroxyl complexation

2.3.1.1. Synthesis of polymer dispersions with pyrrolidone and hydroxyl groups

After the polymerizations, stable latexes with solids content around 50 % were obtained from Runs L1-L6. The monomer conversion and particle size evolution during the synthesis of the dispersions is shown in Figures 2.7.A and 2.7.B, respectively. In addition, the final monomer conversion and particle size, gel content and molecular weight of the polymers are presented in Table 2.5.

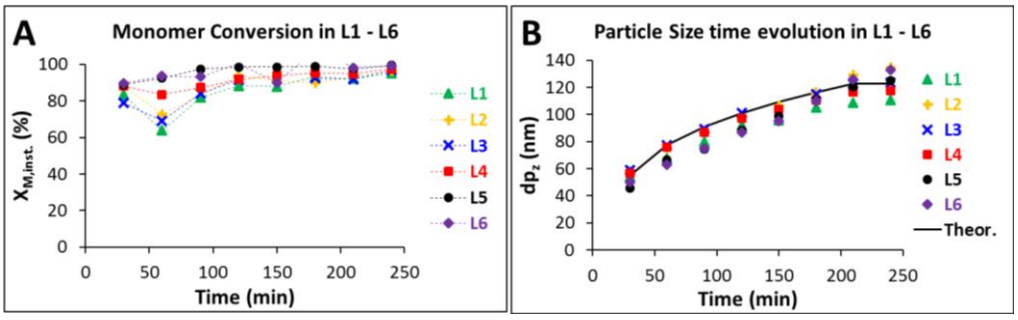

Figure 2.7. (A) Instantaneous monomer conversion and (B) particle size time evolution during the synthesis of Latex 1-6. The theoretical growth of a 55 nm seed assuming that there is neither secondary nucleation nor coagulation during the semibatch stage is shown for comparison.

Table 2.5. Final monomer conversion, particle size, gel content and molecular weight distribution of the polymer dispersions produced in runs L1-L6.

Run	Description	Final X_M (%)	$dp_{z,seed}$ (nm)	$dp_{z,final}$ (nm)	Gel content (%)	M_w (kg/mol)
L1	Blank - 0% F.M.	96.9	54 ± 3	111 ± 2	< 1	480
L2	5% NVP	96.5	58 ± 1	135 ± 1	< 1	680
L3	5% HEMA	97.0	59 ± 1	124 ± 2	< 1	468
L4	5% DHPMA	97.4	57 ± 1	118 ± 1	54	248
L5	2.5% NVP + 2.5% HEMA	99.5	46 ± 1	125 ± 1	13.9 ± 1.3	382
L6	2.5% NVP + 2.5% DHPMA	99.3	50 ± 1	133 ± 1	5.3 ± 0.3	316

Although some differences arose in the instantaneous conversion at short times, largely as a result of some variability in the initial formation of the seed, high instantaneous monomer conversions (X_{inst} > 80%) were obtained during the reactions in all cases. At the end of the reaction, the monomer conversion was higher than 95 % in all polymerizations, suggesting at least the partial incorporation of the functional monomers to the acrylic particles. Regarding the particle size, Figure 2.7.B shows that the polymer seeds formed after 30 minutes of reaction had a particle size of 46 – 59 nm. During the semibatch stage the polymer particles grew until a final particle size between 111 and 135 nm. It is worth mentioning that the experimental particle size values were close to the theoretical dp_z values indicating that no significant secondary nucleation or coagulation of the particles occurred during this stage. Overall, the comparison of the final dp_z values shows that the addition of hydrophilic monomers led to polymer dispersions with slightly higher particle sizes.

Regarding the microstructure of the polymers, the addition of 0.1 % wbm CTA to the formulation led to polymers with gel contents lower than 10 %. The only exception was Latex 4, where 5 wt% DHPMA was copolymerized. This polymer showed a 54 % gel content and the higher crosslinking degree of the polymer was attributed to the presence of 1,3-glyceryl bismethacrylate (the structure is shown in Figure 2.8) that is generated as byproduct in the synthesis of DHPMA. The molar % of this compound in the DHPMA mixture determined by ^{1}H-NMR was ≈ 10 mol%.

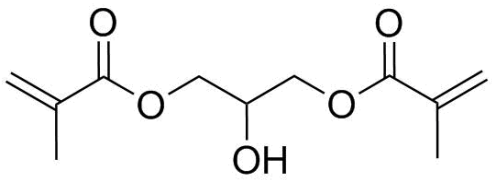

Figure 2.8. Chemical structure of 1,3-glyceryl bismethacrylate.

2.3.1.2. Tensile properties

After the synthesis of the polymer dispersions, the neat dispersions and the latex blends with hydroxyl and pyrrolidone groups were cast and dried for 7 days at standard conditions (23 ± 2 °C and 55 ± 5 % RH). The stress-strain plots are shown in Figure 2.9 and the values obtained from the plots are summarized in Table 2.6.

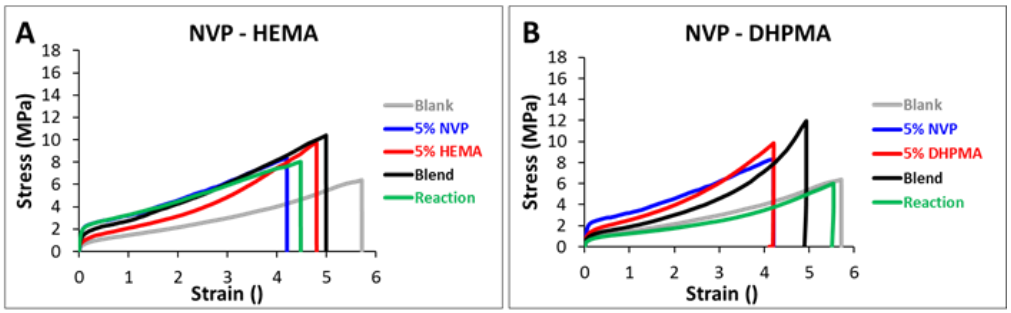

Figure 2.9. Stress−strain plots of the (A) NVP-HEMA and (B) NVP-DHPMA materials with pyrrolidone and hydroxyl groups cast from dispersion and dried for 7 days at standard conditions.

Table 2.6. Mechanical parameters of the NVP-HEMA and NVP-DHPMA materials related to the stress-strain plots presented in Figure 2.9.

Latex	Material	Young's Modulus E (MPa)	Yield stress σ_y (MPa)	Tensile strength σ_{max} (MPa)	Ultimate strain γ_{max} ()
L1	Blank	21 ± 2	0.8 ± 0.1	6.5 ± 1.2	5.4 ± 0.7
L2	5% NVP	57 ± 5	2.1 ± 0.1	8.3 ± 0.1	4.2 ± 0.1
L3	5% HEMA	48 ± 9	1.0 ± 0.1	10.4 ± 0.7	4.9 ± 0.1
L4	5% DHPMA	46 ± 11	1.3 ± 0.5	11.4 ± 0.9	4.1 ± 0.1
L2 -L3 blend	NVP-HEMA blend	53 ± 2	1.5 ± 0.1	9.7 ± 1.1	4.7 ± 0.5
L5	NVP-HEMA same particle	71 ± 12	2.3 ± 0.4	5.3 ± 0.8	8.0 ± 1.2
L2-L4 blend	NVP-DHPMA blend	41 ± 6	1.0 ± 0.1	9.8 ± 2.5	5.3 ± 0.7
L6	NVP-DHPMA same particle	18 ± 3	0.6 ± 0.1	5.9 ± 0.6	5.5 ± 0.6

It can be seen in Figure 2.9 that the blank material without functional monomers prepared from Latex 1 showed the lowest Young's modulus (E), yield stress (σ_y) and tensile strength (σ_{max}) and highest extensibility (γ_{max}). The addition of 5 wt% of NVP, HEMA or DHPMA in Latex 2-4 led to materials with higher E, σ_y and σ_{max}, and lower γ_{max}. In addition, the material with 5 wt% DHPMA showed a strain-hardening behavior caused by the gel fraction of the polymer. However, the materials prepared from the NVP-HEMA and NVP-DHPMA latex blends (black plots) showed

a mechanical behavior in between the starting materials, and no reinforcement coming from the pyrrolidone - hydroxyl H-bond was observed.

There are multiple potential issues that may prevent the establishment of hydrogen bonding and the physical reinforcement of these systems. The first is that in materials prepared from blends of particles with similar particle sizes like the ones discussed herein, the contact points between the two types of particles are limited and this could be a reason for the poor crosslinking and low reinforcement observed for these blends. However, when both pyrrolidone and hydroxyl functionalities were copolymerized in the same dispersion (Latexes 5 and 6), Figure 2.9 shows that there was no major improvement. While the NVP-HEMA Reaction material cast from Latex 5 showed slightly higher E, σ_y and σ_{max} than the analogous NVP-HEMA blend, which could be related to the physical crosslinking of the polymer chains with H-bonds, the NVP-DHPMA Reaction film showed a mechanical behavior similar to the blank, with low E, σ_y and σ_{max}.

To further discard the idea that the lack of reinforcement is due to limited interactions between chains from different particles, the films were annealed for 7 days at 65 °C. The mechanical properties of the annealed films cast from dispersion are presented in Figure 2.10 and Table 2.7. The annealed materials showed higher E, σ_y and σ_{max} which is likely due to the greater interdiffusion of the polymer chains. However, the incorporation of H-bonds did not change the behavior of the NVP-HEMA blend compared to the starting 5% NVP and 5% HEMA films before or after annealing.

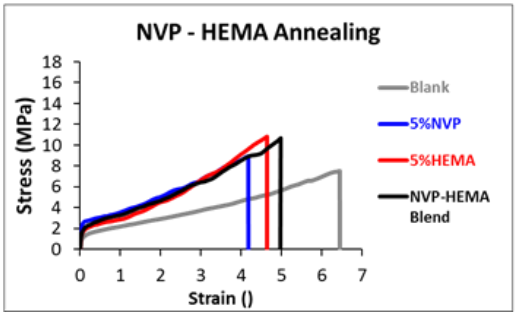

Figure 2.10. Stress−strain plots of the NVP-HEMA and materials with pyrrolidone and hydroxyl groups cast from dispersion, dried for 7 days at standard conditions and 7 days at 65 °C.

Table 2.7. Mechanical parameters of the NVP-HEMA materials related to the stress-strain plots presented in Figure 2.10.

Latex	Material	Young's Modulus E (MPa)	Yield Stress σ_y (MPa)	Tensile strength σ_{max} (MPa)	Ultimate strain γ_{max} ()
L1	Blank	50 ± 9	1.2 ± 0.1	8.4 ± 1.1	6.5 ± 0.5
L2	5% NVP	71 ± 11	2.5 ± 0.2	8.1 ± 0.6	4.2 ± 0.4
L3	5% HEMA	78 ± 10	1.7 ± 0.2	11.6 ± 0.8	4.7 ± 0.1
L2-L3 blend	NVP-HEMA blend	69 ± 9	2.0 ± 0.2	10.2 ± 0.4	5.1 ± 0.5

As a conclusive demonstration that limited interdiffusion and mixing of chains containing different H-bonding groups is not the reason that there is no significant improvement of the mechanical properties, the polymer films cast from the dispersions were redissolved in THF and cast from solution. The tensile test results of the films cast from solution are shown in Figure 2.11 and Table 2.8. The tensile test results show that the pyrrolidone-hydroxyl H-bonds did not affect the mechanical behavior of the films even in the films cast from solution where there is no impediment for the interaction between functional groups or for interdiffusion.

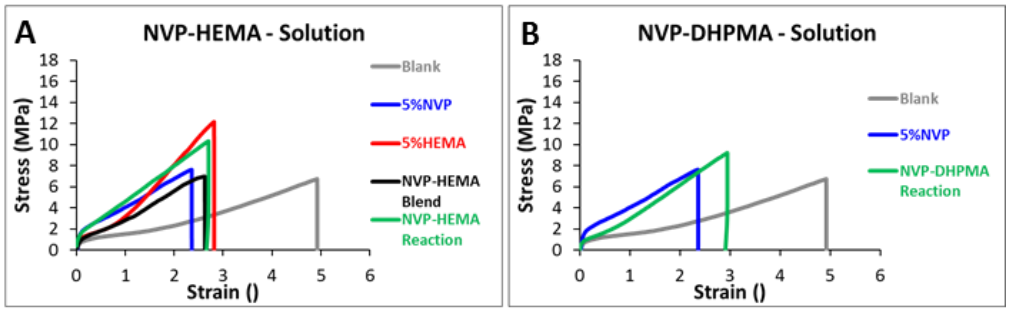

Figure 2.11. Stress−strain plots of the (A) NVP-HEMA and (B) NVP-DHPMA materials with pyrrolidone and hydroxyl groups cast from THF.

Table 2.8. Mechanical parameters of the NVP-HEMA and NVP-DHPMA materials cast from THF solution related to the stress-strain plots presented in Figure 2.11.

Latex	Material	Young's Modulus E (MPa)	Yield stress σ_y (MPa)	Tensile strength σ_{max} (MPa)	Ultimate strain γ_{max} ()
L1	Blank	17 ± 8	0.6 ± 0.2	7.6 ± 1.4	7.6 ± 1.4
L2	5% NVP	32 ± 7	1.4 ± 0.2	7.0 ± 1.3	2.1 ± 0.3
L3	5% HEMA	31 ± 16	1.0 ± 0.2	9.5 ± 2.3	2.8 ± 0.5
L2-L3 blend	NVP-HEMA blend	16 ± 5	0.9 ± 0.2	6.7 ± 1.6	2.6 ± 0.4
L5	NVP-HEMA reaction	46 ± 10	1.2 ± 0.3	10.1 ± 1.2	2.3 ± 0.6
L6	NVP-DHPMA reaction	41 ± 6	0.8 ± 0.1	9.4 ± 1.5	3.1 ± 0.4

An alternative cause of the lack of H-bond reinforcement is the presence of residual water molecules which can interrupt the H-bonds and prevent the physical crosslinking of the polymer chains. To test that hypothesis, the films prepared from the dispersions and dried for 7 days at standard conditions were dried for 2 additional days at 23 °C and high vacuum, to remove the humidity from the polymer films. The results presented in Figure 2.12 and Table 2.9 show that overall the materials showed higher E, σ_y and σ_{max} after drying in vacuum due to the removal of small amounts of water that hydroplasticizes the polymer chains. Nevertheless, the relative

behavior of each material with respect to the others did not change compared to the materials dried at standard conditions and no contribution of the H-bonds was observed. Therefore, the interruption of the physical network by residual water molecules was not the reason for the lack of mechanical reinforcement observed for the H-bonded materials.

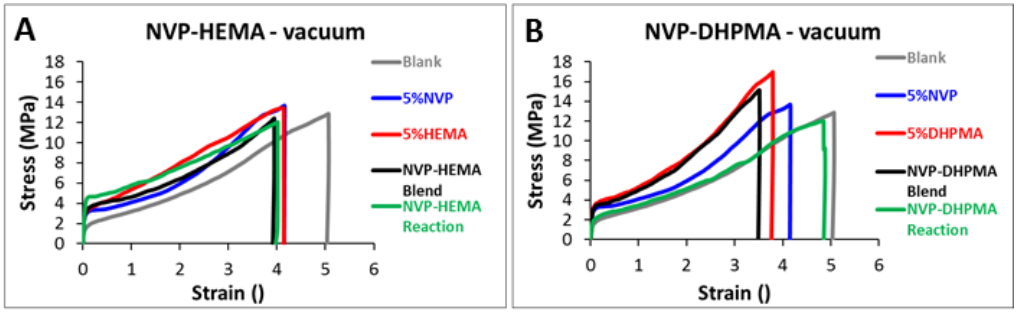

Figure 2.12. Stress−strain plots of the (A) NVP-HEMA and (B) NVP-DHPMA materials with pyrrolidone and hydroxyl groups cast from dispersion and dried for 7 days at standard conditions and 2 days at 23 °C and vacuum.

Table 2.9. Mechanical parameters of the NVP-HEMA and NVP-DHPMA materials related to the stress-strain plots presented in Figure 2.12.

Latex	Material	Young's Modulus E (MPa)	Yield stress σ_y (MPa)	Tensile strength σ_{max} (MPa)	Ultimate strain γ_{max} ()
L1	Blank	67 ± 3	1.4 ± 0.2	10.8 ± 0.2	6.0 ± 0.1
L2	5% NVP	134 ± 45	2.4 ± 0.6	14.2 ± 0.3	3.9 ± 0.2
L3	5% HEMA	125 ± 25.	2.7 ± 0.6	14.2 ± 0.1	4.0 ± 0.2
L4	5% DHPMA	152 ± 23	3.3 ± 0.1	17.2 ± 0.8	3.9 ± 0.1
L2-L3 blend	NVP-HEMA blend	133 ± 19	3.2 ±0.6	14.7 ± 1.6	4.6 ± 0.5
L5	NVP-HEMA reaction	125 ± 9	4.6 ± 0.2	12.7 ± 0.6	3.8 ± 0.2
L2-L4 blend	NVP-DHPMA blend	121 ± 8	2.7 ± 0.5	15.4 ± 1.0	3.7 ± 0.2
L6	NVP-DHPMA reaction	75 ± 16	1.6 ± 0.3	12.2 ± 1.1	5.0 ± 0.3

It is clear from the above that the pyrrolidone-hydroxyl system is not capable of providing significant mechanical reinforcement. This may be related to the relatively low concentration of H-bonds or the limited strength of the H-bonds. Since concentrations above around 5 wt% functional monomer become impractical, we therefore decided to move to the use of stronger H-bonding systems. In the next section, the double H-bond between uracil and adenine groups which has a K_a nearly 100 times greater than the pyrrolidone – hydroxyl complexation was utilized to crosslink the polymer chains and reinforce mechanically the polymer films.

2.3.2. Uracil – adenine complexation

The objective of this part of the work was to produce polymer dispersions with uracil and adenine functional groups to prepare materials reinforced with H-bonds. First, acrylic monomers with uracil and adenine groups were synthesized; then, the functional monomers were incorporated to acrylic polymer dispersions by batch emulsion polymerization and the mechanical properties of the films were analyzed by tensile test.

2.3.2.1. Synthesis of polymer dispersions with uracil and adenine groups

3 weight% of uracil acrylate and adenine acrylate were incorporated to the batch emulsion polymerization of MMA / BA to prepare functional polymer dispersions with uracil and adenine groups in runs NB2 and NB3, respectively. One more dispersion without functional monomers was produced using the same polymerization procedure in NB1 as reference. The monomer conversion during runs NB 1-3 is shown in Figure 2.13. The final monomer conversion, particle size, gel content and molecular weight of the polymers produced in NB 1 – 3 are presented in Table 2.10.

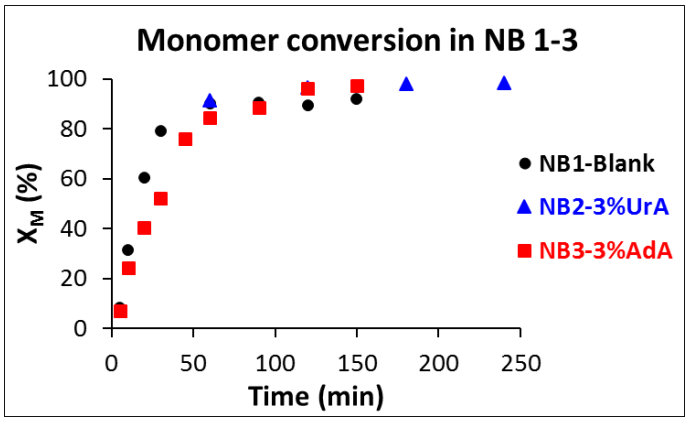

Figure 2.13. Monomer conversion time evolution in runs NB 1–3.

Table 2.10. Final monomer conversion, particle size, gel content and molecular weight distribution (soluble fraction after the Soxhlet extraction) of the polymer dispersions produced in runs NB 1-3.

Latex	Final X_M (%)	$dp_{z,final}$ (nm)	Gel content (%)	$M_{w,\ sol.}$ (kg/mol)	Đ
NB1 - Blank	92	206	26	702	2.0
NB2 – 3% UrA	98	220	84	167	2.6
NB3 – 3% AdA	97	331	50	519	2.2

Stable polymer dispersions with solids content around 40 % were obtained in the three reactions. The monomer conversions at the end of the polymerizations were 92 % in NB1 (blank), 98 % in run NB2 (3 wt% UrA) and 97 % in NB3 (wt% AdA), which suggested at least the partial incorporation of the functional monomers into the polymer backbone. The final particle sizes varied in the range 200 – 300 nm probably due to differences in the nucleation process. The gel content of the blank copolymer with a composition of 50/50 MMA/BA was 26% and the copolymers with 3 wt% UrA and 3 wt% AdA presented gel contents of 84 and 50 %, respectively. In polymerizations carried out without crosslinker, gel is typically formed from intermolecular chain transfer to polymer reactions from acrylic radicals followed by propagation or bimolecular

termination.[21] These reactions are favored at high monomer conversions when the concentration of monomer in the system is low and the concentration of polymer is high, which increases the probability for chain transfer relative to propagation. In runs NB2 and NB3 with 3 wt% of the nucleobase-containing acrylic monomers the monomer conversion was higher than in NB1, which enhanced the chain transfer and crosslinking events at the end of the polymerizations and led to higher gel contents. The extent of crosslinking reactions and thus the gel content was higher in NB2 due to the longer polymerization time.

2.3.2.2. Tensile properties

After the synthesis of the polymer dispersions, the neat latexes and the UrA-AdA latex blend were cast into silicone molds and dried for 7 days at 23 ± 2ºC and 55 ± 5% RH. The effect of the H-bonds on the mechanical properties was evaluated by tensile test. The tensile test results are shown in Figure 2.14 and Table 2.11.

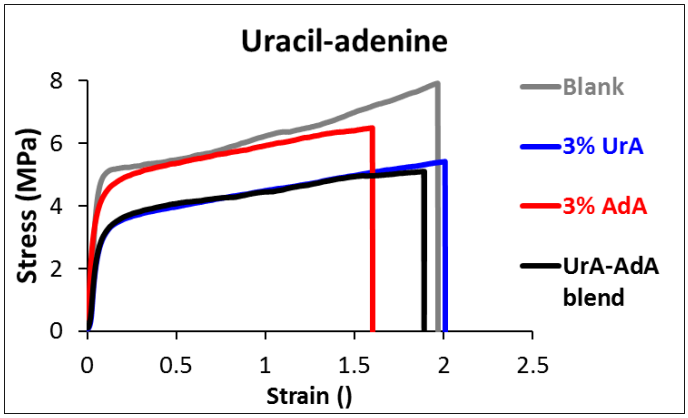

Figure 2.14. Stress−strain plots of the UrA-AdA materials prepared from runs NB1-3.

Table 2.11. Mechanical parameters of the UrA-AdA materials related to the stress-strain plots presented in Figure 2.14.

Latex	Material	Young's Modulus E (MPa)	Yield stress σ_y (MPa)	Tensile strength σ_{max} (MPa)	Ultimate strain γ_{max} ()
NB1	Blank	144 ± 13	5.0 ± 0.4	7.8 ± 0.8	1.7 ± 0.4
NB2	3 wt% UrA	83 ± 14	3.3 ± 0.3	5.5 ± 0.4	1.7 ± 0.4
NB3	3 wt% AdA	155 ± 46	5.1 ± 0.8	7.0 ± 1.0	1.5 ± 0.2
NB2-NB3 blend	UrA-AdA Blend	77 ± 13	3.3 ± 0.2	5.2 ± 0.3	1.7 ± 0.2

All the materials showed an ultimate strain between 1.5 and 2. The blank and 3 wt% AdA materials had an elastic modulus near 150 MPa, a yield stress or around 5 MPa and a tensile strength of 7 MPa, and the 3 wt% UrA and AdA-UrA blend materials showed an elastic modulus of ≈ 80 MPa, a yield stress of 3.3 MPa and a tensile strength between 5.2 and 5.5 MPa. However, no reinforcement coming from the uracil-adenine H-bonds was observed. In these materials, the lack of reinforcement could be related to the low concentration of uracil and adenine groups in the films (≈1 mol%). In addition, the considerable differences in the gel contents and molar masses of the polymers may hide any effect of H-bonds. More importantly, similar to the pyrrolidone-hydroxyl system, the strength of the linkage might still be low to efficiently crosslink the polymer chains and reinforce the films. Thus, in order to gain information about the contribution of the analyzed H-bonds to the mechanical strength of the films, the ability of these relatively weak H-bonds to crosslink the polymer chains in copolymer systems was analyzed in Section 2.3.3.

2.3.3. Rheological behavior of functional low molar mass polymers

The ability of the pyrrolidone-hydroxyl and uracil-adenine H-bonds to physically crosslink low molar mass polymer chains was investigated to evaluate the contribution of these interactions into the mechanical strength of the polymer films and understand the behavior of the systems presented in Sections 2.3.1 and 2.3.2. First, low molar mass copolymers with the functional groups were prepared by high temperature solution polymerization. Then, the rheological response of the materials was analyzed to understand the influence of the H-bonds in each system. The molecular weights of the polymers employed for the analysis were below the critical entanglement molecular weight ($M_{C,MMA} \approx 10\ 000$ g mol^{-1})[22] to eliminate the effect of entanglements and isolate the effect of the H-bonds on the rheological response of the polymers.[23,24]

2.3.3.1. High temperature solution polymerizations

High temperature semibatch solution polymerizations were conducted to synthesize functional acrylic polymers with molecular weights below the critical entanglement molecular weight. First, copolymers with pyrrolidone and hydroxyl groups were prepared in m-xylene copolymerizing 20 wt% NVP (SP2) or HEMA (SP3) with MMA/BA. One copolymer with both functionalities was prepared in SP4 adding 10 wt% NVP and 10 wt% HEMA to the synthesis. Copolymers with uracil and adenine groups were prepared adding 20 wt% uracil acrylate (UrA, SP5) and 20 wt% AdA (SP7) to the copolymerization of MMA/BA in DMF. The blank copolymers without H-bonding groups were also produced in SP1 (in m-xylene) and SP5 (in DMF) to serve as reference. The global monomer conversions in SP1-4 and SP5-7 are shown Figures 2.15.A and 2.15.B, respectively. The theoretical global conversion for an instantaneous monomer conversion of 100% is plotted in Figure 2.15 for comparison. In addition, the final overall

monomer conversion, the final conversion of the functional monomer(s) and the molecular weight distribution results are presented in Table 2.12.

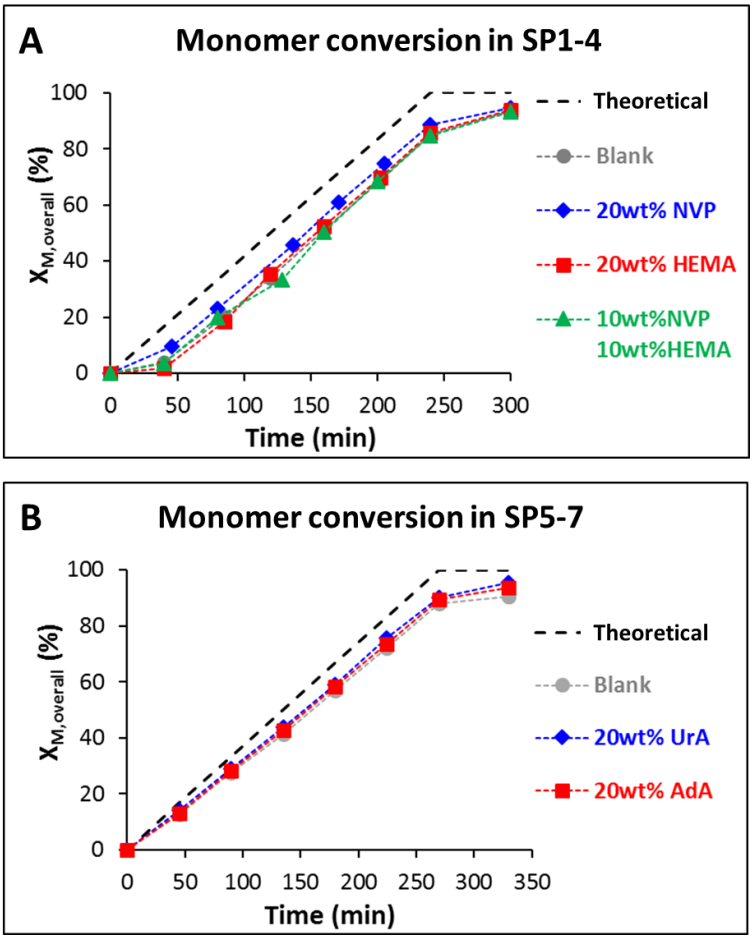

Figure 2.15. Overall monomer conversion time evolution in the high temperature solution polymerizations carried out in (A) m-xylene in SP1-4 and (B) DMF in SP5-7.

Table 2.12. Monomer conversion and SEC results of the copolymers produced in SP1-7. *The monomer conversion given for UrA and AdA corresponds to the conversion of acrylates (BA + nucleobase containing monomers) due to the similarity of the signals in the ^{1}H-NMR spectrum. N is the number average of functional groups per chain calculated according to Equation 2.1.

Copolymer	$X_{M,overall}$ (%)	$X_{F.M.}$ (%)	M_n (g mol^{-1})	M_w (g mol^{-1})	Đ	N
SP1 – Blank	93.4	-	2400	6800	2.9	0
SP2 – 20 wt% NVP	94.7	NVP 87.5	3300	7400	2.2	5.5
SP3 – 20 wt% HEMA	94.0	HEMA 97.2	2400	7600	3.2	3.8
SP4 – 10 wt% NVP + 10 wt% HEMA	93.0	NVP 92.3 HEMA 94.8	2400	7100	2.9	4.0
SP5 – Blank	90.2	-	5500	9500	1.7	0
SP6 – 20 wt% UrA	94.9	UrA* 93.5	4000	8200	2.0	2.5
SP7 – 20 wt% AdA	93.3	AdA* 91.7	3800	7400	1.9	2.2

Figure 2.15 shows that for SP1-4, the monomer conversion and the polymerization rate were low in the first 40 minutes of reaction due to the low monomer concentration in the system. Then, as the amount of monomer fed to the reactor increased, the polymerization rate increased and the global monomer conversion increased with time reaching values higher than 93 % at the end of the reactions. Figure 2.15.B shows that in SP5-7 the global monomer conversion increased linearly and reaching final values higher than 90% at the end of the process. In all the reactions, the conversion of the functional monomers at the end of the polymerizations was higher than 87.5% (Table 2.12), which ensured a high incorporation of the functional groups into the copolymers.

After the synthesis, the molecular weight of the copolymers was measured by SEC in THF. In addition, the average number of functional groups per polymer chain (N) was calculated using the Equation 2.1, where M_n is the number average molar mass of the polymer, $w_{F.M.}$ is the

weight fraction of the functional monomer in the formulation, $X_{F.M.}$ is the conversion of the functional monomer and $MW_{F.M.}$ is the molar mass of the functional monomer.

$$N = \frac{M_n * w_{F.M.} * X_{F.M.}}{MW_{F.M.}} \qquad \text{Equation 2.1}$$

The polymers synthesized in m-xylene (SP1-4) presented a weight average molecular weight (M_W) of around 7000 g mol^{-1} and the polymers prepared in DMF (SP5-7) had slightly higher M_W-s in the range of 7400 and 9500 g mol^{-1}. In both cases, the M_w was below the critical entanglement molecular weight ($M_{C,MMA}$ ≈ 10 000 g mol^{-1})[22] as targeted. The absence of entanglements between the polymer chains ensures that the changes in the mobility of the polymer chains will exclusively be caused by the H-bonds. In addition, from the molecular weight and monomer conversion results it was estimated that there was an average of 5 pyrrolidone groups per chain in SP2, 4 hydroxyl groups per chain in SP3 and 4 pyrrolidone+hydroxyl groups in SP4. For the copolymers produced in DMF in SP6 and SP7, there was an average of 2.5 uracil and 2.2 adenine groups per chain. In all the copolymers, the functionality of the polymer chains was higher than 2 allowing potential formation of a physically crosslinked 3D polymer network.

2.3.3.2. Rheological behavior

The linear viscoelastic behavior of the low molar mass copolymers was analyzed by conducting frequency sweep tests at constant temperatures and applying a strain of 1 %. The frequency mastercurves obtained for the SP1-4 copolymers with different pyrrolidone and hydroxyl contents are presented in Figure 2.16 and the frequency mastercurves obtained for the SP5-7 copolymers with uracil and adenine groups are shown in Figure 2.17.

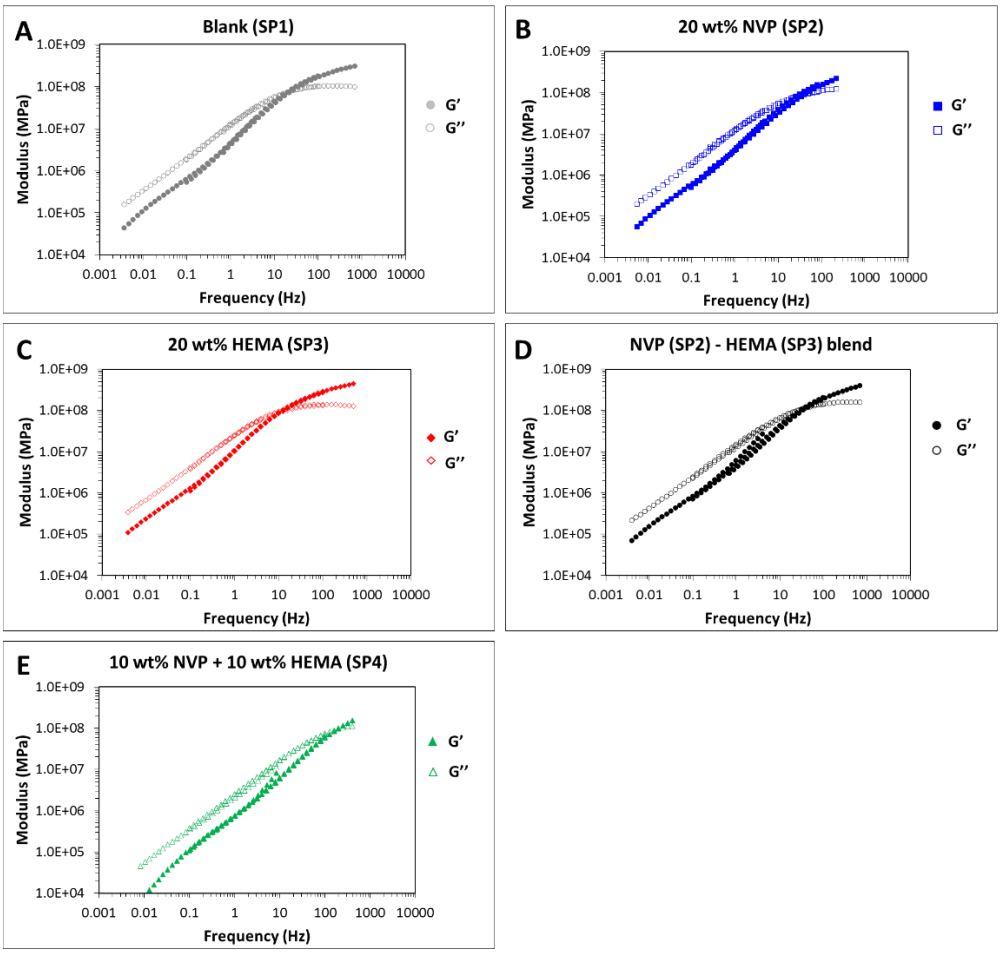

Figure 2.16. Frequency mastercurves of the copolymers with different pyrrolidone and/or hydroxyl contents: (A) blank (SP1), (B) 20 wt% NVP (SP2), (C) 20 wt% HEMA (SP3), (D) 20 wt% NVP (SP2) – 20 wt% HEMA (SP3) blend and (E) 10 wt% NVP + 10 wt% HEMA (SP4). The storage modulus (G') is represented with closed symbols and the loss modulus (G'') with open symbols.

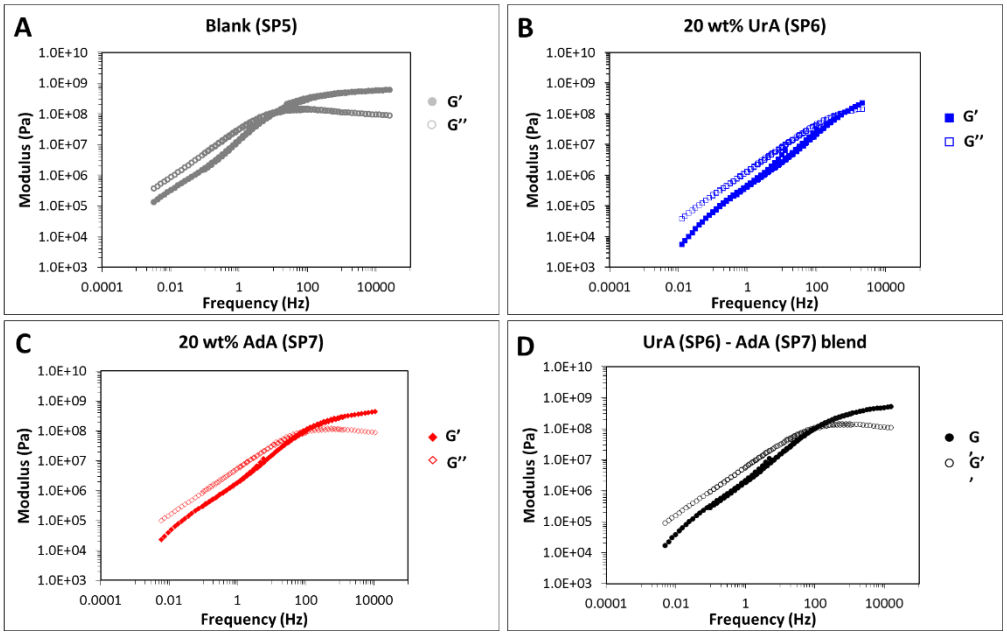

Figure 2.17. Frequency mastercurves of the copolymers with different uracil and adenine contents: (A) blank (SP5), (B) 20 wt% UrA (SP6), (C) 20 wt% AdA (SP7) and (D) 20 wt% UrA (SP6) – 20 wt% AdA (SP7) blend. The storage modulus (G') is represented with closed symbols and the loss modulus (G'') with open symbols.

Analysis of Figures 2.16 and 2.17 shows that all the polymer and polymer blends showed a liquid-like behavior (G'' > G') at low frequencies and solid-like behavior (G' > G'') at high frequencies. The transition between these two regions, namely the G' – G'' crossover, was very similar in the materials provided with and without H-bonds. The results suggested that the pyrrolidone-hydroxyl and uracil-adenine physical interactions did not efficiently crosslink the polymer chains and impact the rheology of the polymer blends. In the next section we will therefore consider theoretically the expected rheological behavior of polymers containing associative hydrogen bonding groups in relation to the results shown in this chapter and the implications for the design of H-bond reinforced films from latex systems.

2.3.4. Fundamental considerations for physically crosslinked waterborne polymer dispersions

Taking the elastic modulus as a primary measure of the influence of the hydrogen bonding on the rheological properties of the material we can characterize a physically bonded system with respect to conventional linear and chemically crosslinked systems (see Figure 2.18).

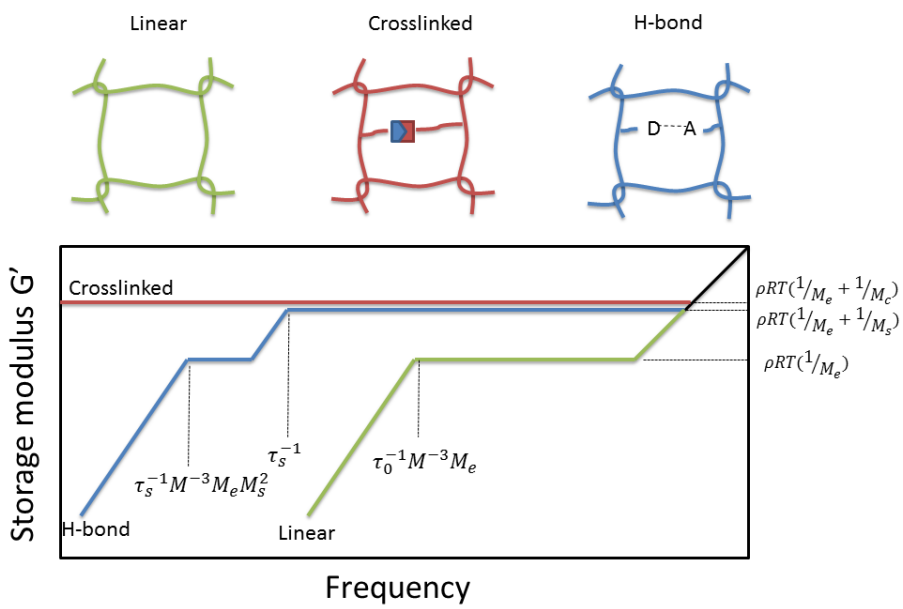

Figure 2.18. Storage modulus (G') behavior for linear, covalently crosslinked and physically crosslinked polymers. Reproduced and modified with permission from Royal Society of Chemistry.[25]

For an entangled, linear polymer the frequency dependent modulus takes a characteristic form with a plateau modulus that is determined by the molecular weight between entanglements, M_e, such that

$$G' = \rho RT(^1/_{M_e}) \qquad \text{Equation 2.2}$$

The reptation of the entangled chains leads to a terminal relaxation time given by

$$\tau_{rep} \approx \frac{\tau_0 M^3}{M_e} \qquad \text{Equation 2.3}$$

where M is the number average molecular weight, M_e is the average molecular weight between entanglements and τ_0 is the monomer relaxation time.[25] In chemically crosslinked systems the plateau modulus is increased due to the crosslink points that are established to give a plateau modulus given by

$$G' = \rho RT({}^{1}/_{M_e} + {}^{1}/_{M_c}) \qquad \text{Equation 2.4}$$

The crosslinking points prevent chain diffusion and therefore the terminal relaxation time present in linear systems disappears. In terms of mechanical properties both the increase in modulus and the absence of relaxation results in improved performance. In a physically crosslinked system, the sticky reptation theory also predicts an increased plateau modulus at times shorter than the timescale on which the hydrogen bonds are dissociated with a value of[26]

$$G' = \rho RT({}^{1}/_{M_e} + {}^{1}/_{M_s}) \qquad \text{Equation 2.5}$$

Where M_s is the molecular weight between hydrogen bonding groups. For a frequency of τ_s^{-1} (the inverse of the lifetime of the H-bond) the hydrogen bonds break and only the entanglements contribute to the value of G'. Furthermore, the terminal relaxation time is increased relative to the linear case to give a relaxation time given by[25]

$$\tau_{Rep,Ass} = \frac{\tau_s M^3}{M_e {M_s}^2} \qquad \text{Equation 2.6}$$

Where τ_s is the lifetime of the hydrogen bond. Thus, in the case of hydrogen bond modified polymer networks, the rheological behavior is dependent on the molecular weight between associative groups and the lifetime of the hydrogen bond.

The average molecular weight between associative groups depends on molar content of the associative groups in the polymer chains but can also be understood as a function of hydrogen bond strength. As explained in the introduction chapter, a hydrogen bond is the electrostatic attraction between an electron-rich electronegative atom (H-bond acceptor) and an electron-deficient proton (H-bond donor).[27,28] Here we consider only isolated bonds but it should be noted that single H-bonds can cooperatively participate in integrated structures leading to complexes with higher binding strengths. Overall, the formation of a H-bond can be expressed as the interaction between group “A” and group “B” to give complex “C” as shown in Scheme 2.2.

$$A + B \rightleftharpoons C$$

Scheme 2.2. Hydrogen bond association equilibrium.

The concentration of “A”, “B” and “C” species in equilibrium is given by the association constant (K_a) of the complex as expressed in Equation 2.7.

$$K_a = \frac{[C]}{[A][B]} \qquad \text{Equation 2.7}$$

For the case the initial concentration of “A” and “B” groups is equal ($[A]_0 = [B]_0$), and defining [A] as $[A]_0 - [C]$, the expression of K_a can be rewritten as in Equation 2.8.

$$K_a = \frac{[C]}{([A]_0 - [C])^2} \qquad \text{Equation 2.8}$$

Then, Equation 2.8 can be solved for [C] as shown in Equation 2.9. Note that the positive solution of the equation is not considered because [C] cannot exceed $[A]_0$.

$$[C] = \frac{2K_a[A]_0+1-\sqrt{4K_a[A]_0+1}}{2K_a} \qquad \text{Equation 2.9}$$

Therefore, Equation 2.8 can be used to estimate the concentration of crosslinks in a polymer system. In addition, a more intuitive and practical way to evaluate and compare crosslinking efficiency of H-bonds is the bonding %, which is defined as the percentage of bonded "C" groups with respect to the initial concentration of "A" groups ($[A]_0$) as expressed in Equation 2.10.[29]

$$Bonding\% = \frac{[C]}{[A]_0} x100 \qquad \text{Equation 2.10}$$

The combination of Equations 2.9 and 2.10 leads to Equation 2.11 which allows the direct calculation of the bonding % in the system for given K_a and $[A]_0$ values. The bonding % in each system will determine the average molar mass between stickers (M_s) and thus, the rheological behavior of physically crosslinked polymer networks.

$$Bonding\% = \frac{[C]}{[A]_0} 100 = \frac{2K_a[A]_0+1-\sqrt{4K_a[A]_0+1}}{2K_a[A]_0} 100 \qquad \text{Equation 2.11}$$

The bonding % in the NVP-HEMA and UrA-AdA solution polymer blends at different concentrations was calculated using equation 2.11 to evaluate the efficiency of crosslinking in each system. In addition, the bonding % in homologous polymers functionalized with guanine-cytosine (G-C) triple H-bonds and self-complementary ureidopyrimidinone (Upy-Upy) quadruple H-bonds were calculated for discussion. The K_a and $[A]_0$ parameters used for the calculations and the bonding % results are presented in Table 2.13. The initial molar concentration of "A" H-

bonding groups ($[A]_0$) was calculated considering the weight fraction of the monomers was 10/10/30/50 FM_A/FM_B/MMA/BA in the pyrrolidone-hydroxyl, uracil-adenine and guanine-cytosine complementary H-bonding polymers and 20/30/50 UPy/MMA/BA in the self-associating polymer.

Table 2.13. K_a, $[A]_0$ and bonding % in polymers functionalized with pyrrolidone-hydroxyl, uracil-adenine, guanine-cytosine and Upy-Upy H-bonds.

H-bond	K_a (L mol^{-1})	$[A]_0$ (mol L^{-1})	Bonding %
Pyrrolidone – hydroxyl	1 (ref.17)	0.90	36.4
Uracil – adenine	100 (ref.4)	0.30	83.3
Guanine – cytosine	1000 (ref.4)	0.29	98.1
Upy – Upy	1000000 (ref.4)	0.61	99.9

Table 2.13 shows that the association constant greatly influences the bonding % and thus, the crosslinking efficiency of a H-bonding system. Pyrrolidone – hydroxyl H-bonds have a low K_a around 1 M^{-1} and thus only 36.4 % of the functional groups were in the complexed state in the SP2-SP3 blend and SP4 polymer presented in Figure 2.16. In the latex system, this value would be substantially lower due to the lower concentrations of H-bonding units. Uracil-adenine H-bonds have a higher association constant near 100 M^{-1} which enhanced the bonding % in the SP6-SP7 blend to 83.3 %. Higher K_a complexes such as guanine-cytosine or Upy-Upy H-bonds are expected show bonding percentages of 98.1 and 99.9 %, respectively. Thus, while the relatively weak NVP-HEMA and uracil-adenine H-bonds utilized in this work can only lead to partial complexation and limited crosslinking of the polymer chains, stronger complexes would allow the complete crosslinking of the system.

The second factor that determines the crosslinking efficiency of H-bonds and their contribution to the rheology and mechanical strength of polymers is lifetime of species “C” before

dissociating into “A” and “B” species. This is crucial to determine whether the hydrogen bonds that are established have any influence on the rheology of the material. This has previously been demonstrated by Lewis and coworkers,[24] who studied the rheological behavior of low molar mass ($M_w < M_c$) polybutyl acrylate (PBA) chains with increasing amounts of acrylamidopyridine (AP), acrylic acid (AA), carboxyethylacrylate (CEA) and ureidopyrimidinone (UPy). Low K_a H-bonds such as the interactions between AP, AA or CEA units, denominated as “weak interactions”, had complex lifetimes shorter than the experimental time scale and no significant influence of the H-bonds on the rheological behavior of the polymers was observed, until very high amounts of functional monomer were added (see Figure 2.19). Similar conclusions for weakly interacting H-bond units were obtained in the work of Hawke *et al*[30] and Shabbir *et al*.[31] In contrast, high K_a associates such as the H-bond between two ureidopyrimidinone units (Upy) have significantly longer lifetimes and display a well-defined G’ plateau, even at Upy contents as low as 1 mol % (see Figure 2.19). This result has been reproduced in a number of similar examples in the literature that show strong H-bonds can efficiently crosslink polymer chains. [1–3,5,13,23,24,32–37]

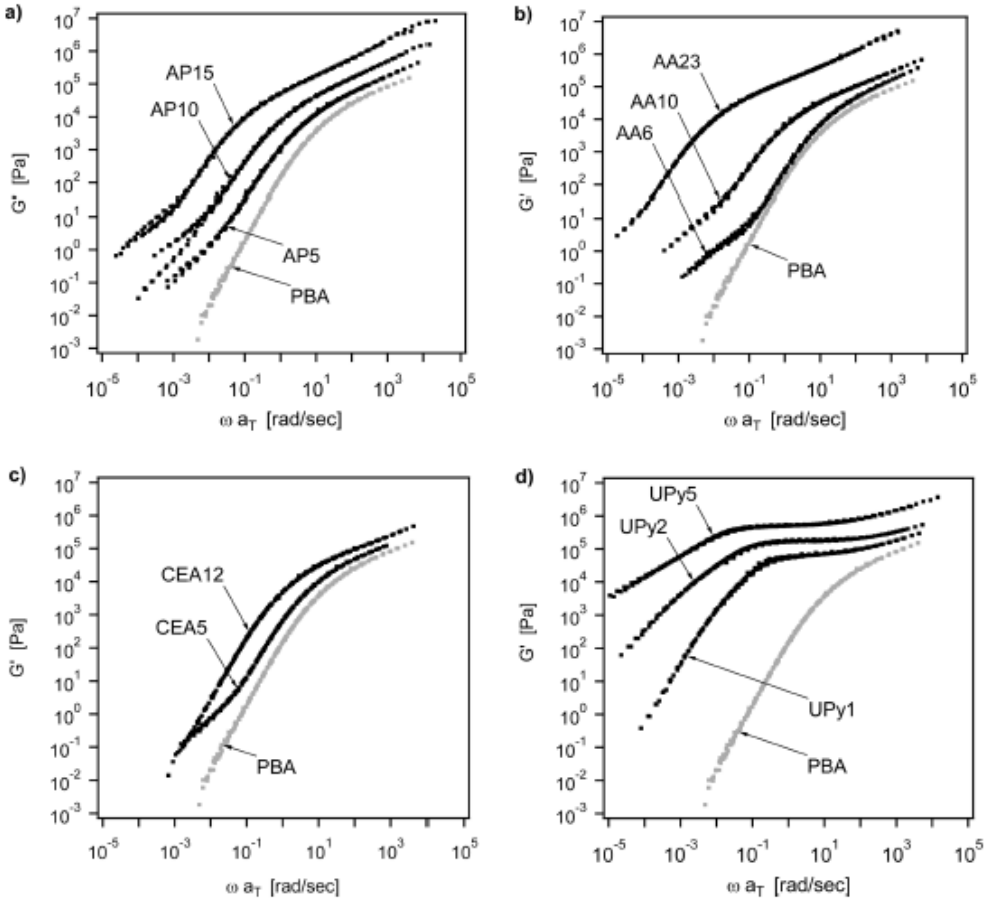

Figure 2.19. Storage modulus mastercurves referenced to 25 °C of linear copolymers containing (a) acrylaminopyridine (AP), (b) acrylic acid (AA), (c) carboxyethyl acrylate (CEA), and (d) UPy acrylate monomers. The number after the functional monomer expresses the mol % of functional monomer employed in the formulation. Reprinted with permission from American Chemical Society.[24]

Based on the results in this chapter and from previous investigations of the rheological behavior of weakly associating hydrogen bonding groups in the literature we can therefore highlight two major stumbling blocks that can arise when using weakly associating H-bond motifs to physically crosslink films cast from polymer latexes. The first is that the association constant

must be sufficient to establish a high number of hydrogen bonds when present at low concentration. The second is that the hydrogen bonds do not efficiently reinforce the mechanical properties unless the bond lifetime is sufficiently high to restrict reptation by interchain associative bonding. This second issue is likely important for most moderately associating H bond systems (K_a<1000 M^{-1}) which form hydrogen bond networks but are highly dynamic.

These results also point to two alternatives to ensure that hydrogen bonds can contribute to the improvement of mechanical properties. The first alternative, which will be the focus of much of the remainder of this thesis, would be the use of weakly associating units at much higher local concentrations and in blocky structures. In these circumstances, weak single H-bonds can work cooperatively to form sticky junctions that present complex lifetimes higher than the individual H-bonds and lead to crosslinked materials.[11]

A second alternative is to use hydrogen bond motifs with higher association constants/longer bond lifetimes. However, although crosslinking of polymer chains by strong H-bonds has been demonstrated in solvent based systems, there are few examples where such chemistries are implemented practically for the mechanical reinforcement of waterborne systems.[7,8,38] In these systems the high equilibrium constants that lead to improved mechanical properties also result in low solubility in typical solvent systems and require cosolvent for successful polymerization. For example, Chen and coworkers reported the emulsion copolymerization of MMA/BA with 1.5 mol% of a Upy-containing monomer, but the synthesis used >100% wbm of chloroform to ensure solubility of the Upy monomer.[38] In the work carried out by Qiu *et al.,* 1 to 5 mol% of Upy-containing monomer was incorporated to the synthesis of acrylic polymer particles using 30 wt% of AA to solubilize the Upy monomer in the monomer mixture.[8] The polymer films showed increasing Young's modulus, yield stress and tensile strength with the Upy content. Nevertheless, the high AA content employed in the formulation

would be expected to make these polymer films very water sensitive, limiting the practical application of this formulation. Similarly, Karikari *et al.* utilized 8 wt% MAA to solubilize 2 wt% of a Upy containing monomer to produce aqueous floor coatings with improved durability.[7]

In order to gauge the potential of such high H-bond strength systems, an attempt was made to incorporate the Upy functionality to an acrylic polymer dispersion. First, a Upy monomer containing an α-methyl styrene polymerizable group was synthesized according to the procedure described by Karikari (chemical structure shown in Figure 2.20).[7]

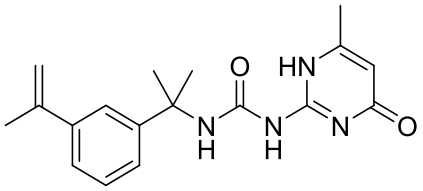

Figure 2.20. Chemical structure of UPy functionalized α-methyl styrene monomer synthesized by Karikari *et al.*[7]

Then, 1 wt% of the Upy monomer was solubilized in a 50/50 MMA/BA monomer mixture using 7 wt% NVP and 1 wt% AA hydrophilic monomers in the formulation and the monomer mixture was polymerized by seeded semibatch emulsion polymerization according to the procedure of Haddock *et al*.[18] Stable latexes were achieved but no influence of the quadruple H-bonds was observed in the tensile test of the films cast from the latex with 1 wt% Upy shown in Figure 2.21, very likely due to the low concentration of UPy groups in the polymer matrix (≈ 0.3 mol%). Increasing the Upy monomer content in the formulation requires higher AA and NVP concentrations which, as in previous examples, would compromise the water sensitivity of the films.

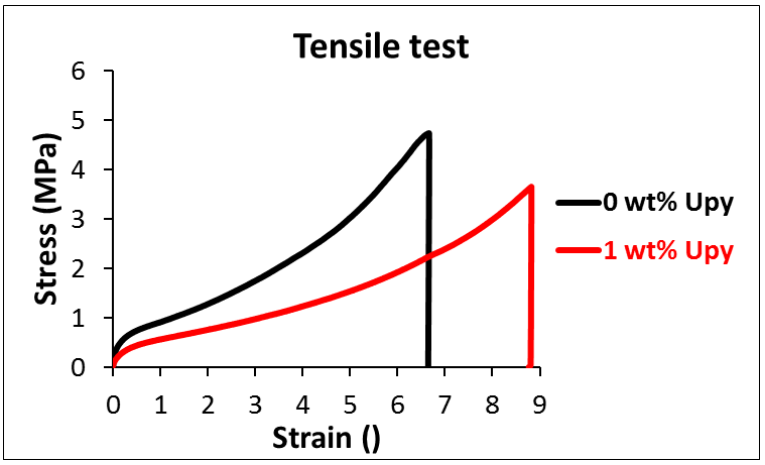

Figure 2.21. Stress−strain plots of the PMMA/BA films functionalized with 0 and 1 wt% (≈ 0.3 mol%) Upy monomer.

2.4. Conclusions

In this chapter, the possibility of using pyrrolidone – hydroxyl and uracil – adenine H-bonds to physically crosslink the polymer chains and mechanically reinforce the polymer films from waterborne dispersions was investigated.

First, functional polymer dispersions with pyrrolidone, hydroxyl, uracil or adenine H-bonding groups were synthesized by emulsion polymerization. Polymer dispersions with complementary H-bonding groups were combined and the dispersions were cast and dried to obtain polymer films provided with pyrrolidone – hydroxyl and uracil – adenine H-bonds. All the materials cast from the functional dispersions and blends showed very similar mechanical behavior, and no influence of the H-bonds on the mechanical properties of the films was observed. In the pyrrolidone – hydroxyl materials, the lack of reinforcement was ascribed to the low binding energy and association constant ($K_a \approx 1\ M^{-1}$) of the interaction which limits the number of hydrogen bonds formed in the films. The uracil – adenine interaction has a higher binding strength which allows the buildup of physical networks. In this case, the lack of reinforcement was attributed to the low concentration of the H-bonds (≈ 1 mol%) coupled with the short lifetime of the hydrogen bond, thus preventing their effective reinforcement of the mechanical properties. It can be concluded that for the mechanical reinforcement of the polymer films, it is necessary to use H-bonding motifs with stronger interactions such as cytosine-guanine or Upy-Upy. Nevertheless, the low solubility of such groups in water, common organic solvents and monomer mixtures limits the practical implementation of these systems. The other alternative is to employ weakly associating units at much higher local concentrations and in blocky structures. In these circumstances, weak single H-bonds can work cooperatively to form sticky junctions that present complex lifetimes higher than the individual H-bonds and may lead to crosslinked materials with greater mechanical resistance.

2.5. References

(1) Yamauchi, K.; Lizotte, J. R.; Long, T. E. Thermoreversible poly(alkyl acrylates) consisting of self-complementary multiple hydrogen bonding *Macromolecules* **2003**, *36*, 1083–1088.

(2) Yamauchi, K.; Kanomata, A.; Inoue, T.; Long, T. E. Thermoreversible Polyesters Consisting of Multiple Hydrogen Bonding (MHB) *Macromolecules* **2004**, *37*, 3519–3522.

(3) Elkins, C. L.; Park, T.; Mckee, M. G.; Long, T. E. Synthesis and Characterization of Poly (2-ethylhexyl methacrylate) Copolymers Containing Pendant, Self-Complementary Multiple-Hydrogen-Bonding Sites *J. Polym. Sci. Part A Polym. Chem.* **2005**, *43*, 4618–4631.

(4) Wilson, A. J. Non-covalent polymer assembly using arrays of hydrogen-bonds *Soft Matter* **2007**, *3*, 409–425.

(5) Feldman, K. E.; Kade, M. J.; Meijer, E. W.; Hawker, C. J.; Kramer, E. J. Model Transient Networks from Strongly Hydrogen-Bonded Polymers *Macromolecules* **2009**, *42*, 9072–9081.

(6) Chen, Y.; Ballard, N.; Gayet, F.; Bon, S. A. F. High internal phase emulsion gels (HIPE-gels) from polymer dispersions reinforced with quadruple hydrogen bond functionality *Chem. Commun.* **2012**, *48*, 1117–1119.

(7) Karikari, A. S.; Tysak, T. Floor coating compositions containing supramolecular polymers. US 2016/0230035 A1, 2016.

(8) Qiu, T.; Wang, X.; Lin, X.; Zhu, Z.; Li, X.; Guo, L. Emulsion Polymerization to Synthesize Self-Healing Films Toward Healing on Fractures: A Feasible Strategy *J. Polym. Sci. Part A Polym. Chem.* **2016**, *54*, 3071–3078.

(9) Sukul, P. K.; Malik, S. Supramolecular hydrogels of adenine: morphological, structural and rheological investigations *Soft Matter* **2011**, *7*, 4234–4241.

(10) Cheng, S.; Zhang, M.; Dixit, N.; Moore, R. B.; Long, T. E. Nucleobase self-assembly in supramolecular adhesives *Macromolecules* **2012**, *45*, 805–812.

(11) Lei, Y. Supramolecular Polymeric Networks via Hydrogen Bonding in Ionic Liquids, University of Minnesota, 2012.

(12) Feldstein, M. M.; Dormidontova, E. E.; Khokhlov, A. R. Pressure sensitive adhesives based on interpolymer complexes *Prog. Polym. Sci.* **2015**, *42*, 79–153.

(13) Ishikawa, N.; Furutani, M.; Arimitsu, K. Adhesive Materials Utilizing a Thymine − Adenine

Interaction and Thymine Photodimerization *ACS Macro Lett.* **2015**, *4*, 741–744.

(14) Ishikawa, N.; Furutani, M.; Arimitsu, K. Pressure-Sensitive Adhesive Utilizing Molecular Interactions Between Thymine and Adenine *Polym. Chem.* **2016**, *54*, 1332–1338.

(15) Liu, X.; Zhang, Q.; Gao, Z.; Hou, R.; Gao, G. A bio-inspired adhesive hydrogel driven by adenine and thymine *ACS Appl. Mater. Interfaces* **2017**, *9*, 17645–17652.

(16) del Prado, A.; González-Rodríguez, D.; Wu, Y. Functional Systems Derived from Nucleobase Self-assembly *Chem. Open* **2020**, *9*, 409–430.

(17) Lomas, J. S.; François, M. Water and alcohol(s): what's the difference? A proton NMR and DFT study of hetero-association with pyridine *J. Phys. Org. Chem.* **2008**, *21*, 464–471.

(18) Haddock, T. H. Presure sensitive adhesive. EP 0130080 B1, 1988.

(19) Martins Camargo, A. P. An electrochemical study of the adsorption and coadsorption behavior of selected purines, pyrimidines and nucleosides on Au(111), Freien University, Berlin, 2004.

(20) Li, D.; Grady, M. C.; Hutchinson, R. A. High-Temperature Semibatch Free Radical Copolymerization of Butyl Methacrylate and Butyl Acrylate *Ind. Eng. Chem. Res.* **2005**, *44*, 2506–2517.

(21) Ballard, N.; Asua, J. M. Radical polymerization of acrylic monomers: An overview *Prog. Polym. Sci.* **2018**, *79*, 40–60.

(22) Porter, R. S.; Johnson, J. F. The entanglement concept in polymer systems *Chem. Rev.* **1966**, *66*, 1–27.

(23) Callies, X.; Fonteneau, C.; Véchambre, C.; Pensec, S.; Chenal, J.-M.; Chazeau, L.; Bouteiller, L.; Ducouret, G.; Creton, C. Linear rheology of bis-urea functionalized supramolecular poly(butylacrylate)s: Part I - weak stickers *Polymer* **2015**, *69*, 233–240.

(24) Lewis, C. L.; Stewart, K.; Anthamatten, M. The Influence of Hydrogen Bonding Side-Groups on Viscoelastic Behavior of Linear and Network Polymers *Macromolecules* **2014**, *47*, 729–740.

(25) Zhang, Z.; Chen, Q.; Colby, R. H. Dynamics of associative polymers *Soft Matter* **2018**, *14*, 2961–2977.

(26) Leibler, L.; Rubinstein, M.; Colby, R. H. Dynamics of Reversible Networks *Macromolecules* **1991**, *24*, 4701–4707.

(27) Li, Z.-T.; Wu, L.-Z. *Hydrogen Bonded Supramolecular Structures*; Springer: Beijing (China), 2015; Vol. 88.

(28) Gilli, G.; Gilli, P. *The Nature of the Hydrogen Bond*; Oxford University Press Inc: New York, 2009.

(29) Zhou, J.; Guimard, N. K.; Inglis, A. J.; Namazian, M.; Lin, C. Y.; Coote, M. L.; Spyrou, E.; Hilf, S.; Schmidt, F. G.; Barner-Kowollik, C. Thermally reversible Diels – Alder-based polymerization: an experimental and theoretical assessment *Polym. Chem.* **2012**, *3*, 628–639.

(30) Hawke, L. G. D.; Ahmadi, M.; Goldansaz, H.; van Ruymbeke, E. Viscoelastic properties of linear associating poly(n-butyl acrylate) chains *J. Rheol.* **2016**, *60*, 297–310.

(31) Shabbir, A.; Hadi, G.; Hassager, O.; van Ruymbeke, E.; Alvarez, N. J. The Effect of Hydrogen Bonding on Linear and Nonlinear Rheology of Entangled Polymer Melts *Macromolecules* **2015**, *48*, 5988–5996.

(32) Kuo, S.-W.; Hsu, C.-H. Miscibility enhancement of supramolecular polymer blends through complementary multiple hydrogen bonding interactions *Polym. Int.* **2010**, *59*, 998–1005.

(33) Wang, J.-H.; Altukhov, O.; Cheng, C.-C.; Chang, F.-C.; Kuo, S.-W. Supramolecular structures of uracil-functionalized PEG complementary hydrogen bonding interactions *Soft Matter* **2013**, *9*, 5196–5206.

(34) Zhang, K.; Aiba, M.; Fahs, G. B.; Hudson, A. G.; Chiang, W. D.; Moore, R. B.; Ueda, M.; Long, T. E. Nucleobase-Functionalized Acrylic ABA Triblock Copolymers and Supramolecular Blends *Polym. Chem.* **2015**, *6*, 2434–2444.

(35) Shabbir, A. Rheology of Supramolecular Polymers, Technical University of Denmark, 2016.

(36) Wu, Y.-S.; Wu, Y.-C.; Kuo, S.-W. Thymine- and Adenine-Functionalized Polystyrene Form Self-Assembled Structures through Multiple Complementary Hydrogen Bonds *Polymers* **2014**, *6*, 1827–1845.

(37) Kuo, S.; Cheng, R.-S. DNA-like interactions enhance the miscibility of supramolecular polymer blends *Polymer* **2009**, *50*, 177–188.

(38) Chen, Y.; Jones, S. T.; Hancox, I.; Beanland, R.; Tunnah, E. J.; Bon, S. A. F. Multiple hydrogen-bond array reinforced cellular polymer films from colloidal crystalline assemblies of soft latex particles *ACS Macro Lett.* **2012**, *1*, 603–608.

Chapter 3. H-bonding complexation of polyvinyl alcohol (PVOH) stabilized polymer dispersions and water-soluble species

3.1. Introduction

In Chapter 2, the use of polymer dispersions with complementary H-bonding groups did not lead to polymer films with improved mechanical properties. In this chapter, a new strategy is adopted that involves using a latex with a H-bonding group attached to the surface, with the complementary group present in the aqueous phase. It is proposed that during the drying of the dispersions, the functional groups will interact at the surface of the polymer particles, leading to H-bonded particle interfaces. Specifically, polyvinyl alcohol (PVOH) stabilized polymer particles are used as functional dispersions and polyvinyl pyrrolidone (PVP), tannic acid (TA) and gallic acid (GA) are used as water-soluble complementary H-bond species. The schematic representation of the system and the chemical structures of the H-bonding molecules are shown in Figure 3.1.

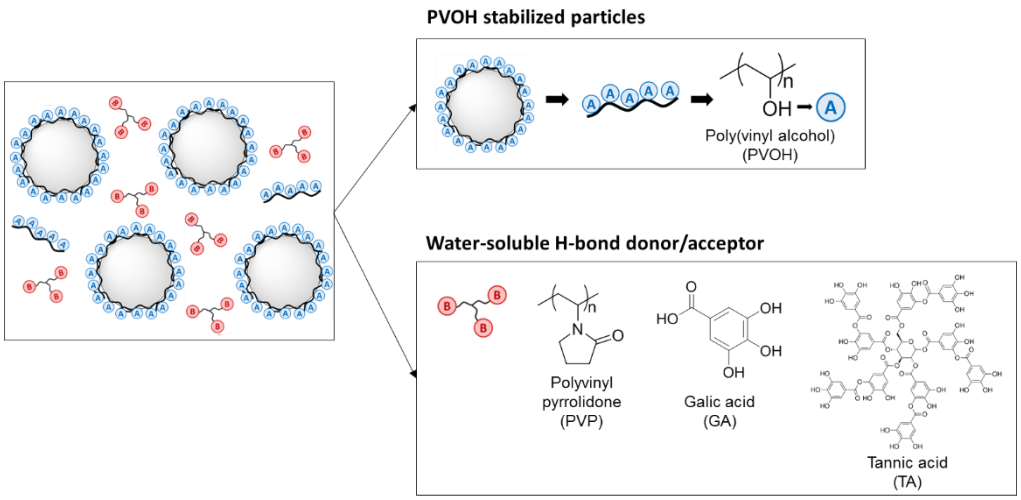

Figure 3.1. Schematic representation of the system composed of PVOH stabilized polymer particles and PVP, GA or TA dissolved in the aqueous phase.

PVOH is a water-soluble polymer with hydroxyl side groups that are able to act both as H-bond donors and acceptors. The hydroxyl groups interact promoting the organization of the polymer chains in 3D structures. As a result, commercial atactic PVOH is semicrystalline with a crystallinity in the range of 30 – 50 %, a melting temperature (T_M) of 230 °C[1] and a T_g of 80 °C.[2] It is worth highlighting that the melting temperature of PVOH is higher than the T_M of other commercial polymers like polyethylene (T_M = 117-135 °C)[1] due to the strength given to the structure by the hydrogen bonds. PVOH is widely used in biomedical applications due to its biocompatibility and low toxocity.[3–5] In the coatings and adhesives field, PVOH is used as steric stabilizer in the (mini)emulsion polymerization vinyl acetate (VAc),[6,7] VAc/VeoVa[8] and acrylic monomers.[9,10] In the films cast from such dispersions, PVOH forms a percolating network around the polymer particles above a critical volume fraction (between 6.5 and 8.8 volume% in the work carried out by J. Richard)[11] that greatly influences the thermomechanical properties of the materials.[11,12]

Polyvinylpyrrolidone (PVP) is a water-soluble polymer with a T_g = 187 °C[13] widely used in medical and pharmaceutical applications due to its biocompatibility[14,15]. PVP is also used as stabilizer for the preparation of nanoparticles.[16] The amide groups in the chemical structure of PVP are particularly good H-bond acceptors and blends of PVP with other H-bond donor polymers such as polyvinyl alcohol or polyacrylic acid have widely been used for the preparation of physically crosslinked[5,17,18] or dually crosslinked (combination of covalent and non-covalent bonds) hydrogels.[3,4,19]

Tannic acid and gallic acid are natural occurring polyphenols that are employed in the food and medical industries due to its antioxidant and astringent properties.[20–23] The high acidity of the phenolic hydroxyl group makes them a particularly good hydrogen donor and this feature has been exploited as non-covalent crosslinker of natural and synthetic polymers.[18,24–33]

In this chapter, PVOH is used as steric stabilizer for the synthesis acrylic polymer particles by miniemulsion polymerization. Aqueous solutions of PVP, TA and GA are added to the PVOH stabilized dispersion to physically crosslink the PVOH grafts with H-bonds and enhance the mechanical strength of the films. The hydrogen bonds between two PVOH units and between a PVOH unit and PVP, TA or GA are shown in Figure 3.2. These H-bonds are low energy interactions with K_a values around 1 M^{-1} and short life-times similar to the pyrrolidone-hydroxyl groups utilized in Chapter 2. Nevertheless, compared to Chapter 2, in the system presented in this chapter the hydrogen bond density at the surface of the particles is higher due to the use of H-bonding homopolymers their specific localization at the surface of the particles, which favors the formation of cohesive H-bond networks. In addition, the H-bonding polymers utilized have high T_g-s, and can act as structural reinforcing agents, potentially further enhancing the strength of the films.

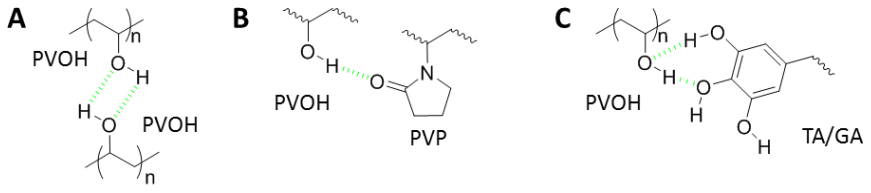

Figure 3.2. (A) H-bond between two hydroxyl groups in PVOH, (B) a hydroxyl group in PVOH and a pyrrolidone of PVP and (C) a hydroxyl group in PVOH and a hydroxyl group in TA or GA.

3.2. Experimental part

3.2.1. Materials

Technical grade monomers methyl methacrylate (MMA, Quimidroga) and n-butyl acrylate (BA, Quimidroga) were used without purification. Stearyl acrylate (SA, 97%, Sigma Aldrich), potassium persulfate (KPS, ≥99.0%, Sigma Aldrich), sodium bicarbonate ($NaHCO_3$, Sigma Aldrich), polyvinyl pyrrolidone (PVP, 1 3000 000 g mol^{-1}, Sigma Aldrich), gallic acid (GA, ≥97.5%, Sigma Aldrich), tannic acid (TA, Sigma Aldrich) hydrochloric acid (HCl, 1M, Sigma Aldrich), acetic acid (Sigma Aldrich) and anhydric acid (Sigma Aldrich) were used as received. Polyvinyl alcohol Mowiol 4.88® (PVOH, 31 000 g mol^{-1} and 88 % degree of hydrolysis) was kindly supplied by Wacker Chemie AG and Dowfax 2A1 was kindly supplied by Dow Chemical Company. Deionized water was used throughout.

3.2.2. Synthesis of polymer dispersions

The synthesis of PVOH stabilized polymer dispersions was carried out by batch miniemulsion polymerization. Two polymer dispersions were prepared using 10 % weight based on monomers (wbm) of PVOH and varying the MMA/BA weight ratio in the formulation: 50/50

MMA/BA was used in PVOH 1 and 40/60 MMA/BA was used in PVOH 2. In addition, the analogous polymer dispersions were produced using 2 % wbm Dowfax 2A1 as stabilizer (50/50 MMA/BA ratio in Dowfax 1 and 40/60 MMA/BA ratio in Dowfax 2). This surfactant does not have H-bonding groups in the structure and these dispersions were used as reference to understand the effect of the H-bond on film properties. The formulations employed for the synthesis are shown in Table 3.1. In the recipes, 4 % wbm SA was used as co-stabilizer, 0.1 % wbm of $NaHCO_3$ as buffer to control the pH and 0.125 % wbm KPS as thermal initiator.

Table 3.1. Formulations employed for the synthesis of the polymer dispersions stabilized with PVOH and Dowfax 2A1.

Latex	Stabilizer (g)	MMA (g)	BA (g)	SA (g)	H_2O (g)	KPS (g)	$NaHCO_3$ (g)
PVOH 1	PVOH 12	60	60	4.8	170	0.15	0.12
PVOH 2	PVOH 12	48	72	4.8	170	0.15	0.12
Dowfax 1	Dowfax 2.4	60	60	4.8	170	0.15	0.12
Dowfax 2	Dowfax 2.4	48	72	4.8	170	0.15	0.12

First, all the ingredients except the initiator were mixed and the coarse emulsions were sonicated using a Branson Digital Sonifier 450 with an amplitude of 80% over 20 minutes under magnetic stirring and inside an ice bath to avoid overheating. Then, the miniemulsions were placed in a 0.5 L glass reactor fitted with a reflux condenser, a stainless steel anchor-type stirrer, a nitrogen inlet, a sampling tube and a thermocouple. The system was purged with N_2 and heated to 70 °C using a water-jacket controlled by an automatic control system (Camile TG, Biotage). The polymerization was initiated with a shot of initiator dissolved in 3 g of water and the polymerizations proceeded for 4 hours and using a stirring velocity of 250 rpm.

3.2.3. Blending and film casting

First, PVP, TA and GA were dissolved in water (10 wt% concentration for PVP and TA and 1 wt% for GA). Then, different amounts of the PVP aqueous solution were added to the PVOH 1 and Dowfax 1 latexes to prepare polymer blends with 0, 2.2, 4.4 and 22 % of PVP based on the weight of the polymer. For the preparation of PVOH – TA and PVOH – GA blends, the required amounts of the TA and GA solutions were added to PVOH 2 and Dowfax 2 to achieve polymer films with 0, 1, 2.5 and 5 wt% polyphenol based on the weight of the polymer.

The neat latexes and the latex blends were cast in silicone molds and dried for 7 days at 23 ± 2ºC and 50 ± 5% of relative humidity (standard conditions). After the water immersion experiments, the materials were dried under standard conditions for 7 days.

3.2.4. Characterization

The monomer conversion was determined gravimetrically and the particle size was measured using Dynamic Light Scattering (DLS). The gel content of the polymers was determined with Soxhlet extractions in THF and the molecular weight of the soluble fractions obtained from the extractions were measured by Size Exclusion Chromatography (SEC) in THF. The detailed description of the latex characterization methods is given in Section I.1 of Appendix I. In PVOH 1 the vinyl alcohol units of PVOH were acetylated mixing 1 g of dried polymer with 10 mL of acetic acid, 10 mL of acetic anhydride and 1 mL of 1M HCl. After 24 hours, the polymer was soluble in the mixture and the solvents were evaporated under vacuum.[34] The Soxhlet extraction of the acetylated PVOH 1 sample was carried out following the method described in Section I.1.3.1 of Appendix I but using cellulose extraction thimbles to hold the sample instead of cellulose pads.

The mechanical properties were measured by tensile test and the water sensitivity of the polymer films was analyzed by immersing the films in water for 5 days. A detailed description of the film characterization methods is given in Section I.2 of Appendix I.

3.3. Results and discussion

3.3.1. Synthesis of polymer dispersions

After the polymerizations stable latexes with solids content between 42 – 44 % were obtained. The final monomer conversion, particle size, gel content and molecular weight of the polymers produced in the reactions are presented in Table 3.2.

Table 3.2. Final monomer conversion, particle size, gel content and molecular weight distribution (soluble fraction after the Soxhlet extraction) of the polymer dispersions stabilized with PVOH or Dowfax.

Latex	Final X_M (%)	Final PS (nm)	Gel content (%)	$M_{W, sol.}$ (kg/mol)	PDI
PVOH 1	> 99	257 ± 1	65	690	1.9
PVOH 2	> 99	214 ± 5	62 ± 17	1 100	2.8
Dowfax 1	> 99	159 ± 1	10	1 300	2.1
Dowfax 2	96.8	203 ± 2	10 ± 5	2 100	2.7

Very high monomer conversions were achieved at the end of the reactions. The particle sizes obtained for the dispersions stabilized with Dowfax were 159 and 203 nm and the particle sizes of the PVOH-stabilized dispersions were 214 and 257 nm. As explained in Section 1.2.2 of the introduction chapter, in a miniemulsification process the final droplet size is the result of consecutive droplet break-up and coagulation of the droplets. If the viscosity of the medium is low and the mechanical energy applied for the breakage of the droplets is sufficiently high, the droplet size is determined by the surfactant available. In the miniemulsion stabilized with PVOH

the weight % of surfactant was 5 times higher than in the reaction stabilized with Dowfax (10 % wbm PVOH and 2 % wbm Dowfax). However, polymer-type surfactants have low adsorption/desorption rates at oil/water interfaces[35] and this limits their migration velocity to cover the newly formed droplets before they coagulate. On the contrary, anionic surfactants like Dowfax have very fast adsorption/desorption kinetics and they can efficiently migrate to cover the newly generated monomer/water interfaces. As result, the polymer dispersions prepared using Dowfax had smaller particles sizes than the PVOH-stabilized latexes.

The gel content was measured with Soxhlet extractions in THF. The polymer dispersions stabilized with Dowfax showed a gel content around 10% and the polymers produced using PVOH as surfactant showed high gel contents in the range of 62 – 65 %. PVOH is not soluble in THF and the high gel contents could be ascribed to free PVOH chains and P(MMA/BA) chains with PVOH grafts. During free radical polymerization of the acrylic monomers, a primary radical coming from the initiator or a growing chain can abstract a hydrogen atom from the methine of the PVOH backbone.[8] The resulting PVOH radical can propagate or undergo bimolecular termination and this leads to acrylic chains grafted with PVOH, which will show very low solubility in THF.[7,9,10,36] To confirm this, an acetylation process of the hydroxyl groups was carried out in PVOH 1 in order to make the grafts THF soluble for the Soxhlet extraction. After the acetylation process, the gel content was 4%. This difference of ~60% in the gel content shows that significant grafting occurred.

3.3.2. Film appearance

After the synthesis of the polymer dispersions, latexes PVOH 1 and Dowfax 1 were combined with different amounts of an aqueous solution of PVP and latexes PVOH 2 and Dowfax 2 were blended with aqueous solutions of TA and GA to prepare materials with different PVP, TA and GA content. The appearance of the polymer films is shown in Figure 3.3.

Figure 3.3 shows that the films prepared from the neat latexes without water-soluble H-bond donor/acceptors were transparent and homogeneous. The addition of PVP to Dowfax 1 and PVOH 1 dispersions did not affect the physical appearance of the films. On the contrary, the addition of the phenolic compounds to PVOH 2 and Dowfax 2 gave an orange tint to the films. GA has a lower absorption coefficient due to its smaller molecular size,[37] and therefore the films prepared with GA were less colored. In addition, comparing the films prepared from PVOH 2 and Dowfax 2 latexes, the PVOH 2 materials with H-bonds were more translucent. This point will be discussed in Section 4.3.3 in Chapter 4, when the morphology of the films is analyzed. Overall, among the materials with phenolic compounds, the PVOH 2 – GA blends showed the smallest change in color. This point is important if these materials are to be implemented practically.

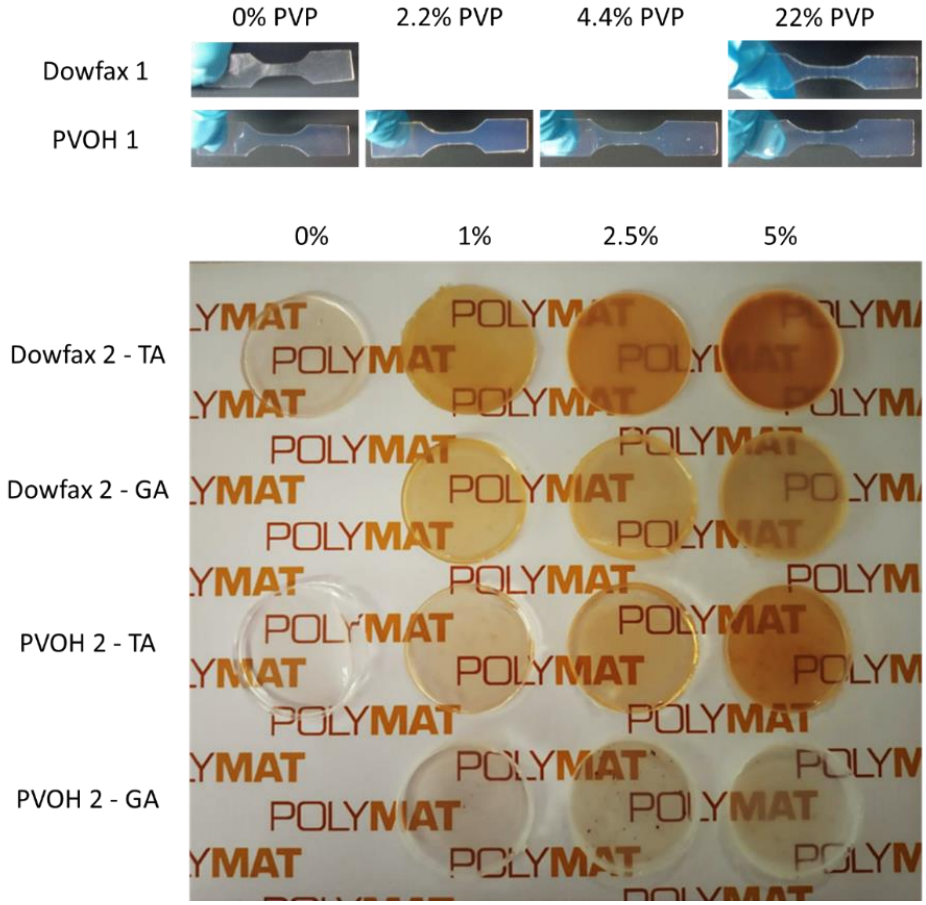

Figure 3.3. Physical appearance of the polymer films prepared from the latex-PVP/TA/GA blends.

3.3.3. Tensile properties

The mechanical properties of the films were measured by tensile test. The stress-strain plots are shown in Figure 3.4 and the values obtained from the plots are presented in Table 3.3.

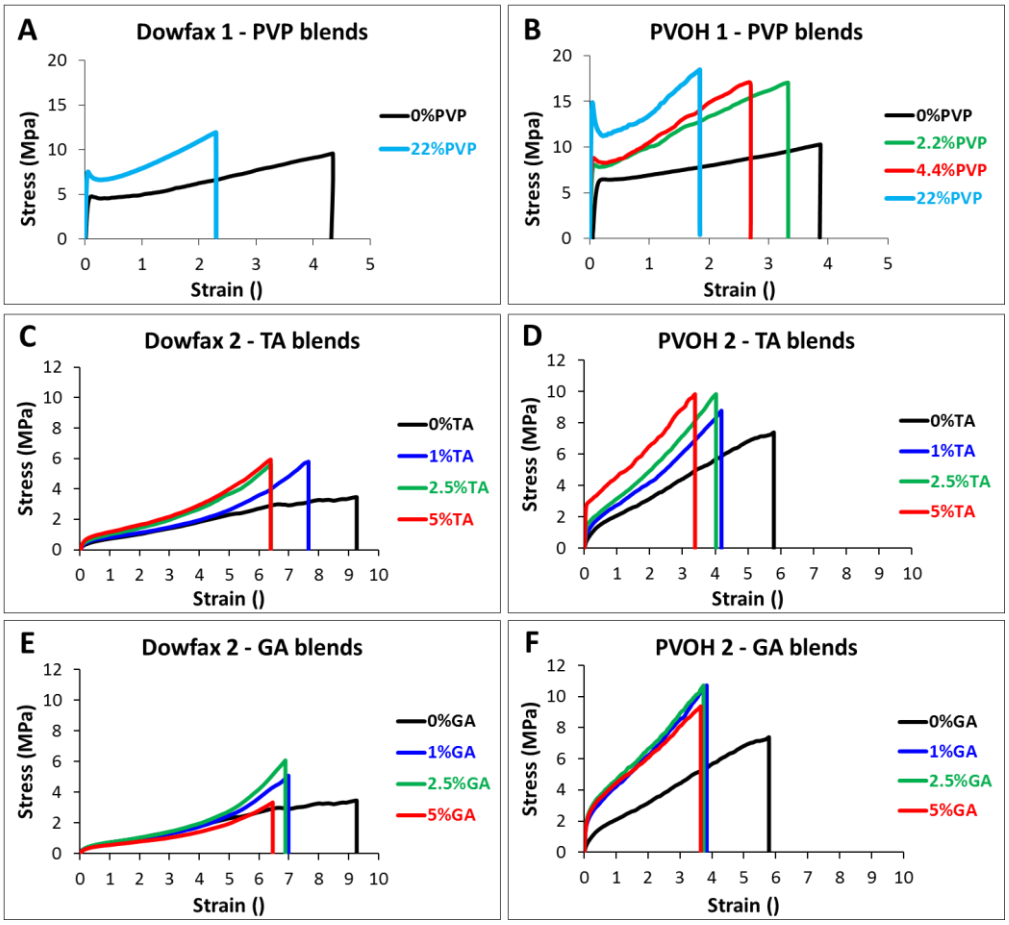

Figure 3.4. Stress−strain plots of the (A) Dowfax 1 – PVP, (B) PVOH 1 – PVP, (C) Dowfax 2 – TA, (D) PVOH 2 – TA, (E) Dowfax 2 – GA and (F) PVOH 2 – GA blends.

Table 3.3. Mechanical parameters of the latex – PVP / TA / GA blends related to the stress-strain plots presented in Figure 3.4.

Blend	PVP / TA / GA %	Young's modulus E (MPa)	Yield stress σ_y (MPa)	Tensile strength σ_{max} (MPa)	Ultimate strain γ_{max} ()
Dowfax 1 - PVP	0	96 ± 25	4.26 ± 0.47	8.6 ± 1.0	4.7 ± 0.5
	22	241 ± 27	6.84 ± 0.76	10.2 ± 1.1	1.9 ± 0.4
PVOH 1 - PVP	0	88 ± 17	6.02 ± 0.43	10.6 ± 0.9	3.5 ± 0.4
	2.2	174 ± 28	8.16 ± 0.59	16.9 ± 0.2	3.1 ± 0.3
	4.4	204 ± 28	8.68 ± 0.39	17.1 ± 1.2	2.7 ± 0.2
	22	466 ± 39	15.28 ± 1.20	18.0 ± 2.4	1.7 ± 0.2
Dowfax 2 - TA	0	4.5 ± 0.6	0.38 ± 0.03	3.6 ± 0.3	8.8 ± 0.4
	1	5.0 ± 2.0	0.36 ± 0.04	5.9 ± 0.2	7.7 ± 0.2
	2.5	8.0 ± 2.0	0.39 ± 0.07	6.4 ± 0.2	5.8 ± 0.2
	5	14.5 ± 5.3	0.59 ± 0.02	6.3 ± 0.3	6.1 ± 1.2
PVOH 2 - TA	0	11.4 ± 1.8	0.91 ± 0.06	7.3 ± 1.3	6.2 ± 1.0
	1	23.7 ± 2.4	1.05 ± 0.05	8.7 ± 0.7	4.2 ± 0.1
	2.5	32.5 ± 2.4	1.39 ± 0.08	9.8 ± 0.6	4.0 ± 2.4
	5	80.6 ± 8.9	2.62 ± 0.14	9.7 ± 0.4	3.3 ± 0.2
Dowfax 2 - GA	0	4.5 ± 0.6	0.38 ± 0.03	3.6 ± 0.3	8.8 ± 0.4
	1	4.7 ± 1.5	0.36 ± 0.03	5.4 ± 0.7	7.0 ± 0.1
	2.5	4.0 ± 1.8	0.35 ± 0.04	5.3 ± 0.9	6.7 ± 0.6
	5	3.2 ± 1.9	0.34 ± 0.04	2.9 ± 0.4	6.1 ± 0.4
PVOH 2 - GA	0	11.4 ± 1.8	0.91 ± 0.06	7.3 ± 1.3	6.2 ± 1.0
	1	35.3 ± 2.6	1.78 ± 0.11	10.0 ± 0.7	3.6 ± 0.3
	2.5	44.8 ± 5.8	2.45 ± 0.17	10.8 ± 1.1	3.7 ± 0.3
	5	42.0 ± 10.7	2.12 ± 0.23	9.4 ± 0.7	3.7 ± 0.1

First, comparing the materials cast from the neat latexes represented with black lines in Figure 3.4, the films prepared from Dowfax 1 and PVOH 1 latexes have higher Young's moduli than the analogous films cast from Dowfax 2 and PVOH 2 due to the higher MMA wt% used in the synthesis of the dispersions (the weight ratio of MMA/BA in latex groups "1" and "2" was 50/50 and 40/60, respectively). Then, comparing the films with and without PVOH, the film cast from PVOH 2 was stiffer and less flexible than the film cast from Dowfax 2 due to the semicrystalline PVOH corona around the polymer particles. The crystalline part of PVOH reinforced the polymer particle boundaries and, hence, the materials cast from the PVOH-stabilized latex were stiffer. The contribution of the PVOH corona was limited in the PVOH 1 film where the MMA/BA ratio was 50/50 and the films prepared from Dowfax 1 and PVOH 1 showed very similar Young's moduli.

The addition of the water-soluble H-bonding species led to a gradual increase in the Young's modulus (E), yield stress (σ_y) and tensile strength (σ_{max}) and lower ultimate strain (γ_{max}) with the PVP/TA/GA content. This was attributed to the structural reinforcement caused by the incorporation of hard components to the polymer films. However, the reinforcement was significantly larger for the PVOH stabilized dispersions. As an example, the addition of 5 weight % TA to Dowfax 2 led to a x3.2 times increase in the Young's modulus while the addition of the same amount of TA to PVOH 2 caused a x7.1 times increase in the modulus of material. In the PVOH-containing materials, the H-bonds between the PVOH grafts and water-soluble molecules led to reinforced polymer particle interfaces.

Focusing on the effect of each water-soluble species, PVP was the least efficient at increasing the modulus of the films and 4.4 wt% of PVP only caused a x2.3 increase in the modulus of the PVOH – PVP blend. The phenolic compounds were more efficient stiffening the materials and the addition of 5 wt% GA and TA increased the modulus of the PVOH-containing

films 3.6 and 7.1 times, respectively. The differences in the reinforcing ability of GA and TA were ascribed to the different molecular size of the phenolic compounds: TA is roughly 10 times bigger than GA, and since it has a higher amount of hydroxyl groups per molecule (25 OH-s in TA vs 4 OH-s in GA, see Figure 3.1), it is able to form a higher number of H-bonds per molecule increasing the strength of the interface between particles. It is worth commenting that the behavior of the PVOH - GA blends was different to the behavior of the PVOH - TA and PVOH - PVP blends. While the addition of PVP and TA caused a gradual stiffening of the materials with the PVP/TA content (see Figures 3.4.B and 3.4.D), in the PVOH - GA blends (see Figure 3.4.F) the addition of 1 wt% GA abruptly stiffened the material and then, the mechanical properties remained nearly constant as the GA content was increased up to 5%. As a possible explanation, the small molecular size of GA could lead to the physical crosslinking of the PVOH segments only within the same particle and therefore would not contribute to strengthening the polymer-polymer interface. In this scenario, the main reinforcement of the films would come from the hardness of the PVOH phase and, therefore, the mechanical properties would be only moderately affected by an increase in the GA content. In the case of PVP and TA, as they are bigger molecules, the chance of physical bonding between PVOH grafted to different particles is higher and therefore the polymer interface is reinforced gradually with the water-soluble polymer content.

3.3.4. Water sensitivity

After the tensile test, the water sensitivity of the films was evaluated by immersing the films in water and measuring the water absorption and weight loss of the polymer films during the test. The materials with PVP showed very poor water sensitivity and absorbed large amounts of water in very short times. Table 3.4 shows that the water absorption of the Dowfax and PVOH materials increased with the PVP content due to the hydrophilic nature of this homopolymer. In

addition, the incorporation of PVOH to the formulation decreased the water resistance of the materials and the PVOH-containing films showed higher absorption values than their Dowfax-containing analogous. The poorer water resistance of the PVOH films was ascribed to the higher concentration of surfactant in the formulation which was 5 times bigger than in the Dowfax stabilized reaction. In addition, the PVOH corona around the polymer particles formed a continuous hydrophilic percolating structure in the dried films that favored the penetration of water to the films. It is worth mentioning, that after only 1 hour of immersion in water the PVOH – 22 wt% PVP film disintegrated due to the high content of hydrophilic components in the material and easy penetration of water through the percolating network.

Table 3.4. Water absorption wt% of the PVOH 1 – PVP and Dowfax 1 – PVP blends after 1 hour of immersion in water.

PVP wt%	Dowfax 1 – PVP blends Water absorption (wt%)	PVOH 1 – PVP blends Water absorption (wt%)
0	0.7 ± 0.3	16.6 ± 1.3
2.2	-	24.9 ± 0.4
4.4	-	34.2 ± 0.3
22	82.9 ± 1.3	Disintegration

On the other hand, the materials with TA and GA showed better water resistance and the films were self-standing even after 5 days in water. The water absorption and weight loss of the PVOH 2 and Dowfax 2 films at different TA and GA concentrations are shown in Figure 3.5.A and 3.5.B, respectively.

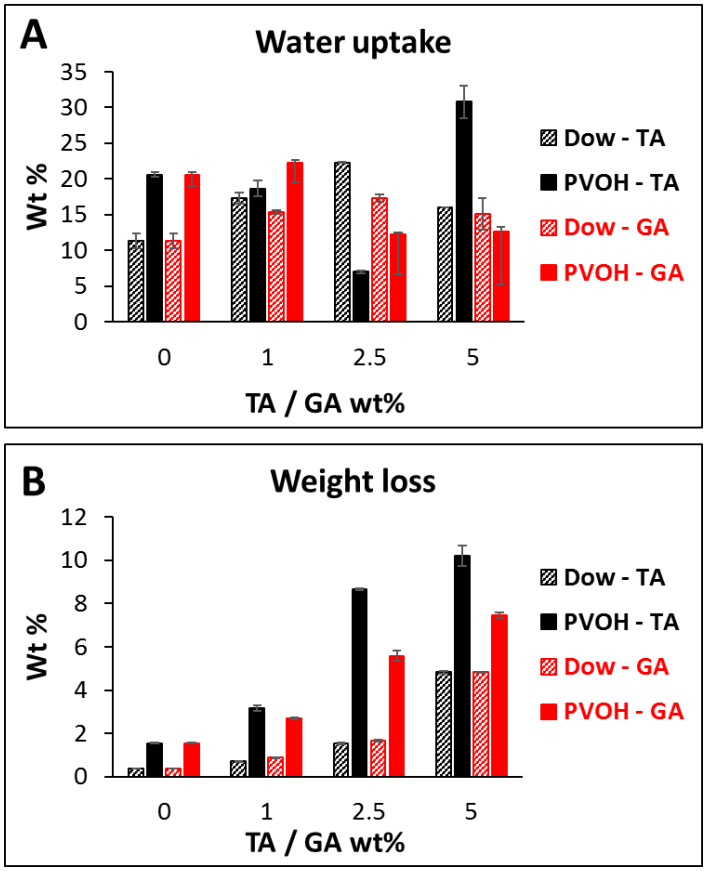

Figure 3.5. (A) Water uptake and (B) weight loss of the latex – TA / GA blends after 5 days of immersion in water.

First, in agreement with the results obtained for latexes Dowfax 1 and PVOH 1, the material cast from the neat PVOH 2 latex showed higher water absorption than the material cast from Dowfax 2, due to the higher surfactant concentration in the formulation. The PVOH 2 material also presented higher weight loss probably as result of non-grafted PVOH chains being dissolved into the aqueous phase.

In the Dowfax 2 – TA and Dowfax 2 - GA blends represented with black and red patterned bars in Figure 3.5, the water uptake and weight loss of the materials gradually increased as the fraction of phenolic compounds increased from 0 to 2.5% due to the hydrophilic nature of these species. When the concentration of the phenolic compounds was increased to 5% the weight loss of the films increased significantly and the water uptake decreased slightly probably due to the considerable amount of hydrophilic material lost from the films.

The PVOH 2 – TA and PVOH 2 – GA blends depicted with black and red full bars in Figure 3.5 also showed a gradual increase in the weight loss with the TA / GA content. However, the weight loss was greater than in the blends prepared from Dowfax 2. In these materials, the hydrophilic PVOH percolating structure favored the penetration of water into the films and this enhanced the release of hydrophilic components from the films. In addition, the fraction of water sensitive components in the PVOH-containing blends was considerably higher than in the Dowfax blends, and therefore, the amount of material that can be easily dissolved from the films was higher. Comparing the PVOH materials with TA or GA, the materials with TA showed higher weight loss, which indicated a greater release of hydrophilic components to the aqueous phase when TA was used. Regarding the water uptake of the PVOH materials, the competition between material release and water absorption makes difficult to distinguish a clear trend on the water uptake results.

During the immersion of the films, the hydrophilic components of the formulations including the surfactants and the phenolic compounds desorbed from the films. In order to isolate the release of TA and GA from the films, the concentration of the phenolic compounds in the aqueous phase was determined after the test using UV-vis spectrometry. The wt% of TA and GA released from the films is presented in Figure 3.6.

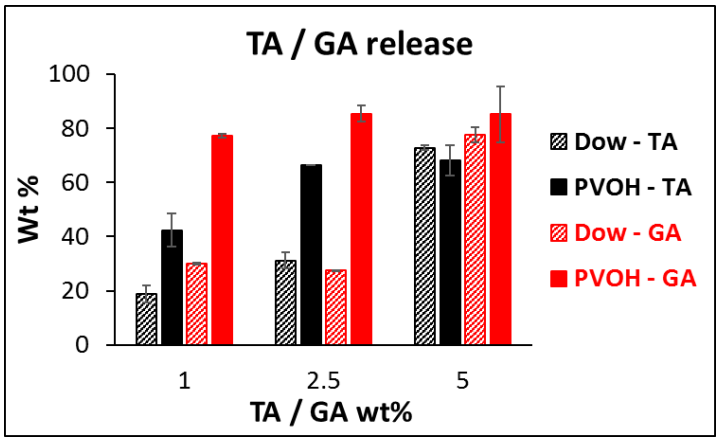

Figure 3.6. TA and GA wt% released from the blends after 5 days of immersion in water.

In general, the TA / GA fraction released to the aqueous phase increased with the amount of phenolic compound incorporated to the films. At low TA / GA contents (1 and 2.5 wt%), the GA and TA amounts released were markedly higher in the case of PVOH very likely because the hydrophilic path favored the release of the hydrophilic compounds. At higher TA / GA content (5 wt%), both Dowfax and PVOH-containing materials showed very high release of the phenolic compounds, higher than 70 wt% in all the cases. Comparing the performance of the PVOH blends, TA desorbed less than GA from the PVOH films. In contrast, the PVOH – TA films showed higher weight losses after the immersion in water than the PVOH – GA blends. These results may be explained based on the ability of polyphenols to link to PVOH chains depending on their functionality. TA is a molecule nearly 10 times bigger than GA and therefore, the chance of TA to link to PVOH chains is greater. As result of the interactions between PVOH and TA, the non-grafted PVOH chains linked to TA were brought to the aqueous phase by TA leading to high weight loss values. In contrast, the small GA molecules had lower linking ability and were not as efficient as TA dragging the non-grafted PVOH chains to the aqueous phase. Regarding the release of phenolic compounds to the aqueous phase, the greater number of interactions

between TA and the grafted PVOH chains reduced the migration of this polyphenol to the aqueous phase.

Overall, the H-bonds between PVOH and TA / GA did not prevent the release of the phenolic compounds from the films and this had a direct impact on the mechanical performance of the materials after being exposed to water. Figure 3.7 shows the reinforcement given by the phenolic compounds faded after the immersion in water, especially in the PVOH – GA blends. Thus, while many of the PVOH systems displayed clear improvement in mechanical properties in the virgin state, the practical use of these materials would be limited due to the water sensitivity.

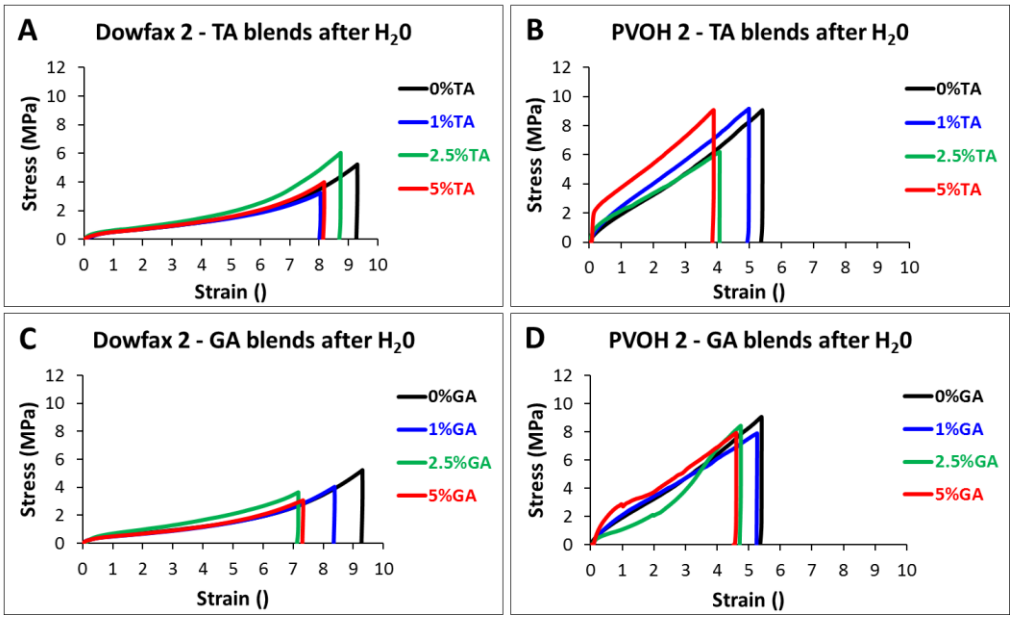

Figure 3.7. Stress−strain plots of the (A) Dowfax 2 – TA, (B) PVOH 2 – TA, (C) Dowfax 2 – GA and (D) PVOH 2 – GA blends after immersion in water.

Table 3.5. Mechanical parameters of the latex – PVP / TA / GA blends related to the stress-strain plots presented in Figure 3.7.

Blend	PVP / TA / GA %	Young's modulus E (MPa)	Yield stress σ_y (MPa)	Tensile strength σ_{max} (MPa)	Ultimate strain γ_{max} ()
Dowfax 2 - TA After H_2O	0	2.7 ± 0.5	0.31 ± 0.01	4.7 ± 0.9	8.8 ± 0.8
	1	2.3 ± 0.5	0.24 ± 0.03	4.0 ± 0.6	8.6 ± 0.7
	2.5	3.3 ± 0.5	0.30 ± 0.02	6.0 ± 0.1	8.8 ± 0.1
	5	2.5 ± 0.5	0.33 ± 0.01	3.8 ± 0.7	7.9 ± 0.6
PVOH 2 - TA After H_2O	0	5.0 ± 1.0	0.26 ± 0.02	8.8 ± 0.3	5.7 ± 0.3
	1	6.7 ± 2.4	0.29 ± 0.07	9.1 ± 0.2	4.9 ± 0.2
	2.5	12.0 ± 2.0	0.99 ± 0.07	6.4 ± 0.2	4.2 ± 0.2
	5	48.0 ± 2.0	1.93 ± 0.09	9.2 ± 0.1	3.9 ± 0.1
Dowfax 2 - GA After H_2O	0	2.7 ± 0.5	0.31 ± 0.01	4.7 ± 0.9	8.8 ± 0.8
	1	1.3 ± 0.5	0.31 ± 0.01	4.3 ± 0.3	7.8 ± 0.6
	2.5	2.3 ± 0.5	0.33 ± 0.02	5.1 ± 0.6	8.7 ± 0.5
	5	2.0 ± 1.0	0.34 ± 0.02	2.7 ± 0.4	7.2 ± 0.1
PVOH 2 - GA After H_2O	0	5.0 ± 1.0	0.26 ± 0.02	8.8 ± 0.3	5.7 ± 0.3
	1	6.5 ± 0.5	0.38 ± 0.03	7.9 ± 0.1	5.2 ± 0.1
	2.5	4.5 ± 2.5	0.41 ± 0.05	7.2 ± 1.2	4.4 ± 0.3
	5	6.7 ± 0.9	0.98 ± 0.66	6.5 ± 1.5	3.8 ± 0.8

3.4. Conclusions

The combination of PVOH-stabilized latexes and water-soluble H-bonding species such as PVP, TA or GA is an efficient and practical approach to prepare mechanically stiff polymer films. However, the materials showed very poor water resistance due to the high fraction of hydrophilic compounds in the formulation. When the films were exposed to water, the non-covalent network was disrupted by the water molecules and the hydrophilic components (PVOH free chains, PVP, TA and GA) were released to the aqueous phase. As a result, the polymer films were not able to retain the mechanical strength after being exposed to water. Therefore, although the H-bond density at the particle boundaries was high in these materials, the H-bonds moieties used in this work (see Figure 3.2) were not strong enough to retain the structural integrity of the materials in the presence of water. In this context, stronger H-bonds such as the interaction between a highly basic pyrrolidone and the highly acidic hydroxyl from a phenolic compound might offer better water resistance to the materials.

3.5. References

(1) Assender, H. E.; Windle, A. H. Crystallinity in poly(vinyl alcohol). 1. An X-ray diffraction study of atactic PVOH *Polymer* **1998**, *39*, 4295–4302.

(2) Rault, J.; Gref, R.; Ping, Z. H.; Nguyen, Q. T.; Néel, J. Glass transition temperature regulation effect in a poly(vinyl alcohol)-water system *Polymer* **1995**, *36*, 1655–1661.

(3) Husain, M. S. B.; Gupta, A.; Alashwal, B. Y.; Sharma, S. Synthesis of PVA/PVP based hydrogel for biomedical applications: a review *Energy Sources, Part A Recover. Util. Environ. Eff.* **2018**, *40*, 2388–2393.

(4) Reena; Kumar, A.; Mahto, V.; Choubey, A. K. Synthesis and characterization of cross-linked hydrogels using polyvinyl alcohol and polyvinyl pyrolidone and their blend for water shut-off treatments *J. Mol. Liq.* **2020**, *310*, 1–33.

(5) Bashyal, S.; Shin, C. Y.; Hyun, S. M.; Jang, S. W.; Lee, S. Preparation, Characterization, and In Vivo Pharmacokinetic Evaluation of Polyvinyl Alcohol and Polyvinyl Pyrrolidone Blended Hydrogels for Transdermal Delivery of Donepezil HCl *Pharmaceutics* **2020**, *12*, 1–16.

(6) Wang, S.; Schork, F. J. Miniemulsion Polymerization of Vinyl Acetate with Nonionic Surfactant *J. Appl. Polym. Sci.* **1994**, *58*, 2157–2164.

(7) Budhlall, B. M.; Sudol, E. D.; Dimonie, V. L.; Klein, A. Role of Grafting in the Emulsion Polymerization of Vinyl Acetate with Poly(vinyl alcohol) as an Emulsifier. I. Effect of the Degree of Blockiness on the Kinetics and Mechanism of Grafting *J. Polym. Sci. Part A Polym. Chem.* **2001**, *39*, 3633–3654.

(8) Bohorquez, S. J.; Asua, J. M. Particle Nucleation in High Solids Batch Miniemulsion Polymerization Stabilized with a Polymeric Surfactant *J. Polym. Sci. Part A Polym. Chem.* **2008**, *46*, 6407–6414.

(9) Kim, N.; Sudol, E. D.; Dimonie, V. L.; El-Aasser, M. S. Poly(vinyl alcohol) stabilization of acrylic emulsion polymers using the miniemulsion approach *Macromolecules* **2003**, *36*, 5573–5579.

(10) Kim, N.; Sudol, E. D.; Dimonie, V. L.; El-Aasser, M. S. Comparison of Conventional and Miniemulsion Copolymerizations of Acrylic Monomers Using Poly(vinyl alcohol) as the Sole Stabilizer *Macromolecules* **2004**, *37*, 2427–2433.

(11) Richard, J. Thermomechanical behaviour of composite polymer films obtained from poly(vinyl acetate) latexes sterically stabilized by poly(vinyl alcohol) *Polymer* **1993**, *34*, 3823–3831.

(12) Richard, J. In *Film Formation in Waterborne Coatings*; Provder, T.; Winnik, M. A.; Urban, M. W., Eds.; 1996; pp. 118–153.

(13) Cassu, S. N.; Felisberti, M. I. Poly(vinyl alcohol) and poly(vinylpyrrolidone) blends: 2. Study of relaxations by dynamic mechanical analysis *Polymer* **1999**, *40*, 4845–4851.

(14) Haaf, F.; Sanner, A.; Straub, F. Polymers of N-vinylpyrrolidone: Synthesis, Characterization and Uses *Polym. J.* **1985**, *17*, 143–152.

(15) Franco, P.; De Marco, I. The Use of Poly(N-vinyl pyrrolidone) in the Delivery of Drugs: A Review *Polymers.* **2020**, *12*, 1–29.

(16) Koczkur, K. M.; Mourdikoudis, S.; Polavarapu, L.; Skrabalak, S. E. Polyvinylpyrrolidone (PVP) in nanoparticle synthesis *Dalt. Trans.* **2015**, *44*, 17883–17905.

(17) Zheng, Y.; Huang, X.; Wang, Y.; Xu, H.; Chen, X. Performance and Characterization of Irradiated Poly(vinyl alcohol)/Polyvinylpyrrolidone Composite Hydrogels Used as Cartilages Replacement *J. Appl. Polym. Sci.* **2009**, *113*, 736–741.

(18) Nam, H. G.; Nam, M. G.; Yoo, P. J.; Kim, J. Hydrogen bonding-based strongly adhesive coacervate hydrogels synthesized using poly(N-vinylpyrrolidone) and tannic acid *Soft Matter* **2019**, *15*, 785–791.

(19) Sohail, K.; Khan, I. U.; Shahzad, Y.; Hussain, T.; Ranjha, N. M. pH-sensitive polyvinylpyrrolidone-acrylic acid hydrogels: Impact of material parameters on swelling and drug release *Brazilian J. Pharm. Sci.* **2014**, *50*, 173–184.

(20) Sahiner, N.; Sengel, S. B. Tannic acid decorated poly(methacrylic acid) micro and nanoparticles with controllable tannic acid release and antioxidant properties *Colloids Surfaces A Physicochem. Eng. Asp.* **2016**, *508*, 30–38.

(21) Ashok, P. K.; Upadhyaya, K. Tannins are Astringent *J. Pharmacogn. Phytochem.* **2012**, *1*, 45–50.

(22) Soltani, R.; Haghighat, A.; Fanaei, M.; Asghari, G. Evaluation of the Effect of Green Tea Extract on the Prevention of Gingival Bleeding after Posterior Mandibular Teeth Extraction: A Randomized Controlled Trial *Evidence-Based Complement. Altern. Med.* **2014**, *2014*, 1–4.

(23) *Tannin Market Analysis By Sources (Plants, Brown Algae), By Product (Hydrolysable, Non-hydrolysable, Phlorotannins), By Application (Leather Tanning, Wine Production, Wood Adhesives), & Segment Forecasts, 2014 - 2025*; 2017.

(24) Erel-Unal, I.; Sukhishvili, S. A. Hydrogen-bonded multilayers of a neutral polymer and a polyphenol *Macromolecules* **2008**, *41*, 3962–3970.

(25) Dai, H.; Huang, Y.; Huang, H. Enhanced performances of polyvinyl alcohol films by introducing tannic acid and pineapple peel-derived cellulose nanocrystals *Cellulose* **2018**, *25*, 4623–463.

(26) Bedran-Russo, A. K. B.; Yoo, K. J.; Ema, K. C.; Pashley, D. H. Mechanical properties of tannic-acid-treated dentin matrix *J. Dent. Res.* **2009**, *88*, 807–811.

(27) López, C. M.; Pich, A. Supramolecular Stimuli-Responsive Microgels Crosslinked by Tannic Acid *Macromol. Rapid Commun.* **2018**, *39*, 1700808.

(28) Tsukruk, V. V; Kozlovskaya, V.; Harbaugh, S.; Drachuk, I.; Shchepelina, O.; Kelley-loughnane, N.; Stone, M.; Tsukruk, V. V. Hydrogen-bonded LbL shells for living cell surface engineering *Soft Matter* **2011**, *7*, 2364–2372.

(29) Euti, E. M.; Wolfel, A.; Picchio, M. L.; Romero, M. R.; Martinelli, M.; Minari, R. J.; Igarzabal, C. I. A. Controlled Thermoreversible Formation of Supramolecular Hydrogels Based on Poly(vinyl alcohol) and Natural Phenolic Compounds *Macromol. Rapid Commun.* **2019**, *0*, 1900217.

(30) Chen, Y.-N.; Peng, L.; Liu, T.; Wang, Y.; Shi, S.; Huiliang, W. Poly(vinyl alcohol)-Tannic Acid Hydrogels with Excellent Mechanical Properties and Shape Memory Behaviors *ACS Appl. Mater. Interfaces* **2016**, *8*, 27199–27206.

(31) Kaczmarek, B.; Mazur, O. Collagen-Based Materials Modified by Phenolic Acids - A review *Materials.* **2020**, *13*, 1–18.

(32) Picchio, M. L.; Linck, Y. G.; Monti, G. A.; Gugliotta, L. M.; Minari, R. J.; Igarzabal, C. I. A. Casein films crosslinked by tannic acid for food packaging applications *Food Hydrocoll.* **2018**, *84*.

(33) Fan, H.; Wang, L.; Feng, X.; Bu, Y.; Wu, D.; Jin, Z. Supramolecular Hydrogel Formation Based on Tannic Acid *Macromolecules* **2017**, *50*, 666–676.

(34) Agirre, A.; Weitzel, H. P.; Hergeth, W. D.; Asua, J. M. Process intensification of VAc-VeoVa10 latex production *Chem. Eng. J.* **2015**, *266*, 34–47.

(35) Ballard, N.; Urrutia, J.; Eizagirre, S.; Schäfer, T.; Diaconu, G.; de la Cal, J. C.; Asua, J. M. Surfactant Kinetics and Their Importance in Nucleation Events in (Mini)emulsion Polymerization Revealed by Quartz Crystal Microbalance with Dissipation Monitoring *Langmuir* **2014**, *30*, 9053–9062.

(36) Okaya, T.; Suzuki, A.; Kikuchi, K. Effect of initiators on grafting in the initial stage of the emulsion polymerization of methyl methacrylate using poly(vinyl alcohol) as a protective colloid *Colloid Polym. Sci.* **2002**, *280*, 188–192.

(37) Katwa, L. C.; Ramakrishna, M.; Rao, M. R. R. Spectrophotometric assay of immobilized tannase *J. Biosci.* **1981**, *3*, 135–142

Chapter 4. N-vinyl pyrrolidone (NVP) and tannic acid complexation for coatings applications

4.1. Introduction

In Chapter 3, the addition of hard water-soluble molecules with H-bonding groups such as polyvinyl pyrrolidone, tannic acid or gallic acid to PVOH-stabilized latexes was shown to lead to the formation of stiff materials. However, those materials showed very poor water resistance due to the high content of hydrophilic components in the films (≈ 15 weight %) and the low strength of the H-bonds between the PVOH chains and the water-soluble species.

In this chapter, we propose a similar approach for the mechanical reinforcement of the polymer films that uses stronger H-bonding motifs. In order to do so, a polymer dispersion containing 5 wt % N-vinyl pyrrolidone (NVP) was combined with tannic acid dissolved in the aqueous phase. The schematic representation of the system and the chemical structures of NVP and TA are shown in Figure 4.1. Compared to the PVOH - TA combination, the use of the pyrrolidone functionalized dispersion offers two main advantages. First, pyrrolidones are particularly strong H-bond acceptors due to the basicity of the amide groups and they form very strong complexes with TA[1,2] (H-bond shown in Figure 4.2). Second, the hydrophilic component is incorporated directly to the polymer particles which on one hand renders the dispersion inherently less hydrophilic and on the other avoids the mobility of the H-bond acceptor in humid conditions. These two features will contribute to the water resistance of the films.

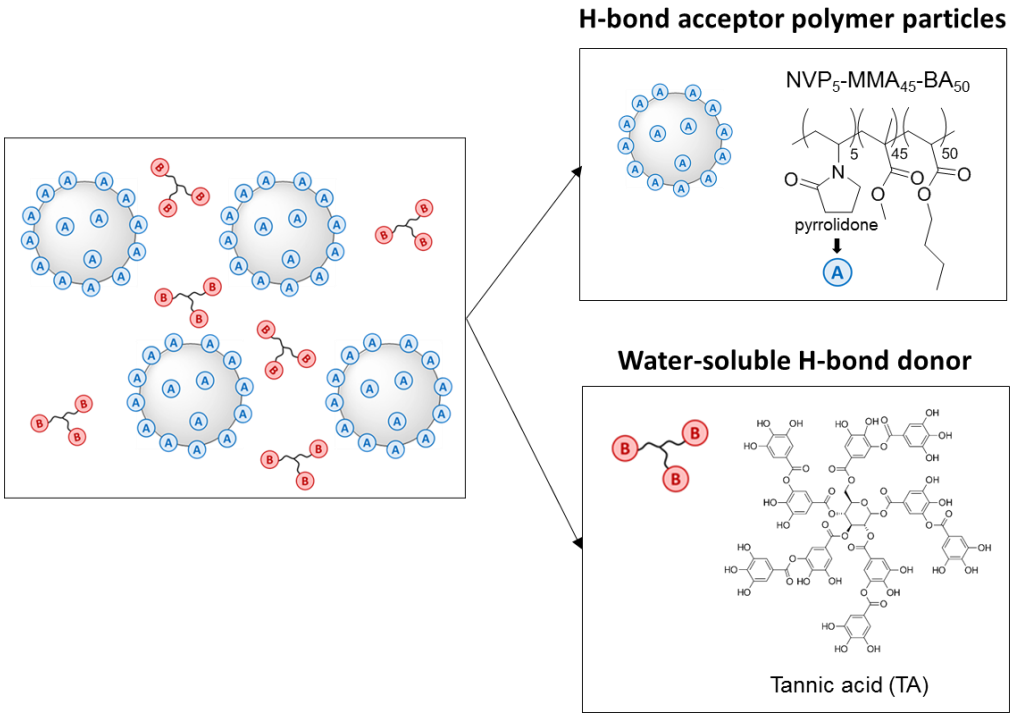

Figure 4.1. Schematic representation of the system composed of NVP functionalized polymer particles and TA dissolved in the aqueous phase. In the scheme, the subscripts after the monomer units express the weight % of the monomers used for the synthesis.

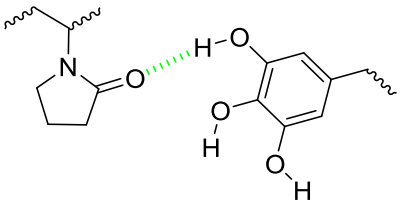

Figure 4.2. H-bond between a pyrrolidone and the aromatic hydroxyl group of TA.

In this chapter, the mechanical properties of the polymer films formed from the combination of acrylic dispersions with pyrrolidone groups and TA in the aqueous phase are examined. The improvement in the mechanical strength of the materials is explained by exploring the effect of TA on the internal morphology of the polymer films. Then, the water uptake and the sensitivity of the mechanical properties to water are analyzed. The versatility of the approach for other latexes (e.g. varying the H-bond acceptor monomer) is also studied. The effect of the molecular weight of the H-bond donating cross-linker and nature of the hydroxyl group is investigated by substitution of TA by gallic acid (GA, the repeat unit of TA) and polyvinyl alcohol (PVOH). In the last part, the potential use of the system as formulated product is examined.

4.2. Experimental part

4.2.1. Materials

Technical grade monomers methyl methacrylate (MMA, Quimidroga) and n-butyl acrylate (BA, Quimidroga) were used without purification. N-vinyl pyrrolidone (NVP, >99 %, Sigma Aldrich), N-vinyl caprolactam (NVC, 98 %, Sigma Aldrich), acrylic acid (AA, 99 %, Sigma Aldrich), ammonium persulfate (APS, ≥98 %, Sigma Aldrich), sodium bicarbonate ($NaHCO_3$, Sigma Aldrich), n-dodecanethiol (DSH, ≥97 %, Sigmal Aldrich), tannic acid (TA, Fluka), gallic acid (GA, ≥ 97.5 %, Sigma Aldrich) and polyvinyl alcohol Mowiol ® 4.88 (PVOH, Mw = 31 kDa and 88 % degree of hydrolysis, kindly supplied by Wacker Chemie AG) were used as received. Dowfax 2A1 was kindly supplied by Dow Chemical Company. AA 4140, BYK 24, Kronos 2190 and Natrosol® 250 HR were provided by BASF. Deionized water was used as polymerization media.

4.2.2. Synthesis of polymer dispersions

The polymer dispersions were produced by seeded semibatch emulsion polymerization according to the procedure described by Haddock *et al.*[3] The same polymerization process was utilized in Chapter 2 for the synthesis of the polymer dispersions with pyrrolidone and hydroxyl groups. Thus, to unambiguously identify the dispersions, the latexes prepared using the procedure described by Haddock are numbered from 1 to 21 along the manuscript. In this chapter, in total 8 polymer dispersions were used: Latexes 7 – 12 were synthesized in the University of the Basque Country and Latex 13 – 14 were produced in BASF. The formulations used for the synthesis of Latexes 7 -14 are shown in Table 4.1. No functional monomer was incorporated in Latexes 7 and 13 to be used as reference and 5 % weight based on monomers (wbm) of N-vinyl pyrrolidone (NVP) was used in Latexes 8, 10, 11 and 14. First, the effect of lowering the pyrrolidone content from 5 wt % to 2 wt % was investigated comparing Latexes 9 and 8. The effect of the presence of AA (often used in latexes for coatings) and the absence of CTA was studied in Latexes 10 and 11, respectively. Finally, the possibility of using N-vinyl caprolactam (NVC) as alternative H-bond acceptor monomer was checked in Latex 12. Comparing their chemical structures (Figure 4.3), they contain cyclic amides but the ring has 5 members in the case of NVP and 7 members in NVC.

Table 4.1. Formulations employed for the synthesis of the functional latexes according to the procedure proposed by Haddock.[3] *The latexes synthesized in BASF are marked with an asterisk (*).

		F.M. (g)	MMA (g)	BA (g)	AA (g)	DSH (g)	H_2O (g)	Dowfax (g)	APS (g)	$NaHCO_3$ (g)
Latex 7 0% F.M.	Seed	-	10	10	-	-	160	4.28	0.267	1
	F1	-	-	-	-	-	37.3	2.38	1.333	-
	F2	-	90	90	-	0.18	-	-	-	-
Latex 8 5% NVP	Seed	NVP 1	9	10	-	-	160	4.28	0.267	1
	F1	-	-	-	-	-	37.3	2.38	1.333	-
	F2	NVP 9	81	90	-	0.18	-	-	-	-
Latex 9 2% NVP	Seed	NVP 0.4	9.6	10	-	-	160	4.28	0.267	1
	F1	-	-	-	-	-	37.3	2.38	1.333	-
	F2	NVP 3.6	86.4	90	-	0.18	-	-	-	-
Latex 10 5% NVP 1% AA	Seed	NVP 1	9	10	-	-	160	4.28	0.267	1
	F1	-	-	-	-	-	37.3	2.38	1.333	-
	F2	NVP 9	79	90	2	0.18	-	-	-	-
Latex 11 5% NVP no CTA	Seed	NVP 1	9	10	-	-	160	4.28	0.267	1
	F1	-	-	-	-	-	37.3	2.38	1.333	-
	F2	NVP 9	81	90	-	-	-	-	-	-
Latex 12 5% NVC	Seed	NVC 1	9	10	-	-	160	4.28	0.267	1
	F1	-	-	-	-	-	37.3	2.38	1.333	-
	F2	NVC 9	81	90	-	0.18	-	-	-	-
Latex 13* 0% F.M.	Seed	-	20	20	-	-	320	8.6	0.56	2
	F1	-	-	-	-	-	74	4.8	2.7	-
	F2	-	180	180	-	0.36	-	-	-	-
Latex 14* 5% NVP	Seed	NVP 2	18	20	-	-	320	8.6	0.56	2
	F1	-	-	-	-	-	74	4.8	2.7	-
	F2	NVP 18	162	180	-	0.36	-	-	-	-

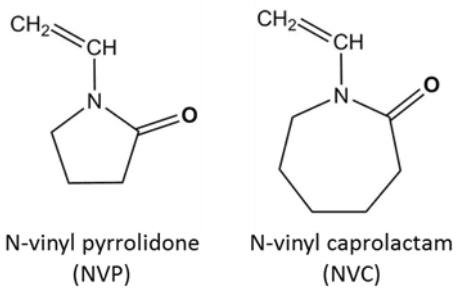

Figure 4.3. Chemical structures of NVP and NVC.

Similar to Chapter 2, the reactions were carried out in glass reactors fitted with a reflux condenser, a nitrogen inlet, a sampling tube, a thermocouple, and a stainless steel anchor-type stirrer. The reactor temperature was controlled by an automatic control system (Camile TG, Biotage). First, a seed of 11% solids content containing 10% of the total monomers was produced in situ for 30 min in batch, and then the rest of the monomers and an aqueous solution of the initiator (APS) and the emulsifier (Dowfax 2A1) were fed for 3 h in two independent streams. DSH was fed together with the monomers with a concentration of 0.1% wbm in order to suppress the gel content of the latexes and remove from considering the influence of this parameter on the results. At the end of the feeding, the reaction temperature was held for an additional 30 min to ensure monomer consumption. The reactions were carried out under nitrogen atmosphere at 70 °C and 200 rpm.

4.2.3. Blending and film casting

Different amounts of a 10% tannic acid water solution were added to the latexes and the blends were stirred for 30 min before film casting. The TA contents were: 0%, 0.5%, 1% 2.5%, 5%, 25% and 50% based on polymer. Similarly, the gallic acid (GA) blends with 0.5%, 2.5% and 5% of GA were prepared adding different amounts of 1% gallic acid aqueous solutions to the latexes. The polymer blends using polyvinyl alcohol as physical crosslinker were prepared using the same hydroxyl concentration as in the TA blends in order to figure out the influence of the hydroxyl nature (aliphatic in PVOH and aromatic in TA).

The latexes or the latex blends were cast in silicone molds and they were dried for 7 days at 23 ± 2ºC and 50 ± 5% of relative humidity (standard conditions). After the water immersion experiments, the materials were dried under standard conditions for 7 days.

In order to prepare the polymer films cast from solution, the materials with different TA % cast from dispersion were redissolved in THF, cast in silicone molds and dried for 5 days at standard conditions and 2 days at 60ºC.

4.2.4. Formulation of white paints

Standard white paints were prepared using as binders the polymer dispersions with 0 and 5 wt% NVP synthesized in BASF (Latexes 13 and 14). First, a white paste based on titanium dioxide (TiO_2) was prepared using the formulation shown in Table 4.2. The components of the formulation were added to the mixture following the order employed in Table 4.2, from the top to the bottom of the list. First, the first three components of the paste were weighed and stirred for 20 minutes. Then, the pH of the dispersion was increased to 9.5 using a 10 wt% aqueous solution of NaOH and after, the last two components were added under stirring. 24 hours after of the

preparation of the white paste, 20 g of the latex - TA blends were added to 40 g of the white paste under stirring. The mixtures were stirred for additional 10 minutes at 1000 rpm and stored overnight. In total, 5 paints were prepared using the following latex - TA blends as binders: Blank – 0%TA, 5%NVP – 0%TA, 5%NVP – 1%TA, 5%NVP – 2.5%TA and 5 %NVP – 5%TA. The paints are named according to the latex - TA blend used as binder.

Table 4.2. Formulation of the TiO_2-based paste employed for the preparation of white paints.

Component	Function	Concentration	Weight %
H_20	Dispersing medium		38.7
AA 4140	Dispersant	0.3 wt % in H_2O	0.24
Kronos 2190	TiO_2, pigment		35.0
BYK 24	Surfactant		0.37
Natrosol® 250 HR	Cellulose, thickener	3 wt % in H_2O	25.6

4.2.5. Characterization

The monomer conversion was determined by gravimetry. In Latexes 7 – 12, the particle size was measured by Dynamic Light Scattering (DLS) and the gel content was determined using Soxhlet extractions in THF. In Latexes 13 – 14 produced in BASF, the particle size was measured using Hydrodynamic Capillary Chromatography (HDC) and the gel content was defined as the insoluble polymer fraction in methyl ethyl ketone (MEK). The molecular weight distribution of the polymers was determined with Size Exclusion Chromatography in THF in all cases. The detailed description of the latex characterization methods and experimental conditions is given in Section I.1 of Appendix I. In addition, in Latex 8 the individual monomer conversions were measured by gas chromatography (GC). The column employed for the separation was a BP21 (FFAP) (from SGE analytical science) of 25 m, an inner diameter of 0.53 mm, and a film thickness of 0.5 μm.

The mechanical properties of the films were measured by tensile test. The glass transition temperatures of the polymer and polymer blends were determined by differential scanning calorimetry (DSC). The internal morphology of the films was investigated by transmission electron microscopy (TEM). The films were stained with RuO_4 to increase the contrast of the aromatic-rich areas, namely, the TA-rich zones. The water sensitivity of the polymer films was assessed by immersing the polymer films in water for 7 days and measuring water uptake, weight loss and release of tannic acid to the aqueous phase. The mechanical properties of the films after extensive exposure to water were also determined by tensile test. Detailed information these characterization methods is given in Section 1.2 of Appendix I.

The formation of H-bonds between pyrrolidone and TA was analyzed by Fourier transform infrared spectroscopy with a Nicolet 6700 spectrophotometer equipped with a single reflection ATR system (Specac Golden Gate). Dynamic mechanical analysis (DMA) measurements were carried out in a Triton 2000 DMA (Triton Technology) equipped with a liquid nitrogen cooling system. The measurements were performed in tension mode at 1 % deformation and a single frequency of 1 Hz. The samples were cooled down to ≈ −50 °C and heated with a rate of 4 °C min^{-1} until ≈ 100 °C. The linear viscoelastic behavior of the low molar mass copolymer-TA blends was analyzed by conducting frequency sweep tests (0.1 – 100 Hz) at constant temperature and applying a strain of 0.1 %. The Lab values of the surface of the white paints were determined with a X-RITE Ci64 spectrophotometer.

4.3. Results and discussion

4.3.1. Synthesis of polymer dispersions

Stable latexes of approximately 50 wt % solids content were obtained from runs Latex 7 – Latex 14. The monomer conversion and particle size time evolution during the synthesis of the dispersions are shown in Figures 4.4.A and 4.4.B, respectively. In addition, the final monomer conversion and particle size, gel content and molecular weight of the polymers are presented in Table 4.3.

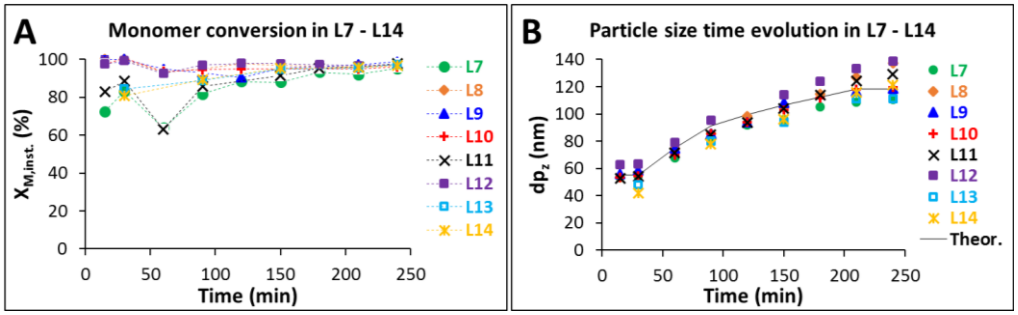

Figure 4.4. (A) Instantaneous monomer conversion and (B) particle size time evolution during the synthesis of Latex 7-14. The theoretical growth of a 55 nm seed assuming there is no secondary nucleation during the semibatch stage is shown for comparison.

Table 4.3. Main characteristics of the polymer dispersions produced in Latex 7 - 14. Latexes 13 and 14 marked with (*) were synthesized in BASF. Data determined by [a]gravimetry, [b]DLS, [c]HDC, [d]Soxhlet extractions in THF, [e]insoluble polymer fraction in MEK and [f]SEC in THF.

Latex	Description	Final X_M[a] (%)	$dp_{z,seed}$[b,c] (nm)	$dp_{z,final}$[b,c] (nm)	Gel content[d,e] (%)	M_w[f] (kg/mol)
L7	Blank - 0% F.M.	95.2	54 ± 1[b]	110 ± 1[b]	< 1[d]	684
L8	5% NVP	97.0	53 ± 1[b]	137 ± 2[b]	< 1[d]	744
L9	2% NVP	98.8	59 ± 1[b]	119 ± 2[b]	< 1[d]	524
L10	5% NVP + 1% AA	95.9	54 ± 1[b]	129 ± 1[b]	2.6 ± 0.5[d]	502
L11	5% NVP –no CTA	97.8	63 ± 1[b]	139 ± 1[b]	32.9 ± 1.7[d]	324
L12	5% NVC	97.3	54 ± 1[b]	120 ± 1[b]	< 1[d]	446
L13*	Blank - 0% F.M.	97.4	48 ± 13[c]	111 ± 17[c]	< 1[e]	606
L14*	5% NVP	96.7	42 ± 17[c]	121 ± 20[c]	< 1[e]	635

Similar to Chapter 2, high instantaneous monomer conversions ($X_{M,inst}$ > 80%) were obtained during the reactions. At the end of the reaction, the monomer conversions were higher than 95 % in all the cases, suggesting at least the partial incorporation of the functional monomers to the acrylic particles. Nevertheless, due to the large disparity in reactivity ratios between (meth)acrylates and NVP (r_{MMA} = 1.69 and r_{NVP} = 0.03[4]; r_{BA} = 0.80 and r_{NVP} = 0.02[5]), gas chromatography measurements were performed on Latex 8 in order to confirm the incorporation of NVP. Figure 4.5 shows that after 30 minutes of reaction, when the seed was formed, the conversion of NVP was slightly lower that the conversions of the other two monomers due to its lower reactivity and the batch process used in this initial stage. However, this was overcome during the semibatch process where all the monomers showed very high instantaneous conversions. In addition, the total monomer conversion was nearly 100 % at the end of the reaction. With these results it was concluded that the NVP did not accumulate along

the reaction and that it was successfully incorporated to the polymer particles. Similarly, since NVP and NVC have the same polymerizable bond, it was assumed that NVC was also satisfactorily incorporated to the polymer particles.

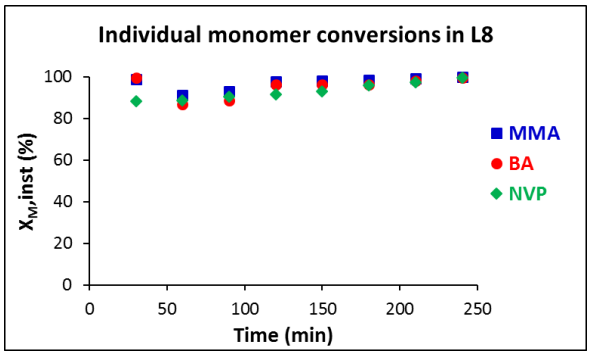

Figure 4.5. Individual monomer conversions measured by gas chromatography in Latex 8.

Regarding the particle size, it can be seen in Figure 4.4.B that the seeds formed after 30 minutes of batch polymerization had sizes between 42 and 63 nm. Then, during the semibatch stage the particles grew achieving final particles sizes between 110 and 137 nm. Table 4.3 shows that the gel content was suppressed in all the latexes with the incorporation of 0.1% wbm of n-dodecanethiol to the formulation. The polymers prepared with CTA presented weight average molecular weights in the range of 450 − 750 kg/mol. On the other hand, the polymer prepared in Latex 11 without CTA presented 33% of gel and the lowest M_w, which is a consequence of the incorporation of the high-molecular-weight chains into the gel.

4.3.2. Tensile properties

In order to investigate the effect of the hydrogen bond interaction between the pyrrolidone and TA in the system, films were cast from the 0 and 5 % NVP latexes (L7 and L8) with different TA contents. The mechanical performance of the materials was evaluated by tensile testing. The stress−strain plots obtained for the reference material (L7) and for the latex functionalized with 5% of pyrrolidone (L8) are presented in Figures 4.6.A and 4.6.B, respectively. The mechanical parameters obtained from the curves shown in Figure 4.6 are summarized in Table 4.4. To give an estimate of the molar ratios in these experiments, a latex with 5 wt % NVP and 2.5 wt % TA corresponds to a molar ratio of NVP/TA = 31 and a molar ratio of H-bond acceptor(amide)/H-bond donor(hydroxyl) = 1.2.

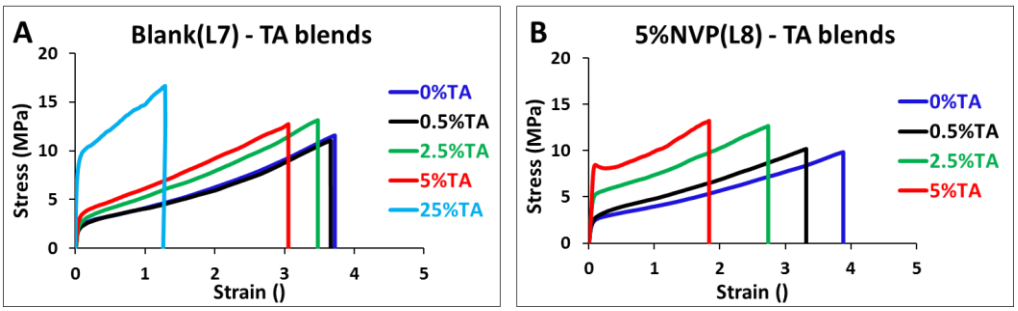

Figure 4.6. Stress−strain plots obtained from tensile measurements of the materials prepared from the (A) reference latex (L7) without the pyrrolidone and (B) latex containing 5% of NVP (L8). The 25% TA sample is not shown because it was too brittle to carry out the measurement.

Table 4.4. Mechanical parameters of the Blank (L7) - TA and 5% NVP (L8) - TA blends related to the stress –strain plots represented in Figure 4.6.

Latex	TA %	Young's modulus E (MPa)	Yield stress σ_y (MPa)	Tensile strength σ_{max} (MPa)	Ultimate strain γ_{max} ()
Blank (Latex 7)	0	84 ± 22	2.3 ± 0.4	11.6 ± 0.6	3.7 ± 0.1
	0.5	86 ± 19	2.2 ± 0.5	11.1 ± 0.8	3.7 ± 0.1
	2.5	104 ± 33	2.8 ± 0.4	13.1 ± 0.7	3.5 ± 0.2
	5	125 ± 24	3.3 ± 0.1	12.7 ± 1.3	3.1 ± 0.2
	25	299 ± 48	10.6 ± 1.0	18.8 ± 2.1	2.2 ± 0.3
5% NVP (Latex 8)	0	78 ± 7	2.5 ± 0.1	9.8 ± 0.3	3.9 ± 0.1
	0.5	76 ± 14	2.7 ± 0.4	10.2 ± 0.1	3.3 ± 0.4
	2.5	129 ± 18	5.1 ± 0.3	12.7 ± 1.3	2.7 ± 0.2
	5	225 ± 14	8.4 ± 0.7	13.2 ± 1.6	1.8 ± 0.4

Figure 4.6 and Table 4.4 show that for the blank latex, at low tannic acid contents (up to 5%) there was little change in the mechanical properties with increasing tannic acid content. Nevertheless, it was possible to discern that increasing the tannic acid content, the materials showed slightly higher Young's moduli and yield stress and lower ultimate strain. When the tannic acid content was increased to 25%, an abrupt change in the mechanical behavior was observed, as the material became substantially stiffer and brittle.

On the other hand, in the NVP - tannic acid blends (Latex 8 - TA), the mechanical properties were efficiently modified with the tannic acid content even at low tannic acid fractions. As in the blank latex, the addition of tannic acid led to the formation of stiffer (higher Young's modulus and yield stress) and less flexible materials. Comparison of Figures 4.6.A and 4.6.B

clearly indicates that the effect of the addition of TA was considerably greater when NVP was present. This is perhaps most notable in the increase of the yield strength of the NVP materials with added tannic acid. Similar behavior was observed in Chapter 3 where the addition of PVP, TA or GA to PVOH-stabilized latexes led to the formation of stiffer materials. The modification in the mechanical properties reported in Chapter 3 and in this chapter through a non-covalent network is similar to the systems that employ chemical crosslinking.[6–11] The addition of water-soluble H-bonding species (TA in this case) led to a loss in extensibility, but in coatings applications, the loss in extensibility does not necessarily affect the final performance of the materials, since they will not suffer high deformations under normal conditions. Instead, the most significant effect on mechanical properties relates to increased stiffness as this determines the hardness of the coating.

4.3.3. Film morphology

In order to explain these drastic differences in mechanical properties with addition of tannic acid for the two latexes, the morphology of the films was investigated by transmission electron microscopy. The films were stained with ruthenium tetroxide, which complexes with the aromatic rings. Therefore, the darker regions observed correspond to tannic acid rich areas. The images obtained for the blank (L7) - TA blends are shown in Figure 4.7.

The image of the initial P(MMA/BA) film without tannic acid is shown in Figure 4.7.A. As expected, due to the absence of tannic acid it was homogeneous, without darker zones. When 5 wt% of tannic acid was added (Figure 4.7.B) some dark isolated aggregates were observed which corresponded to tannic acid. Analyzing the TEM images and the tensile test results simultaneously for this sample, it can be seen that the material became slightly stiffer due to the presence of TA aggregates dispersed in the polymer matrix. When the TA content was increased

to 25 %, Figures 4.7.C and 4.7.D show that the tannic acid formed a honeycomb structure. The size of each cell was of around 120 nm which was in agreement with the DLS particle size results, indicating that each cell corresponded to an individual polymer particle. These kinds of materials, also known as cellular solids, present superior mechanical properties such as stiffness and tensile strength and are used in a variety of applications: from sandwich panels for the building sector to aerospace components.[12] The formation of the honeycomb structure in the film cast from the blank latex and 25 % of TA had a great effect on the mechanical properties where an abrupt change was observed as seen in Figure 4.6.A.

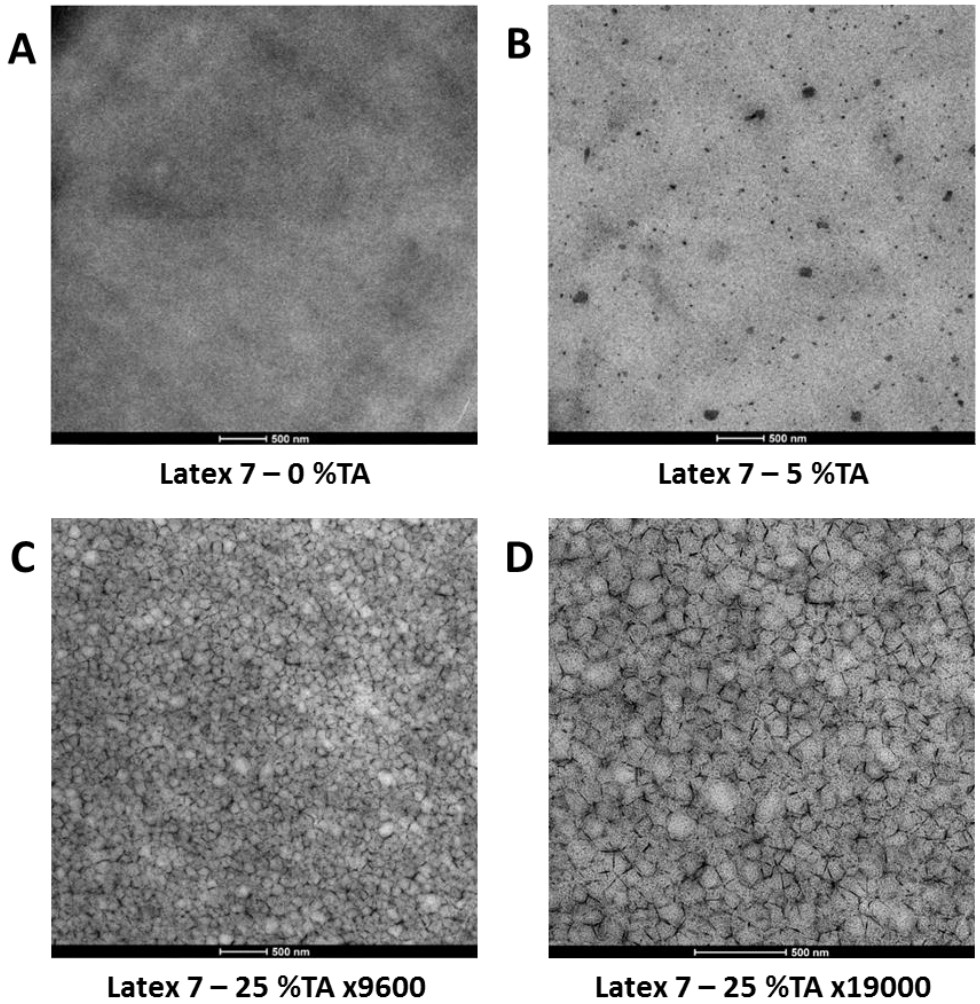

Figure 4.7. TEM images of the blank latex (L7) - TA blends without the pyrrolidone and with different TA contents: A) Pure P(MMA/BA) without tannic acid, B) 5 wt% TA C) 25 wt% TA at x9600 amplification and D) 25 wt% TA at x19000 amplification.

Moving to the images of the pyrrolidone containing blends shown in Figure 4.8, the honeycomb microstructure was detected from very low tannic acid contents. Even at 0.5 % TA (Figure 4.8.A) it was possible to visualize the honeycomb microstructure. These results were in agreement with the tensile test results, in which the mechanical properties were efficiently modified with small tannic acid contents. This early formation of the honeycomb allows for the stiffening of the materials from very low TA contents. Comparison with the results obtained with the blank latex shows that the presence of hydrogen accepting groups in the latex particles bound the tannic acid to the surface of the particles during film formation and therefore led to the honeycomb structure. Translating these findings to the tensile properties of the PVOH – PVP / TA / GA blends discussed in Chapter 3 (see Figure 3.4), the efficient stiffening observed for the PVOH materials very likely arose from the better distribution of PVP, TA and GA around the polymer particles thanks to the H-bonds between PVOH and the water-soluble species.

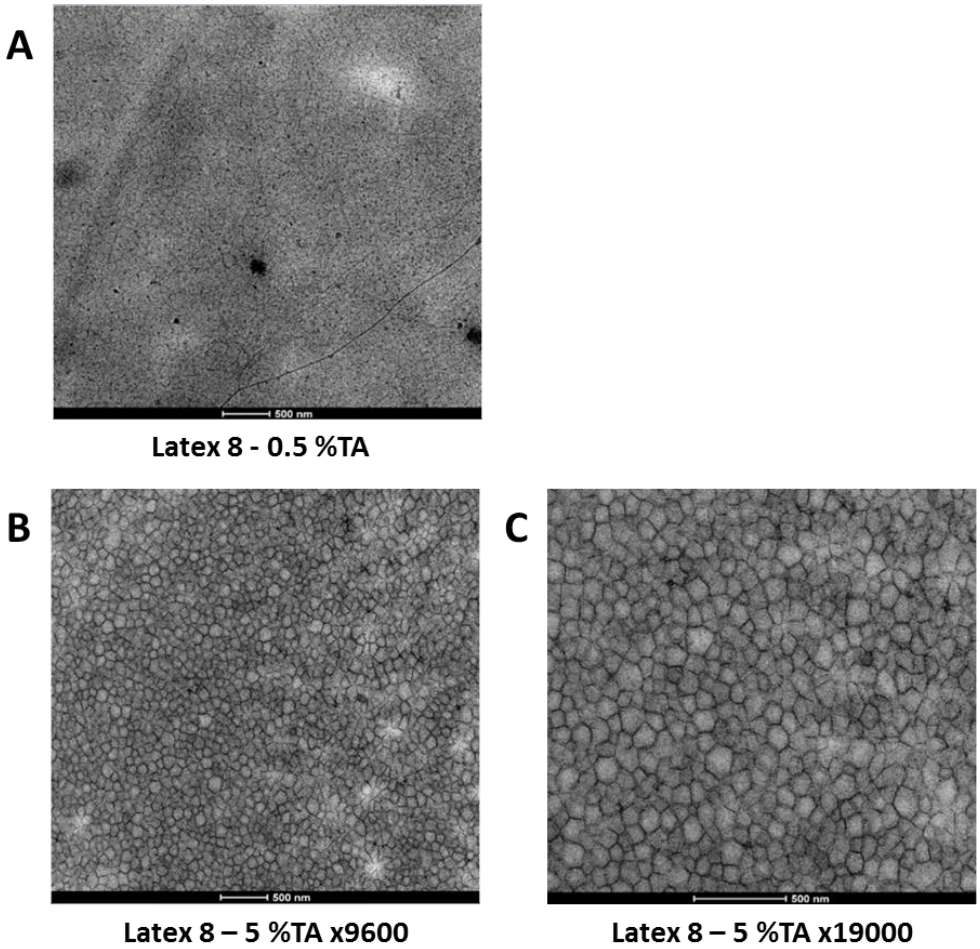

Figure 4.8. TEM images of the Latex 8 - TA blends with 5 wt% of NVP and different TA ratios: A) 0.5 wt% TA, B) 5 wt% TA at x9600 of magnification and C) 5 wt% TA at x19000 of magnification.

The differences in microstructure of the films between the blank and 5% NVP latexes can also be seen in the optical properties of the materials as shown in Figure 4.9. In the case of the blank latexes, the tannic acid aggregates in the film led to increased light scattering and increased the opacity of the films, while the honeycomb structure given by the NVP-containing latexes gives significantly less scattering and more translucent films were obtained. A similar

behavior was observed in Chapter 3, where the H-bonded PVOH – TA / GA blends were more translucent than the reference Dowfax – TA / GA materials. The transparency of the PVOH – TA / GA films suggests that in presence of H-bonds the polyphenols arranged around the PVOH-stabilized polymer particles forming a honeycomb microstructure and this explains the efficient stiffening observed for these materials.

In addition, similar to the PVOH – TA blends, the addition of tannic acid altered the color of the blank and 5% NVP materials, showing increasing orange tint with the tannic acid content. This fact would prevent the use of these materials as clear coats in many applications, but should not impede their application as binders in pigmented coatings or wood coatings since tannins are the main components responsible for the color of the wood.

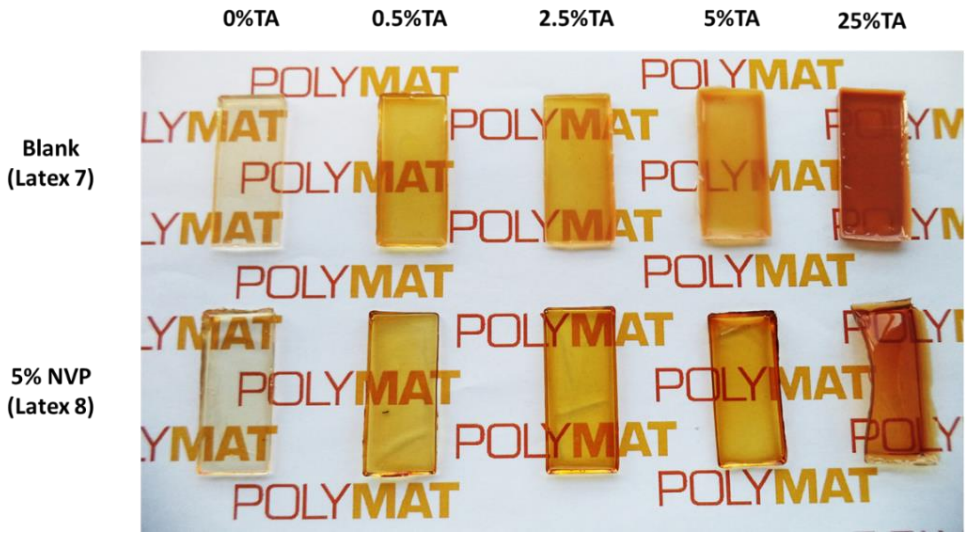

Figure 4.9. Appearance of the films with different tannic acid content: First line, materials prepared with the blank latex (L7) which were used as reference; and second line, materials prepared with the NVP latex (L8), which had the pyrrolidone functional groups.

4.3.4. Dynamic mechanical properties

The dynamic mechanical properties of the materials were also measured by Dynamic Mechanical Thermal Analysis (DMTA). The tanδ temperature sweep results obtained for the blank (L7) - TA blends and the 5% NVP (L8) - TA blends are presented in Figures 4.10.A and 4.10.B, respectively.

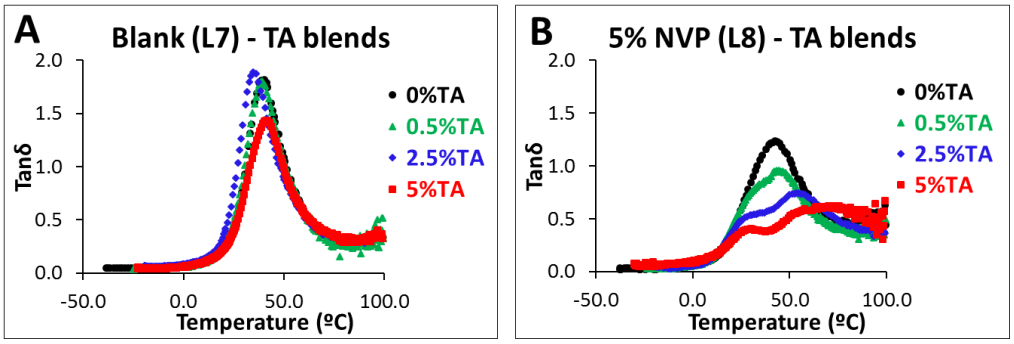

Figure 4.10. DMTA measurements of A) Latex 7 - TA and B) Latex 8 - TA blends.

For blank - TA blends, the addition of tannic acid did not have any significant influence on the glass transition temperature (T_g), which was around 40 ºC for all tannic acid contents. It is worth highlighting that 40 ºC is a very high T_g for a 50/50 P(MMA/BA) copolymer (theoretical T_g ≈10 ºC). The T_g measured with DSC was 19 ºC (Figure 4.11), which was closer to the theoretical value. For the blank materials, the reason for the limited influence of TA on the T_g was that the tannic acid formed aggregates and therefore the interaction between the polymer in the particles and the tannic acid was limited. However, in the materials functionalized with pyrrolidones, two different transitions were observed. The starting 5% NVP – 0 wt% TA material presented a single T_g but this peak was split in two when the tannic acid was added. In addition, the distance between the two maxima of the peaks increased with the tannic acid content. It is thought that this shift is a result of the restricted motion of the polymer chains bound to the tannic acid

(showing a shift towards higher T_g) while the mobility of the chains of the interior part of the particles would remain the same. In order to understand this hypothesis, it is convenient to think about the distribution of the pyrrolidone functional groups within the polymer particles. As they are hydrophilic, they will tend to go to the surface of the particles that are in contact with water. As a consequence, two different populations of polymer chains can be defined: P(MMA/BA) chains basically devoid of pyrrolidone in the interior part of the particles and pyrrolidone rich polymer chains in the exterior part. The polymer chains richer in NVP will present slightly higher T_g as the PVP homopolymer has a T_g of 187 ºC[13] and therefore the T_g peak at 0 wt% TA was broader for the latex with pyrrolidone (Latex 8).

When the tannic acid is added to the system, the pyrrolidone moieties that are mainly located in the outside part of the particles interact via H-bonding with the hydroxyl groups of the tannic acid and therefore the movement of the polymer chains that are next to the TA is restricted. Hence, when the TA is added, the T_g of the polymer chains with NVP is shifted to higher temperatures whilst the non-interacting P(MMA/BA) chains remain at the same T_g. This behavior was not observed in the reference materials where the polymer chains were not able to interact via H-bonding. These results can be considered as proof of the formation of hydrogen bonding interactions which modify the mobility of the polymer chains and the mechanical dynamic behavior of the materials.

These results were corroborated by Differential Scanning Calorimetry (DSC). The thermograms of the blends prepared from Latex 7 (blank) and Latex 8 (5% NVP) with 5 wt% TA are shown in Figure 4.11. In agreement with the DMTA results, the blank - TA materials only showed one T_g at 19 ºC whilst the 5% NVP - TA materials showed two: the first one at 9 ºC and the second one at 52 ºC. The appearance of the high T_g chain population was attributed to the

mobility constraints produced by the hydrogen bonds between the pyrrolidone and the hydroxyl groups.

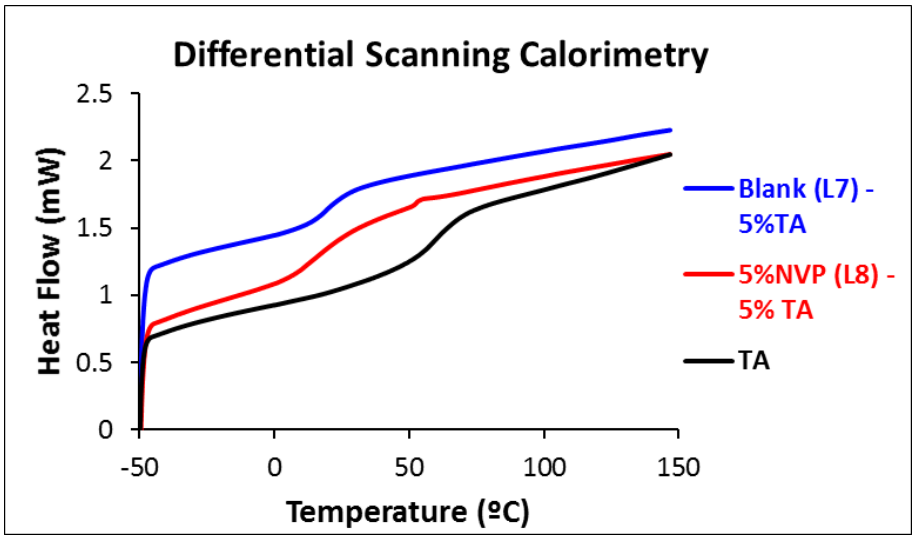

Figure 4.11. Thermograms of the blends prepared from Latex 7 (blank) and Latex 8 (5% NVP) with 5% TA.

4.3.5. Fourier Transform Infrared Spectroscopy (FTIR)

In order to further confirm that the hydrogen bonds were responsible for the formation of the microstructure, the films were analyzed by FTIR. The absorption spectra of the reference and pyrrolidone containing materials are shown in Figure 4.12. The TA concentration increases upwards, as the broad signal of the hydroxyl groups of tannic acid at around 3400 cm^{-1} increases. The results obtained for the 25 wt% TA and 50 wt% TA blends are included Figure 4.12 in order to emphasize the chemical shifts related to the H-bond interactions.

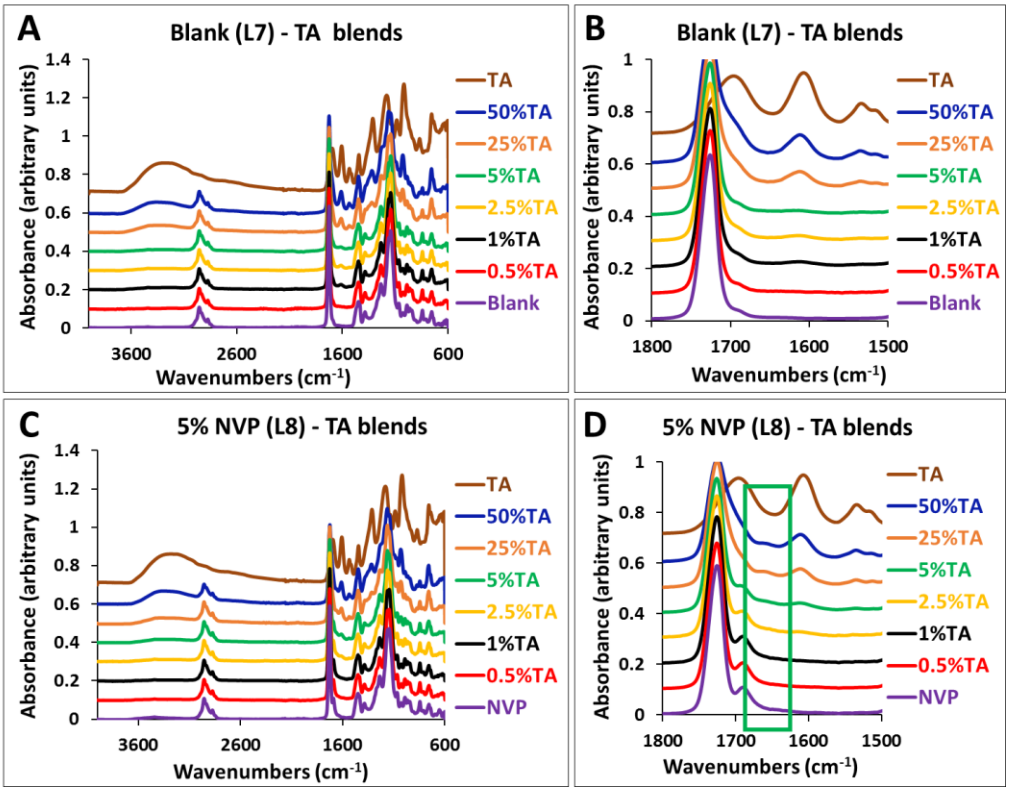

Figure 4.12. FTIR of the blank - TA blends without pyrrolidone are shown in parts A and B and results of the 5% NVP - TA blends are shown in parts C and D. Parts A and C show the whole FTIR spectrum and parts B and D display the carbonyl region.

In both sets of materials the spectra obtained were very similar. Only a small difference was detected in the carbonyl region (1500-1800 cm^{-1}, see Figures 4.12.B and 4.12.D). Starting from the carbonyl region of the blank latex (L7), the big peak at 1720 cm^{-1} corresponded to the acrylic and methacrylic carbonyls of the copolymer. However, the pyrrolidone containing polymer (L8) showed two peaks: A big peak at 1720 cm^{-1} (acrylic and methacrylic carbonyls) and a small peak at 1690 cm^{-1} which corresponded to the amide carbonyl of the pyrrolidone. In addition, in the pyrrolidone containing materials, the formation of a new small peak was observed at 1660

cm^{-1} at high TA contents (marked with a green rectangle in Figure 4.12.D). This peak was not detected in the reference blends, and therefore, it could correspond the complexed amide carbonyl peak which was shifted to lower wavenumbers. This shift is in good agreement with previous FTIR studies of the interaction between phenols and pyrrolidone as recently reported by Nam *et al*, where the addition of TA to polyvinyl pyrrolidone (PVP) shifted the PVP carbonyl absorption peak 29 units downfield, from 1661 cm^{-1} to 1632 cm^{-1}.[2]

4.3.6. Influence of microstructuring

In order to investigate the influence of film nanostructuring on the mechanical performance of the materials, the polymer - tannic acid blends were dissolved in THF and the films were cast from solution. The TEM images of the Blank (L7) – 5 %TA and 5%NVP (L8) – 5 %TA materials cast from solution are shown in Figure 4.13. In both cases the films cast from solution did not show the honeycomb microstructure but contained aggregates of tannic acid in the polymer matrix. However, in the pyrrolidone containing material the aggregates observed were smaller and they were homogeneously dispersed in the polymer matrix. This could be attributed to the formation of H-bonds between the pyrrolidone and tannic acid.

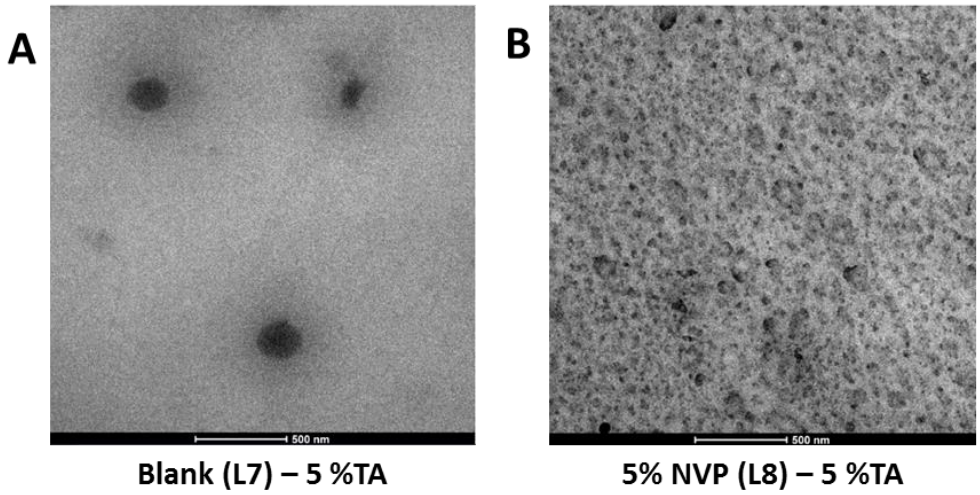

Figure 4.13. TEM images of the materials with 5% TA cast from solutions in THF: A) Blank (L7) – 5 %TA and B) 5% NVP (L8) – 5 %TA .

The mechanical properties of the films cast from solution were also measured by tensile test. The stress-strain plots of Blank - TA and 5% NVP - TA blends cast from solution are presented in Figure 4.14 and the mechanical parameters obtained from the curves are summarized in Table 4.5.

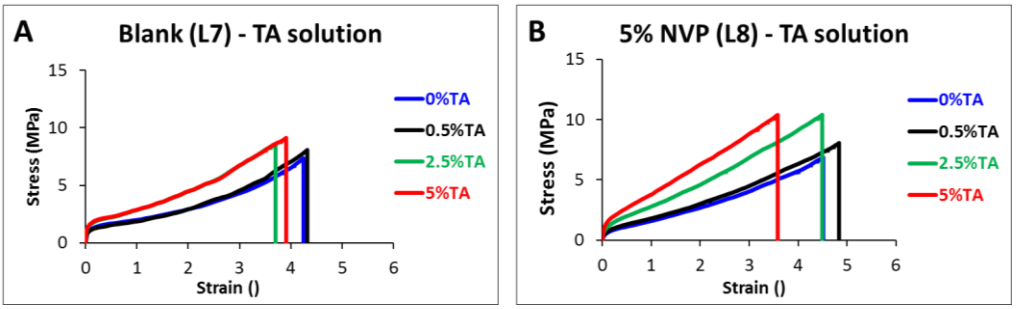

Figure 4.14. Mechanical properties of the materials cast from solutions in THF: A) Blank (L7) - TA blends and B) 5% NVP (L8) - TA blends.

Table 4.5. Mechanical parameters related to the stress-strain plots represented in Figure 4.14.

Latex	TA %	Young's modulus E (MPa)	Yield stress σ_y (MPa)	Tensile strength σ_{max} (MPa)	Ultimate strain γ_{max} ()
Blank (Latex 7)	0	52 ± 29	1.8 ± 0.18	7.4 ± 1.7	4.2 ± 0.6
	0.5	56 ± 35	1.12 ± 0.10	8.1 ± 1.7	4.3 ± 0.1
	2.5	85 ± 38	1.74 ± 0.12	9.1 ± 0.6	3.9 ± 0.4
	5	103 ± 8	2.02 ± 0.09	10.1 ± 1.6	4.2 ± 0.7
5% NVP (Latex 8)	0	15 ± 8	0.60 ± 0.16	6.8 ± 1.4	4.5 ± 0.3
	0.5	31 ± 10	0.66 ± 0.10	9.1 ± 1.6	4.8 ± 0.1
	2.5	47 ± 17	0.95 ± 0.11	10.4 ± 0.7	4.5 ± 0.3
	5	64 ± 13	1.42 ± 0.04	10.40± 1.3	3.6 ± 0.4

First of all, it is important to clarify that even in the case where no tannic acid was added, some plasticizing effect of THF traces could be observed and therefore the results obtained from solution and dispersion cannot be directly compared. As in the case of the materials cast from dispersion, the materials showed an increase in the Young's modulus, yield stress and tensile strength and a decrease in the elongation at break with the tannic acid content. In addition, the

incorporation of NVP to the materials resulted in a greater improvement of the mechanical properties. However, unlike the case of the materials cast from dispersion the absence of the honeycomb structure meant that the improvement in mechanical properties, and in particular the stiffness of the material, was not as noticeable. This highlights the importance of the film microstructure. First, the hard TA honeycomb provided structural reinforcement to the polymer films. In addition, the arrangement of TA around the pyrrolidone-rich polymer particles led to a high density of H-bonds at the particle interfaces which further enhanced the mechanical strength of the materials.

4.3.7. Water sensitivity

One important aspect in the practical use of polymer films cast from waterborne dispersions is the sensitivity to water. In previous works, including the PVOH – PVP / TA / GA blends presented in Chapter 3, this has been one of the major issues in films which are held together by hydrogen bonds due to disruption of the network and loss of the mechanical integrity by small amounts of water.[14] Therefore, in order to investigate this, the films were immersed in water for 7 days and the water absorption and weight loss of the films was determined. The water uptake and weight loss results are presented in Figures 4.15.A and 4.15.B.

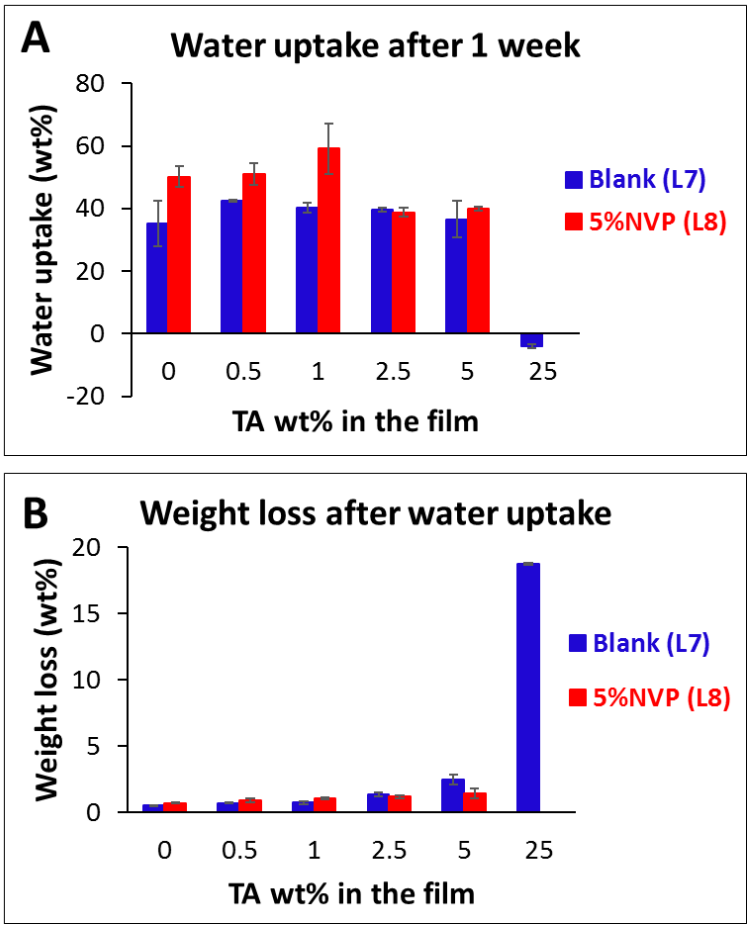

Figure 4.15. (A) Water uptake and (B) weight loss of the films after one week of immersion in water.

In general, the pyrrolidone containing samples absorbed more water than the reference ones as NVP is a hydrophilic monomer. However, unlike the PVOH-containing materials studied in Chapter 3, the values of water uptake were comparable to conventional latex films. This improvement in the water sensitivity could be due to a decrease of the water-sensitive species from 10 wt% PVOH to 5 wt% NVP and the incorporation of the NVP into a hydrophobic copolymer system. The blank (L7) – 25 wt% TA material showed a negative water uptake value very likely

due to the release of water-soluble species during the water uptake. To confirm this, the films were dried and weighed in order to determine the weight loss of the films after the immersion in water. The weight loss results presented in Figure 4.15.B show that the blank – 25 wt% TA film disintegrated during the test. In addition, while the weight loss of the 5% NVP materials remained nearly constant, the weight loss in the blank materials increased gradually with the TA content. This suggested that the component that was being leached out was the tannic acid. To confirm this, the amount of tannic acid released during the water uptake was determined by UV-vis spectroscopy.

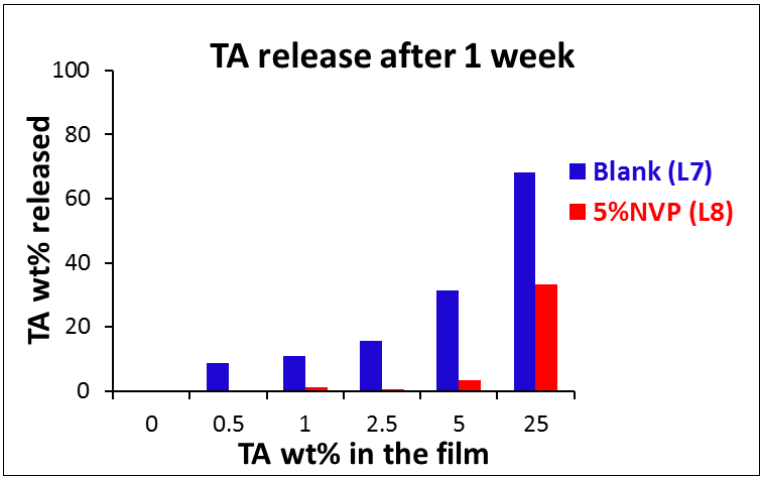

Figure 4.16. Fraction of tannic acid released from the films during the water uptake measurements.

Looking at Figure 4.16, it can be noticed that in all the proportions, the tannic acid leached out of the film to a lesser extent in the pyrrolidone containing materials due to the H-bonding interactions. At tannic acid concentrations up to 5 %, almost no tannic acid was released from the pyrrolidone containing materials while more than 10 % of the tannic acid was released in the reference materials. In order to check the ability of the pyrrolidone groups to retain higher concentrations of tannic acid in the film, a blend of 5% NVP (L8) with 25 wt% TA was prepared

and the tannic acid released from its film measured. Figure 4.16 shows that the fraction of TA released substantially increased. This is perhaps to be expected as in the case of the pyrrolidone containing latex at 25 wt% TA the molar ratio of NVP/TA = 3 and the ratio amide/phenol = 0.1. This means that there are likely to be at any given time a fraction of tannic acid molecules that do not have any H-bonding interactions with vinyl pyrrolidone.

In the case of the reference material, for which there are limited interactions with the polymer at all concentrations, the abrupt increase in dissolution of the tannic acid may be a result of the formation of the honeycomb structure at tannic acid contents equal or higher than 25 wt% (see Figure 4.6.D). Thus, while at lower tannic acid concentration the tannic acid is in isolated pockets and dissolution requires transport through the acrylic film, at higher tannic acid concentration the formation of the honeycomb structure created a connected pathway for the entrance of water and dissolution of TA, provoking the observed weight loss and partial disintegration of the films.

Although water uptake gives an idea of water sensitivity, in materials held together by H-bonds, one critical aspect is how the mechanical properties are affected following contact with water. This is obvious from the results in Chapter 3 where the improvement of mechanical properties was completely removed following extensive contact with water. In order to explore this for the PVP – tannic acid system, the tensile properties of the films were tested before and after being immersed in water. The tensile test results are presented in Figure 4.17 and Table 4.6.

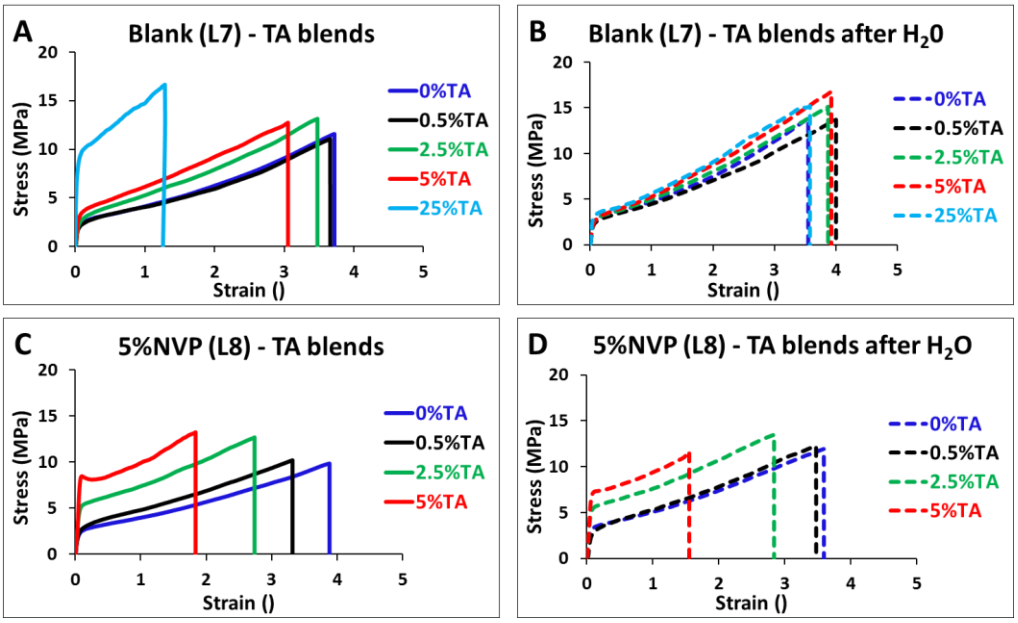

Figure 4.17. Tensile test results of: A) Blank (L7) - TA blends prior to immersion in water, B) Blank (L7) - TA after immersion in water, C) 5% NVP (L8) - TA blends before immersion in water and D) 5% NVP (L8) - TA after immersion in water.

Table 4.6. Mechanical parameters of the Blank (L7) - TA and 5 wt% NVP (L8) - TA blends related to the stress-strain plots represented in Figure 4.17 before and after immersion in water. [a]Only one measurement recorded.

Latex	TA %	Young's modulus E (MPa)	Yield stress σ_y (MPa)	Tensile strength σ_{max} (MPa)	Ultimate strain γ_{max} ()
Blank (Latex 7) BEFORE	0	84 ± 22	2.3 ± 0.4	11.6 ± 0.6	3.7 ± 0.1
	0.5	86 ± 19	2.2 ± 0.5	11.1 ± 0.6	3.7 ± 0.1
	2.5	104 ± 33	2.8 ± 0.4	13.1 ± 0.7	3.5 ± 0.2
	5	125 ± 24	3.3 ± 0.1	12.7 ± 1.3	3.1 ± 0.2
	25	299 ± 48	10.6 ± 1.0	18.8 ± 2.1	2.2 ± 0.3
Blank (Latex 7) AFTER	0	116 ± 42	2.8 ± 0.8	13.8 ± 1.1	3.6 ± 0.1
	0.5	88 ± 5	2.4 ± 0.3	13.7 ± 0.6	4.0 ± 0.2
	2.5	100 ± 16	2.8 ± 0.3	15.1 ± 1.1	3.9 ± 0.2
	5	95 ± 11	2.7 ± 0.2	16.8 ± 1.5	3.9 ± 0.3
	25	170 ± 11	3.2 ± 0.1	15.2 ± 1.1	3.6 ± 0.2
5% NVP (Latex 8) BEFORE	0	78 ± 7	2.5 ± 0.1	9.8 ± 0.2	3.9 ± 0.1
	0.5	76 ± 14	2.7 ± 0.4	10.2 ± 0.1	3.3 ± 0.4
	2.5	129 ± 18	5.1 ± 0.3	12.7 ± 1.3	2.7 ± 0.2
	5	225 ± 14	8.4 ± 0.7	13.2 ± 1.6	1.8 ± 0.4
5% NVP (Latex 8) AFTER	0	98 ± 6	3.3 ± 0.1	12.4 ± 1.9	3.8 ± 0.7
	0.5[a]	74	3.0	12.2	3.5
	2.5	138 ± 18	5.4 ± 0.6	13.5 ± 0.2	2.8 ± 0.1
	5	169 ± 37	7.1 ± 1.5	11.6 ± 4.5	1.6 ± 0.5

In the case of the reference materials, it can be observed that all the improvements of mechanical properties by the presence of tannic acid were drastically reduced following immersion in water and all samples showed similar mechanical behavior (Figure 4.17.B). This observation is expected based on the loss of tannic acid as observed in Figure 4.16 which results in the disintegration of the honeycomb structure. On the other hand, in the case of the pyrrolidone containing blends, the mechanical properties were maintained after the immersion in water due to the retention in the system of the tannic acid by the strong hydrogen bonds. In order to confirm the structural differences between the reference and the pyrrolidone containing films, TEM images were obtained following immersion in water (see Figure 4.18). In agreement with the water uptake results and the tensile testing shown above, in the reference sample, immersion in water leads to dissolution of a substantial part of the tannic acid and loss of the honeycomb microstructure in the case of high TA content. On the contrary, the sample containing N-vinyl pyrrolidone showed similar structure before and after immersion in water.

Compared to the PVOH – TA / GA system discussed in Chapter 3, the pyrrolidone – phenol H-bonds were stronger than the PVOH – phenol H-bonds. In consequence, when the PVOH film were put in contact with water the disruption of the non-covalent network led to the partial disintegration of the polymer films. In addition, in Chapter 3 the release of non-grafted PVOH chains enhanced the decomposition of the films. On the contrary, the strong pyrrolidone – TA H-bonds endured in contact with water and this allowed the retention of the morphology and mechanical properties of the films.

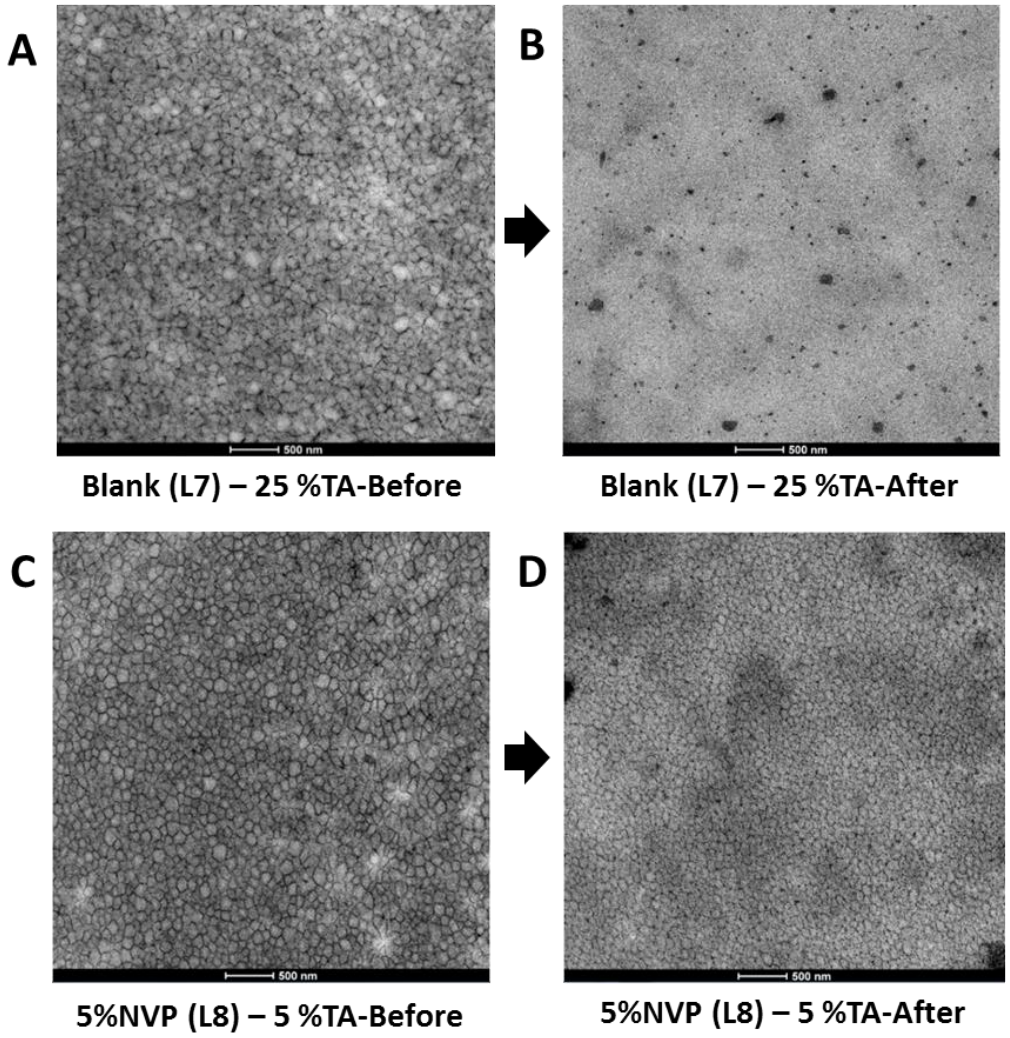

Figure 4.18. TEM images before and after water immersion of the films: A) Blank (L7) - 25 wt% TA before water immersion, B) Blank (L7) - 25 wt% TA after water immersion, C) 5% NVP (L8) - 5 wt% TA before water immersion and D)) 5% NVP (L8) - 5 wt% TA after water immersion.

4.3.8. Investigation of industrially interesting variables

Having demonstrated the possibility of a hydrogen bond induced structuring and stiffening of acrylic polymer films, the versatility of the approach for other latexes was studied. First, the effect of lowering the concentration of NVP from 5 to 2 wt% was investigated using Latex 9. Then, the effect of the presence of acrylic acid (often used in latexes for coatings) and the absence of CTA was studied in Latexes 10 and 11, respectively. Finally, the possibility of using a different hydrogen acceptor was checked in Latex 12. The tensile measurements of the films cast from blends of these latexes and varying amounts of tannic acid are presented in Figure 4.19 and Table 4.7. First it was confirmed using Latex 9 that even at lower pyrrolidone concentrations, a similar stiffening effect could be observed, although to a reduced extent. Second, it was shown that in the presence of acrylic acid (Latex 10), a commonly used comonomer in emulsion polymerization, and in the absence of any CTA such that high molecular weight polymers are obtained (Latex 11), the addition of tannic acid also had a reinforcing effect on the mechanical behavior of the film. In addition, it was shown using Latex 12 that the stiffening effect through hydrogen bonding also applied to alternative amide monomers as demonstrated by the use of N-vinyl caprolactam (NVC).

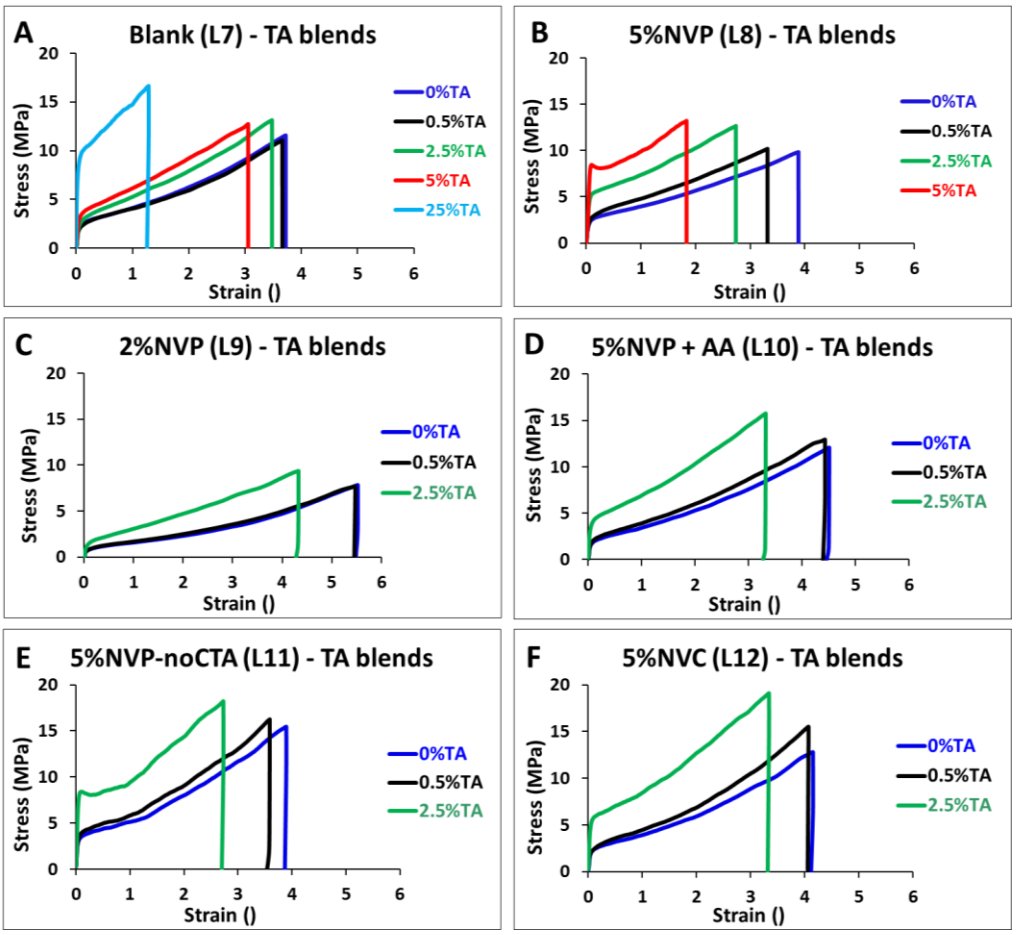

Figure 4.19. Tensile test results of: A) Latex 7 - TA blends without pyrrolidone used as reference, B) Latex 8 – TA blends with 5 %NVP and CTA, C) Latex 9 - TA blends with 2 %NVP, D) Latex 10 - TA blends incorporating 5 %NVP and 1 %AA, E) Latex 11 – TA blends with 5 %NVP but without CTA and F) Latex 12 – TA using 5 %NVC.

Table 4.7. Mechanical parameters related to the stress-strain plots represented in Figure 4.19.

Latex	TA %	Young's modulus E (MPa)	Yield stress σ_y (MPa)	Tensile strength σ_{max} (MPa)	Ultimate strain γ_{max} ()
Blank Latex 7	0	84 ± 22	2.3 ± 0.4	11.6 ± 0.6	3.7 ± 0.1
	0.5	86 ± 19	2.2 ± 0.5	11.1 ± 0.8	3.7 ± 0.1
	2.5	104 ± 33	2.8 ± 0.4	13.1 ± 0.7	3.5 ± 0.2
	5	125 ± 24	3.3 ± 0.1	12.7 ± 1.3	3.1 ± 0.2
	25	299 ± 48	10.6 ± 1.0	18.8 ± 2.1	2.2 ± 0.3
5% NVP Latex 8	0	78 ± 7	2.5 ± 0.1	9.8 ± 0.2	3.9 ± 0.1
	0.5	76 ± 14	2.7 ± 0.4	10.2 ± 0.1	3.3 ± 0.4
	2.5	129 ± 18	5.1 ± 0.3	12.7 ± 1.3	2.7 ± 0.2
	5	225 ± 14	8.4 ± 0.7	13.2 ± 1.6	1.8 ± 0.4
2% NVP Latex 9	0	30 ± 3	0.8 ± 0.1	8.0 ± 0.2	5.6 ± 0.1
	0.5	26 ± 10	0.9 ± 0.1	7.4 ± 0.3	5.5 ± 0.5
	2.5	54 ± 14	1.7 ± 0.2	11.0 ± 2.6	4.3 ± 0.3
5% NVP +AA Latex 10	0	64 ± 6	1.9 ± 0.1	11.6 ± 0.7	4.4 ± 0.1
	0.5	109 ± 27	3.1 ± 0.9	14.5 ± 1.4	4.1 ± 0.6
	2.5	130 ± 75	3.9 ± 2.2	15.9 ± 3.2	3.8 ± 0.6
5% NVP - noCTA Latex 11	0	130 ± 16	3.4 ± 0.4	15.5 ± 0.3	3.9 ± 0.1
	0.5	137 ± 11	3.7 ± 0.2	16.1 ± 0.9	3.6 ± 0.1
	2.5	228 ± 53	7.4 ± 0.8	18.5 ± 1.0	2.8 ± 0.1
5% NVC Latex 12	0	65 ± 12	2.1 ± 0.2	13.2 ± 0.4	4.1 ± 0.1
	0.5	86 ± 19	2.4 ± 0.6	14.9 ± 0.5	4.0 ± 0.1
	2.5	150 ± 30	4.7 ± 0.9	17.9 ± 1.7	3.3 ± 0.3

In addition to these experiments varying the latex and the H-bond acceptor, the influence of the molecular weight and nature of the H-bond donor used as physical crosslinker was studied employing different crosslinkers and maintaining constant the hydroxyl concentration. Gallic acid (the repeat unit of tannic acid) was selected to analyze the effect of the molecular size of the crosslinker (see Figure 4.20.A, and Table 4.8). Whilst being chemically similar, gallic acid contains 3 phenolic OH groups per molecule as opposed to 25 in tannic acid. Starting from the 5% NVP (L8) - GA blends, as in the case of tannic acid (Figure 4.6.A for the 5% NVP (L8) – TA blends), the materials became stiffer and less flexible with the increasing fraction of crosslinker. However, from the comparison of the materials with the same crosslinker amount, it was observed that the gallic acid was less efficient modifying the mechanical properties. This is because the reduction in the number of OH groups per molecule reduces the probability of linking two different polymer particles and therefore reinforcing the materials. A second effect may be related to the stiffness of the percolating, polyphenol rich network. As tannic acid has a larger number of hydrogen bonding groups per molecule we expect the stiffness of the honeycomb to also be higher in the case of tannic acid. Polyvinyl alcohol (PVOH) was employed to evaluate the influence of the acidity of the hydroxyl group and therefore the strength of the H-bond. The aromatic hydroxyl groups are more acidic; hence, they are able to form stronger H-bonds. From the results shown in Figure 4.20.B and Table 4.8, it was observed that, in contrast to tannic acid, the addition of PVOH did not lead to the formation of stiffer films. The Young's moduli of the materials only increased slightly with the PVOH content but the mechanical properties were not significantly modified. Therefore, it was concluded that the acidity of the phenolic hydroxyls plays a key role when forming H-bonds with the pyrrolidone groups and promoting the formation of the reinforcing honeycomb microstructures.

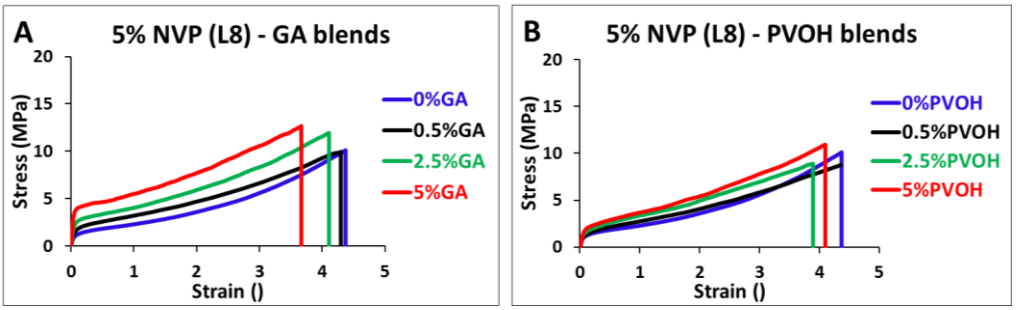

Figure 4.20. Mechanical behavior of the pyrrolidone functionalized materials physically crosslinked with H-bond donors: A) 5 %NVP (L8) - GA blends and B) 5 %NVP (L8) - PVOH blends.

Table 4.8. Mechanical parameters of the 5% NVP (L8) - GA and 5% NVP (L8) - PVOH blends related to the stress-strain plots represented in Figure 4.20 used to analyze the influence of the physical crosslinker.

Latex	CL %	Young's modulus E (MPa)	Yield stress σ_y (MPa)	Tensile strength σ_{max} (MPa)	Ultimate strain γ_{max} ()
5% NVP (L8) - GA	0	23 ± 1	1.2 ± 0.1	10.1 ± 0.6	4.4 ± 0.2
	0.5	43 ± 6	1.9 ± 0.1	10.0 ± 0.5	4.3 ± 0.4
	2.5	87 ± 17	2.6 ± 0.2	11.9 ± 0.5	4.1 ± 0.2
	25	154 ± 44	3.9 ± 0.9	12.7 ± 0.4	3.7 ± 0.2
5% NVP (L8) - PVOH	0	23 ± 1	1.2 ± 0.1	10.1 ± 0.6	4.4 ± 0.2
	0.5	32 ± 6	1.4 ± 0.1	8.9 ± 1.0	4.4 ± 0.1
	2.5	40 ± 7	1.7 ± 0.1	8.7 ± 1.0	3.9 ± 0.2
	5	47 ± 8	2.0 ± 0.1	10.9 ± 0.4	4.1 ± 0.3

4.3.9. Application tests

The applicability of the NVP-TA system for coating applications (white paints) was investigated during the internship in BASF. The first objective was to examine if the reinforcement provided by TA was still functional in the presence of further formulation components. The second objective was to analyze if the color given to the films by TA was still visible in the presence of TiO_2 white pigment.

First, polymer dispersions with 0 and 5% NVP were prepared following procedure of Haddock *et al.* (Latex 13 and 14 in Table 4.1). Then, the latexes were combined with different amounts of TA to prepare five latex – TA blends: Blank (L13) – 0 wt% TA, 5 %NVP (L14) – 0 wt% TA, 5 %NVP (L14) – 1 wt% TA, 5 %NVP (L14) - 2.5 wt% TA and 5 %NVP (L14) – 5 wt% TA. These blends were used as binders and were combined with a white paste containing TiO_2, Natrosol (thickener) and surfactants to prepare the paints. As result, stable white paints were obtained for all blends with ≤ 1 wt% TA. On the contrary, the paints with 2.5 and 5 wt% TA collapsed and big aggregates were visible. To identify the formulation component responsible for the instability of the paints, TA was independently blended with the latexes, TiO_2 and Natrosol thickener in water. The latex – TA blends were stable and no changes in solids content or viscosity were detected after 1 week at 60 °C. In contrast, the addition of TA to TiO_2 and Natrosol led to the immediate formation of insoluble aggregates as a result of the strong H-bond interactions between the components. These strong interactions caused the instability of the paints and imply a great challenge for the preparation of formulated products with tannic acid.

Finally, relatively stable paints with 2.5 and 5 wt% TA were achieved removing Natrosol from the formulation. These two paints still contained small aggregates but were stable enough to cast a film. The final color of the films was quantitatively compared using the Lab values. “Lab”

is a color space that expresses color as three values: “L” expresses the lightness from 0 to 100, “a” is relative to the green–red opponent colors and “b” represents the blue-yellow opponents. “a” and “b” values can range from -127 to 128 being more positive numbers stronger in the red and yellow components. The appearance of the white coats and their corresponding Lab values are shown in Figure 4.21.

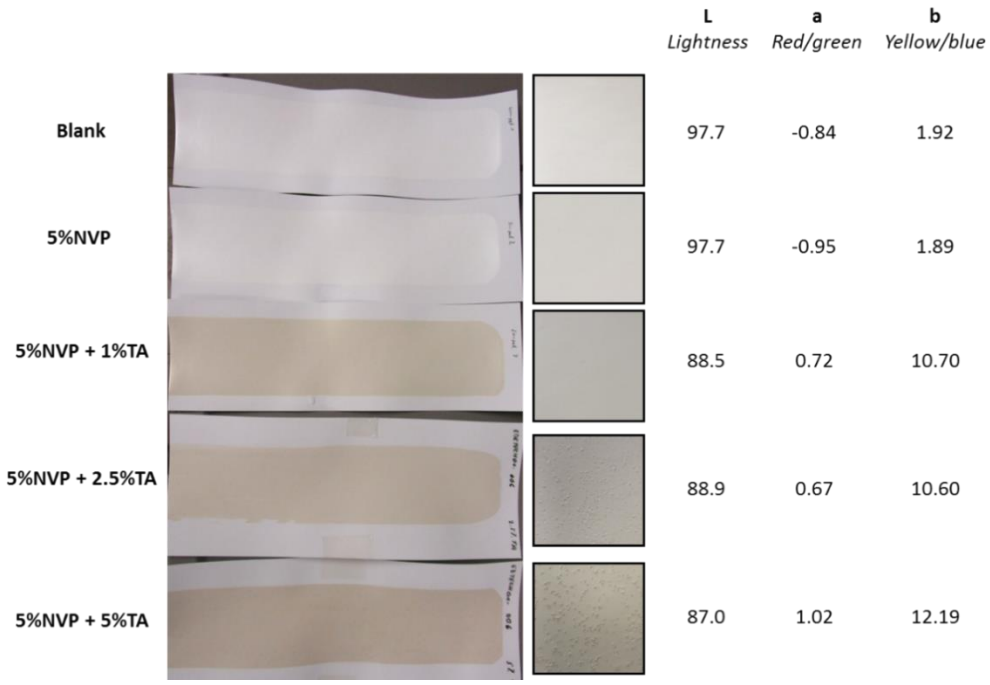

Figure 4.21. Physical appearance and Lab values of the white paints prepared from the NVP - TA system.

First, from the comparison of the paints prepared from the Blank and 5% NVP latexes with 0 wt% TA, it was concluded that the addition of pyrrolidone moieties to the dispersion does not affect the color of the paint since the blank and 5% NVP products showed very similar Lab values. Second, the addition of tannic acid gave an orange tint to the paints even in the presence of the TiO_2 pigment. This coloration was manifested in the Lab values with a decrease in the

lightness (“L”), slight increase in the redness (“a” value) and a considerable increase in the yellowness (“b” value) with the tannic acid content.

Besides the application of the NVP - TA system as white paints, the tannin blocking ability of the latex with 5% NVP was tested. The strong H-bonds between pyrrolidone and TA prevented the migration of TA from the films to the aqueous phase during the immersion in water and in this part of the work, the ability of these strong H-bonds to prevent the free migration of the tannins from the wood was investigated. The tannin blocking ability of the blank (L13) and 5% NVP (L14) was tested as non-formulated primer but no contribution coming from the pyrrolidone H-bond acceptors was observed.

4.4. Conclusions

In conclusion, it has been demonstrated that the addition of a water-soluble polyphenol compound, tannic acid, to a waterborne acrylic latex containing hydrogen bond accepting group leads to materials with improved Young's modulus and yield strength. The reinforcement was attributed to the formation of a honeycomb microstructure which was promoted by the hydrogen bonding interactions between pyrrolidone groups in the polymer backbone and phenolic OH groups in the tannic acid. While water uptake was similar to the blank, leaching of TA from the films was almost completely prevented by the H-bond network and therefore led to retention of mechanical performance even after extensive water exposure. The stiffening mechanism was applied to a variety of latexes (with different molecular weight polymers, variable H-bond acceptor monomer content, including AA in the formulation or employing NVC as alternative H-bond acceptor) proving the versatility of the approach. The nature and molecular size of the crosslinker were shown to directly influence the final performance of the materials: less acidic OH groups (PVOH) were not able to form strong interactions and reinforce the materials, and smaller molecular size phenolic compounds (GA) were less efficient stiffening the materials. The presented amide - TA H-bonding complexation offers a practical route to hard acrylic films cast from aqueous dispersions. However, when used as formulated product the strong interactions between TA and the main coating components led to unstable products, which makes the use of TA in formulated products challenging.

4.5. References

(1) Mullens, J.; Yperman, J.; François, J. P.; Van Poucke, I. C. Simultaneous Calorimetric Determination of Equillibrium Constant and Enthalpy Change of Hydrogen-bond Complexes in Dillute Solutions of Phenol with Pyridine in Carbon Tetrachloride *J. Phys. Chem.* **1985**, *89*, 2937–2941.

(2) Nam, H. G.; Nam, M. G.; Yoo, P. J.; Kim, J. Hydrogen bonding-based strongly adhesive coacervate hydrogels synthesized using poly(N-vinylpyrrolidone) and tannic acid *Soft Matter* **2019**, *15*, 785–791.

(3) Haddock, T. H. Presure sensitive adhesive. EP 0130080 B1, 1988.

(4) Parambil, A. M.; Puttaiahgowda, Y. M.; Shankarappa, P. Copolymerization of N-Vinyl pyrrolidone with methyl methacrylate by Ti(III)-DMG redox initiator *Turkish J. Chem.* **2012**, *36*, 397–409.

(5) Al-Issa, M. A.; Davis, T. P.; Huglin, M. B.; Yip, D. C. F. Copolymerizations involving N-vinyl-2-pyrrolidone *Polymer* **1985**, *26*, 1869–1874.

(6) Zosel, A. Mechanical Properties of Films from Polymer Latices *Polym. Adv. Technol.* **1995**, *6*, 263–269.

(7) Zosel, A.; Ley, G. Influence of crosslinking on Structure, Mechanical Properties, and Strength of Latex Films *Macromolecules* **1993**, *26*, 2222–2227.

(8) Mazuel, F.; Bui, C.; Charleux, B.; Cabet-deliry, E.; Winnik, M. A. Interdiffusion and Self-Cross-Linking in Acetal-Functionalized Latex Films *Macromolecules* **2004**, *37*, 6141–6152.

(9) Wang, R.; Ma, J.; Zhou, X.; Wang, Z.; Kang, H.; Zhang, L.; Hua, K.; Kulig, J. Design and Preparation of a Novel Cross-Linkable, High Molecular Weight, and Bio-Based Elastomer by Emulsion Polymerization *Macromolecules* **2012**, *45*, 6830–6839.

(10) Joshi, R. G.; Provder, T.; Ziemer, P.; Mao, W.; Shen, W.; Jones, F. N. Investigation of the effect of precoalescence or postcoalescence crosslinking on film formation, properties, and latex morphology *J. Coatings Technol. Res.* **2009**, *6*, 47–65.

(11) Pinenq, P.; Toronto, W. Polymer Diffusion and Mechanical Properties of Films Prepared from Crosslinked Latex Particles *J. Coatings Technol.* **2000**, *72*, 45–61.

(12) Gibson, L.; Ashby, M. E. Cellular Solids Structure and Properties, 1997.

(13) Cassu, S. N.; Felisberti, M. I. Poly(vinyl alcohol) and poly(vinylpyrrolidone) blends: 2.

Study of relaxations by dynamic mechanical analysis *Polymer* **1999**, *40*, 4845–4851.

(14) Richard, J.; Maquet, J. Dynamic micromechanical investigations into particle/particle interfaces in latex films *Polymer* **1992**, *33*, 4164–4173.

Chapter 5. N-vinyl pyrrolidone (NVP) and tannic acid complexation for Pressure Sensitive Adhesives (PSAs)

5.1. Introduction

Pressure sensitive adhesives (PSAs) are soft, viscoelastic materials that adhere to a substrate upon application of light pressure.[1–3] In any given PSA, the adhesive performance is dependent on a delicate balance of the rheological properties of the polymer, which necessitates the fine tuning of the polymer structure.[4,5] On the one hand, the polymer should display some "liquid-like" viscoelastic behavior; this leads to the requirement that the elastic modulus should be fairly low (Dahlquist criterion: G'<0.1 MPa)[6] and there should be a significant contribution of the viscous component. Liquid-like behavior ensures good contact with the substrate and promotes the formation and growth of fibrils during debonding, which contributes to improved tack and peel strength.[7–9] On the other hand, liquid-like behavior results in poor shear resistance as well as a tendency to debond by cohesive failure of the material,[10,11] which is generally undesirable. It should be noted that the failure mode is particularly dependent on the large strain behavior of the material and therefore the adhesive behavior cannot be simply described by the linear viscoelastic properties.[12–15] Thus, the final behavior of a PSA is the result of a complex tug-of-war between the viscous and elastic components and an appropriate balance is crucial for good adhesive performance.[16]

Acrylic PSAs are formed from the radical (co)polymerization of low glass transition temperature (T_g) acrylic monomers such as n-butyl acrylate (BA) and 2-ethylhexyl acrylate (2-

EHA). The emulsion copolymerization of acrylic monomers, where water is used as polymerization medium, has gained popularity as an environmentally friendly tool for the production PSAs.[17,18] Thanks to the versatility of the polymerization process, the performance of the adhesives can be easily tuned during synthesis by varying the copolymer composition and T_g of the copolymer,[19–22] or changing the polymer architecture[12,23–29] (molecular weight distribution, crosslinking degree). However, in general it is not possible to independently control improvements in shear resistance and peel strength and some compromise must be made. For example, by increasing the extent of crosslinking of the polymer the cohesive strength is improved and thus the shear resistance of the adhesive tends is increased, but this usually comes with a concomitant decrease in the peel strength.[30,31]

In general, waterborne acrylic PSAs are characterized by relatively good peel strength, but tend to suffer from poor shear resistance, especially when compared to their solvent based counterparts. A common approach to improve the shear resistance of water-based acrylic PSAs is through the use of composite materials[32–40] or through the use of microstructured materials that contain a connected hard phase around the soft polymer cores.[41–44] In the latter case, the structured hard phase enhances the cohesion of the PSAs whilst the soft cores dissipate energy and allow high peel strength. As a result, microstructured materials generally show relatively high shear resistance while still preserving a good adhesive/cohesive balance.

The objective of this work is to explore the potential of the H-bond directed formation approach for the preparation of microstructured films discussed in Chapter 4 to tune the adhesive properties of water-based acrylic PSAs. In this approach, acrylic polymer particles functionalized with pyrrolidone groups were combined with aqueous solutions of tannic acid as shown in Figure 5.1. In Chapter 4, the monomer composition used was 5/45/50 NVP/MMA/BA and led to copolymers with a $T_g \approx 15$ °C, suitable for coatings applications. In this chapter, the MMA fraction

was reduced to adjust the T_g of the copolymers to around -45 °C and prepare adhesive polymer layers. During the drying of the latex – TA blends, the H-bonds between the pyrrolidone groups on the surface of the acrylic particles and the hydroxyl groups of TA in the aqueous phase (see Figure 5.2) would promote the organization of TA around the polymer particles leading to the formation of microstructured materials. Physical bonding by H-bonds has previously been used to produce supramolecular adhesives.[45–51] However, in PSA systems, while the physical crosslinking of the polymer chains led to materials with greater elastic moduli in linear rheology experiments, the disruption of the H-bonds at large deformations tended to lead to shear-thinning behavior, which promoted cohesive failure.[52] In this chapter, we seek to avoid this issue by combining H-bonding with structural reinforcement.

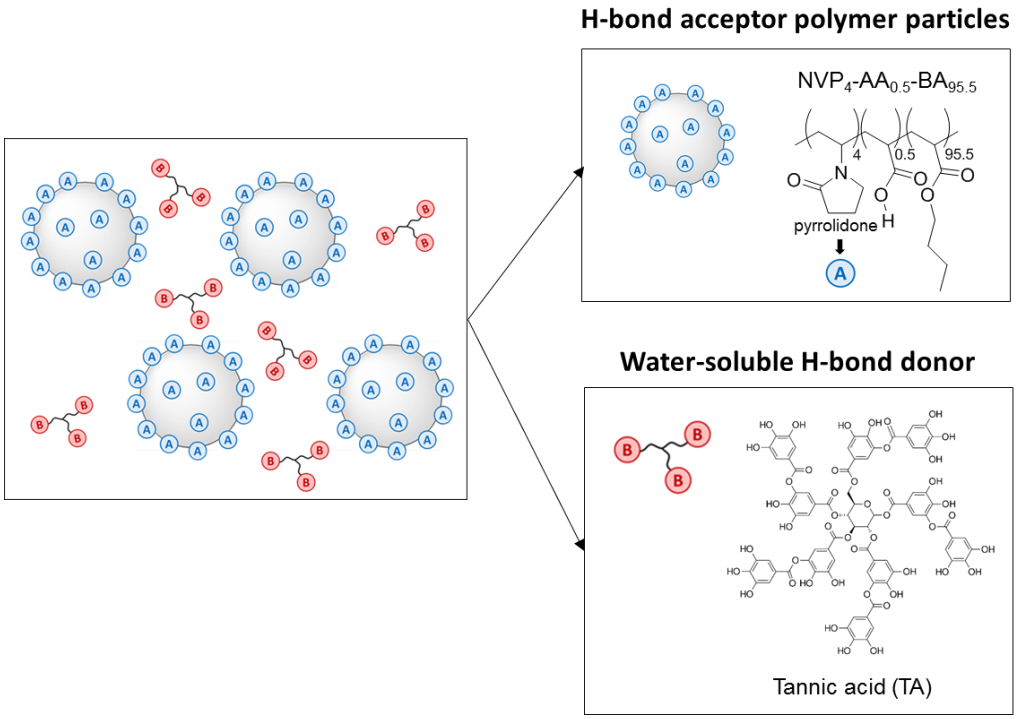

Figure 5.1. Schematic representation of the system composed of NVP functionalized polymer particles and TA dissolved in the aqueous phase. In the scheme, the subscripts after the monomer units express the weight % of the monomers used for the synthesis.

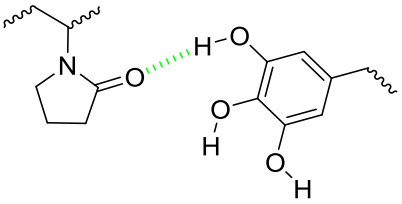

Figure 5.2. H-bond between a pyrrolidone and the aromatic hydroxyl group of TA.

5.2. Experimental part

5.2.1. Materials

Butyl acrylate (BA, technical grade, Quimidroga), N-vinyl pyrrolidone (NVP, >99 %, Sigma Aldrich), acrylic acid (AA, 99 %, Sigma Aldrich), ammonium persulfate (APS, ≥98 %, Sigma Aldrich), sodium bicarbonate ($NaHCO_3$, Sigma Aldrich), n-dodecanethiol (DSH, ≥97 %, Sigma Aldrich) and tannic acid (TA, Sigma Aldrich) was used as received. Dowfax 2A1 was kindly supplied by Dow Chemical Company. Ureido methacrylate (UMA) and Lumiten I-SC were kindly provided by BASF. Deionized water was used as polymerization media.

5.2.2. Synthesis of polymer dispersions

The adhesive polymer dispersions were produced by seeded semibatch emulsion polymerization following the polymerization process described by Haddock *et al*.[53] The formulations used for the synthesis of the polymer dispersions are shown in Table 5.1. Latex 15 and 16 were synthesized in the University of the Basque Country (UPV/EHU) and Latexes 17 – 21 were produced in BASF during the internship. The main monomer used for the synthesis of the PSAs was BA and 0.5 wt% AA was added to the formulations to enhance the stability and wettability of the polymer dispersions. No functional monomer was incorporated in Latexes 15 and 17 to be used as reference, 1 and 2 % wbm N-vinyl pyrrolidone (NVP) was incorporated in Latexes 18 and 19 and 4 % wbm NVP was used in Latexes 16 and 20. One more dispersion with 1 % wbm of ureido methacrylate (UMA) was prepared in run Latex 21 to explore the possibility of using UMA as alternative H-bond acceptor monomer. The chemical structures of NVP and UMA are shown in Figure 5.3.

Table 5.1. Formulations employed for the synthesis of the functional latexes according to the procedure proposed by Haddock *et al*.[53] *The latexes synthesized in BASF are marked with an asterisk (*).

		F.M. (g)	MMA (g)	BA (g)	AA (g)	DSH (g)	H_2O (g)	Dowfax (g)	APS (g)	$NaHCO_3$ (g)
Latex 15 0% F.M.	Seed	--	-	19.8	0.2	-	160	4.28	0.267	1
	F1	-	-	-	-	-	37.3	2.38	1.333	-
	F2	.-	-	179.2	0.8	0.18	-	-	-	-
Latex 16 4% NVP	Seed	NVP 0.8	-	19	0.2	-	160	4.28	0.267	1
	F1	-	-	-	-	-	37.3	2.38	1.333	-
	F2	NVP 7.2	-	172	0.8	0.18	-	-	-	-
Latex 17* 0% Ff.M.	Seed	-	1.2	38.2	0.2	-	320	8.6	0.56	2
	F1	-	-	-	-	-	74	4.8	2.7	-
	F2	-	10.8	347.4	1.8	0.36	-	-	-	-
Latex 18* 1% NVP	Seed	NVP 0.4	1.2	38.2	0.2	-	320	8.6	0.56	2
	F1	-	-	-	-	-	74	4.8	2.7	-
	F2	NVP 3.6	10.8	343.8	1.8	0.36		-	-	-
Latex 19* 2% NVP	Seed	NVP 0.8	2.4	36.6	0.2	-	320	8.6	0.56	2
	F1	-	-	-	-	-	74	4.8	2.7	-
	F2	NVP 7.2	21.6	329.4	1.8	0.36		-	-	-
Latex 20* 4% NVP	Seed	NVP 1.6	-	38.2	0.2	-	320	8.6	0.56	2
	F1	-	-	-	-	-	74	4.8	2.7	-
	F2	NVP 14.4	-	343.8	1.8	0.36	-	-	-	-
Latex 21* 1% UMA	Seed	UMA 0.4	1.2	38.2	0.2	-	320	8.6	0.56	2
	F1	-	-	-	-	-	74	4.8	2.7	-
	F2	UMA 3.6	10.8	343.8	1.8	0.36	-	-	-	-

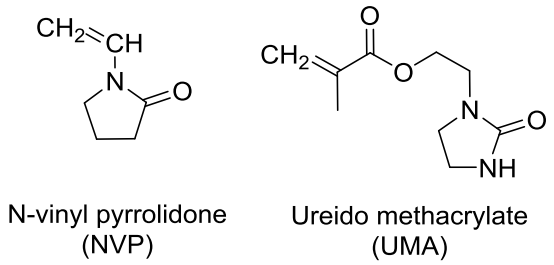

Figure 5.3. Chemical structures of NVP and UMA.

The reactions were carried out in glass reactors fitted with a reflux condenser, a nitrogen inlet, a sampling tube, a thermocouple, and a stainless steel anchor-type stirrer. The reactor temperature was controlled by an automatic control system (Camile TG, Biotage). First, a seed of 11% solids content containing 10% of the total monomers was produced in situ for 30 min in batch, and then the rest of the monomers and an aqueous solution of the initiator (APS) and the emulsifier (Dowfax 2A1) were fed for 3 h in two independent streams. 0.1 wbm% DSH was fed together with the monomers to limit the formation of gel during the synthesis of the latexes. At the end of the feeding, the reaction temperature was held for an additional 30 min to ensure monomer consumption. The reactions were carried out under the nitrogen atmosphere at 70 °C and 200 rpm.

5.2.3. Blending and film casting

For the polymer dispersions prepared in UPV/EHU, first the solids content of Latexes 15 and 16 was increased to 55 wt% by rotary evaporation to prevent dewetting during the preparation of the adhesive film. Then, TA was dissolved in water at a concentration of 20 wt% and different amounts of the TA aqueous solution were added to the polymer dispersions to prepare blends with 0, 0.5, 1, 2 and 3 wt% TA based on polymer. For the probe tack measurements, the blends were cast on glass panels using a gap applicator to obtain polymer

films with a final thickness of around 110 µm. For the shear adhesion and 180° peel tests, the dispersions were cast over a flame-treated polyethylene terephthalate sheet with a gap applicator to prepare polymer films of around 60 µm. After film casting, the dispersions were dried for 13 h at 23 ± 2 °C and 50 ± 5% relative humidity (standard conditions) and protected from dust with a silicone release paper. For the tensile measurements, the right amounts of the blends necessary to achieve final film thicknesses of 400–600 µm were cast into 1 cm × 5 cm silicone molds and dried for 5 days at standard conditions. For the water uptake and weight loss tests, 1 cm diameter and 1 mm thick discs were obtained after drying the blends in silicone molds for 5 days.

Regarding the films prepared in BASF, first 0.5 wt% Lumiten I-SC based on the weight of the latex was added to Latexes 17 – 21 under stirring to improve their wettability. After 24 hours, a previously prepared 30 wt % tannic acid aqueous solution was added to the polymer dispersions with Lumiten I-SC to obtain blends with 0, 1 and 3 tannic acid wt% based on polymer. The blends were stirred at 150 rpm for 10 minutes and kept still for additional 20 minutes. Then, the blends were cast on a HOSTAPHAN RN36 polyester substrate with a film applicator and dried for 3 minutes at 90 °C. The thickness of the dry adhesive films was 21 – 22 g m^{-2} (≈ 21 – 22 µm). Finally, the adhesive tapes were covered with a silicone based easy removable paper for their protection and easy manipulation.

5.2.4. Characterization

The monomer conversion was determined by gravimetry. In Latexes 15 – 16, the particle size was measured by Dynamic Light Scattering (DLS) and the gel content was determined using Soxhlet extractions in THF. In Latexes 17 - 21 produced in BASF, the particle size was measured using Hydrodynamic Capillary Chromatography (HDC) and the gel content was defined as the

insoluble polymer fraction in methyl ethyl ketone (MEK). The molecular weight distribution of the polymers was determined with Size Exclusion Chromatography in THF in all cases. The detailed description of the latex characterization methods and experimental conditions is given in Section I.1 of Appendix I.

The glass transition temperatures of the polymer and polymer blends were determined by differential scanning calorimetry (DSC). The internal morphology of the films was investigated by transmission electron microscopy (TEM). The films were stained with RuO_4 to increase the contrast of the aromatic-rich areas, namely, the TA-rich zones. The water sensitivity of the polymer films was assessed by immersing the polymer films in water for 7 days and measuring water uptake, weight loss and release of tannic acid to the aqueous phase. To determine the adhesive properties in humid conditions the films were immersed in water for 60 minutes before the probe tack test. Detailed information these characterization methods is given in Section 1.2 of Appendix I.

The probe tack, 180° peel tests and tensile tests performed in UPV/EHU were carried out in a TA.HD.plus Texture Analyser (Stable Micro Systems, UK) at 23 ± 2 °C and 50 ± 5% relative humidity. The probe tack tests were carried out employing a 1” stainless steel spherical probe. The ball was brought in contact with the adhesive layer and a compressive force of 4.5 N was applied for 1 s. The probe was then retracted from the adhesive at a crosshead speed of 0.055 mm/s. This corresponds to a nominal strain rate of ~0.5 s^{-1} which is roughly comparable to the strain rate used in the peel test.[54] The dimensionless strain was defined as the displacement divided by initial thickness of the film (100 μm) and the debonding stress was given by the measured force divided by the probe-adhesive contact area. In order to check the reproducibility of the results, each material was tested at least 10 times and the probe tack results given in Table 5.3 are the average values of all the measurements. For the determination of adhesive

properties in humid conditions, the samples were immersed in water for 60 minutes, and they were wiped out with a paper cloth right before the probe tack test. For more details on the probe tack measurement the reader is directed to refs.[8,55] The 180° peel tests were performed on stainless steel substrates according to ASTM D3330. PSA tapes of 25 mm width were attached to the stainless steel substrate and pressed four times with a 2 kg rubber-coated roller. The PSA tape end unattached to the substrate was held to the upper grip of the tensile machine and the tape was peeled off from the substrate with an angle of 180° and a rate of 5 mm/s. The average force needed to detach a 25 mm x 60 mm tape is reported. To verify the reproducibility of the test, each material was tested at least 3 times and the average results are shown in Figure 5.9. Tensile tests were performed based on a modified procedure from ASTM D638-14. 1 cm x 5 cm polymer films were stretched at a constant rate of 50 mm/min. The dimensionless strain (λ) was defined as the distance elongated divided by the initial length of the sample. At least 3 samples were tested for each material to examine the reproducibility of the results. The mechanical parameters presented are the average values calculated from the stress-strain plots.

The shear adhesion tests of the PSAs prepared in UPV/EHU were carried out in a Binder FED (E2) oven (Chem instruments, model SS-HT-8). The tapes were attached to stainless steel panels with a contact area of 25 mm x 25 mm and they were pressed 20 times with a 1 kg rubber-coated roller. Then, 1 kg weights were loaded to the free ends of the tapes and the time the adhesives were able to stand the load at 25 °C was recorded. The results reported are the average values of four tests.

The loop tack tests performed of the PSAs prepared in BASF were carried out in a Zwick Roell tensile machine at room temperature, using one inch width adhesive stripes and stainless steel substrates. First, the strips were held on the superior grip of the analyser with the adhesive part looking downwards, they were put in contact with the substrate for a short time (≈2 s) and

they were detached from the substrate with a constant rate of 300 mm/min. The force needed to remove the adhesive tapes during the detachment was measured. For the shear adhesion tests performed in BASF, the adhesive strips were attached to stainless steel substrates with a contact area of 1 inch x 1 inch or ½ inch x ½ inch (it will be specified in the results for each case). The samples were pressed 4 times with a 2 kg roller and allowed to dwell for 10 minutes. Then, they were hung vertically on the wall and a 1 kg weight was loaded. The time needed for the failure of the adhesive was recorded. To verify the reproducibility of the tests, each material was tested at least 3 times and the average results are presented herein.

5.3. Results and discussion

5.3.1. Synthesis of polymer dispersions

Stable latexes of approximately 50 wt % solids content were obtained from runs Latex 15 – Latex 21. Latex 15 and 16 with 0 and 4 wt% NVP were synthesized in UPV/EHU and Latexes 17 – 20 with 0, 1, 2 and 4 wt% NVP and Latex 21 with 1 wt% UMA were produced in BASF as part of the internship. The monomer conversion and particle size time evolution during the synthesis of the dispersions are shown in Figures 5.4.A and 5.4.B, respectively. In addition, the final monomer conversion and particle size, gel content and molecular weight of the polymers are presented in Table 5.2.

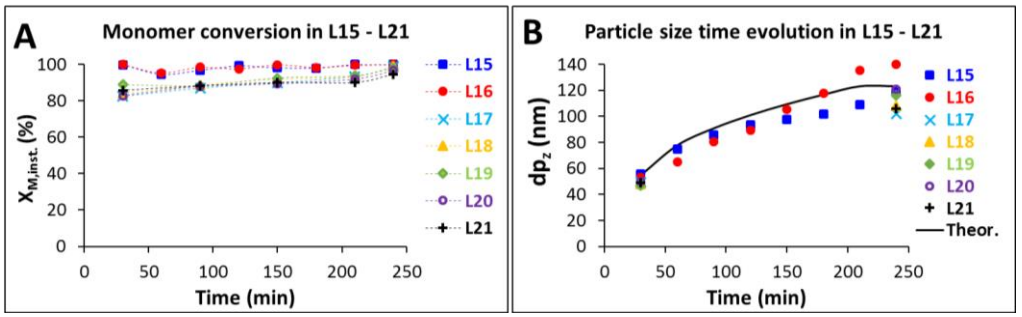

Figure 5.4. (A) Instantaneous monomer conversion and (B) particle size time evolution during the synthesis of Latexes 15-21. The theoretical growth of a 55 nm seed assuming there is no secondary nucleation during the semibatch stage is shown for comparison.

Figure 5.4.A shows that the instantaneous monomer conversions during the polymerizations were very high ($X_{M,inst}$ > 80%), especially in Latexes 15 and 16 synthesized in UPV/EHU. It is worth highlighting that the monomer conversion in these polymerizations was slightly higher than in the synthesis of the latexes produced for coatings applications in Chapters 2 and 4, very likely due to the high propagation rate coefficient of butyl acrylate, which was the main component of the recipe. In addition, although the reactivity ratios between NVP and acrylates do not favor the copolymerization of NVP (r_{BA} = 0.80 and r_{NVP} = 0.02[56]), the high instantaneous monomer conversions and final monomer conversions achieved in the polymerizations of Latexes 16 and 18-20 ensured the incorporation of NVP into the polymer backbone. For UMA, although the final monomer conversion in Latex 21 was slightly lower, the incorporation of this functional monomer was assumed due to the favorable reactivity ratios of methacrylates with acrylates (*e.g.* for the MMA/BA copolymerization system r_{MMA}=1.789 and r_{BA}=0.298).[57]

The polymer seeds formed after 30 minutes of polymerization had particle sizes between 47 and 54 nm. During the semibatch period, the particles grew showing values close to the

theoretical particle sizes calculated for a seed of 55 nm indicating no significant nucleation or coagulation occurred during the feeding. At the end of the polymerizations, the latexes had particle sizes between 102 and 140 nm. The comparison dispersions with increasing amounts NVP (compare L15 and L16, and L17-L20) shows that the dispersions presented an increasing particle size with the NVP content.

Table 5.2. Main characteristics of the polymer dispersions produced in Latex 15 - 21. Latexes 17 - 21 marked with (*) were synthesized in BASF. Data determined by [a]gravimetry, [b]DLS, [c]HDC, [d]Soxhlet extractions in THF, [e]insoluble polymer fraction in MEK and [f]SEC in THF.

Latex	Description	Final X_M[a] (%)	$dp_{z,seed}$[b,c] (nm)	$dp_{z,final}$[b,c] (nm)	Gel content[d,e] (%)	M_w[f] (kg/mol)
L15	Blank - 0% F.M.	100	54 ± 1[b]	119 ± 2[b]	52 ± 7[d]	151
L16	4% NVP	99.9	52 ± 1[b]	140 ± 1[b]	57 ± 1[d]	123
L17*	Blank - 0% F.M.	98.6	49 ± 13[c]	102 ± 5[c]	49.0 ± 11.0[e]	430
L18*	1% NVP	98.8	48 ± 12[c]	108 ± 5[c]	75.4 ± 2.2[e]	390
L19*	2% NVP	97.8	47 ± 12[c]	116 ± 13[c]	57.5 ± 14.4[e]	350
L20*	4% NVP	98.9	50 ± 13[c]	121 ± 19[c]	66.5 ± 1.6[e]	300
L21*	1% UMA	94.6	49 ± 13[c]	106 ± 13[c]	77.7 ± 1.2[e]	226

Regarding the microstructure of the polymers, the PSAs presented relatively high gel content values of around 50–70 %. This can be attributed to the high fraction of acrylates in the formulation, which typically undergo chain transfer reactions during emulsion polymerization, leading to internal crosslinking and gel formation.[58,59] Overall, the blank and 1, 2 and 4 wt% NVP latexes (L15-20) showed similar gel content and number average molar masses. These similarities show that the incorporation of up to 4 wt% NVP to the formulation did not influence significantly the polymer architecture and therefore any differences in the mechanical response

of these adhesives should be directly related to the presence of the pyrrolidone groups. Latex 21 with 1 wt% UMA showed the highest gel content which could be explained by residual amounts of a bis-methacrylate derivative (shown in Figure 5.5), that is formed as by-product during the synthesis of UMA. On first glance, the difference may not seem significant, but the higher gel content was coupled with different physical appearance of the gel fraction of the PSA samples. In contrast to the blank and the NVP-containing materials, whose insoluble polymer fraction was a highly viscous liquid unable to pass the filter, the insoluble polymer fraction of the UMA-containing dispersions was a solid. Therefore, although the gel content values of the PSAs presented in Table 5.2 are similar, it can be assumed that the 1% UMA sample had a different microstructure compared to the rest of the PSAs with a tighter crosslinking network. This observation will be relevant to understand the adhesive properties of the PSAs prepared from these dispersions.

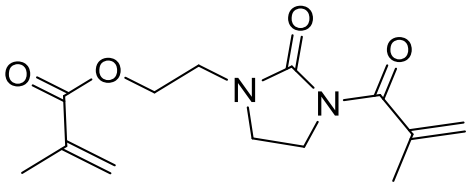

Figure 5.5. Bis-ureidomethacrylate crosslinker formed as byproduct during the synthesis of UMA.

5.3.2. Film morphology

After the synthesis, the polymer dispersions were blended with different amounts of a TA aqueous solution and dried to prepare materials with different TA content. In order to observe the internal morphology of the adhesive films, they were microtomized and stained with RuO_4 to increase the contrast of the aromatic rings and therefore, the tannic acid-rich areas are the darker regions. The TEM images of the blank (L15) and NVP (L16) materials with 3 wt% TA are shown in Figure 5.6.

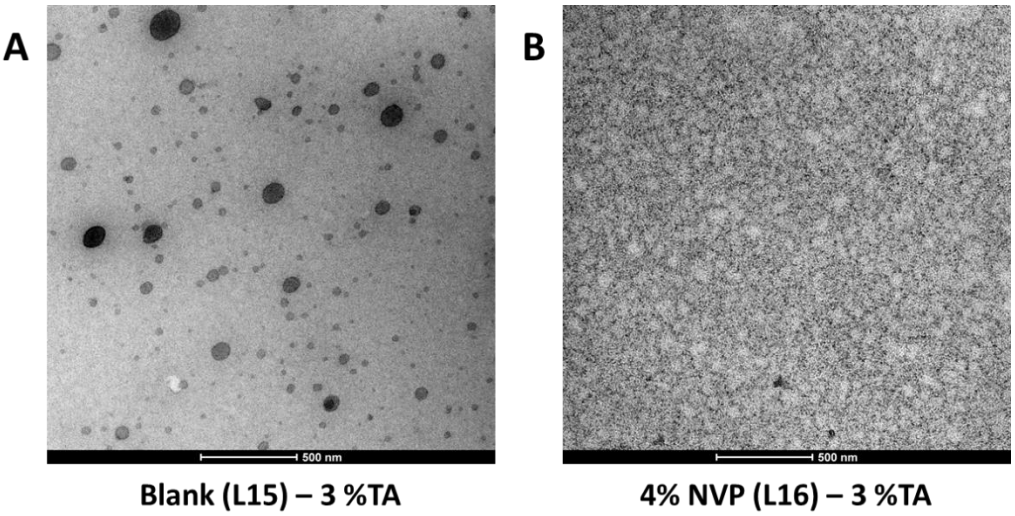

Figure 5.6. TEM images of the (A) blank (L15) - 3 wt% TA and (B) 4% NVP (L16) - 3 wt% TA PSAs.

In the blank materials without pyrrolidone groups, TA formed relatively large aggregates in the soft polymer matrix with domain sizes on the order of 100 nm (see Figure 5.6.A). In contrast, in the 4 wt% NVP materials with pyrrolidone groups, the TA was distributed homogeneously to form a continuous network around the deformed polymer particles (see Figure 5.6.B). Although the shape of each cell was irregular and slightly deformed due to the low modulus of the latex, their size was in reasonable agreement with the particle size reported in Table 5.2, indicating that each cell corresponded to a polymer particle. Comparing the microstructure of the blank and 4% NVP materials, it can be concluded that similar to Chapter 4, the incorporation of pyrrolidone groups to the polymer particles promoted the formation of a TA network around the polymer particles due to the hydrogen bond interactions between the phenolic groups in tannic acid and the pyrrolidone group in the polymer (see Figure 5.2).

5.3.3. Glass transition temperature (T_g)

In order to have a better understanding of the microstructure of the PSAs, the glass transition temperatures (T_g) of the materials were measured by differential scanning calorimetry (DSC). Figures 5.7.A and 5.7.C show the heat flow and derivative heat flow thermograms obtained for the blank (L15) - TA materials and Figures 5.7.B and 5.7.D show the thermograms obtained for the 4% NVP (L16) - TA materials. All the films showed two transitions, one at around -40 ºC and a second transition at around 15 ºC. The first transition is related to the T_g of the main BA rich polymer and is in reasonable agreement with reported values of T_g of the PBA homopolymer in the literature.[60] In the case of the NVP latex this transition was shifted slightly to higher temperatures (-40 ºC instead of -44 ºC) due to the incorporation of NVP ($T_{g,PVP}$ = 187 °C[61]). Indeed, taking the T_g of the poly(BA-co-AA) polymer as -44 ºC and incorporating 4 wt% of NVP, the Fox equation gives an estimate of the NVP copolymer of -40 °C, which is in excellent agreement with the experimental result and indicates good incorporation of the NVP into the copolymer. The second transition at 15 °C, which was more pronounced when NVP was used, likely arises from small amounts of polymer that are formed in the aqueous phase and are rich in AA and NVP. This is more obvious in the case of Latex 16 (4% NVP) since the amount of water soluble monomer used in the formulation is higher than in Latex 15 (blank).

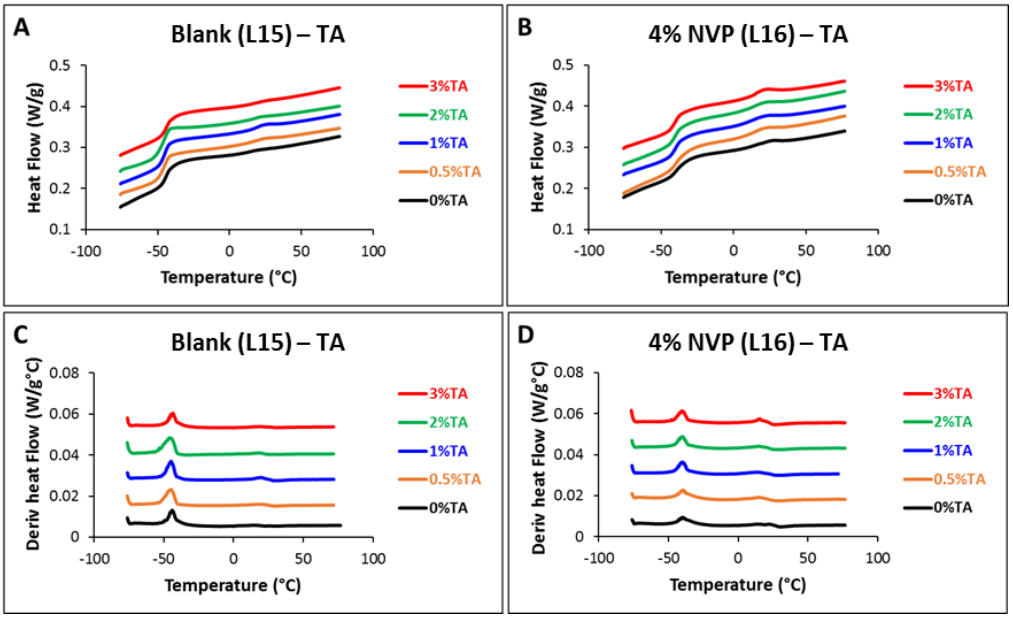

Figure 5.7. (A) and (B) display the heat flow thermograms and (C) and (D) show the derivative heat flow thermograms for the blank (L15) - TA and 4% NVP (L16) - TA materials.

5.3.4. Adhesive properties: Probe tack, 180° peel and shear adhesion tests

In order to evaluate the adhesive properties of these materials, first, the probe tack test of the PSAs with different TA contents was carried out employing a 1” spherical stainless steel probe. The stress-strain curves obtained for the blank (L15) - TA and 4% NVP (L16) - TA blends are presented in Figures 5.8.A and 5.8.B respectively. The maximum stress, elongation and work of adhesion of the materials obtained from the stress-strain plots are summarized in Table 5.3.

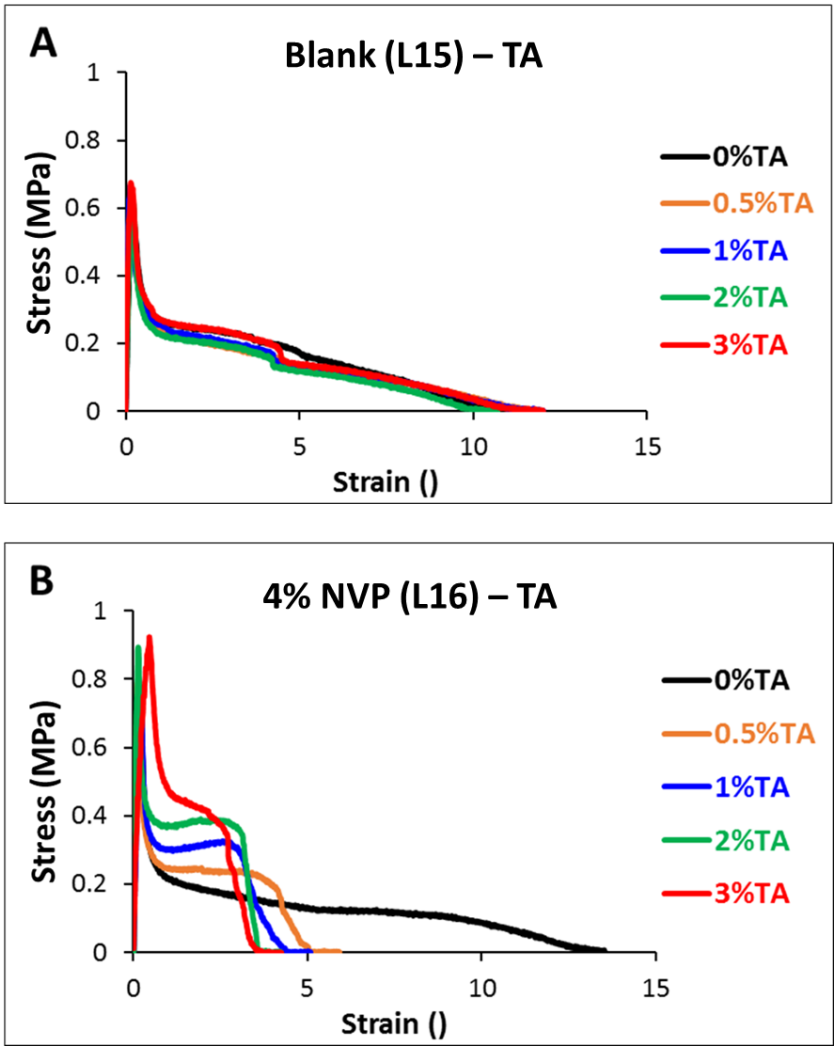

Figure 5.8. Probe tack results of (A) blank (L15) - TA and (B) 4% NVP (L16) - TA PSAs.

Table 5.3. Maximum stress, strain at break and work of adhesion results calculated from the probe tack plots presented in Figure 5.8.

Latex	TA %	Maximum stress (MPa)	Strain at break (-)	Work of adhesion (J m^{-2})
Blank (Latex 15)	0	0.62 ± 0.04	11.1 ± 1.3	176 ± 12
	0.5	0.65 ± 0.03	11.4 ± 0.5	158 ± 14
	1	0.66 ± 0.04	11.9 ± 2.4	155 ± 19
	2	0.61 ± 0.04	10.7 ± 0.5	154 ± 8
	3	0.65 ± 0.01	11.8 ± 1.3	176 ± 12
4% NVP (Latex 16)	0	0.75 ± 0.03	14.4 ± 2.1	213 ± 18
	0.5	0.72 ± 0.08	5.1 ± 1.2	133 ± 12
	1	0.71 ± 0.08	4.2 ± 0.3	128 ± 13
	2	0.85 ± 0.04	3.9 ± 0.4	155 ± 18
	3	0.90 ± 0.07	3.6 ± 0.4	151 ± 35

Starting from the blank (L15) - TA materials shown in Figure 5.8.A, it can be seen that all of the materials showed very similar probe tack profile. They presented a maximum stress of around 0.65 MPa, a liquid-like deformation without a fibrillation plateau and a maximum elongation between 10.7 and 11.9. The work of adhesion of the blank materials varied slightly from 154 to 176 J m^{-2} but with no discernible trend. In addition, all the blank materials resulted in cohesive failure, leaving adhesive residue on the probe. From these results, it can be concluded that the addition of TA to the blank polymer dispersion Latex 15 did not influence the tack properties of the blank - TA PSAs.

Moving to the 4% NVP (L26) - TA materials shown in Figure 5.8.B, first, it can be seen that the addition of 4 wt% NVP to the formulation in Latex 16 influenced the adhesive properties

of the PSA, since even in the absence of TA the NVP sample showed higher maximum stress, strain at break and work of adhesion than the blank PSAs. In addition, it showed a fibrillation plateau, which was an indicative of the higher cohesion of the 4% NVP - 0 wt% TA PSA compared to the blank PSAs. This reinforcement was attributed to the contribution of NVP to the formation of a more rigid shell at the latex surface.

Unlike the blank materials, the addition of TA had a significant impact on the probe tack behavior of the 4% NVP PSAs. The addition of only 0.5 wt% TA caused a dramatic decrease in the strain at break, and with increasing TA content the strain at break continued to decrease. This decrease in the strain at break was related to the formation of the continuous TA phase observed in the TEM images and the probe tack results suggested that this structure was formed from very low TA contents, even at 0.5 wt% TA. The maximum stress and the stress of the fibrillation plateau increased with the tannic acid content. This indicated a progressive increase in the elastic modulus of the PSAs since higher forces were required for cavitation and to elongate the fibrils. In addition, the 4% NVP materials showed some strain hardening in the plateau region as a result of the continuous percolating TA network. The gradual addition of TA increased the density of the H-bond network, as well as the thickness and internal strength of the TA phase. A shift in the rheological behavior was also detected from the failure mechanism, as all the 4% NVP - TA blends showed adhesive failure and detached from the probe without leaving any residue. The work of adhesion increased moderately with the TA content because of the stiffness provided by the continuous TA phase to the materials, although it was lower than the reference 4% NVP - 0 wt% TA. In this case, the high cohesion of the structured materials restricted the deformation of the fibrils to low elongations and reduced their capacity to dissipate energy before debonding. Overall, the work of adhesion of the 4% NVP blends was similar to that of the blank system.

The adhesive properties were also evaluated by a 180° peel test. The results for the blank (L15) - TA and 4% NVP (L16) - TA materials are displayed in Figure 5.9. The PSAs prepared from the blank latex with different TA content showed very similar peel forces with values ranging from 18 to 22 N/25mm, with no obvious influence of the addition of the TA. In addition, these materials underwent debonding by cohesive failure. These results are in agreement with the probe tack results where a liquid-like behaviour of the blank PSAs was observed. On the other hand, in the pyrrolidone containing materials, the addition of TA gradually decreased the average peel force as the cohesion of the materials increased. The 4% NVP - 0 wt% TA material showed a combined adhesive and cohesive failure but the rest of the 4% NVP - TA PSAs showed an adhesive failure due to the enhanced internal strength provided by the H-bond network and the film microstructure.

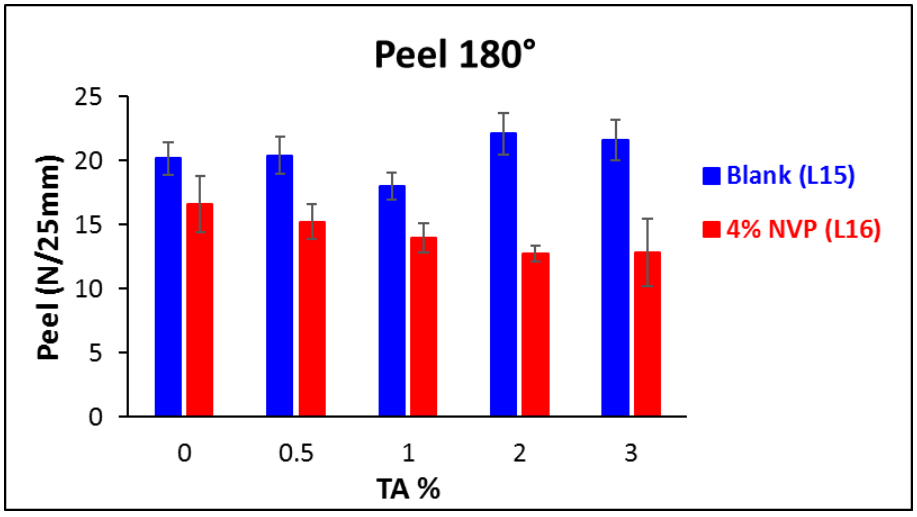

Figure 5.9. 180° peel test results of for the blank (L15) - TA and 4% NVP (L16) - TA materials.

Finally, the shear adhesion test of the PSAs was carried out to directly evaluate the cohesive strength of the materials. In this test, the time the adhesive is able to stand a 1 kg shear

load is measured. The higher the holding time, the greater is the shear resistance of the adhesive. The failure time results obtained for the blank (L15) - TA and 4% NVP (L16) - TA materials are shown in Figure 5.10.

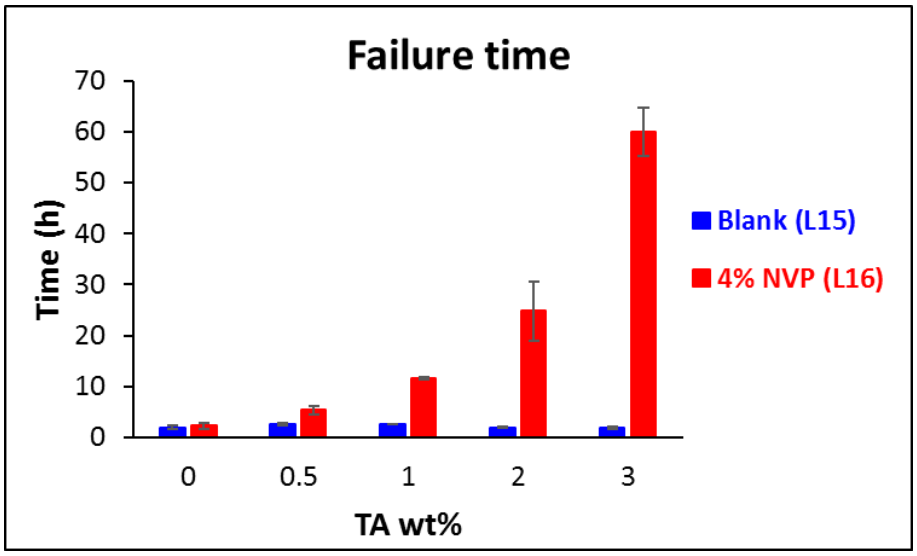

Figure 5.10. Holding times of the blank (L15) - TA and 4% NVP (L16) - TA PSAs.

Figure 5.10 shows that the addition of TA did not influence the holding time of the materials prepared from the blank polymer dispersion. On the contrary, the holding time of the 4% NVP materials increased significantly with the TA content, which meant that the hard TA network enhanced the shear resistance of the 4% NVP materials. These results are in agreement with the probe tack test results where the addition of TA increased the maximum stress and fibrillation stress of the PSAs.

5.3.5. Tensile properties

The change in adhesive behavior can be attributed to the influence of the percolating network of tannic acid. In order to explore this further, tensile experiments were conducted to investigate the large strain behavior of the materials. As mentioned in the introduction, the PSAs must show a certain degree of strain-hardening to ensure adhesive failure.[16] One practical way to represent the tensile test results and discuss the non-linear behavior of a PSA is the Mooney-Rivlin plot where the reduced stress (σ_R) is represented against the inverse of the strain ($1/\lambda$).[62] The reduced stress, defined in Equation 5.1, normalizes the nominal stress (σ_N) obtained in the tensile measurement by the predicted behavior of a neo-Hookean rubber in uniaxial tension.

$$\sigma_R = \frac{\sigma_N}{(\lambda - \frac{1}{\lambda^2})} \qquad \text{Equation 5.1}$$

In the absence of strain hardening, the reduced stress progressively decreases with the deformation. This is the characteristic behavior of a viscoelastic liquid.[16] The stress-strain and Mooney-Rivlin plots of the blank (L15) - TA and 4% NVP (L16) - TA materials are presented in Figure 5.11. In addition, the values obtained for the main mechanical parameters obtained from the stress-strain curves in Figures 5.11.A and 5.11.B are shown in Table 5.4.

Starting from the blank (L15) - TA materials presented in Figure 5.11.A, it can be seen that all of them showed very similar mechanical behavior. The materials presented a Young's modulus between 51 and 72 kPa, a tensile strength equal or below 57 kPa and a toughness around 25×10^{-6} J m^{-3}. The maximum elongation varied from 5 to 8 without a clear trend very likely due to the high sensitivity of these soft materials towards the presence of defects that cause fracture. More importantly, the blank materials behave as viscoelastic liquids and did not show any strain hardening. This liquid-like behavior was also clearly seen in the Mooney-Rivlin plots

presented in Figure 5.11.C where the reduced stress progressively decreased with the deformation without showing any minimum. These tensile results were in agreement with the probe tack test results where the materials showed a liquid-like deformation with no fibrillation plateau and detached giving a cohesive failure.

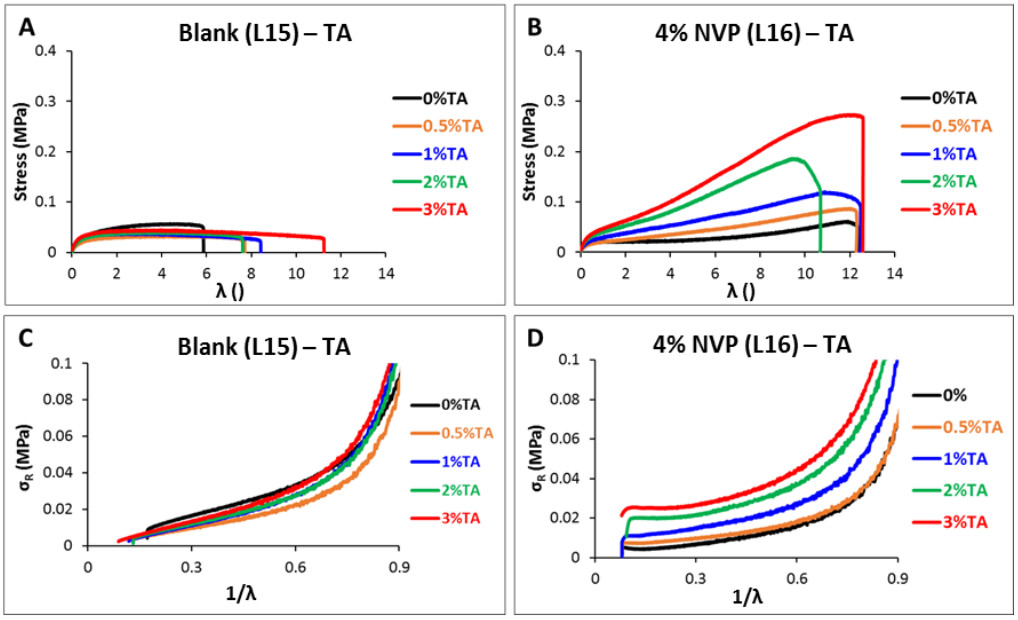

Figure 5.11. Stress-strain plots obtained from the tensile tests of the (A) blank (L15) - TA and (B) 4% NVP (L16) - TA blends. Mooney-Rivlin representations of tensile results for the (C) blank (L15) - TA and (D) 4% NVP (L16) - TA blends.

Table 5.4. Main mechanical parameters obtained from the stress-strain plots shown in Figure 5.11.

Latex	TA %	Young's Modulus (kPa)	Tensile Strength (kPa)	Maximum elongation ()	Toughness 10^6 ($J\ m^{-3}$)
Blank (Latex 15)	0	67 ± 7	57 ± 2	5.3 ± 0.9	26 ± 6
	0.5	59 ± 6	36 ± 4	7.0 ± 1.3	23 ± 6
	2.5	60 ± 7	39 ± 4	8.1 ± 1.1	27 ± 1
	2	51 ± 9	38 ± 3	8.1 ± 0.9	27 ± 1
	3	72 ± 7	46 ± 6	8.6 ± 2.3	34 ± 7
4% NVP (Latex 16)	0	34 ± 4	55 ± 9	11.5 ± 1.1	35 ± 7
	0.5	48 ± 8	100 ± 18	11.5 ± 0.7	65 ± 10
	1	53 ± 12	135 ± 33	9.4 ± 3.1	73 ± 15
	2	66 ± 4	182 ± 17	10.6 ± 0.5	111 ± 13
	3	74 ± 4	289 ± 19	11.6 ± 1.4	193 ± 33

Moving to the 4% NVP (L16) - TA materials, Figure 5.11.B shows that the addition of TA strongly influenced the tensile behavior of the PSAs. The materials showed higher Young's modulus, tensile strength and toughness with increasing tannic acid content. In these materials, the H-bond driven formation of the hard TA network and its gradual thickening with the TA content caused the progressive reinforcement of the materials. One of the main differences between the two set of materials was the strain hardening given by the 4% NVP - TA PSAs compared to the liquid-like behavior shown by the blank - TA blends. First, comparing the neat PSAs without TA, it can be seen that the addition of 4 wt% NVP to the formulation changed the behavior of the PSA and caused some strain hardening, very likely due to the existence of a pyrrolidone-rich shell formed during the synthesis of the polymer dispersion. The addition of TA to the NVP materials and its arrangement in a network, led to stronger and more cohesive materials with a well-defined strain hardening behavior. As a practical example, the addition of 3 wt% TA to the

NVP polymer dispersion doubled the Young's modulus and increased around five times the tensile strength and toughness of the PSA.

The strain hardening of the 4% NVP - TA blends was also observed in the Mooney-Rivlin plots shown in Figure 5.11.D where the reduced stress did not progressively decrease with the deformation. Instead, the reduced stress showed a plateau and a slight increase at small 1/ λ values. In addition, the stress of the plateau in the Mooney-Rivlin plot increased with the TA content which indicated the gradual strengthening of the materials with the addition of TA. These results suggest an adhesive failure would be more likely in these materials and are in agreement with the probe tack and 180° peel tests discussed above.

5.3.6. Water sensitivity

The impact of incorporating hydrophilic pyrrolidone and TA species on the water resistance of the PSAs was evaluated measuring the water uptake and weight loss of the films after 7 days in water. Figure 5.12.A and 5.12.B show that, despite the relatively high NVP fraction in the formulation (4 wt%), the water uptake and weight loss of the 4% NVP materials was only moderately higher than the ones of blank PSAs without showing any trend with the TA content. For the blank materials, the weight loss increased with the TA content due to the release of TA from the films to the aqueous phase. Figure 5.12.C shows that whilst the amount of TA released to the aqueous phase increased with the TA content in the blank materials, the H-bonds between the pyrrolidone groups and tannic acid prevented the leaching of TA from the films in the 4% NVP materials. The adhesive performance of the PSAs in wet conditions was also investigated by conducting probe tack tests before and after 60 minutes of immersion in water. Figure 5.12.D shows that the immersion in water led to a similar reduction in the peak stress of the probe tack measurement, without any further decrease related to the presence of pyrrolidone and TA

groups. More importantly, during the test the blank - TA PSA films detached from the glass substrates while all the 4% NVP - TA materials showed a standard adhesive failure and detached from the steel probe without leaving any residue.

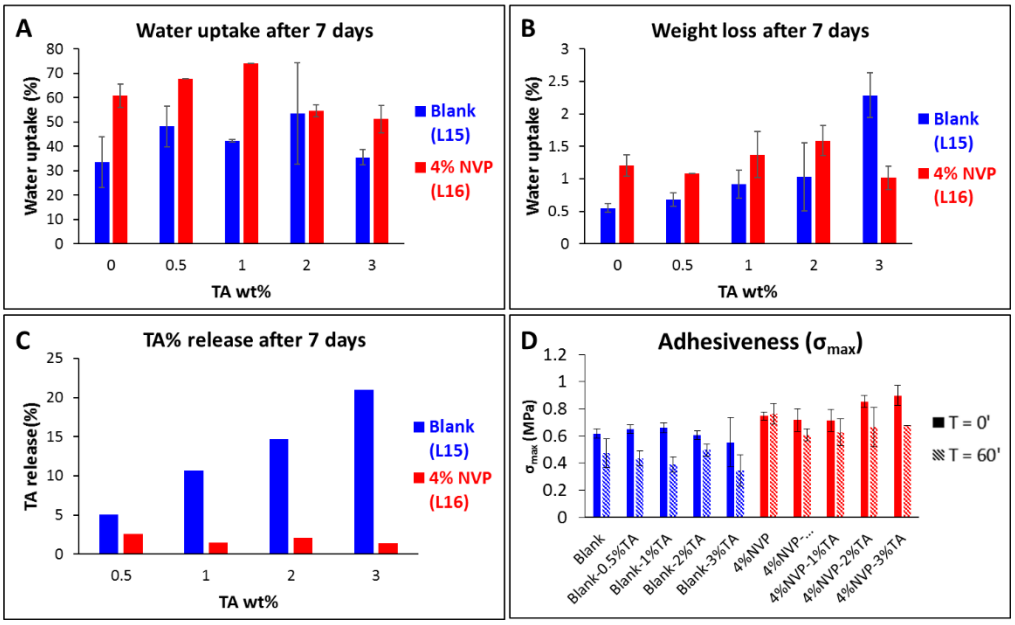

Figure 5.12. (A) Water uptake and (B) weight loss of the PSA films after 7 days of immersion in water. (C) TA % released from the films to the aqueous phase after 7 days of immersion in water. (D) Peak stress obtained in probe tack measurement of the PSAs with different TA % before and after 60 minutes of immersion in water.

5.3.7. Investigation of industrially interesting variables

Having understood the behavior of the microstructured PSAs with 4 % NVP at different TA contents, industrially interesting variables were investigated during the internship in BASF. First, the possibility of reducing the NVP wt% in the formulation was analyzed using polymer dispersions with 0, 1, 2 and 4 wt% in Latexes 17 – 20. Second, the possibility of using 1 wt% ureido methacrylate (UMA) as alternative H-bond acceptor monomer was studied using Latex 21.

First, the adhesive properties were evaluated using loop tack tests. The work of adhesion (W) of the samples is plotted in Figure 5.13.

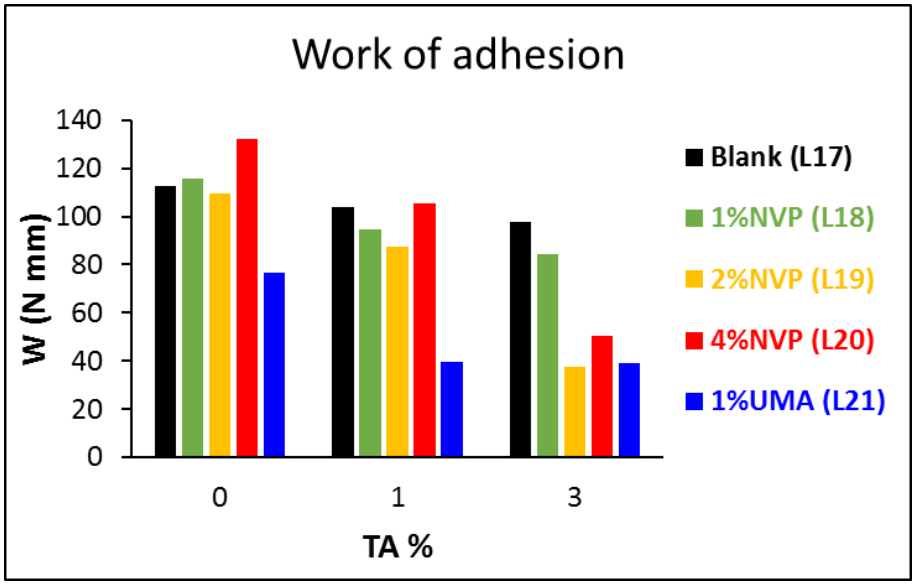

Figure 5.13. Work of adhesion of the PSAs prepared from Latexes 17 – 21 with different TA contents in the loop tack measurements.

Figure 5.13 shows that the gradual addition of TA to the blank dispersion without any functional monomer (L17) caused a moderate decrease in the work of adhesion. The PSAs with 1% NVP (L18) showed very similar behavior to the blank PSAs. On the contrary, a drastic decrease in the work of adhesion was observed for the samples with 2 and 4 weight % NVP. Very likely, in these samples the H-bond density was high enough to promote the organization of TA around the polymer particles and create a reinforcing honeycomb microstructure. The sample with 1% UMA also showed a decrease in the work of adhesion with the TA content. Nevertheless, it is worth highlighting that in general, all the PSAs prepared from the 1% UMA dispersion showed low work of adhesion. As discussed in section 5.3.1, the polymer produced in Latex 21 with 1 wt% UMA had a higher gel content, which explains the low tack of these PSAs. All the samples showed adhesive failure in the loop tack test.

The cohesion of the PSAs was tested with shear adhesion tests at room temperature and using 1 kg loads. The contact area used for the test and holding time of the PSAs are shown in Table 5.5. First, the blank and NVP PSAs showed little cohesion in the absence of tannic acid and failed in between 3 and 6 hours. Then, the addition of TA increased the holding time of the adhesives gradually. In addition, the cohesion increased with the NVP content indicating that the reinforcement of the PSAs depended on the density of the H-bonding network. In agreement with the loop tack results, the blank and 1% NVP samples behaved in a similar way and showed a moderate increase in the cohesion with the TA content. On the contrary, the materials with 2% and 4% NVP showed a considerable increase in the cohesion with the TA amount. Specifically, the holding times of the 2% NVP and 4% NVP PSAs with 3 wt% TA were x3 and x8 greater than the holding time of the analogous PSA with only 1% NVP. The results suggested that a minimum amount of 2 wt% NVP was necessary to drive the microstructuring of TA around the polymer particles. Furthermore, while the addition of TA caused a similar decrease in the work of adhesion

in the samples with 2 and 4 wt% NVP, the increase in the cohesion for the 4% NVP PSAs was remarkable. In this material, the greater amount H-bonds led to the development of a highly cohesive physical network.

Regarding the UMA-containing materials, the three 1%UMA PSAs showed holding times of more than 100 hours, even in the absence of TA. The high cohesion of these samples was attributed to the high gel content of the 1% UMA polymer. In addition, the H-bond interactions between the urea units on the surface of the polymer particles may also reinforce the particle interfaces and contribute to the cohesive strength of the PSAs. In order to find out the reinforcing effect of TA in the 1% UMA dispersion, the contact area with the steel substrate was reduced from 1 x 1 inch to ½ x ½ inch. It can be seen from these results that the addition of TA to the 1% UMA dispersion led to great enhancement in the holding time and cohesive strength of the PSAs.

Table 5.5. Shear adhesion test results carried out at room temperature and 1 kg weight.

		Holding time (h)		
Latex	**Contact area**	**0% TA**	**1% TA**	**3% TA**
Blank (Latex 17)	1 inch x 1 inch	6.5 ± 0.1	6.0 ± 0.1	19.8 ± 0.0
1% NVP (Latex 18)	1 inch x 1 inch	3.2 ± 0.2	4.7 ± 0.6	13.2 ± 0.6
2% NVP (Latex 19)	1 inch x 1 inch	5.5 ± 0.0	13.1 ± 0.8	38.4 ± 1.4
4% NVP (Latex 20)	1 inch x 1 inch	4.7 ± 0.4	32.0 ± 0.4	> 100
1% UMA (Latex 21)	1 inch x 1 inch	> 100	> 100	> 100
1% UMA (Latex 21)	1/2 inch x 1/2 inch	1.0 ± 0.5	3.4 ± 1.5	> 100

For a better comparison of the NVP- and UMA-containing samples and in order to highlight the strengthening effect of TA in each dispersion, the shear adhesion results were normalized by dividing the holding time of each sample with the holding time of the material in the absence of tannic acid. The normalized holding time results are shown in Figure 5.14.

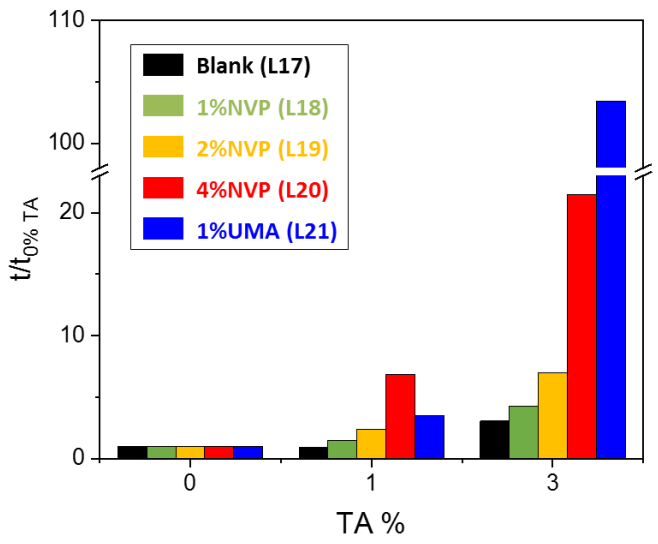

Figure 5.14. Normalized shear adhesion test results for the Latex 17–21 – TA blends. $t/t_{0\%\ TA}$ is the holding time of each adhesive divided by the holding time of the same polymer in the absence of TA.

The normalized results shown in Figure 5.14 clearly revealed that the strengthening effect of TA depended on the H-bonding sites on the surface of the polymer particles which promoted a better distribution of TA around the polymer particles and led to the formation of a more cohesive physical network. In addition, the reinforcement efficiency of TA in the PSA with only 1 wt% UMA was very high, even greater than for the PSA with 4 wt% NVP. Considering the dispersion with only 1 wt% NVP behaved similar to the blank, it was concluded that the incorporation of UMA with two H-bonding sites in its structure was more efficient than NVP which only has one H-bonding site for enhancing the cohesive strength of the PSAs.

5.4. Conclusions

In conclusion, a H-bond directed approach has been presented for the preparation of nanostructured acrylic PSAs with enhanced shear resistance. The system is composed of a soft acrylic dispersion functionalized with N-vinyl pyrrolidone (NVP) and tannic acid (TA), a water-soluble polyphenol. The H-bonds between the pyrrolidone groups in the polymer particles and the hydroxyl groups in TA promoted the arrangement of a continuous network of TA around the soft polymer particles. The physically crosslinked and microstructured PSAs showed an increasing mechanical and cohesive strength with the NVP and TA content. In addition, while the increase in the cohesion was remarkable (x26 times increase in the holding time with the addition of 4% NVP and 3 wt% TA) the formation of the TA microstructure only caused a moderate decrease in the work of adhesion (25 % decrease with the addition of 4% NVP and 3 wt% TA) and peel strength. Thus, through simple post-synthesis addition of a naturally occurring polyphenol waterborne acrylic PSAs with significantly improved shear resistance were obtained with only a slight decrease in the peel strength.

5.5. References

(1) Benedek, I. Pressure-Sensitive Adhesives and Applications; New York, 2004.

(2) Creton, C.; Ciccotti, M. Fracture and adhesion of soft materials: a review Reports Prog. Phys. 2017, 79, 1–107.

(3) Creton, C. Pressure-Sensitive Adhesives: An Introductory Course MRS Bull. 2003, 28, 434–439.

(4) Sun, S.; Li, M.; Liu, A. A review on mechanical properties of pressure sensitive adhesives Int. J. Adhes. Adhes. 2013, 41, 98–106.

(5) Rudawska, A. Adhesives and Adhesive Joints in Industry Applications; 2019.

(6) Dahlquist, C. A. In Treatise on adhesion and adhesives, Vol 2; Patrick, R. L., Ed.; New York, 1969.

(7) Brown, K.; Hooker, J. C.; Creton, C. Micromechanisms of Tack of Soft Adhesives Based on Styrenic Block Copolymers Macromol. Mater. Eng. 2002, 287, 163–179.

(8) Lakrout, H.; Sergot, P.; Creton, C. Direct Observation of Cavitation and Fibrillation in a Probe Tack Experiment on Model Acrylic Pressure-Sensitive-Adhesives J. Adhes. 1999, 69, 307–359.

(9) Zosel, A. Adhesive Failure and Deformation Behaviour of Polymers J. Adhes. 1989, 30, 135–149.

(10) Zosel, A. Shear Strength of Pressure Sensitive Adhesives and its Correlation to Mechanical Properties J. Adhes. 1994, 44, 1–16.

(11) Sosson, F.; Chateauminois, A.; Creton, C. Investigation of shear failure mechanisms of pressure-sensitive adhesives J. Polym. Sci. Part B Polym. Phys. 2005, 43, 3316–3330.

(12) Lindner, A.; Lestriez, B.; Mariot, S.; Creton, C.; Maevis, T.; Lühmann, B.; Brummer, R. Adhesive and Rheological Properties of Lightly Crosslinked Model Acrylic Networks J. Adhes. 2007, 83, 267–310.

(13) Drzal, P. L.; Shull, K. R. Adhesive Failure of Model Acrylic Pressure Sensitive Adhesives J. Adhes. 2005, 81, 397–415.

(14) Creton, C.; Hu, G.; Deplace, F.; Morgret, L.; Shull, K. R. Large-Strain Mechanical Behavior of Model Block Copolymer Adhesives Macromolecules 2009, 42, 7605–7615.

(15) Chopin, J.; Villey, R.; Yarusso, D.; Barthel, E.; Creton, C.; Ciccotti, M. Nonlinear Viscoelastic Modeling of Adhesive Failure for Polyacrylate Pressure-Sensitive Adhesives Macromolecules 2018, 51, 8605–8610.

(16) Deplace, F.; Carelli, C.; Mariot, S.; Retsos, H.; Chateauminois, A.; Ouzineb, K.; Creton, C. Fine Tuning the Adhesive Properties of a Soft Nanostructured Adhesive with Rheological Measurements J. Adhes. 2009, 85, 18–54.

(17) Jovanovic, R.; Dubé, M. A. Emulsion-Based Pressure-Sensitive Adhesives: A Review J. Macromol. Sci. Part C Polym. Rev. 2004, 44, 1–51.

(18) Mallégol, J.; Dupont, O.; Keddie, J. L. Obtaining and Interpreting Images of Waterborne Acrylic Pressure-Sensitive Adhesives by Tapping-Mode Atomic Force Microscopy Langmuir 2001, 17, 7022–7031.

(19) Márquez, I.; Alarcia, F.; Velasco, J. I. Synthesis and Properties of Water-Based Acrylic Adhesives with a Variable Ratio of 2-Ethylhexyl Acrylate and n-Butyl Acrylate for Application in Glass Bottle Labels Polymer 2020, 12, 1–14.

(20) Aymonier, A.; Papon, E.; Villenave, J.-J.; Tordjeman, P.; Pirri, R.; Gérard, P. Design of Pressure-Sensitive Adhesives by Free-Radical Emulsion Copolymerization of Methyl Methacrylate and 2-Ethylhexyl Acrylate. 1. Kinetic Study and Tack Properties Chem. Mater. 2001, 13, 2562–2566.

(21) Laureau, C.; Vicente, M.; Barandiaran, M. J.; Leiza, J. R.; Asua, J. M. Effect of the Composition Profile of 2-Ethyl Hexyl Acrylate/Methyl Methacrylate Latex Particles on Adhesion J. Appl. Polym. Sci. 2001, 81, 1258–1265.

(22) Xu, H.; Wang, N.; Qu, T.; Yang, J.; Yao, Y.; Qu, X.; Lovell, P. A. Effect of the MMA Content on the Emulsion Polymerization Process and Adhesive Properties of Poly(BA-co-MMA-co-AA) Latexes J. Appl. Polym. Sci. 2011, 123, 1068–1078.

(23) Agirre, A.; Nase, J.; Degrandi, E.; Creton, C.; Asua, J. M. Miniemulsion Polymerization of 2-Ethylhexyl Acrylate. Polymer Architecture Control and Adhesion Properties Macromolecules 2010, 43, 8924–8932.

(24) Badía, A.; Agirre, A.; Barandiaran, M. J.; Leiza, J. R. Easy removable and UV tunable biobased waterborne pressure sensitive adhesives Int. J. Adhes. Adhes. 2021, 108, 102860.

(25) Tobing, S. D.; Klein, A. Molecular parameters and their relation to the adhesive performance of acrylic pressure-sensitive adhesives J. Appl. Polym. Sci. 2001, 79, 2230–2244.

(26) Tobing, S. D.; Klein, A. Molecular parameters and their relation to the adhesive performance of emulsion acrylic pressure-sensitive adhesives. II. Effect of crosslinking

J. Appl. Polym. Sci. 2001, 79, 2558–2564.

(27) Qie, L.; Dubé, M. A. Manipulation of chain transfer agent and cross-linker concentration to modify latex micro-structure for pressure-sensitive adhesives Eur. Polym. J. 2010, 46, 1225–1236.

(28) Fonseca, G. E.; McKenna, T. F. L.; Dubé, M. A. Effect of Bimodality on the Adhesive Properties of Pressure Sensitive Adhesives: Role of Bimodal Particle Size and Molecular Weight Distributions Ind. Eng. Chem. Res. 2010, 49, 7303–7312.

(29) Chauvet, J.; Asua, J. M.; Leiza, J. R. Independent control of sol molar mass and gel content in acrylate polymer/latexes Polymer 2005, 46, 9555–9561.

(30) Zosel, A. Effect of Cross-Linking on Tack and Peel Strength of Polymers J. Adhes. 1991, 34, 201–209.

(31) Czech, Z. Crosslinking of pressure sensitive adhesive based on water-borne acrylate Polym. Int. 2003, 52, 347–357.

(32) Degrandi-Contraires, E.; Udagama, R.; Bourgeat-Lami, E.; McKenna, T.; Ouzineb, K.; Creton, C. Mechanical Properties of Adhesive Films Obtained from PU−Acrylic Hybrid Particles Macromolecules 2011, 44, 2643–2652.

(33) Lopez, A.; Degrandi-Contraires, E.; Canetta, E.; Creton, C.; Keddie, J. L.; Asua, J. M. Waterborne polyurethane-acrylic hybrid nanoparticles by miniemulsion polymerization: applications in pressure-sensitive adhesives. Langmuir 2011, 27, 3878–3888.

(34) Yamamoto, Y.; Fujii, S.; Shitajima, K.; Fujiwara, K.; Hikasa, S.; Nakamura, Y. Soft polymer-silica nanocomposite particles as filler for pressure-sensitive adhesives Polymer 2015, 23, 77–87.

(35) Bonnefond, A.; Micusik, M.; Paulis, M.; Leiza, J. R.; Teixeira, R. F. A.; Bon, S. A. F. Morphology and properties of waterborne adhesives made from hybrid polyacrylic/montmorillonite clay colloidal dispersions showing improved tack and shear resistance Colloid Polym. Sci. 2013, 291, 167–180.

(36) Li, H.; Yang, Y.; Yu, Y. Acrylic emulsion pressure-sensitive adhesives (PSAS) reinforced with layered silicate J. Adhes. Sci. Technol. 2004, 18, 1759–1770.

(37) Dastjerdi, Z.; Cranston, E. D.; Dubé, M. A. Pressure sensitive adhesive property modification using cellulose nanocrystals Int. J. Adhes. Adhes. 2018, 81, 36–42.

(38) Fabbroni, E. F.; Shull, K. R.; Hersam, M. C. Adhesive and mechanical properties of soft nanocomposites: Model studies with blended latex films J. Polym. Sci. Part B Polym. Phys. 2001, 39, 3090–3102.

(39) Wang, T.; Lei, C.; Dalton, A. B.; Creton, C.; Lin, Y.; Fernando, K. A. S.; Sun, Y.-P.; Manea, M.; Asua, J. M.; Keddie, J. L. Waterborne, Nanocomposite Pressure-Sensitive Adhesives with High Tack Energy, Optical Transparency, and Electrical Conductivity Adv. Mater. 2006, 18, 2730–2734.

(40) Wang, T.; Colver, P. J.; Bon, E. A. F.; Keddie, J. L. Soft polymer and nano-clay supracolloidal particles in adhesives: synergistic effects on mechanical properties Soft Matter 2009, 5, 3842–3849.

(41) Chenal, M.; Véchambre, C.; Chenal, J.-M.; Chazeau, L.; Humblot, V.; Bouteiller, L.; Creton, C.; Rieger, J. Mechanical properties of nanostructured films with an ultralow volume fraction of hard phase Polymer 2017, 109, 187–196.

(42) Chenal, M.; Rieger, J.; Véchambre, C.; Chenal, J.-M.; Chazeau, L.; Creton, C.; Bouteiller, L. Soft Nanostructured Films with an Ultra-Low Volume Fraction of Percolating Hard Phase Macromol. Rapid Commun. 2013, 34, 1524–1529.

(43) Gurney, R. S.; Morse, A.; Siband, E.; Dupin, D.; Armes, S. P.; Keddie, J. L. Mechanical properties of a waterborne pressure-sensitive adhesive with a percolating poly(acrylic acid)-based diblock copolymer network: Effect of pH J. Colloid Interface Sci. 2015, 448, 8–16.

(44) Deplace, F.; Rabjohns, M. A.; Yamaguchi, T.; Foster, A. B.; Carelli, C.; Lei, C. H.; Ouzineb, K.; Keddie, J. L.; Lovell, P. A.; Creton, C. Deformation and adhesion of a periodic soft-soft nanocomposite designed with structured polymer colloid particles Soft Matter 2009, 5, 1440–1447.

(45) Courtois, J.; Baroudi, I.; Nouvel, N.; Degrandi, E.; Bouteiller, L.; Pensec, S.; Ducouret, G.; Chanéac, C.; Creton, C. Supramolecular Soft Adhesive Materials Adv. Funct. Mater. 2010, 20, 1803–1811.

(46) Callies, X.; Herscher, O.; Fonteneau, C.; Robert, A.; Bouteiller, L.; Ducouret, G.; Creton, C. Combined effect of Chain Extension and Supramolecular Interactions on Rheological and Adhesive Properties of Acrylic Pressure-Sensitive-Adhesives Appl. Mater. Interfaces 2016, 8, 33307–33315.

(47) Cheng, S.; Zhang, M.; Dixit, N.; Moore, R. B.; Long, T. E. Nucleobase self-assembly in supramolecular adhesives Macromolecules 2012, 45, 805–812.

(48) Viswanathan, K.; Ozhalici, H.; Elkins, C. L.; Heisey, C.; Ward, T. C.; Long, T. E. Multiple Hydrogen Bonding for Reversible Polymer Surface Adhesion Langmuir 2006, 22, 1099–1105.

(49) Heinzmann, C.; Coulibaly, S.; Roulin, A.; Fiore, G. L.; Weder, C. Light-Induced Bonding and Debonding with Supramolecular Adhesives Appl. Mater. Interfaces 2014, 6, 4713–4719.

(50) Heinzmann, C.; Salz, U.; Moszner, N.; Fiore, G. L.; Weder, C. Supramolecular Cross-Links in Poly (Alkyl Methacrylate) Copolymers and Their Impact on the Mechanical and Reversible Adhesive Properties ACS Appl. Mater. Interfaces 2015, 7, 13395–13404.

(51) Heinzmann, C.; Weder, C.; De Espinosa, L. M. Supramolecular polymer adhesives: Advanced materials inspired by nature Chem. Soc. Rev. 2016, 45, 342–358.

(52) Callies, X.; Fonteneau, C.; Pensec, S.; Bouteiller, L.; Ducouret, G.; Creton, C. Adhesion and Non-Linear Rheology of Adhesives with Supramolecular Crosslinking Points Soft Matter 2016, 12, 7174–7185.

(53) Haddock, T. H. Presure sensitive adhesive. EP 0130080 B1, 1988.

(54) Pandey, V.; Fleury, A.; Villey, R.; Creton, C.; Ciccotti, M. Linking peel and tack performances of pressure sensitive adhesives Soft Matter 2020, 16, 3267–3275.

(55) Josse, G.; Sergot, P.; Creton, C.; Dorget, M. Measuring interfacial adhesion between a soft viscoelastic layer and a rigid surface using a probe method J. Adhes. 2004, 80, 87–118.

(56) Al-Issa, M. A.; Davis, T. P.; Huglin, M. B.; Yip, D. C. F. Copolymerizations involving N-vinyl-2-pyrrolidone Polymer 1985, 26, 1869–1874.

(57) Dubé, M. A.; Penlidis, A. A systematic approach to the study of multicomponent polymerization kinetics-the butyl acrylate/methyl methacrylate/vinyl acetate example: 1. Bulk copolymerization Polymer 1995, 36, 587–598.

(58) Hamzehlou, S.; Reyes, Y.; Leiza, J. R. Detailed Microstructure Investigation of Acrylate/Methacrylate Functional Copolymers by Kinetic Monte Carlo Simulation Macromol. React. Eng. 2012, 6, 1–11.

(59) Moghadam, N.; Liu, S.; Srinivasan, S.; Grady, M. C.; Rappe, A. M.; Soroush, M. Theoretical study of intermolecular chain transfer to polymer reactions of alkyl acrylates Ind. Eng. Chem. Res. 2015, 54, 4148–4165.

(60) Fernández-García, M.; Cuervo-Rodriguez, R.; Madruga, E. L. Glass Transition Temperatures of Butyl Acrylate – Methyl Methacrylate Copolymers J. Polym. Sci. Part B Polym. Phys. 1999, 37, 2512–2520.

(61) Cassu, S. N.; Felisberti, M. I. Poly(vinyl alcohol) and poly(vinylpyrrolidone) blends: 2. Study of relaxations by dynamic mechanical analysis Polymer 1999, 40, 4845–4851.

(62) Roos, A.; Creton, C. Effect of the Presence of Diblock Copolymer on the Nonlinear Elastic and Viscoelastic Properties of Elastomeric Triblock Copolymers Macromolecules 2005, 38, 7807–7818

Chapter 6. Fundamental insights into free radical polymerization in the presence of catechols and catechol functionalized monomers

6.1. Introduction

In Chapter 4, the combination of acrylic polymer dispersions with pyrrolidone units and tannic acid, a naturally occurring polyphenol, led to the H-bond directed formation of microstructured materials with enhanced stiffness. The materials also showed high water resistance and the films maintained the microstructure and mechanical strength after extensive exposure to water thanks to the high strength of the amide – phenol H-bonds. However, the addition of TA gave an orange tint to the polymer films which was visible even in the white paints prepared with TiO_2 pigment. Moreover, when used as formulated product the strong interactions between TA and the main coating components led to unstable products, which limits the potential application of TA in formulated products. A potential route to overcome these limitations is the synthesis of copolymers containing catechol units in place of TA.

Catechols are aromatic compounds containing two hydroxyl groups in ortho position (chemical structure shown in Figure 6.1) that have attracted great interest for use in polymer materials in a variety of applications.[1–5] Catechol-containing polymers can be used to mimic adhesive proteins used in nature, making them particularly suitable for use as adhesives[6–13] and to anchor polymer chains to surfaces.[14–20] Similar to TA, the phenolic hydroxyl groups of catechols are strong H-bond donors, and H-bond interactions arising from catechols have been reported to physically crosslink linear polymers for the formation of mechanically robust polymer

films[21,22] as well as hydrogels and microgels.[12,23–27] Furthermore, catechols form strong bonds with metal ions, a feature that has been advantageously used in self-healing polymers,[28] water purification hydrogels[29] and in crosslinking catechol containing polymers.[30–32] Finally the catechol/*o*-benzoquinone redox couple has been exploited for use in electronic applications such as organic cathode materials for batteries.[33–37]

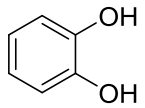

Catechol

Figure 6.1. Chemical structure of catechol.

There are a number of techniques that can be used to synthesize catechol containing polymers such as ring opening polymerization of catechol containing N-carboxyanhydride monomers,[38] oxidative polymerization of catechols,[19,39,40] side chain functionalization[41,42] and free radical polymerization. The use of free radical polymerization is particularly attractive due to its versatility. However, the incorporation of catechols into polymers by free radical polymerization processes is challenging. In fact, catechol-containing compounds such as 4-*tert*-butylcatechol and other phenolic molecules are widely employed as free radical inhibitors and commercial monomers are shipped containing ppm amounts of them in order to prevent polymerization during storage. As catechols are known inhibitors of polymerization, in the design of catechol functionalized polymers they are commonly incorporated into the formulation as protected monomers that have to be later deprotected.[7,13,17,18,33,43,44] Despite this, there are widespread reports of successful radical copolymerizations using catechol containing monomers.[1,8,12,16,27,37,45–49] The reason for the success of some radical copolymerizations

containing catechol moieties can at least partially be understood in the context of the mechanism by which they inhibit polymerization.

Due to the commercial importance of the use of phenols as inhibitors, the reaction between carbon centered radicals and phenols/catechols has been well studied.[50,51] Scheme 6.1 shows the general picture that can be used to understand the inhibitory activity of catechols in radical polymerization. The primary reaction of a phenol is not directly with carbon centered radicals, but rather with peroxyl radicals arising from addition of oxygen to the propagating chain end (I).[52–54] This hydrogen transfer generates a phenoxyl radical (II) that can potentially proceed to terminate an additional radical. In the absence of inhibitor, the peroxyl radicals (I) can react with monomer, leading to a carbon centered radical that can again consume oxygen. Thus, when no inhibitor is present, for each radical that is generated a large number of oxygen molecules are consumed and oxygen is depleted rapidly, resulting in a rapid polymerization.

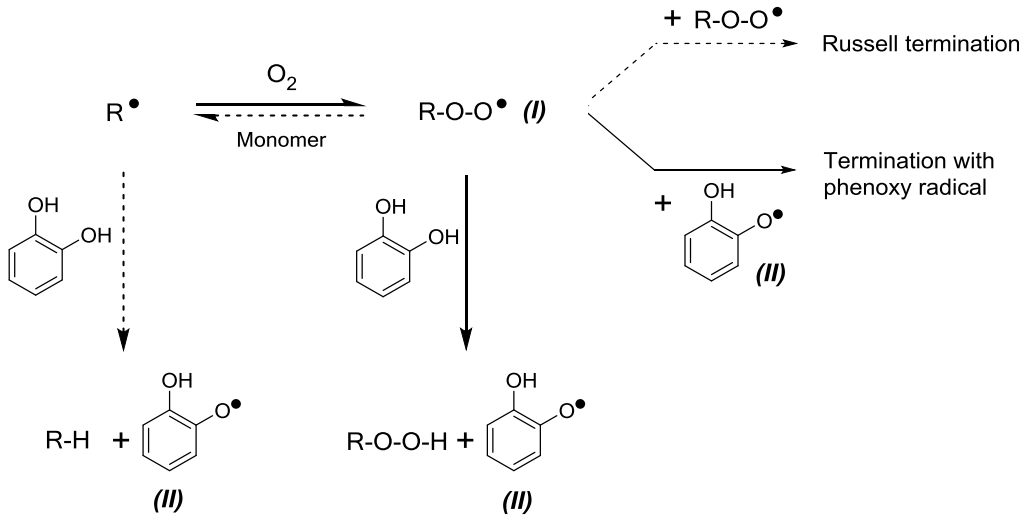

Scheme 6.1. Inhibition of radical polymerization in the presence of oxygen. R* represents the propagating radical species. The full lines show the predominant pathway when both oxygen and inhibitor are present.

In a radical polymerization that is conducted in an inert atmosphere, the presence of phenols/catechols can therefore only influence the polymerization in the case of hydrogen abstraction of the phenolic hydrogen by the propagating radical.[55] Compared to the rate of combination with oxygen this reaction is substantially slower and, unlike the inhibition effect in the presence of oxygen, is highly dependent on the nature of the propagating radical.[56–58] For example, benzene-1,2-diol has been reported to lead to a significantly reduced rate and molecular weight in the polymerization of styrene with estimated transfer constant, C_{TR}, of 0.13 at 60°C,[59] but has been seen to have no measurable effect in the polymerization of methyl methacrylate.[56] Seemingly in contradiction to this Samal *et al.* have reported that in the case of methyl methacrylate inhibition and retardation occur with a decrease in the molecular weights in the presence of phenols.[60]

In (co)polymerizations that contain appreciable fractions of catechol functionalized monomers there is an additional issue with respect to the reactivity of the radicals that are generated following chain transfer event to catechol (see Scheme 6.2, species I). In the case that propagation or termination by combination occurs with this species, branched chain structures will be generated (species II in Scheme 6.2). Thus, the chain transfer reaction can lead to insolubility of the polymer through formation of a crosslinked network. Although many radical polymerizations of catechol containing monomers have been reported, there are few examples of detailed examination of the resulting products. Yang *et al.* reported the copolymerization of dopamine methacrylamide and 2-methoxyethyl acrylate.[10] At high dopamine methacrylamide content (>25 mol%) the reaction was observed to form an insoluble gel which was attributed to termination and transfer events arising from the catechol moiety. Below this value the extent of branching was seen to increase with increasing catechol concentration. Xue *et al.* reported the synthesis of poly(*N*-isopropylacrylamide) microgels using dopamine

methacrylamide as a comonomer. At low concentration of dopamine methacrylamide no microgels were formed whereas at concentrations above 5% microgel formation was observed. This was attributed to the combination of chemical crosslinking arising from transfer reactions of the propagating radical to the catechol and termination reactions involving the resulting phenoxy radical.[61]

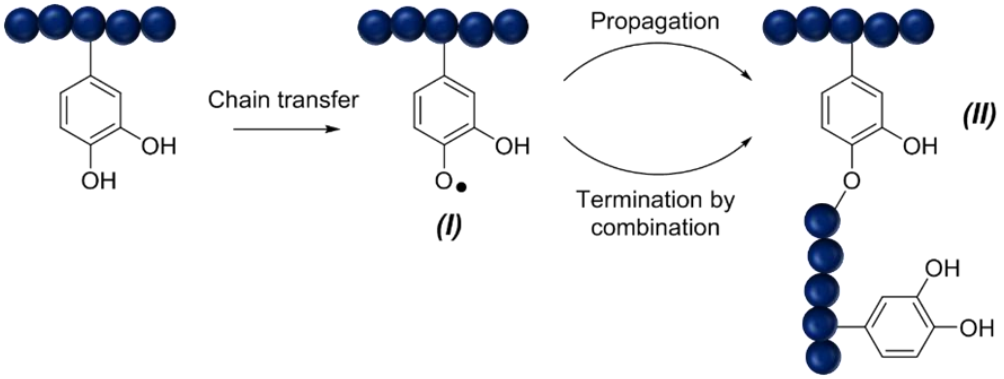

Scheme 6.2. Chain transfer to catechol and potential reaction of phenoxy radical in the absence of oxygen, modified from reference 1.

It is clear that while the radical polymerization of catechol containing monomers is possible to some extent, the nature and reactivity of the catechol during the reaction and the result it has on polymer structure is uncertain. This is an important point if catechol functionalized polymers are to be implemented practically. Therefore, the objective of the work conducted in this chapter is to explore the fundamental behavior of catechol groups in the radical polymerization of common monomers and demonstrate that this knowledge can be used to circumvent many of the problems that are faced when incorporating catechols.

First, a comprehensive kinetic and structural study is performed using styrene, methyl methacrylate and methyl acrylate in the presence of pyrocatechol as a model catechol molecule.

The reaction kinetics, molar mass distribution and polymer microstructure are examined in order to determine the influence and reactivity of the catechol in each case. Subsequently, the chain transfer constants of the 3 monomer systems are determined. The differences in transfer activity are attributed to the varying steric and electronic configurations of the polymerizing radical species and are confirmed by density functional theory calculations. Then, the investigation is extended to (meth)acrylamide monomers validating the results obtained for (meth)acrylates. Finally, the consequences that these results have on the targeted synthesis of catechol containing polymers by radical polymerization are discussed. The information gained in this study will be utilized in Chapter 7 for the synthesis of catechol-containing water-soluble H-bond donors, as synthetic alternative to TA.

6.2. Experimental part

6.2.1. Materials

Unless otherwise stated, the commercial monomers employed in this work were used without purification: methyl methacrylate (MMA, technical grade, Quimidroga), styrene (S, technical grade, Quimidroga) methyl acrylate (MA, 99 %, Sigma Aldrich), acrylamide (AM, ≥98 %, Fluka), methacrylamide (MAM, >98 %, Merck) 2-methoxyethyl methacrylate (2-MOMA, 99 %, Sigma Aldrich) and 2-methoxyethyl acrylate (2-MOA, Merck). Styrene was distilled under reduced pressure to remove inhibitor traces for Runs 5, 6, 9-11 in Table 6.4. 2,2'-azobis(2-methylpropionitrile) (AIBN, ≥98 %, Sigma Aldrich), lauryl peroxide (LPO, 97 %, Sigma Aldrich) and 4,4'-azobis(4-cyanovaleric acid) (V-501, >98 %, Sigma Aldrich) were used as received. Toluene (Lab reagent grade, Fischer), dimethyl formamide (DMF, ≥99.8 %, Sigma Aldrich), cyclohexane (≥99.5 %, Sigma Aldrich) and deionized water were employed as polymerization media. Pyrocatechol (PC, ≥99 %, Sigma Aldrich), sodium chloride (NaCl, synthesis grade,

Scharlau), sodium phosphate monobasic (NaH_2PO_4, ≥99 %, Sigma Aldrich), tetrahydrofuran (THF, GPC grade, Scharlab), and acetonitrile (>99.9 %, Panreac) were used as received. Deuterated dimethyl sulfoxide (d_6-DMSO, 99.8 %D, Eurisotop) was used as solvent for the kinetic study in Runs 1-4 and 7-10 in Table 6.4 and deuterated chloroform ($CDCl_3$, 99.5%D, Eurisotop) was used as solvent for Runs 5, 6 and 11 in Table 6.4. Dopamine methacrylamide (DMA) was synthesized from dopamine and methacryloyl chloride based on a procedure reported by Xu *et al.*[62] Vinyl catechol (VC) was synthesized from caffeic acid according to the procedure described by Takeshima *et al.*[63] The experimental details about the synthesis of DMA and VC are given in Sections II.1 and II.2 of Appendix II.

6.2.2. Synthetic procedures

Set 1. Radical polymerizations of MMA, S and MA in presence of pyrocatechol

In polymerizations conducted under inert conditions, the inhibitory activity of catechols only depends on the nature of the propagating radical. In order to gain an insight into the reactivity of catechols with different radical types, methyl methacrylate (MMA), methyl acrylate (MA) and styrene (S) were polymerized in presence of increasing amounts of pyrocatechol (PC) as model catechol compound. The formulations employed for the reactions are shown in Table 6.1. The reactions were carried out in a commercial calorimetric reactor (RTCal™, Metler Toledo) comprised of 1 L glass jacket reactor, a platinum resistance thermometer, an anchor impeller, a nitrogen inlet and a sampling tube. Initially, the monomer and solvent were charged into the reactor and the system was purged for 30 minutes with N_2. Then, the system was heated to 70 °C and the system was left until the heat flow stabilized. The reaction was initiated with a shot of a solution of the initiator in toluene. The reactions were conducted under nitrogen atmosphere, at 70 °C and 200 rpm for 6 hours.

Table 6.1. Formulations employed for the radical polymerizations of different vinyl monomers and different pyrocatechol concentrations.

Run	Catechol (wt%)[a]	MMA (g)	S (g)	MA (g)	Toluene (g)	AIBN (g)	S (g)	LPO (g)	Pyrocatechol (g)
S-1	0	-	100	-	200	2	-	0	0.02
S-2	5	-	100	-	195	2	-	5	0.02
S-3	10	-	100	-	190	2	-	10	0.02
MA-1	0	-	-	100	200	2	-	0	0.02
MA-2	5	-	-	100	195	2	-	5	0.02
MA-3	10	-	-	100	190	2	-	10	0.02
MA-4	50	-	-	100	150	2	-	50	0.02
MMA-1	0	100	-	-	200	2	-	0	0.02
MMA-2	10	100	-	-	190	2	-	10	0.02
MMA-3	50	100	-	-	150	2	-	50	
MMA-4	0	100	-	-	200	-	2	0	0.02
MMA-5	10	100	-	-	190	-	2	10	0.02

[a] Weight based on monomer weight.

Set 2. Radical polymerizations for the determination of the chain transfer constants

MMA, S and MA were polymerized in presence of different amounts of pyrocatechol in order to determine the chain transfer constant at 70 °C for each monomer-catechol combination and to quantitatively compare the reactivity of catechol with each radical type. The polymerizations of MMA and S were carried out in bulk and the polymerizations of MA were carried out in solution to avoid the significant exotherm that was observed to occur in bulk reactions. The recipes employed for the reactions are shown in Table 6.2. The reactions were carried out in 25 mL round bottom flasks, under magnetic stirring and employing an oil bath at 70 °C. For each monomer, first a stock solution containing all the ingredients except the catechol was prepared. Then, mixtures with different monomer/pyrocatechol ratio were prepared adding the corresponding amounts of pyrocatechol to aliquots of the stock solution. The reaction vessels

were purged with N_2 for 20 minutes and then they were immersed in an oil bath at 70 °C for the polymerization. The reaction time was 10 minutes in the polymerizations of MMA and S, and 12 minutes in the case of MA. After the reaction, the polymerizations were quenched by immersing the vessels in ice.

Table 6.2. Formulations employed for the determination of the chain transfer constants of MMA, S and MA with pyrocatechol.

Run	MMA (g)	S (g)	MA (g)	Cyclohexane (g)	AIBN (g)	Pyrocatechol (g)
MMA-Ct-1	5	-	-	-	0.025	0
MMA-Ct-2	5	-	-	-	0.025	0.1
MMA-Ct-3	5	-	-	-	0.025	0.5
MMA-Ct-4	5	-	-	-	0.025	1
MMA-Ct-5	5	-	-	-	0.025	2.5
S-Ct-1	-	5	-	-	0.025	0
S-Ct-2	-	5	-	-	0.025	0.0125
S-Ct-3	-	5	-	-	0.025	0.05
S-Ct-4	-	5	-	-	0.025	0.1
MA-Ct-1	-	-	5	10	0.025	0
MA-Ct-2	-	-	5	10	0.025	0.05
MA-Ct-3	-	-	5	10	0.025	0.1
MA-Ct-4	-	-	5	10	0.025	0.3

Set 3. Radical polymerizations of acrylamide (AM) and methacrylamide (MAM) in presence of pyrocatechol

Acrylamide (AM) and methacrylamide (MAM) were polymerized in presence of 0% and ≈10 wt% pyrocatechol to understand the effect of the catechol groups on the polymerization of (meth)acrylamides. The polymerizations were conducted in water and using 4,4'–azobis(4–cyanovaleric acid) (V-501) as water soluble azo initiator. The reactions were carried out in 50 ml round bottom flasks, under magnetic stirring and using an oil bath to set the temperature at 70 °C. The reaction vessels were purged with nitrogen for 20 minutes before the reactions and then, they were immersed in the oil bath at 70 °C to start the polymerizations. The formulations employed for the reactions and the reaction times are presented in Table 6.3.

Table 6.3. Formulations employed for the polymerizations of AM and MAM in presence of pyrocatechol.

Run	Reaction time (min)	AM (g)	MAM (g)	H_2O (g)	V-501 (g)	Pyrocatechol (g)
AM-1	20	0.95	-	29.05	0.004	0
AM-2	80	0.95	-	29.05	0.004	0.1
MAM-1	60	-	0.85	10	0.004	0
MAM-2	60	-	0.85	10	0.004	0.1

Set 4. Copolymerization of catechol monomers

Two catechol containing monomers (DMA and VC) were used. DMA was copolymerized with 2-methoxyethyl methacrylate (2-MOMA), 2-methoxyethyl acrylate (2-MOA) and styrene (S) in DMF using AIBN as initiator (Runs 1-6). VC was copolymerized with 2-MOMA (Run 7). As VC has a styrenic double bond and a catechol moiety, there was uncertainty on the cause of the

effects observed (styrenic double bond vs. catechol moiety). Therefore, to separate the effect of catechol and styrene type double bond, 2-MOMA was polymerized in presence of pyrocatechol or/and styrene in Runs 8-10. Styrene was polymerized in presence of pyrocatechol in DMF to understand the effect of the solvent on the activity of catechol (Run 11). The chemical structures of 2-MOMA, 2-MOA, S and the catechol containing monomers are shown in Figure 6.2, and the formulations used for the reactions are shown in Table 6.4.

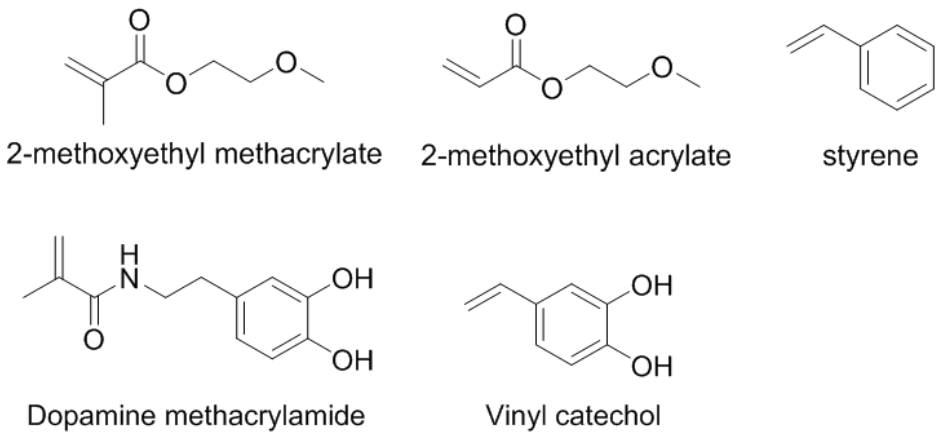

Figure 6.2. Chemical structures of 2-methoxyethyl methacrylate (2-MOMA), 2-methoxyethyl acrylate (2-MOA, styrene (S), dopamine methacrylamide (DMA) and vinyl catechol (VC).

For the reactions, all the ingredients were charged in a 25 mL round bottom flask and the mixture was purged with nitrogen for 30 minutes under magnetic stirring. Then, the vessels were immersed in an oil at 70 °C for 24 hours. Samples were withdrawn from the reaction medium along time to follow the conversion of the monomers and molecular weight distributions of the polymers.

Table 6.4. Formulations employed for the radical polymerizations of different vinyl monomers and different pyrocatechol concentrations.

Run	Description	catechol mol %	DMA (g)	VC (g)	Pyro-catechol (g)	2MOMA (g)	2MOA (g)	S (g)	DMF (g)	AIBN (g)
1	2-MOMA	0	-	-	-	2	-		8	0.02
2	2-MOMA +DMA	15	0.43	-	-	1.57	-		8	0.02
3	2-MOA	0	-	-	-	-	2		8	0.02
4	2-MOA+DMA	15	0.46	-	-	-	1.54		8	0.02
5	S	0	-	-	-	-	-	2	8	0.02
6	S+DMA	8	0.34	-	-	-	-	1.84	8	0.02
7	2-MOMA+VC	8	-	0.29	-	1.71	-		8	0.02
8	2-MOMA+cat.	8	-	-	0.12	2	-	-	8	0.02
9	2-MOMA+S	8	-	-	-	1.84	-	0.12	8	0.02
10	2-MOMA +cat.+S	8	-	-	0.12	1.84	-	0.12	8	0.02
11	S+cat.	8	-	-	0.17	-	-	2	8	0.02

6.2.3. Isolation of polymers

The polymers produced in toluene (Set 1 of experiments, Table 6.1) and the polymers synthesized in the experiments to determine the chain transfer constants (Set 2, Table 6.2) were precipitated in cold methanol. The functional copolymers containing catechol monomers (Set 4, Table 6.4) were precipitated in deionized water. After the precipitation, the polymers were filtered and dried at 30 °C and high vacuum. For the analysis of the time evolution of the molecular weight distribution of the polymers produced in Runs 1-7 (Table 6.4), the samples were dried for 5 days at room temperature and 3 days at 65 °C. In these measurements, the non-volatile monomers (DMA and VC) were not removed from the polymers.

6.2.4. Characterization

6.2.4.1. Monomer conversion

In the experiments carried out in the calorimeter reactor (set 1, Table 6.1) the monomer conversion was determined from the heat released from the reaction medium. In the copolymerizations of catechol monomers (set 4 of experiments, Table 6.4), the individual monomer conversions were determined by ^{1}H -NMR on a Bruker 400 MHz equipment. The ^{1}H-NMR spectra were recorded at room temperature setting a relaxation time (D1) of 20 s and 16 scans. d_6-DMSO was used as solvent in Runs 1-5 and 7-10 and the spectra were recorded in $CDCl_3$ in Runs 5, 6 and 11. For the analysis, 100 µL of the samples withdrawn from the reaction medium at different times were diluted in 600 µL of the deuterated solvent. The monomer conversion was determined from the disappearance of the vinyl protons using the signal of DMF at 8.03 ppm as internal standard to normalize the signals of the vinyl protons.

6.2.4.2. Molar mass distribution

The molecular weight distributions of the polymers produced in Sets 1, 2 and 4 of experiments were measured using size exclusion chromatography (SEC) in THF at 35 °C with a THF flow rate of 1 mL min^{-1}. The SEC instrument consisted of an injector, a pump (Waters 510), three columns in series (Styragel HR2, HR4, and HR6), a differential refractometer detector (Waters 2410) and dual λ absorbance detector (Waters 2487, wavelength 265 nm). The equipment was calibrated using polystyrene standards. The absolute molar masses of PS, PMMA and PMA were determined using a universal calibration curve considering the following Mark Houwink constants: K=0.0158 ml/g and a=0.704 for PS at 35 °C in THF,[64] K=0.0122 ml/g and a=0.690 for PMMA at 35 °C in THF,[64] and K=0.0168 ml/g and a=0.696 for PMA at 30 °C in

THF.[65] The molar masses reported for the P(2-MOA), P(2-MOMA) and PS (co)polymers produced in DMF (Table 6.4) relate to polystyrene.

The molecular weight distributions of the PAM and PMAM polymers produced in Set 3 of reactions were measured by size exclusion chromatography employing a mixed eluent composed of 80 wt% 0.15 mol L^{-1} NaCl and 0.03 mol L^{-1} NaH_2PO_4 aqueous solution and 20 wt% of acetonitrile at 35 °C and with a flow rate of 1 mL min^{-1}. The equipment was composed by a LC20 pump (Shimadzu) coupled to a miniDAWN Treos multiangle (3 angles) light scattering laser photometer equipped with an He-Ne laser (l¼658 nm) and an Optilab T-Rex differential refractometer (658 nm) (all from Wyatt Technology Corp., USA). Separation was carried out using three columns in series (Waters Ultra-hydrogel 120, 250, and 2000 with pore sizes of 120, 250, and 2000 A˚ respectively). The molar mass of the polymers was calculated from the MALS/RI data using the Debye plot (with first order Zimm formalism) assuming a dn/dc of the polymers of 0.142 mL g^{-1}.[64] Note that this value corresponds to the reported dn/dc for polyacrylamide and therefore the reported values of molar mass of the polymethacrylamide samples have limited accuracy.

6.2.4.3. Matrix-assisted laser desorption/ionization time of flight mass spectrometry (MALDI-TOF-MS)

MALDI-TOF MS measurements were performed on a Bruker Autoflex Speed system (Bruker, Germany) instrument equipped with a 355 nm Nd:YAG laser. The spectra of the PS (co)polymers were acquired using silver trifluoroacetate (AgTFA, 10mg L^{-1} in THF) and the spectra of the PMA, P(2-MOMA) and P(2-MOA) (co)polymers were acquired using sodium trifluoroacetate (NaTFA, 10mg L^{-1} in THF) as cationic ionization agent. Trans-2-[3-(4-tert-butylphenyl)-2-methyl-2-propenylidene]malononitrile (DCTB) was used as matrix for all the

measurements at a concentration of 20 g L^{-1} in THF. The polymers were dissolved at 10 mg L^{-1} in THF. The matrix:salt:polymer ratio varied between 10:1:5 and 10:1:10. The spectra of the polymers produced in Set 1 of experiments were acquired in positive linear mode and the spectra of the polymers produced in Set 4 of reactions in positive reflectron mode (accelerating voltage 20 kV, pressure 5 x 10^{-6} mbar). Approximately 0.5 µL of the mixtures were hand spotted on the ground steel target plate. External calibration was performed in quadratic mode with a mixture of different polyethylene glycol standards (PEO, Varian).

6.2.5. Computational work

All geometry optimizations were carried out within density functional theory (DFT) using the M062X functional[66] combined with the 6-31+G(d,p) basis set.[67] To confirm that the optimized structures were minima or transition states on the potential energy surfaces, frequency calculations were carried out at the same level of theory. These frequencies were then used to evaluate the zero-point vibrational energy (ZPVE) and the thermal corrections at T = 298.15 K, in the harmonic oscillator approximation. Single-point calculation using the 6-311++G(2df,2p) basis set[68] were performed in the optimized structures in order to refine the electronic energy. All calculations were performed with the Gaussian 16 suite of programs.[69]

6.3. Results and discussion

6.3.1. Polymerizations in presence of pyrocatechol

A number of radical polymerizations using either styrene, methyl acrylate or methyl methacrylate were conducted using pyrocatechol as a model catechol-containing compound in order to gain an insight into the reactivity towards radicals (see Table 6.1 for formulations). The

monomer conversions of the experiments are presented in Figure 6.3. For easier interpretation of the results, the results obtained for each monomer are presented in separate graphs.

Figures 6.3.A and 6.3.B show that the addition of pyrocatechol reduced the rate of polymerization of styrene (S) and methyl acrylate (MA). This effect was particularly notable in the polymerization of styrene, where 10 wt% of catechol decreased the monomer conversion from ~60 % to ~20 % after 6 h of polymerization. On the contrary, no retardation was observed during the polymerization of methyl methacrylate when AIBN was used as initiator (Figure 6.3.C). It is worth pointing out that even 50 wt% of catechol did not affect the polymerization kinetics of MMA and in fact a slight increase in the polymerization rate can be observed in MMA-3 with 50 wt% catechol due to the slightly higher molar concentration of monomer in the formulation. These first results clearly revealed that the reactivity of radicals towards catechol depends heavily on the nature of the propagating radical.

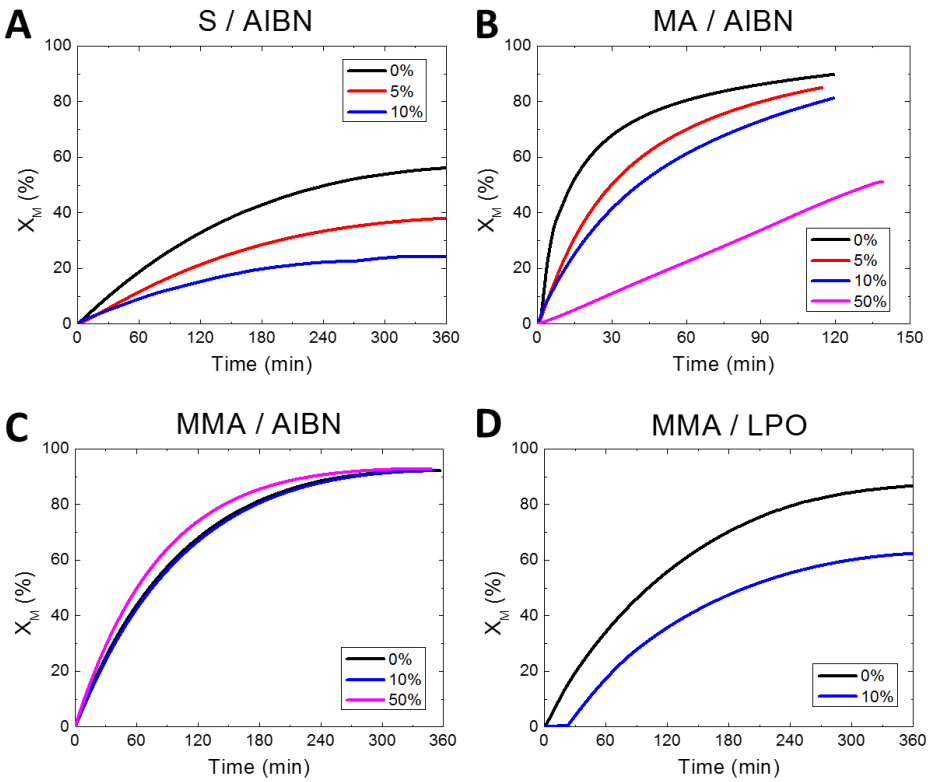

Figure 6.3. Monomer conversions of the polymerizations carried out in the presence of varying amounts of pyrocatechol in set 1 of reactions: (A) Runs S 1-3, (B) Runs MA 1-4, (C) Runs MMA 1-3 and (D) Runs MMA 4-5.

The importance of the initiating radical species was also explored by using lauryl peroxide (LPO) instead of AIBN in the polymerization of MMA. First, in the reactions without catechol, although the rate coefficient of initiator decomposition is slightly higher for LPO, the rate of polymerization was actually slower when using LPO due to the lower molar concentration of this initiator in the formulation. Then, Figure 6.3.D shows that, unlike reactions carried out with AIBN, the polymerization of MMA initiated by lauryl peroxide (LPO) showed an inhibition period and

retardation in the presence of pyrocatechol. These results suggest that pyrocatechol reacts with oxygen centered radicals arising from the decomposition of LPO, which lowers the efficiency of the initiation process, and therefore lowers the number of propagating radicals.

Coupled with changes in the polymerization rate there were significant differences in the molecular weight distributions of polymerizations containing varying concentrations of catechol as can be seen from the molecular weight distributions shown in Figure 6.4 and the values of M_n, M_w and $Đ$ presented in Table 6.5. Figures 6.4.A and 6.4.B show that the molecular weight of the PS and PMA chains decreased with the catechol content, which indicates the occurrence of chain transfer reactions. In addition, the decrease in the molecular weight observed for PS was greater than for PMA, suggesting a higher amount of chain transfer events occurring during the polymerization of S.

Moving to the polymerizations of MMA initiated by AIBN and LPO (see Figures 6.4.C and 6.4.D), the addition of catechol to the peroxide initiated system led to lower molar masses, whilst the PMMA polymers synthesized using AIBN showed very similar molecular weight distributions. Lower molecular weights in the LPO system is perhaps surprising since the lower rate of polymerization in this reaction suggests lower concentrations of propagating radicals, which would be expected to lead to higher molecular weights (less bimolecular termination). However, if the phenoxy radicals generated by the reaction of pyrocatechol with LPO derived radicals do not propagate but do undergo bimolecular termination with propagating radicals, lower rates of polymerization would be coupled with lower molar masses, as observed experimentally. In the MMA/AIBN system, even with 50 wt% of catechol the molecular weight of the polymer was not affected, further indicating that the chain transfer events between methacrylate based radicals and the catechols are negligible. In line with these findings, Haddleton and coworkers showed

that the ATRP polymerization of MMA in presence of substituted phenols proceeded without any evidence of chain transfer events with the phenolic hydroxyls.[70]

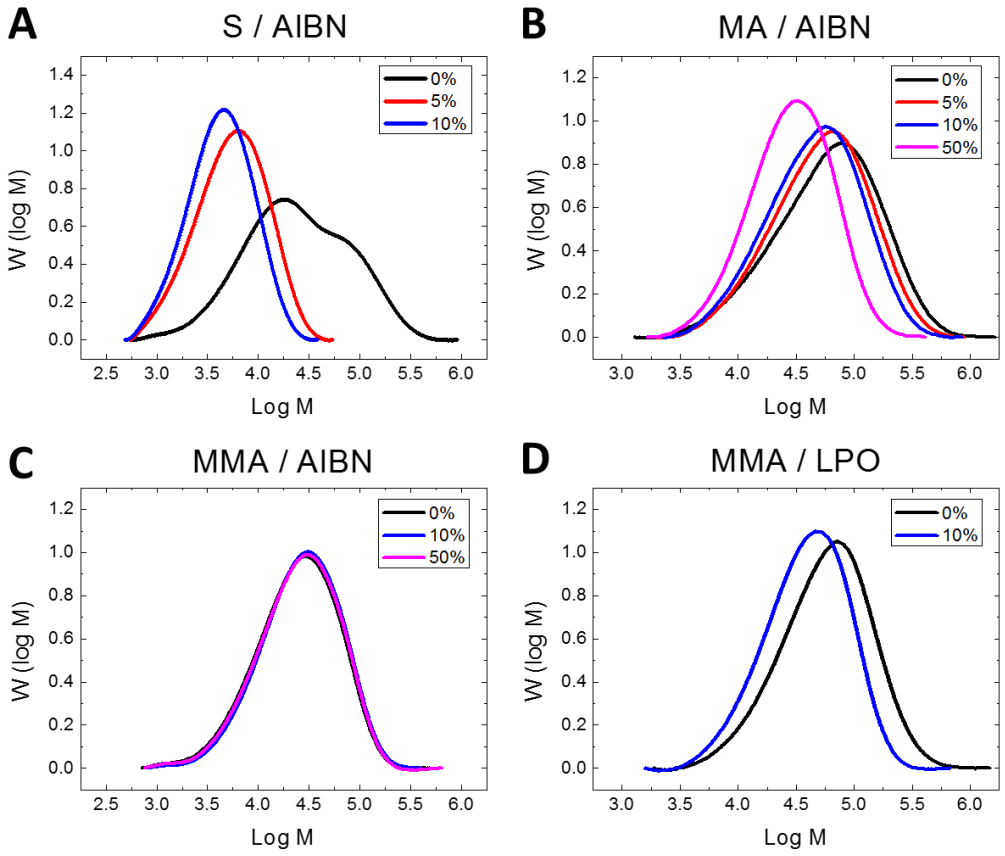

Figure 6.4. Molecular weight distributions of the polymers produced in the presence of catechol in set 1 of reactions: (A) Runs S 1-3, (B) Runs MA 1-4, (C) Runs MMA 1-3 and (D) Runs MMA 4-5.

Table 6.5. Molecular weight number and weight averages and *Đ* values of the polymers produced in the presence of pyrocatechol in set 1 of reactions.

Run	Monomer	Initiator	Catechol (wt %)	M_n (g mol^{-1})	M_w (g mol^{-1})	*Đ*
S-1	S	AIBN	0	12 000	46 400	3.9
S-2	S	AIBN	5	3 900	7 300	1.9
S-3	S	AIBN	10	3 300	5 500	1.7
MA-1	MA	AIBN	0	33 300	94 400	2.8
MA-2	MA	AIBN	5	32 400	78 100	2.4
MA-3	MA	AIBN	10	29 000	66 100	2.3
MA-4	MA	AIBN	50	20 300	38 900	1.9
MMA-1	MMA	AIBN	0	14 900	35 100	2.4
MMA-2	MMA	AIBN	10	16 900	37 600	2.2
MMA-3	MMA	AIBN	50	15 500	36 000	2.3
MMA-4	MMA	LPO	0	37 700	81 800	2.2
MMA-5	MMA	LPO	10	27 300	51 900	1.9

In order to gain information about the nature of chain transfer reactions that may be occurring during the polymerizations of S and MA in the presence of catechol, the microstructure of the polymer chains was investigated using MALDI-TOF-MS. The spectra were interpreted on the basis of the proposed reaction mechanisms presented in Scheme II.3 of Appendix II. The mass spectra of the PS polymers produced in Runs S-1 (0 wt% pyrocatechol) and S-3 (10 wt% pyrocatechol) in the range 2550-3050 Da are shown in Figures 6.5.A and 5.B respectively and the species assigned in the figure are given in Table 6.6. The full spectra are shown in Figure II.3 of Appendix II for reference. Figure 6.5.A shows that in the absence of catechol, the main species (species A) was the product of the termination by combination of growing chains initiated by AIBN. In addition, there were species of lower intensity (species B) formed by either

disproportionation or chain transfer events (e.g. to toluene solvent). However, the absence of toluene-initiated polymer chains suggests that the termination mechanism corresponding to the species B was termination by disproportionation. The origins of peaks C and D are unclear but may be attributed to the fragmentation of PS chains during MALDI-TOF-MS analysis as has previously been observed.[71,72] Peak E is assigned to polymer chains initiated by AIBN and terminated by combination (similar to species A) with one methacrylonitrile (MAN) unit in the polymer backbone. MAN is generated from the termination by disproportionation of two tertiary radicals formed after the decomposition of AIBN[73] as shown in Scheme II.4 in Appendix II. Moving to Figure 6.5.B, in the presence of 10 wt% catechol the intensity of the species formed by termination by combination decreased drastically (species A) and the main species was the product of chains terminated via chain transfer reactions (species B). This alteration on the intensity of the species indicated a change of the main termination mechanism of polystyrene in the presence of catechol from termination by combination to chain transfer to pyrocatechol.

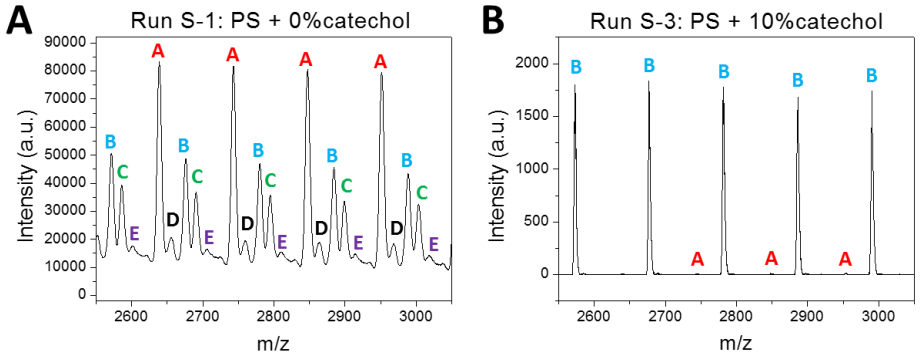

Figure 6.5. MALDI-TOF-MS spectra (range: 2550-3050) of the PS polymers produced in Runs S-1 (part A) and S-3 (part B) in presence of 0 wt% and 10 wt% pyrocatechol. The whole spectra are shown in Figure II.3 Appendix II.

Table 6.6. Species assigned to the mass spectra of PS shown in Figure 6.5.

	Signal	Species	Termination mechanism	Species type (Sch. II.3, II.4)	Molar mass of Ag adduct (g/mol)
	A	AIBN-S_n-AIBN	Combination	I	2639 ± n104
	B	AIBN-S_n-2x and AIBN-S_n-H	Disproportionation	IV / III	2675 ± n104 / 2677 ± n104
	B	AIBN-S_n-H	Chain transfer	II	2677 ± n104
	C	AIBN-S_n-(+methylene)	Fragmentation during MALDI analysis	-	2689 ± n104
	D	AIBN-S_n-(-methylene)	Fragmentation during MALDI analysis	-	2663 ± n104
	E	AIBN-S_n-MAN-AIBN	Combination	I	2602 ± n104

The mass spectra in the 3500-3850 range of the PMA polymers synthesized in Runs MA-1 (0 wt% pyrocatechol) and MA-4 (50 wt% pyrocatechol) are presented in Figures 6.6.A and 6.6.B, respectively. The full spectra are shown in Figure II.4 in Appendix II. The species highlighted in Figure 6.6 are attributed to the structures shown in Table 6.7. In the polymerization of MA, the main species formed both in absence and presence of catechol were chains initiated by AIBN radicals and terminated by chain transfer (species A). Note that although this peak may be linked to termination by disproportionation, peak A is accompanied by a signal of similar intensity which is attributed to chains initiated by toluene (species B). This suggests that the predominant termination mechanism was chain transfer to solvent. Additional peaks of lower intensity (species D and E) were also observed that may be attributed to β-scission reactions of midchain radicals arising from chain transfer to polymer reactions.[74,75] In the absence of catechol (Figure 6.6.A) it was possible to detect the species related to termination by combination of radicals (species C) whilst this species was not visible in the spectrum of the polymer produced in presence of 50 wt% catechol. In addition, in the presence of catechol, the relative intensity of the AIBN initiated species (species A) compared to the toluene initiated species (species B)

increased. Although MALDI-TOF is not a precise quantitative technique, this increase in the intensity of the AIBN-MA_n-H peak could be explained by the occurrence chain transfer to catechol which competes with chain transfer to toluene.

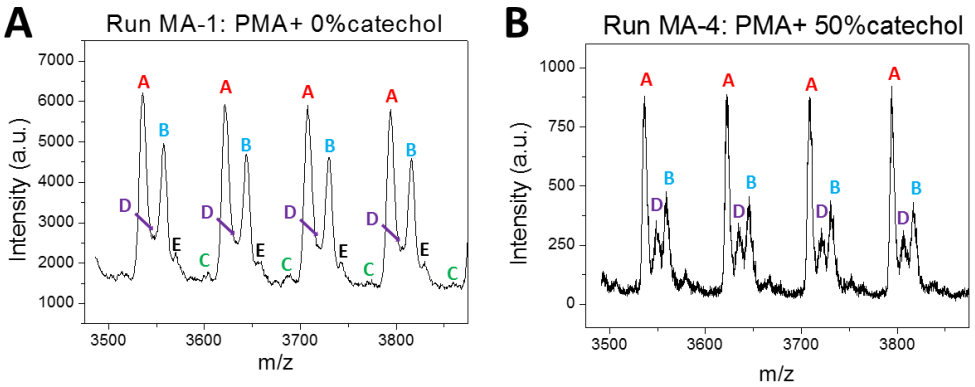

Figure 6.6. MALDI-TOF-MS spectra (range: 3500-3850) of the PMA polymers produced in Runs MA-1 (part A) and MA-4 (part B) in presence of 0 wt% and 50 wt% pyrocatechol. The whole spectra are shown in Figure II.4 in Appendix II.

Table 6.7. Species assigned to the mass spectra of PMA shown in Figure 6.6.

	Signal	Species	Termination mechanism	Species type (Sch. II.3)	Molar mass of Na adduct (g/mol)
	A	AIBN-MA_n-H	Chain transfer	II	3620 ± n86
	B	Toluene-MA_n-H	Chain transfer	II	3643 ± n86
	C	AIBN-MA_n-AIBN	Combination	I	3601 ± n86
	D	AIBN-MA_n-2x	Intramolecular chain transfer + β-scission	V	3632 ± n86
	E	Toluene-MA_n-2x	Intramolecular chain transfer + β-scission	V	3655 ± n86

From the analysis of the microstructure, it can therefore be concluded that the addition of catechol to the polymerization of styrene and methyl acrylate leads to an increase in the extent of chain transfer reactions. These chain transfer events explain the decrease in the average molecular weights of the polymers with increasing catechol content. In addition, it is worth mentioning that no catechol-initiated chains were detected in the mass-spectra of the polymers. Thus, according to these results, the phenoxyl radicals formed via chain transfer to catechol do not reinitiate the polymerization and chain transfer to catechol can be classified as a degradative chain transfer mechanism. Therefore, chain transfer to catechol results in a decrease in the propagating radical concentration which would explain the retardation of the monomer conversion observed in the kinetic study of the first part of the work.

6.3.2. Determination of chain transfer constants with pyrocatechol

The combination of the parameters studied so far indicated that the reactivity of the monomers towards catechol increased in the order methacrylate << acrylate < styrene. In order to get quantitative information about the extent of chain transfer events during the polymerizations, the chain transfer constants of S, MA and MMA with pyrocatechol were determined using the Mayo equation for polymers synthesized at low conversion in the presence of varying amounts of pyrocatechol.[76] The Mayo equation (Equation. 6.1) expresses the change in the number average degree of polymerization (DP_n) with the chain transfer agent / monomer concentration ratio ([catechol]/[M]). In Eq. 6.1 $DP_{n,0}$ represents the number average degree of polymerization of the polymer in the absence of CTA. The chain transfer constant (C_{TR}), defined in Equation 6.2 as the ratio between the chain transfer (k_{tr}) and propagation rate coefficients (k_p), is obtained from the slope of the Mayo plot.

$$\frac{1}{DP_n} = \frac{1}{DP_{n,0}} + C_{TR}\frac{[catechol]}{[M]} \qquad \text{Equation 6.1}$$

$$C_{TR} = \frac{k_{tr}}{k_p} \qquad \text{Equation 6.2}$$

The Mayo plots with the experimental data fitted to the Mayo equation are shown in Figure 6.7, and the values of the chain transfer constants obtained from the Mayo plots are presented in Table 6.8. In agreement with the previous results, styrene showed the highest chain transfer constant with catechol (C_{TR} = 0.28), methyl acrylate showed a chain transfer constant two orders of magnitude lower (C_{TR} = 0.0075) and methyl methacrylate did not show a measurable change in the degree of polymerization up to 50 wt% pyrocatechol.

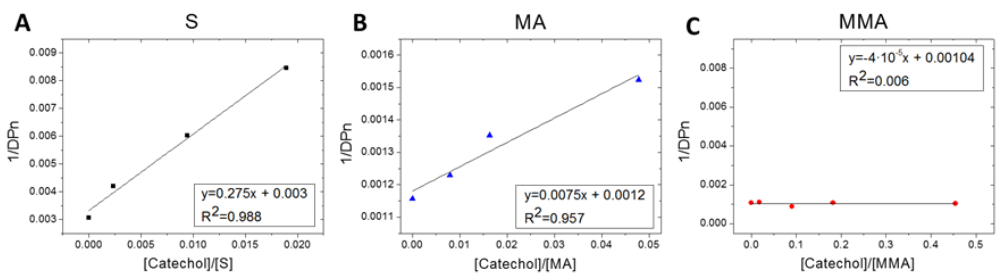

Figure 6.7. Mayo plots for the determination of the chain transfer constants with catechol: (A) S-catechol pair, (B) MA-catechol pair and (C) MMA-catechol pair.

Table 6.8. Chain transfer constants of S, MA and MMA with pyrocatechol.

Monomer	C_{TR} with pyrocatechol
S	0.2752
MA	0.0075
MMA	-

Comparing the chemical structure of MMA and MA, the only difference is in the methyl group attached to the carbon where the radical is located. These results suggest that the

relatively high stability of the tertiary radicals formed in the methacrylate reduces the rate of chain transfer reactions with pyrocatechol. The reduction in the reactivity of the radicals towards catechol from acrylates to methacrylates was also observed for the polymerization of acrylamide and methacrylamide in water. It is shown in Table 6.9 that the addition of ≈10 wt% catechol to the polymerization reduced the molecular weight of the polyacrylamide chains by roughly 2.5 times, while the molecular weight of the polymethacrylamide chains remained essentially unaltered by the presence of pyrocatechol.

Table 6.9. Molecular weight of the PAM and PMAM polymers produced in presence of 0 and ≈10 wt% pyrocatechol in set 3 of reactions.

Run	M_n (kg mol^{-1})	M_w (kg mol^{-1})	*Đ*
AM-1	1601	2365	1.48
AM-2	605	982	1.62
MAM-1	89	159	1.78
MAM-2	104	135	1.30

6.3.3. Theoretical calculations

In order to have a better fundamental understanding of the different reactivity of radicals with pyrocatechol, the hydrogen transfer reaction to a styrene, methacrylate and acrylate radical (termination mechanism B, Scheme II.3) was investigated using density functional theory (DFT). The reaction profiles corresponding to these reactions are presented in Figure 6.8. First, comparing the energy difference between the products and the reactants for the three radical types, it can be seen that the energy gap increased in the order methacrylate < styrene < acrylate (-3.74, -7.31 and -11.42 kcal/mol, respectively). This means that hydrogen abstraction is thermodynamically less favorable for a methacrylate. Second, looking at the activation energies

of the reactions, namely the energy differences between the reactant complexes and the transition states (represented with vertical arrows), the methacrylate radical showed the highest activation energy (16.00 kcal/mol) and S and MA showed lower and very similar activation energies (12.28 and 11.89 kcal/mol, respectively). Thus, the energy barrier for the hydrogen transfer reaction was the highest for MMA, indicating a lower rate for the hydrogen transfer reaction to a MMA radical, in agreement with the experimental results shown above. The difference between MMA and MA can be ascribed to the geometrical structure of the transition state. In the case of the MA, the transition state resembles the reactants (early transition state[77]), facilitating the molecular rearrangement to surpass the reaction barrier. In contrast, for MMA the transition state takes place later, with geometrical features of the products more developed. It may be noted that although the calculated activation energies for the transfer reactions with styrene and methyl acrylate are similar, as the rate coefficient for propagation is substantially higher for methyl acrylate than for styrene, the chain transfer constant would be expected to be lower in the case of methyl acrylate, in agreement with the experimental results.

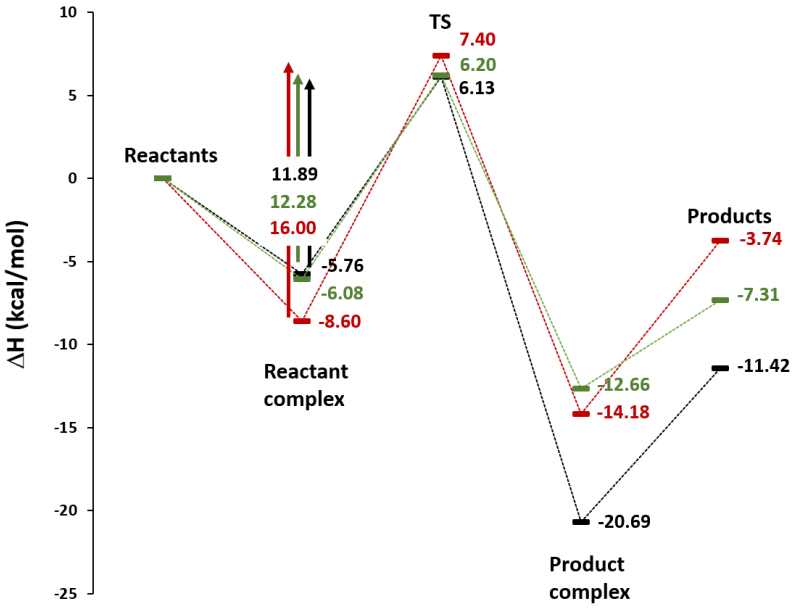

Figure 6.8. Reaction profiles obtained by DFT calculations for the hydrogen transfer reaction to a styrene (green), acrylate (black) or methacrylate (red) radical.

6.3.4. Copolymerization of catechol containing monomers

The difference in the reactivity of the propagating radicals with catechol suggests that in polymerizations incorporating catechol functional monomers, both the main monomer and the nature of the polymerizable moiety on the catechol functional monomer are important. To explore this, a series of copolymerizations were carried out varying both the nature of the main monomer (methacrylate, acrylate or styrene-type) and the nature of the catechol monomer (vinyl catechol or dopamine methacrylamide).

6.3.4.1. Effect of the solvent

Dimethylformamide (DMF) was chosen as polymerization medium for being a good solvent for all the components including the catechol monomers. The reactivity of the functional groups can change depending on the interactions with the solvent,[78] and thus, the effect of the solvent on the reactivity of catechol as CTA was first analyzed by comparing the polymerization of styrene in presence of catechol in toluene or DMF. Figure 6.9.A shows that, the addition of 8 mol% (≈ 8.5 wt%) pyrocatechol to the polymerization in DMF (Run 11) led to a decrease in the polymerization rate of S. However, while the addition of 10 wt% catechol to the polymerization of S in toluene decreased the monomer conversion from 60 to 20 % after 6 h polymerization (Run S-3, see Figure 6.3.A), the addition of 8.5 wt% catechol to the polymerization of S in DMF only decreased the conversion of S from 35 to 27 %. Moreover, in the polymerization in DMF, the addition of catechol only caused a slight decrease in the molecular weight of PS (see Figure 6.9.B). The lower activity of catechol in DMF solution can be ascribed to the stabilization of the hydroxyl groups of catechol via H-bonding with the carbonyl groups of DMF. Similar findings were described by Takeshima *et al.*, where the strong H-bonds between the phenol and the acetonitrile solvent prevented the side reactions and allowed the cationic polymerization of catechol bearing vinyl monomers.[79] Thus, the use of polar solvents with strong H-bond acceptor appears to facilitate the (co)polymerization of catechol-containing monomers.

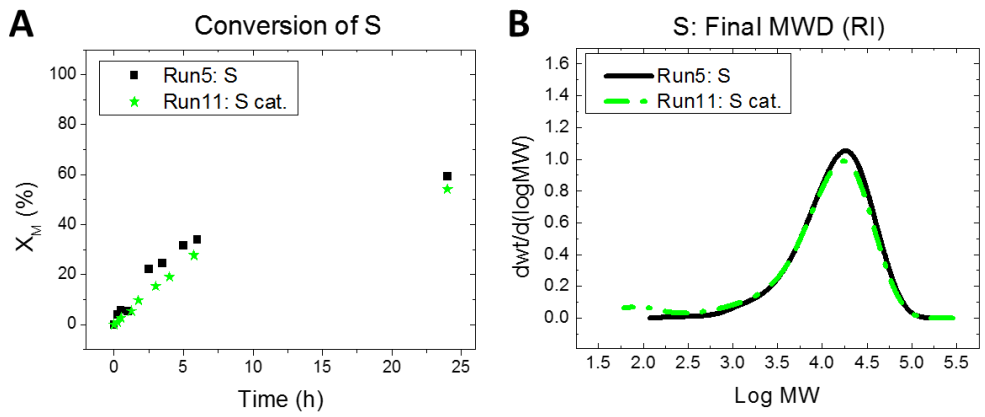

Figure 6.9. Influence of catechol on the polymerization of S in DMF: (A) monomer conversion and (B) molecular weight distribution (MWD).

6.3.4.2. Effect of the nature of the main monomer

To investigate the effect of the nature of the main monomer, the copolymerization of DMA with 2-methoxyethyl methacrylate (2-MOMA), 2-methoxyethyl acrylate (2-MOA) and styrene (S) was investigated. 2-MOMA and 2-MOA were selected as model (meth)acrylates for the polymerizations due to their widespread use in the literature in copolymerization with catechol functional monomers.[8,10,80] The conversion of the 2-MOMA, 2-MOA and S in the (co)polymerizations is compared in Figure 6.10 while the individual monomer conversions in each reaction are reported in Figure II.7. in Appendix II. Figure 6.10 shows that the incorporation of 15 mol% DMA did not influence the monomer conversion of 2-MOMA, but caused a slight decrease in the polymerization rate of 2-MOA. In the case of S, the addition of only 8 mol% DMA caused a slow down in the polymerization similar to the retardation observed with the addition of 8 mol% catechol, which suggests that S is sensitive to the presence of DMA monomer, even though it contains a methacrylamide-type polymerizable group. These results are in general agreement with the previous sections but it should be noted that the effect of catechol on the

polymerizations was less pronounced due to the solvent stabilization effect. In addition, in the copolymerization of catechol containing monomers, it should be noted that any changes in rate can be related to either reaction with the catechol or due to changes in the average propagation rate coefficient.

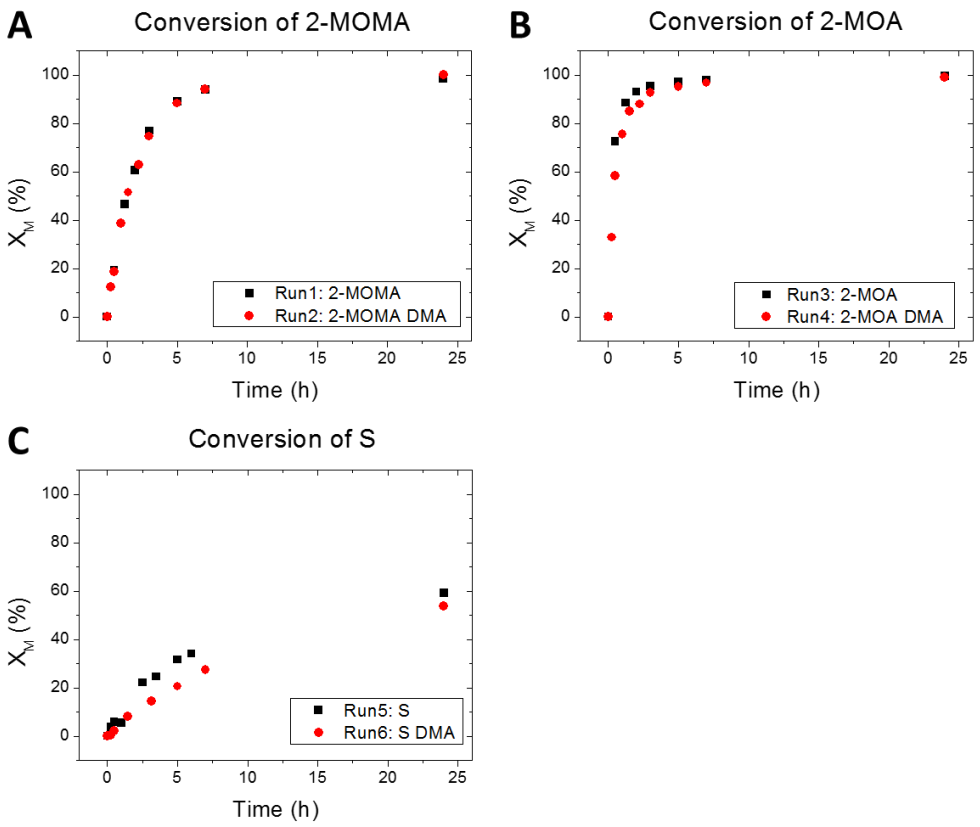

Figure 6.10. Influence of DMA on the copolymerization with 2-MOMA, 2-MOA and S. Conversion of (A) 2-MOMA in Runs 1-2, (B) 2-MOA in Runs 3-4, (C) S in Runs 5-6.

The molecular weight distribution of the polymers were measured to investigate the extent and effect of the chain transfer reactions with the catechol units during the polymerization. The final molecular weight distributions (MWDs) of the polymers are compared in Figure 6.11 and the time evolution of the molecular weight distributions in Runs 1-6 is shown in Figure II.8 in Appendix II. It is worth noting that the peak at very low molar masses that is seen in the reactions containing DMA is DMA monomer that is not removed from the system. The comparison of the final MWDs of the polymers with and without DMA in Figures 6.11.A-C, shows that the incorporation of DMA comonomer did not significantly influence the final MWD for any of the three monomer systems. These results were reasonable since the addition of catechol to the polymerization of S in DMF did not influence considerably the final MWD of the polymer.

The time evolution of the MWDs presented in Figure II.8 shows the molecular weight distributions got broader as the polymerization proceeded. In the case of the copolymerization of DMA with styrene, the molecular weight of the polymer shifted to higher molar masses with increasing time (see Figure II.8.F1) which is likely a result of the higher initial rate of consumption of styrene relative to DMA as can be seen from the individual monomer conversion plots in Figure II.7.F which leads to a significant composition drift during the experiment.

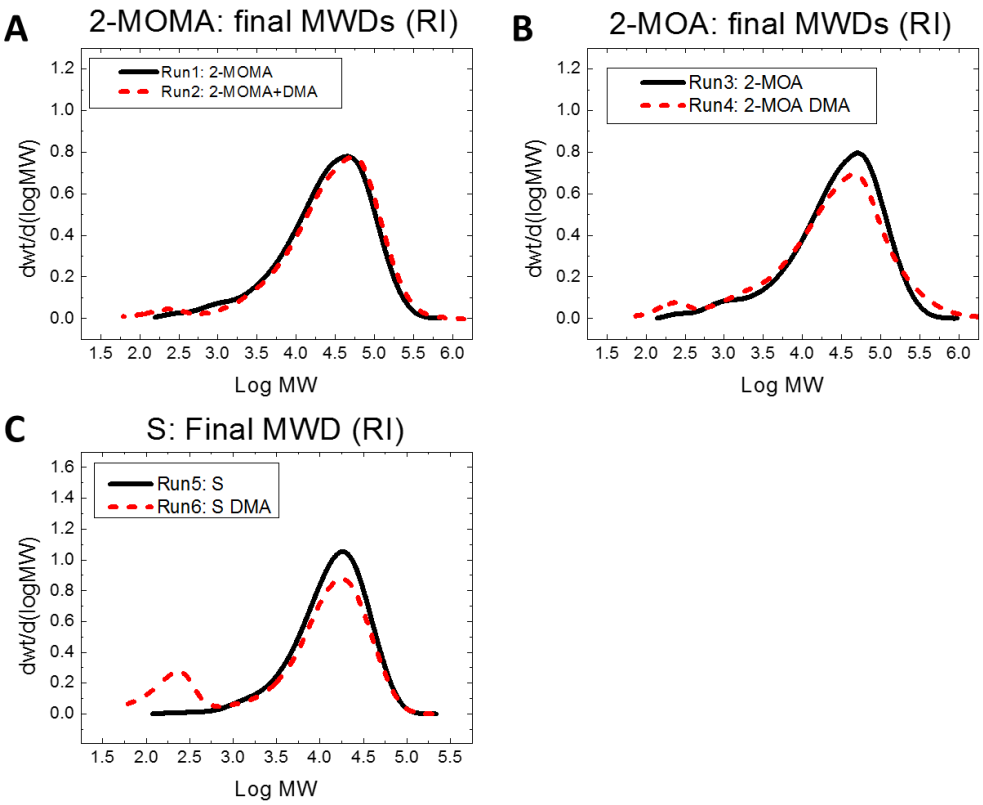

Figure 6.11. Molecular weight distributions obtained with the RI detector for (A) P(2-MOMA) in Runs 1-2, (B) P(2-MOA) in Runs 3-4 and (C) PS in Runs 5-6.

To further investigate any additional termination processes in these reactions the microstructure of the (co)polymers was investigated by MALDI-TOF to gain information about the termination mechanisms during the reactions. The 1800 – 2200 Da range mass spectra of the (co)polymers produced in Runs 1 and 2 are presented in Figure 6.12 and the description of the species marked in the figure is given in Table 6.10. Figure 6.12 shows that the main termination mechanism in the P(2-MOMA) (co)polymers produced in Runs 1 and 2 was termination by disproportion (signals A+B). Although the chains terminated by disproportionation

and chain transfer give an overlapping peak in the MALDI spectra, the isotopic distribution of signals A and B in Run 1 shown in Figure II.6 indicates that the chains were indeed terminated by disproportionation. In addition, a small fraction of species terminated by combination were detected (signal C). In the case of the copolymerization with DMA a number of additional peaks could be observed which are attributed to the copolymer with varying number of DMA units (signals D-H). This indicates that DMA copolymerized homogeneously with 2-MOMA without any additional termination/transfer issues as expected based on the results in the first part of the work.

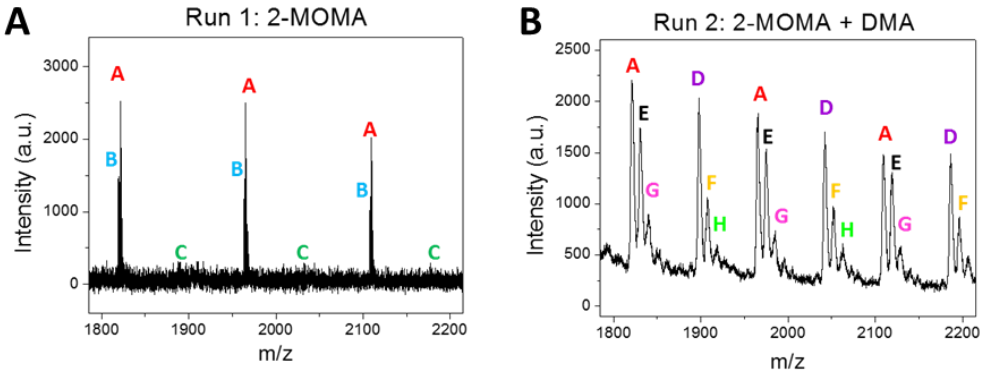

Figure 6.12. 1800-2200 Da range MALDI-TOF-MS spectra of (A) Run 1 – 2-MOMA, (B) Run 2 – 2-MOMA + DMA. Whole spectra are shown in Figures II.5.A and II.5.B.

Table 6.10. Species assigned to the mass spectra of P(2-MOMA) (co)polymers presented in Figure 6.12.

	Signal	Species	Termination mechanism	Species type (Sch. II.3)	Molar mass of Na adduct (g/mol)
	A	AIBN-2MOMA$_n$-H	Chain transfer / disproportionation	II / III	1821 ± n144
	B	AIBN-2MOMA$_n$-2x	Disproportionation	IV	1819 ± n144
	C	AIBN-2MOMA$_n$-AIBN	Combination	I	1888 ± n144
	D	AIBN-2MOMA$_n$-DMA$_1$-H	Chain transfer / disproportionation	II / III	1898 ± n144
	E	AIBN-2MOMA$_n$-DMA$_2$-H	Chain transfer / disproportionation	II / III	1831 ± n144
	F	AIBN-2MOMA$_n$-DMA$_3$-H	Chain transfer / disproportionation	II / III	1908 ± n144
	G	AIBN-2MOMA$_n$-DMA$_4$-H	Chain transfer / disproportionation	II / III	1841 ± n144
	H	AIBN-2MOMA$_n$-DMA$_5$-H	Chain transfer / disproportionation	II / III	1918 ± n144

The mass spectra of the P(2-MOA) (co)polymers are shown in Figure 6.13. Due to the complexity of the spectra, only the main species are marked in Figure 6.13 and assigned in Table 6.11. The analysis of the spectra shows that the main termination mechanism for the acrylates was termination by chain transfer (peak A). A number of other peaks including that arising from transfer to solvent (peak B), as well as peaks arising from chain transfer to polymer and β-scission reactions (peaks E and F) were also detected. In the copolymerization the same peaks but with additional DMA units incorporated into the structure can be observed (labelled A* and A** in Figure 6.13). In the absence of DMA, evidence for termination by combination was also observed. However, the comparison of the spectra revealed that no species were formed from termination by combination in presence of DMA (signal C), which indicated a slight increase of chain transfer events in the presence of catechol.

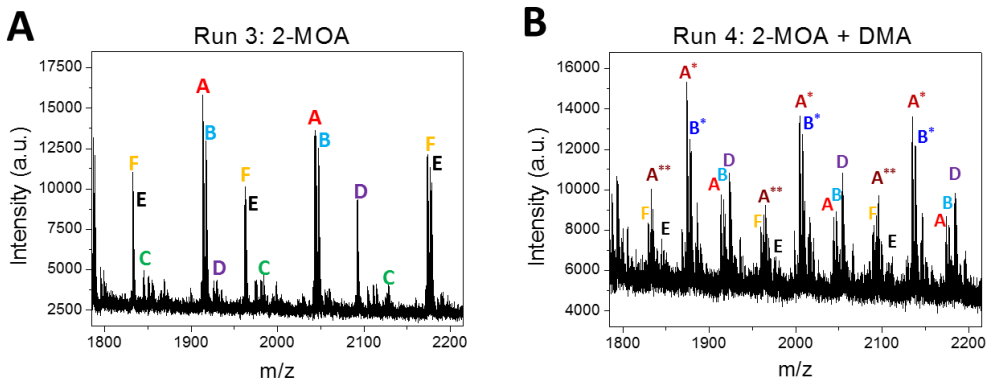

Figure 6.13. 1800-2200 Da range MALDI-TOF-MS spectra of (A) Run 3 – 2-MOA, (B) Run 4 – 2-MOA + DMA. Whole spectra are shown in Figures II.5.C and II.5.D.

Table 6.11. Main species assigned to the mass spectra of P(2-MOA) (co)polymers presented in Figure 6.13.

	Signal	Species	Termination mechanism	Species type (Sch. II.3)	Molar mass of Na adduct (g/mol)
	A	AIBN-2MOA$_n$-H	Chain transfer	II	1914 ± n130
	B	DMF-2MOA$_n$-H	Chain transfer	II	1918 ± n130
	C	AIBN-2MOA$_n$-AIBN	Combination	I	1851 ± n130
	D	AIBN-2MOA$_n$-2x	Intramolecular chain transfer + β-scission	V	1926 ± n130
	E	H-2MOA$_n$-2x	Intramolecular chain transfer + β-scission	VI	1844 ± n130
	F	β-2MOA$_n$-H	Initiating radical from β-scission + chain transfer	II	1833 ± n130
	A*	AIBN-2MOA$_n$-DMA$_1$-H	Chain transfer	II	1875 ± n130
	B*	DMF-2MOA$_n$-DMA$_1$-H	Chain transfer	II	1879± n130
	A**	AIBN-2MOA$_n$-DMA$_2$-H	Chain transfer	II	1836 ± n130

Lastly, the MALDI-TOF-MS spectra for the reactions using styrene are shown in Figure 6.14. Unlike the other monomers where there were limited observable differences, in the case of styrene substantial differences between the two polymers could be observed. When homopolymerized, the MALDI spectra showed the predominant formation of chains terminated by combination (peak A), as well as a fraction of chains terminated by disproportionation (peak B). When copolymerized with DMA, as well as the appearance of a copolymer with one and two DMA units (peaks C* and D), the peak corresponding to termination by combination decreased drastically suggesting the addition of DMA switched the main termination mechanism from combination (signal A) to chain transfer/disproportionation (signals B and C*).

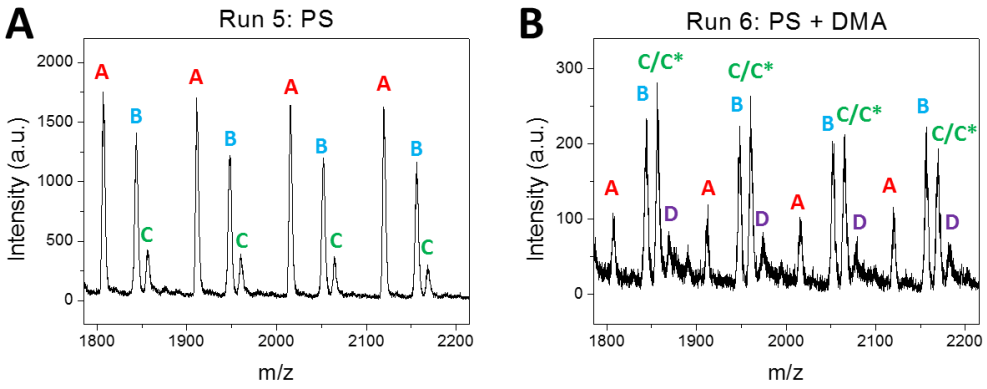

Figure 6.14. 1800-2200 Da range MALDI-TOF-MS spectra of (A) Run 5 – S, (B) Run 6 – S + DMA. Whole spectra are shown in Figures II.5.E and II.5.F.

Table 6.12. Species assigned to the mass spectra of PS (co)polymers presented in Figure 6.14. Signal C* only corresponds to Figure 6.14.B.

	Signal	Species	Termination mechanism	Species type (Sch. II.3)	Molar mass of Ag adduct (g/mol)
	A	AIBN-S_n-AIBN	Combination	I	1806 ± n104
	B	AIBN-S_n-H	Chain transfer / disproportionation	II / III	1843 ± n104
	C	AIBN-S_n-(+ methylene)	Fragmentation during MALDI analysis	-	1855 ± n104
	C*	AIBN-S_n-DMA_1-H	Chain transfer / disproportionation	II / III	1856 ± n104
	D	AIBN-S_n-DMA_2-H	Chain transfer / disproportionation	II / III	1869 ± n104

6.3.4.3. Effect of the nature of the catechol monomer

Since methacrylates were the least affected radicals by the presence of catechol, 2-MOMA was selected as main monomer to investigate the effect of the nature of the catechol functional monomer. The conversion of 2-MOMA in the absence, or presence of 15 mol% DMA and 8 mol% VC is compared in Figure 6.15.A. As mentioned above, the incorporation of 15 mol% DMA in Run 2 did not influence the polymerization rate of 2-MOMA due to the low reactivity of methacrylate and methacrylamide radicals with catechol. However, the addition of 8 mol% VC to the polymerization of 2-MOMA in Run 7 slowed down significantly the copolymerization rate.

This decrease in the rate of polymerization may be related to the lower propagation rate of the VC monomer (styrene type double bond)[81] or to chain transfer events with catechol. In order to separate and understand the contribution of each functionality, 2-MOMA was also polymerized in presence of pyrocatechol and/or styrene in Runs 8-10. The conversion of 2-MOMA in these reactions is presented in Figure 6.15.B. First, the addition of pyrocatechol in Run 8 did not influence the polymerization kinetics of 2-MOMA as previously observed with MMA.

Then, the addition of S to the polymerization in Run 9 decreased the polymerization rate of 2-MOMA due to the lower propagation rate coefficient of S. The further addition of pyrocatechol to the copolymerization of 2-MOMA and S in Run 10 did not cause an additional decrease in the polymerization rate of 2-MOMA. These results suggested that the main contributor to the decrease in the polymerization rate observed in Run 7 was the copolymerization of a styrene-type monomer. Although the retardation in Run 7 using VC was greater than in Run 10 combining S and pyrocatechol, this may simply be the result of a lower k_p of VC as compared to styrene, or due to additional transfer events.

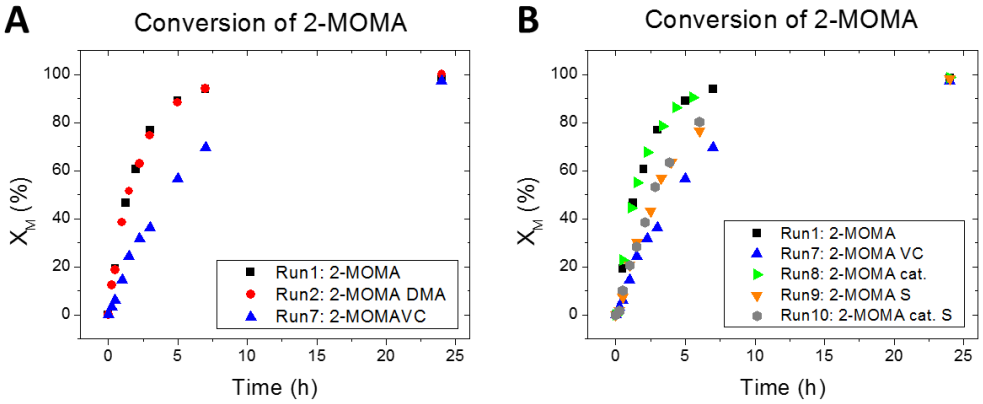

Figure 6.15. (A) Influence of DMA and VC on the copolymerization with 2-MOMA. (B) Influence of VC, catechol and S on the copolymerization with 2-MOMA in Runs 1, 7-10.

While as commented above, the addition of DMA had no effect on the molecular weight distribution, the addition of VC to the polymerization of 2-MOMA led to a broad MWD shifted to lower MW values. The time evolution of the MWDs in Run 1 (2-MOMA) and Run 7 (2-MOMA + VC) presented in Figure 6.16 shows that in the presence of VC, low molecular weight chains of around 1000 g/mol were generated early in the reaction when the conversion of VC was higher than the conversion of 2-MOMA. It is shown in Figure II.7.G that after 2.5 hours of polymerization

the conversions of VC and 2-MOMA were 70 and 30 % respectively. Very likely, the relatively high fraction of VC radicals at low reaction times increased the sensitivity of the polymerization towards the presence of catechol and led to low molecular weight polymer chains as a result of chain transfer events between styrene-type radicals and catechol moieties. Then, after the consumption of VC, the polymerization of the remaining 2-MOMA led to higher molecular weight polymer chains and the P(2-MOMA/VC) copolymer obtained at the end of the reaction presented a very broad MWD. In addition, comparing the MWDs obtained with the RI and UV detectors, the distribution obtained with the UV detector was shifted to lower MWs, which indicates that the low molecular weight polymer chains were richer in VC. The MALDI-TOF-MS spectrum (Figure 6.17) indicates the incorporation of VC into the polymer but do not show any evidence of a change in transfer mechanisms due to the primary termination mechanism of methacrylates being termination by disproportionation in any case.

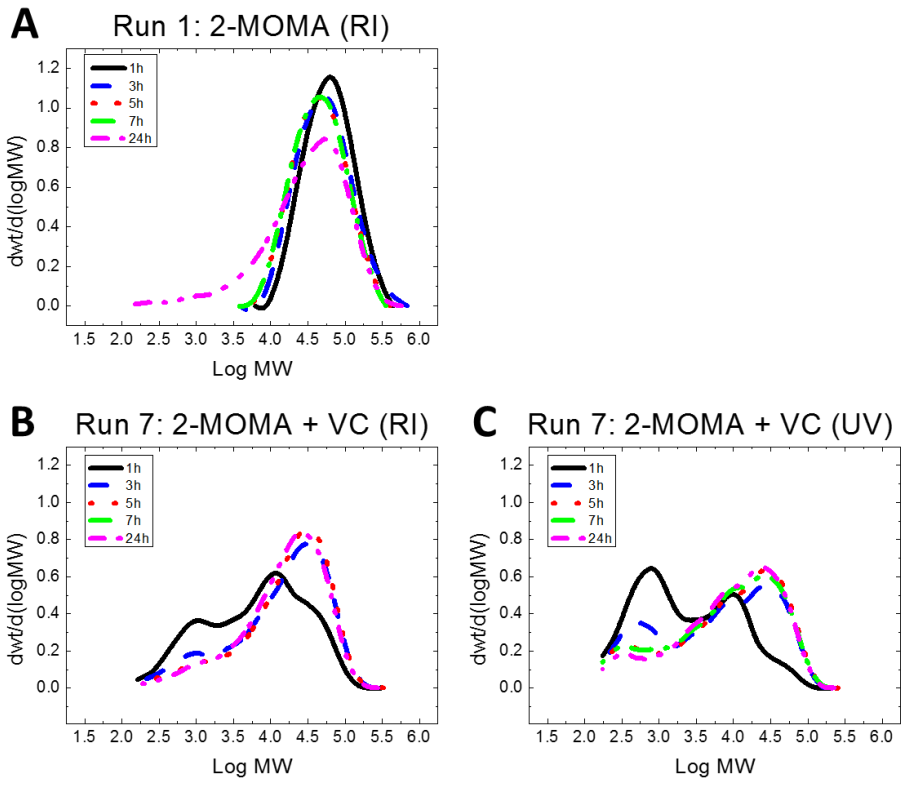

Figure 6.16. Time evolution of the weight distributions in (A) Run 1 – 2-MOMA with the RI detector, (B) Run 7 – 2-MOMA + VC with the RI detector and (C) Run 7 – 2-MOMA + VC with the UV detector.

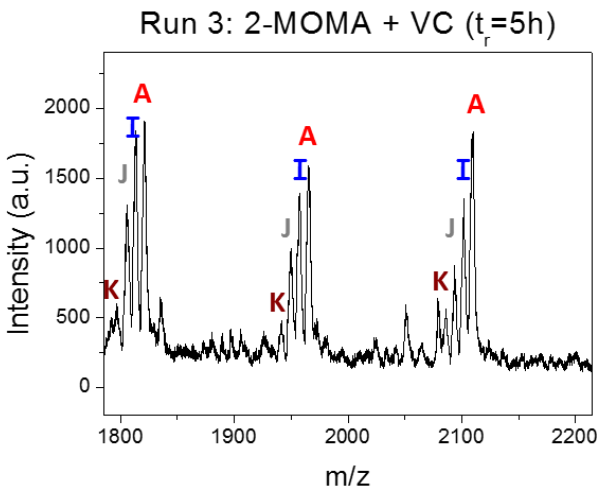

Figure 6.17. 1800-2200 Da range MALDI-TOF-MS spectra of the polymer produced in Run 7 – 2-MOMA + VC after 5 hours of reaction. Whole spectra are shown in Figure II.5.G.

Table 6.13. Species assigned to the mass spectra of the P(2-MOMA) (co)polymer presented in Figure 6.17.

	Signal	Species	Termination mechanism	Species type (Sch. II.3)	Molar mass of Na adduct (g/mol)
	A	AIBN-2MOMA$_n$-H	Chain transfer / disproportionation	II / III	1821 ± n144
	I	AIBN-2MOMA$_n$-VC$_1$-H	Chain transfer / disproportionation	II / III	1957 ± n144
	J	AIBN-2MOMA$_n$-VC$_2$-H	Chain transfer / disproportionation	II / III	1949 ± n144
	K	AIBN-2MOMA$_n$-VC$_3$-H	Chain transfer / disproportionation	II / III	1941 ± n144

6.4. Conclusions

In this work, the reactivity of catechols with common monomer systems used in free radical polymerization has been explored. A systematic study of the polymerizations in the presence of pyrocatechol revealed that for styrene and acrylic monomers chain transfer to catechol leads to a reduction in the rate of polymerization and a decrease in the molecular weight. In the presence of DMF, a polar solvent capable of hydrogen bonding with catechols, the influence of the catechol on the polymerizations was significantly reduced. For methacrylic monomers, even when the catechol was present in large amounts (50 wt%) there was no measurable effect on the rate of polymerization of molecular weight distribution. Based on experimental results with methacrylamide it appears this result can be generalized to methacrylamide type monomers as well.

Similar behavior was also seen in copolymerizations which allows to make some general comments on the possibility for (co)polymerization of catechol-containing monomers. First, the choice of co-monomer is critical when using non-polar solvents. Methacrylate and methacrylamide based radicals are essentially unreactive towards catechol and therefore monomers containing these functional groups are the best choice. While the use of acrylic monomers is feasible, in large quantities catechols will retard the polymerization and result in lower molecular weight polymers. In contrast to these two systems, styrene readily undergoes chain transfer to catechol, and therefore both conversion and molecular weights are limited. These monomer-based effects are also applicable to the choice of catechol containing monomer and therefore the most suitable monomers are those such as dopamine methacrylamide/methacrylate which are less reactive towards the catechol moiety. Styrenic type catechol containing monomers such as vinyl catechol suffer from two issues. First, the type of radicals that are generated appear to lead to increased rates of transfer to catechol. Second, the

rate coefficient of propagation of styrenic-type monomers is low, such that polymerizations are retarded. The effects of chain transfer to catechol can be mitigated by the use of polar solvents with strong H-bond acceptor groups such as DMF which stabilize the aromatic hydroxyl groups of catechol and decrease the rate of chain transfer reactions to catechol. This allows for the successful polymerization of most systems, even those that contain a substantial fraction of styrene type double bonds that cause issues for polymerizations conducted in apolar solvents. These results demonstrate that through appropriate selection of monomers and reaction conditions, catechol containing monomers can be readily incorporated into polymers made by free radical polymerization.

6.5. References

(1) Faure, E.; Falentin-Daudré, C.; Jérôme, C.; Lyskawa, J.; Fournier, D.; Woisel, P.; Detrembleur, C. Catechols as versatile platforms in polymer chemistry *Prog. Polym. Sci.* **2013**, *38*, 236–270.

(2) Zhang, H.; Zhao, T.; Newland, B.; Liu, W.; Wang, W.; Wang, W. Catechol functionalized hyperbranched polymers as biomedical materials *Prog. Polym. Sci.* **2018**, *78*, 47–55.

(3) Rahim, M. A.; Kristufek, S. L.; Pan, S.; Richardson, J. J.; Caruso, F. Phenolic Building Blocks for the Assembly of Functional Materials *Angew. Chemie Int. Ed.* **2019**, *58*, 1904–1927.

(4) Sedó, J.; Saiz-Poseu, J.; Busqué, F.; Ruiz-Molina, D. Catechol-Based Biomimetic Functional Materials *Adv. Mater.* **2013**, *25*, 653–701.

(5) Patil, N.; Jérôme, C.; Detrembleur, C. Recent advances in the synthesis of catechol-derived (bio)polymers for applications in energy storage and environment *Prog. Polym. Sci.* **2018**, *82*, 34–91.

(6) Shao, H.; Stewart, R. J. Biomimetic Underwater Adhesives with Environmentally Triggered Setting Mechanisms *Adv. Mater.* **2010**, *22*, 729–733.

(7) White, J. D.; Wilker, J. J. Underwater Bonding with Charged Polymer Mimics of Marine Mussel Adhesive Proteins *Macromolecules* **2011**, *44*, 5085–5088.

(8) Lee, H.; Lee, B. P.; Messersmith, P. B. A reversible wet/dry adhesive inspired by mussels and geckos *Nature* **2007**, *448*, 338–341.

(9) Waite, J. H. Mussel power *Nat. Mater.* **2008**, *7*, 8–9.

(10) Yang, J.; Keijsers, J.; van Heek, M.; Stuiver, A.; Cohen Stuart, M. A.; Kamperman, M. The effect of molecular composition and crosslinking on adhesion of a bio-inspired adhesive *Polym. Chem.* **2015**, *6*, 3121–3130.

(11) Waite, J. H.; Tanzer, M. L. Polyphenolic Substance of Mytilus edulis: Novel Adhesive Containing L-Dopa and Hydroxyproline *Science* **1981**, *212*, 1038–1040.

(12) White, E. M.; Seppala, J. E.; Rushworth, P. M.; Ritchie, B. W.; Sharma, S.; Locklin, J. Switching the Adhesive State of Catecholic Hydrogels using Phototitration *Macromolecules* **2013**, *46*, 8882–8887.

(13) Lee, S.-B.; González-Cabezas, C.; Kim, K.-M.; Kim, K.-N.; Kuroda, K. Catechol-Functionalized Synthetic Polymer as a Dental Adhesive to Contaminated Dentin Surface for a Composite Restoration *Biomacromolecules* **2015**, *16*, 2265–2275.

(14) Charlot, A.; Sciannaméa, V.; Lenoir, S.; Faure, E.; Jérôme, R.; Jérôme, C.; Van De Weerdt, C.; Martial, J.; Archambeau, C.; Willet, N.; Duwez, A.-S.; Fustin, C.-A.; Detrembleur, C. All-in-one strategy for the fabrication of antimicrobial biomimetic films on stainless steel *J. Mater. Chem.* **2009**, *19*, 4117–4125.

(15) Falentin-Daudré, C.; Faure, E.; Svaldo-Lanero, T.; Farina, F.; Jérôme, C.; Van De Weerdt, C.; Martial, J.; Duwez, A.-S.; Detrembleur, C. Antibacterial Polyelectrolyte Micelles for Coating Stainless Steel *Langmuir* **2012**, *28*, 7233–7241.

(16) Puertas-Bartolomé, M.; Fernández-Gutiérrez, M.; García-Fernández, L.; Vázquez-Lasa, B.; San Román, J. Biocompatible and bioadhesive low molecular weight polymers containing long-arm catechol-functionalized methacrylate *Eur. Polym. J.* **2018**, *98*, 47–55.

(17) Faure, E.; Lecomte, P.; Lenoir, S.; Vreuls, C.; Van De Weerdt, C.; Archambeau, C.; Martial, J.; Jérôme, C.; Duwez, A.-S.; Detrembleur, C. Sustainable and bio-inspired chemistry for robust antibacterial activity of stainless steel *J. Mater. Chem.* **2011**, *21*, 7901–7904.

(18) Isakova, A.; Topham, P. D.; Sutherland, A. J. Controlled RAFT Polymerization and Zinc Binding Performance of Catechol-Inspired Homopolymers *Macromolecules* **2014**, *47*, 2561–2568.

(19) Lee, H.; Dellatore, S. M.; Miller, W. M.; Messersmith, P. B. Mussel-Inspired Surface Chemistry for Multifunctional Coatings *Science* **2007**, *318*, 426–430.

(20) Ye, Q.; Zhou, F.; Liu, W. Bioinspired catecholic chemistry for surface modification *Chem. Soc. Rev.* **2011**, *40*, 4244–4258.

(21) Jiménez, N.; Ballard, N.; Asua, J. M. Hydrogen Bond-Directed Formation of Stiff Polymer Films Using Naturally Occurring Polyphenols *Macromolecules* **2019**, *52*, 9724–9734.

(22) Guan, Y.; Shao, L.; Dong, D.; Wang, F.; Zhang, Y.; Wang, Y. Bio-inspired natural polyphenol cross-linking poly(vinyl alcohol) films with strong integrated strength and toughness *RSC Adv.* **2016**, *6*, 69966–69972.

(23) Chen, Y.-N.; Peng, L.; Liu, T.; Wang, Y.; Shi, S.; Huiliang, W. Poly(vinyl alcohol)-Tannic Acid Hydrogels with Excellent Mechanical Properties and Shape Memory Behaviors *ACS Appl. Mater. Interfaces* **2016**, *8*, 27199–27206.

(24) López, C. M.; Pich, A. Supramolecular Stimuli-Responsive Microgels Crosslinked by Tannic Acid *Macromol. Rapid Commun.* **2018**, *39*, 1700808.

(25) Euti, E. M.; Wolfel, A.; Picchio, M. L.; Romero, M. R.; Martinelli, M.; Minari, R. J.; Igarzabal, C. I. A. Controlled Thermoreversible Formation of Supramolecular Hydrogels Based on Poly(vinyl alcohol) and Natural Phenolic Compounds *Macromol. Rapid*

Commun. **2019**, *0*, 1900217.

(26) Fan, H.; Wang, J.; Jin, Z. Tough, Swelling-Resistant, Self-Healing, and Adhesive Dual-Cross-Linked Hydrogels Based on Polymer–Tannic Acid Multiple Hydrogen Bonds *Macromolecules* **2018**, *51*, 1696–1705.

(27) Vatankhah-Varnoosfaderani, M.; Ina, M.; Adelnia, H.; Li, Q.; Zhushma, A. P.; Hall, L. J.; Sheiko, S. S. Well-Defined Zwitterionic Microgels: Synthesis and Application as Acid-Resistant Microreactors *Macromolecules* **2016**, *49*, 7204–7210.

(28) Krogsgaard, M.; Nue, V.; Birkedal, H. Mussel-Inspired Materials: Self-Healing through Coordination Chemistry *Chem. - A Eur. J.* **2016**, *22*, 844–857.

(29) Gallastegui, A.; Porcarelli, L.; Palacios, R. E.; Gómez, M. L.; Mecerreyes, D. Catechol-Containing Acrylic Poly(ionic liquid) Hydrogels as Bioinspired Filters for Water Decontamination *ACS Appl. Polym. Mater.* **2019**, *1*, 1887–1895.

(30) Holten-Andersen, N.; Harrington, M. J.; Birkedal, H.; Lee, B. P.; Messersmith, P. B.; Lee, K. Y. C.; Waite, J. H. pH-induced metal-ligand cross-links inspired by mussel yield self-healing polymer networks with near-covalent elastic moduli *Proc. Natl. Acad. Sci.* **2011**, *108*, 2651–2655.

(31) Zeng, H.; Hwang, D. S.; Israelachvili, J. N.; Waite, J. H. Strong reversible Fe3+-mediated bridging between dopa-containing protein films in water *Proc. Natl. Acad. Sci.* **2010**, *107*, 12850–12853.

(32) Yang, J.; Cohen Stuart, M. A.; Kamperman, M. Jack of all trades: versatile catechol crosslinking mechanisms *Chem. Soc. Rev.* **2014**, *43*, 8271–8298.

(33) Patil, N.; Aqil, A.; Ouhib, F.; Admassie, S.; Inganäs, O.; Jérôme, C.; Detrembleur, C. Bioinspired Redox-Active Catechol-Bearing Polymers as Ultrarobust Organic Cathodes for Lithium Storage *Adv. Mater.* **2017**, *29*, 1703373.

(34) Pirnat, K.; Casado, N.; Porcarelli, L.; Ballard, N.; Mecerreyes, D. Synthesis of Redox Polymer Nanoparticles Based on Poly(vinyl catechols) and Their Electroactivity *Macromolecules* **2019**, *52*, 8155–8166.

(35) Patil, N.; Aqil, M.; Aqil, A.; Ouhib, F.; Marcilla, R.; Minoia, A.; Lazzaroni, R.; Jérôme, C.; Detrembleur, C. Integration of Redox-Active Catechol Pendants into Poly(ionic liquid) for the Design of High-Performance Lithium-Ion Battery Cathodes *Chem. Mater.* **2018**, *30*, 5831–5835.

(36) Patil, N.; Mavrandonakis, A.; Jérôme, C.; Detrembleur, C.; Palma, J.; Marcilla, R. Polymers Bearing Catechol Pendants as Universal Hosts for Aqueous Rechargeable H+, Li-Ion, and Post-Li-ion (Mono-, Di-, and Trivalent) Batteries *ACS Appl. Energy Mater.* **2019**, *2*, 3035–3041.

(37) Gallastegui, A.; Minudri, D.; Casado, N.; Goujon, N.; Ruipérez, F.; Patil, N.; Detrembleur, C.; Marcilla, R.; Mecerreyes, D. Proton trap effect on catechol–pyridine redox polymer nanoparticles as organic electrodes for lithium batteries *Sustain. Energy Fuels* **2020**, *4*, 3934–3942.

(38) Yu, M.; Deming, T. J. Synthetic Polypeptide Mimics of Marine Adhesives *Macromolecules* **1998**, *31*, 4739–4745.

(39) Liu, Y.; Ai, K.; Lu, L. Polydopamine and Its Derivative Materials: Synthesis and Promising Applications in Energy, Environmental, and Biomedical Fields *Chem. Rev.* **2014**, *114*, 5057–5115.

(40) Dreyer, D. R.; Miller, D. J.; Freeman, B. D.; Paul, D. R.; Bielawski, C. W. Perspectives on poly(dopamine) *Chem. Sci.* **2013**, *4*, 3796–3802.

(41) Ochs, C. J.; Hong, T.; Such, G. K.; Cui, J.; Postma, A.; Caruso, F. Dopamine-Mediated Continuous Assembly of Biodegradable Capsules *Chem. Mater.* **2011**, *23*, 3141–3143.

(42) Xu, L. Q.; Jiang, H.; Neoh, K.-G.; Kang, E.-T.; Fu, G. D. Poly(dopamine acrylamide)-co-poly(propargyl acrylamide)-modified titanium surfaces for 'click' functionalization *Polym. Chem.* **2012**, *3*, 920–927.

(43) Patil, N.; Falentin-Daudré, C.; Jérôme, C.; Detrembleur, C. Mussel-inspired protein-repelling ambivalent block copolymers: controlled synthesis and characterization *Polym. Chem.* **2015**, *6*, 2919–2933.

(44) Boulding, N. A.; Millican, J. M.; Hutchings, L. R. Understanding copolymerisation kinetics for the design of functional copolymers via free radical polymerisation *Polym. Chem.* **2019**, *10*, 5665–5675.

(45) Ham, H. O.; Liu, Z.; Lau, K. H. A.; Lee, H.; Messersmith, P. B. Facile DNA Immobilization on Surfaces through a Catecholamine Polymer *Angew. Chemie Int. Ed.* **2011**, *50*, 732–736.

(46) Glass, P.; Chung, H.; Washburn, N. R.; Sitti, M. Enhanced Wet Adhesion and Shear of Elastomeric Micro-Fiber Arrays with Mushroom Tip Geometry and a Photopolymerized p(DMA-co-MEA) Tip Coating *Langmuir* **2010**, *26*, 17357–17362.

(47) Chung, H.; Glass, P.; Pothen, J. M.; Sitti, M.; Washburn, N. R. Enhanced Adhesion of Dopamine Methacrylamide Elastomers via Viscoelasticity Tuning *Biomacromolecules* **2011**, *12*, 342–347.

(48) Lee, B. P.; Huang, K.; Nunalee, F. N.; Shull, K. R.; Messersmith, P. B. Synthesis of 3,4-dihydroxyphenylalanine (DOPA) containing monomers and their co-polymerization with PEG-diacrylate to form hydrogels *J. Biomater. Sci. Polym. Ed.* **2004**, *15*, 449–464.

(49) Vatankhah-Varnoosfaderani, M.; GhavamiNejad, A.; Hashmi, S.; Stadler, F. J. Hydrogen Bonding in Aprotic Solvents, a New Strategy for Gelation of Bioinspired Catecholic Copolymers with N-Isopropylamide *Macromol. Rapid Commun.* **2015**, *36*, 447–452.

(50) Georgieff, K. K. Relative inhibitory effect of various compounds on the rate of polymerization of methyl methacrylate *J. Appl. Polym. Sci.* **1965**, *9*, 2009–2018.

(51) Tüdos, F.; Földes-Berezsnich, T. Free-radical polymerization: Inhibition and retardation *Prog. Polym. Sci.* **1989**, *14*, 717–761.

(52) Levy, L. B. Inhibition of acrylic acid polymerization by phenothiazine and p-methoxyphenol *J. Polym. Sci. Polym. Chem. Ed.* **1985**, *23*, 1505–1515.

(53) Caldwell, R. G.; Ihrig, J. L. The Reactivity of Phenols toward Peroxy Radicals. I. Inhibition of the Oxidation and Polymerization of Methyl Methacrylate by Phenols in the Presence of Air *J. Am. Chem. Soc.* **1962**, *84*, 2878–2886.

(54) Kurland, J. J. Quantitative aspects of synergistic inhibition of oxygen and p-methoxyphenol in acrylic acid polymerization *J. Polym. Sci. Polym. Chem. Ed.* **1980**, *18*, 1139–1145.

(55) Bird, R. A.; Harpell, G. A.; Russell, K. E. Deuterium isotope effects in abstraction of hydrogen atoms from phenols *Can. J. Chem.* **1962**, *40*, 701–704.

(56) Barton, S. C.; Bird, R. A.; Russell, K. E. The effect of phenols and aromatic thiols on the polymerization of methyl methacrylate *Can. J. Chem.* **1963**, *41*, 2737–2742.

(57) Bird, R. A.; Russell, K. E. The effect of phenols on the polymerization of vinyl acetate *Can. J. Chem.* **1965**, *43*, 2124–2125.

(58) Lilles, H.; Parnell, R. D.; Russell, K. E. A Kinetic and Electron Spin Resonance Study of the Polymerization of Vinyl Acetate Retarded by 2,4,6-Tri-t-butylphenol *Can. J. Chem.* **1972**, *50*, 3304–3309.

(59) Godsay, M. P.; Harpell, G. A.; Russell, K. E. The effect of phenols on the polymerization of styrene *J. Polym. Sci.* **1962**, *57*, 641–650.

(60) Samal, R. K.; Sahoo, P. K.; Bhattacharjee, S. P.; Samantaray, H. S. Kinetics of Inhibition and Retardation of Methyl Methacrylate Polymerization by Phenols *J. Macromol. Sci. Part A - Chem.* **1986**, *23*, 203–220.

(61) Xue, J.; Zhang, Z.; Nie, J.; Du, B. Formation of Microgels by Utilizing the Reactivity of Catechols with Radicals *Macromolecules* **2017**, *50*, 5285–5292.

(62) Xu, H.; Nishida, J.; Ma, W.; Wu, H.; Kobayashi, M.; Otsuka, H.; Takahara, A. Competition

between oxidation and coordination in cross-linking of polystyrene copolymer containing catechol groups *ACS Macro Lett.* **2012**, *1*, 457–460.

(63) Takeshima, H.; Satoh, K.; Kamigaito, M. Scalable Synthesis of Bio-Based Functional Styrene: Protected Vinyl Catechol from Caffeic Acid and Controlled Radical and Anionic Polymerizations Thereof *Sustain. Chem. Eng.* **2018**, *6*, 13681–13686.

(64) Provder, T.; Urban, M. W.; Barth, H. G. *Chromatographic Characterization of Polymers: Hyphenated and Multidimensional Techniques*; American Chemical Society: Washington, DC, 1995.

(65) Buback, M.; Feldermann, A.; Barner-kowollik, C.; Lacík, I. Propagation Rate Coefficients of Acrylate-Methacrylate Free-Radical Bulk Copolymerizations *Macromolecules* **2001**, *34*, 5439–5448.

(66) Zhao, Y.; Truhla, D. G. The M06 suite of density functionals for main group thermochemistry, thermochemical kinetics, noncovalent interactions, excited states, and transition elements: two new functionals and systematic testing of four M06-class functionals and 12 other function *Theor. Chem. Acc.* **2008**, *120*, 215–241.

(67) Hehre, W. J.; Ditchfield, R.; Pople, J. A. Self — Consistent Molecular Orbital Methods. XII. Further Extensions of Gaussian — Type Basis Sets for Use in Molecular Orbital Studies of Organic Molecules *J. Chem. PhysicsJournal Chem* **1972**, *56*, 2257–2261.

(68) Dunning, T. H. Gaussian basis sets for use in correlated molecular calculations. I. The atoms boron through neon and hydrogen Gaussian basis sets for use in correlated molecular calculations. *J. Chem. Phys.* **1989**, *90*, 1007–1023.

(69) Frisch, M. J.; Trucks, G. W.; Schlegel, H. B.; ScuserIa, G. E.; Robb, M. A.; Cheeseman, J. R.; Scalmani, G.; Barone, V.; Petersson, G. A.; Nakatsuji, H.; Li, X.; Caricato, M.; Marenich, A. V.; Bloino, J.; Janesko, B. G.; Gomperts, R.; Mennucci, B.; Hratchian, H. P.; Ortiz, J. V.; Izmaylov, A. F.; Sonnenberg, J. L.; Williams-Young, D.; Ding, F.; Lipparini, F.; Egidi, F.; Goings, J.; Peng, B.; Petrone, A.; Henderson, T.; Ranasinghe, D.; Zakrzewski, V. G.; Gao, J.; Rega, N.; Zheng, G.; Liang, W.; Hada, M.; Ehara, M.; Toyota, K.; Fukuda, R.; Hasegawa, J.; Ishida, M.; Nakajima, T.; Honda, Y.; Kitao, O.; Nakai, H.; Vreven, T.; Throssell, K.; Montgomery, J. A.; Peralta, J. E.; Ogliaro, F.; Bearpark, M. J.; Heyd, J. J.; Brothers, E. N.; Kudin, K. N.; Staroverov, V. N.; Keith, T. A.; Kobayashi, R.; Normand, J.; Raghavachari, K.; Rendell, A. P.; Burant, J. C.; Iyengar, S. S.; Tomasi, J.; Cossi, M.; Millam, J. M.; Klene, M.; Adamo, A.; Cammi, R.; Ochterski, J. W.; Martin, R. L.; Morokuma, K.; Farkas, O.; Foresman, J. B.; Fox, D. J. Gaussian 16, Revision A.03, 2016.

(70) Haddleton, D. M.; Clark, A. J.; Crossman, M. C.; Duncalf, D. J.; Heming, A. M.; Morsley, S. R.; Shooter, A. J. Atom transfer radical polymerisation (ATRP) of methyl methacrylate in the presence of radical inhibitors *Chem. Commun.* **1997**, 1173–1174.

(71) Craig, A. G.; Derrick, P. J. Production and Characterization of Beams of Polystyrene Ions* *Aust. J. Chem.* **1986**, *39*, 1421–1434.

(72) Zammit, M. D.; Davis, T. P.; Haddleton, D. M.; Suddaby, K. G. Evaluation of the Mode of Termination for a Thermally Initiated Free-Radical Polymerization via Matrix-Assisted Laser Desorption Ionization Time-of-Flight Mass Spectrometry *Macromolecules* **1997**, *9297*, 1915–1920.

(73) Moad, G.; Solomon, D. H.; Johns, S. R.; Willing, R. I. Fate of the Initiator in the Azobis (isobutyronitrile) -Initiated Polymerization of Styrene *Macromolecules* **1984**, *17*, 1094–1099.

(74) Koo, S. P. S.; Junkers, T.; Barner-Kowollik, C. Quantitative Product Spectrum Analysis of Poly(butyl acrylate) via Electrospray Ionization Mass Spectrometry *Macromolecules* **2009**, *42*, 62–69.

(75) Ballard, N.; Veloso, A.; Asua, J. M. Mid-Chain Radical Migration in the Radical Polymerization of n-Butyl Acrylate. *Polymers*, 2018, *10*, 765.

(76) Mayo, F. R. Chain Transfer in the Polymerization of Styrene: The Reaction of Solvents with Free Radicals *J. Am. Chem. Soc.* **1943**, *65*, 2324–2329.

(77) Hammond, G. S. A Correlation of Reaction Rates *J. Am. Chem. Soc.* **1955**, *77*, 334–338.

(78) Reichardt, C. *Solvents and Solvent Effects in Organic Chemistry*; Weinheim, 2003.

(79) Takeshima, H.; Satoh, K.; Kamigaito, M. R–Cl/SnCl4/n-Bu4NCl-induced direct living cationic polymerization of naturally-derived unprotected 4-vinylphenol, 4-vinylguaiacol, and 4-vinylcatechol in CH3CN *Polym. Chem.* **2019**, *10*, 1192–1201.

(80) Glass, P.; Chung, H.; Washburn, N. R.; Sitti, M. Enhanced reversible adhesion of dopamine methacrylamide-coated elastomer microfibrillar structures under wet conditions *Langmuir* **2009**, *25*, 6607–6612.

(81) Beuermann, S.; Buback, M. Rate coefficients of free-radical polymerization deduced from pulsed laser experiments *Prog. Polym. Sci.* **2002**, *27*, 191–254.

Chapter 7. Catechol-containing copolymers as water-soluble H-bond donors

7.1. Introduction

The acidic nature of phenolic hydrogens has led to the fairly widespread use of phenol (or catechol) containing molecules to physically crosslink polymer networks.[1–8] For example, in Chapter 4 it was shown that the addition of the natural occurring polyphenol tannic acid (TA) to acrylic polymer dispersions with H-bond acceptors such as pyrrolidone groups is an efficient approach to prepare microstructured materials with enhanced mechanical strength. While the use of naturally occurring polyphenols is desirable in many respects, it leaves little scope for controlling the properties and therefore in this chapter we seek to exploit the knowledge gained in Chapter 6 in the production of synthetic catechol-containing water-soluble copolymers for reinforcing the mechanical properties of latex dispersions. The use of catechol-containing copolymers as synthetic substitutes of TA offers the opportunity to tune and adjust the properties of the water-soluble H-bond donor by designing the copolymer architecture. For example, varying the nature and ratio of the monomers employed for the synthesis it is possible to easily modulate the T_g[9,10] and hydrophilicity[11,12] of the copolymers and the molecular weight of the polymer chains can be adjusted adding chain transfer agents to the polymerization.[13–16] In addition, the use of (meth)acrylate-type copolymers as water-soluble donors could contribute decreasing the water-sensitivity and final color of the polymer films due to the relatively low content of hydrophilic and photo-active phenol groups in the structure of the copolymer compared to TA. Thus, the objective in this chapter was to synthesize catechol-containing water-soluble H-bond donors and use them

in combination with pyrrolidone-containing acrylic dispersions for the production of stiff polymer films.

The work in Chapter 6 has shown that the polymerizations of (meth)acrylate and (meth)acrylamide type monomers are minimally affected by the presence of catechols. Accordingly, dopamine methacrylamide (DMA, chemical structure shown in Figure 7.1) was selected in this chapter as catechol-containing monomer and methacrylate and acrylamide type monomers were used as comonomers for the synthesis of the copolymers. Dimethyl formamide (DMF) was used as solvent for the polymerizations since the results showed in Chapter 6 indicated that the chain transfer reactions to catechol are minimized when polar H-bond acceptor solvents such as DMF are used.

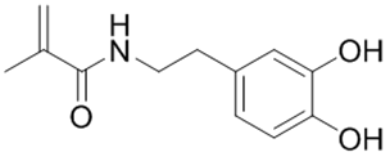

Dopamine methacrylamide
(DMA)

Figure 7.1. Chemical structure of dopamine methacrylamide (DMA).

DMA and the PDMA homopolymer are insoluble in water. Thus, to enhance the solubility in water of the catechol-containing copolymers, three different hydrophilic monomers were copolymerized: methacrylic acid (MAA), short chain poly(ethylene glycol) methacrylate (PEGMA) and 2-acrylamido-2-methyl-1-propanesulfonic acid (AMPS). The chemical structures of the water-soluble monomers are shown in Figure 7.2.

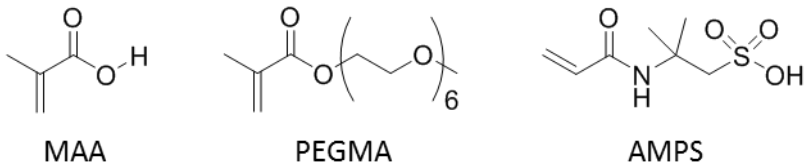

Figure 7.2. Chemical structures of methacrylic acid (MAA), poly(ethylene glycol) methacrylate (PEGMA) and 2-acrylamido-2-methyl-1-propanesulfonic acid (AMPS).

Acrylic acid (AA) and methacrylic acid (MAA) are hydrophilic pH sensitive monomers with a pk_a around 4.5[17] commonly used in small fractions (≈ 1 wt% of the monomers) in emulsion polymerization to enhance the colloidal stability[18–22] and adhesion of the polymer dispersions.[23,24] The addition of these hydrophilic monomers to emulsion polymerization can lead to the formation of microstructured particles with (M)AA-rich hard shells ($T_{g,PMAA}$ = 227 °C[25] and $T_{g,PAA}$ = 105 °C[26]) that enhance the mechanical strength of the films prepared from these dispersions.[27–29] MAA and AA are also commonly used in combination of hydrophobic monomers for the synthesis of Alkali Soluble Resins (ASRs), low molar mass and pH sensitive copolymers used as electrosteric stabilizers in (mini)emulsion polymerization.[30–35]

Polyethylene glycol (PEG) also called polyethylene oxide (PEO) is a water-soluble polymer used in a wide variety of applications including drug carrier in pharmacological applications,[36,37] solid state polymer electrolyte in batteries[38–40] or non-ionic surfactant in cosmetics and detergents.[41,42] In the field of waterborne adhesives and coatings, PEG is recurrently used to enhance the hydrophilicity of the crosslinkers, which allows their subsequent addition to the aqueous polymer dispersions as water solutions/dispersions.[43–48] The physico-chemical properties of PEG highly depend on the molecular weight: PEGs with molecular weights below 700 g/mol (≤ 16 monomer units) are liquids at room temperature, PEGs in the range of

700 – 2000 g/mol (16 – 45 units) are soft solids and PEGs with MWs above 2000 g/mol are hard crystalline solids with a T_g around - 22 °C and a T_M of 63 °C.[37]

2-Acrylamido-2-methyl-1-propanesulfonic acid (AMPS) is a water-soluble ionic monomer. Similar to (meth)acrylic acids, AMPS and other sulfonate monomers are used in emulsion polymerization to provide electrostatic stabilization to the polymer colloids.[49–55] Compared to carboxylic acids, sulfonates have much lower pK_a values (pK_a of para-toluene sulfonic acid is around – 2.7)[56] and display a higher stability over a wide range of temperature and pH.[49,50]

In this work, three types of copolymers with catechol groups were synthesized using the three water-soluble monomers. Then, aqueous solutions of the copolymers were combined with acrylic polymer dispersions functionalized with 5 wt% NVP and the appearance, mechanical properties, morphology and water-sensitivity of the films cast from these blends was analyzed. The schematic representation of the system is given in Figure 7.3 and the pyrrolidone – catechol H-bond is shown in Figure 7.4.

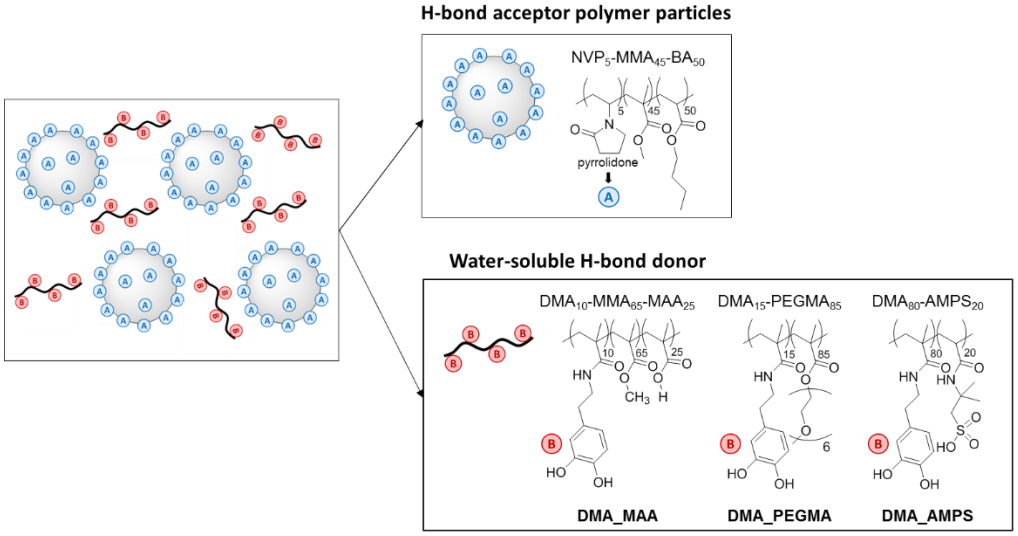

Figure 7.3. Schematic representation of the system composed of polymer particles with 5 wt% NVP and water-soluble catechol-containing copolymers. In the scheme, the subscripts after the monomer units express the weight % of the monomers used for the synthesis.

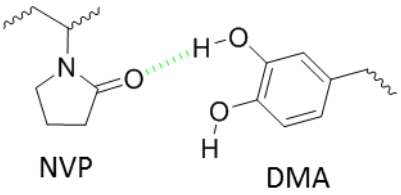

Figure 7.4. H-bond between a pyrrolidone and a hydroxyl of catechol.

7.2. Experimental part

7.2.1. Materials

Methyl methacrylate (MMA, technical grade, Quimidroga), butyl acrylate (BA, technical grade, Quimidroga), N-vinyl pyrrolidone (NVP, >99 %, Sigma Aldrich), methacrylic acid (MAA, 95.5 %, Acros Organics), poly(ethylene glycol) methacrylate (PEGMA, M_n = 360 Da, Sigma Aldrich), 2-acrylamido-2-methyl-1-propanesulfonic acid (AMPS, BASF), ammonium persulfate (APS, ≥98 %, Sigma Aldrich), 2,2′-Azobis(2-methylpropionitrile) (AIBN, >98 %, Sigma Aldrich), sodium bicarbonate ($NaHCO_3$, Sigma Aldrich), n-dodecanethiol (DSH, ≥97 %, Sigmal Aldrich), n-butanethiol (BSH, 97 %, Fluka), 2-ethylhexyl thioglycolate (EHTG, BASF), dimethyl formamide (DMF, ≥99.8 %, Sigma Aldrich) and diethyl ether (synthesis grade, Scharlau) were used as received. Dowfax 2A1 was kindly supplied by Dow Chemical Company. Deionized water was used as polymerization media in the emulsion polymerizations. The DMA used in Runs 1-4 was synthesized based on the procedure described by Xu *et al*[57] (see Appendix II.1 for the experimental details of the monomer synthesis) and the DMA used in Run 5 was purchased from Arkema.

7.2.2. Synthesis of polymer dispersions

Polymer dispersions with 0 and 5 wt% NVP were prepared by seeded semibatch emulsion polymerization following the polymerization process described by Haddock *et al*.[58] The formulations used for the synthesis are presented in Table 7.1. 0 wt% NVP was used in Latexes 1 and 13, and 5 wt% NVP was copolymerized in Latexes 2 and 14. Latexes 1 and 2 were synthesized in UPV/EHU and Latexes 13 and 14 were synthesized in BASF. The reactions were carried out in glass reactors stirred with an anchor type mechanical stirrer at 200 rpm, 70 °C and N_2 atmosphere. The synthesis of these latexes was already described in Chapter 2 for Latexes

1-2 and Chapter 4 for Latexes 13-14 and the reader is referred to those chapters for more experimental details.

Table 7.1. Formulations employed for the synthesis of the polymer dispersions with 0 and 5 wt% NVP in runs Latex 1, 2, 13 and 14. *The latexes synthesized in BASF are marked with an asterisk (*).

		F.M. (g)	MMA (g)	BA (g)	DSH (g)	H_2O (g)	Dowfax (g)	APS (g)	$NaHCO_3$ (g)
Latex 1 0% F.M.	Seed	-	10	10	-	160	4.28	0.267	1
	F1	-	-	-	-	37.3	2.38	1.333	-
	F2	-	90	90	0.18	-	-	-	-
Latex 2 5% NVP	Seed	NVP 1	9	10	-	160	4.28	0.267	1
	F1	-	-	-	-	37.3	2.38	1.333	-
	F2	NVP 9	81	90	0.18	-	-	-	-
Latex 13* 0% F.M.	Seed	-	20	20	-	320	8.6	0.56	2
	F1	-	-	-	-	74	4.8	2.7	-
	F2	-	180	180	0.36	-	-	-	-
Latex 14* 5% NVP	Seed	NVP 2	18	20	-	320	8.6	0.56	2
	F1	-	-	-	-	74	4.8	2.7	-
	F2	NVP 18	162	180	0.36	-	-	-	-

7.2.3. Synthesis of catechol-containing water-soluble copolymers

The copolymers were produced by batch free radical polymerization in DMF. The catechol groups were incorporated to the polymer chains through the copolymerization of dopamine methacrylamide (DMA). In addition, three different hydrophilic monomers were used to provide water-solubility to the polymer chains: MAA, PEGMA and AMPS. The copolymers were named according to the hydrophilic monomer used to make the polymer chains soluble in water: DMA_MAA, DMA_PEGMA and DMA_AMPS. In addition, two analogous copolymers without catechol units were produced as reference, which were named as blank_MAA and

blank_PEGMA. The formulations used for the synthesis of the copolymers are shown in Table 7.2.

Table 7.2. Formulations employed for the synthesis of the catechol-containing water-soluble copolymers.

Run	Copolymer	DMA (wt%)	DMA (g)	MMA (g)	MAA (g)	PEGMA (g)	AMPS (g)	BSH (g)	EHTG (g)	DMF (g)	AIBN (g)
1	Blank_MAA	0	0	6	2	-	-	0.1	-	32	0.128
2	DMA_MAA	10	0.8	5.2	2	-	-	0.1	-	32	0.128
3	Blank_PEGMA	0	0	-	-	8	-	0.1	-	32	0.128
4	DMA_PEGMA	15	1.2	-	-	6.8	-	0.1	-	32	0.128
5	DMA_AMPS	80	8	2	-	-	-	-	0.125	40	0.125

The copolymers produced in Runs 1-4 with MAA and PEGMA were synthesized in UPV/EHU using 1.6 % weight based on monomers (wbm) of AIBN as thermal initiator and 1.25 % wbm BSH as CTA to control the chain length of the polymers. 10 and 15 wt % DMA was used in Runs 2 and 4, respectively. The PEGMA selected for the synthesis had a molar mass of 360 g/mol (6 ethylene oxide units) and therefore, it was liquid and non-crystalline. The DMA_AMPS copolymer (Run 5) was synthesized in BASF during the internship. In this reaction, the DMA content was increased to 80 wt% and 20 wt% AMPS was used to make the polymer chains water-soluble. In this synthesis, 1.25 % wbm 2-ethylhexyl thioglycolate was used as CTA and 3 % wbm AIBN as thermal initiator. No reference AMPS-copolymer without catechol units was produced in this case.

The polymerizations were carried out in round bottom flasks using an oil bath and a thermocouple to control the temperature. First, the reaction medium was purged with nitrogen for 30-60 minutes and then the flask was immersed in the oil bath at 65 °C for 24 hours. In Runs

1-4 the initiator was placed inside the reaction medium from the beginning of the process and in Run 5, the initiator was fed dissolved in DMF during the first hour of polymerization.

7.2.4. Isolation of the copolymers

The MAA copolymers prepared in Runs 1 and 2 were precipitated from deionized water. The PEGMA (co)polymers synthesized in Runs 3 and 4 were precipitated from diethyl ether. The AMPS copolymer from Run 5 was precipitated three times from diethyl ether. The resulting polymers were dried at 40 °C under vacuum.

7.2.5. Blending and film casting

First, the copolymers were dissolved in water at a concentration of around 10 wt%. In the case of the DMA_MAA and blank_MAA copolymers, the pH was increased to 7-9 using NH_4OH and the system was heated to 60 °C to deprotonate the carboxylic acids and dissolve the polymer chains. Then, aqueous solutions of the MAA and PEGMA copolymers prepared in Runs 1-4 were blended with the Latex 1 (blank) and Latex 2 (5 wt% NVP) and the DMA_AMPS copolymer synthesized in Run 5 was combined with Latex 13 (blank) and 14 (5 wt% NVP) to prepare materials with copolymer fractions between 0 and 10 wt % (based on the weight of the polymer). The blends were stirred for 30 minutes, cast in silicone molds and dried for 7 days at 23 ± 2 °C and 55 ± 5 % relative humidity. The final thickness of the films varied from 600 to 800 µm.

7.2.6. Characterization

During the synthesis of the polymer dispersions, the monomer conversion was determined by gravimetry. In Latexes 1 and 2, the particle size was measured by Dynamic Light Scattering (DLS) and the gel content was determined using Soxhlet extractions in THF. In

Latexes 13 – 14 produced in BASF, the particle size was measured using hydrodynamic capillary chromatography (HDC) and the gel content was defined as the insoluble polymer fraction in methyl ethyl ketone (MEK). The molecular weight distribution of the polymers was determined with Size Exclusion Chromatography in THF in all cases. The detailed description of the latex characterization methods and experimental conditions is given in Section I.1 of Appendix I.

In the solution polymerizations, the individual monomer conversions were determined by ^{1}H-NMR on a Bruker 400 MHz equipment. The ^{1}H-NMR spectra were recorded at room temperature using d_6-DMSO was used as solvent. For the analysis, 100 µL of the samples withdrawn from the reaction medium at different times were diluted in 600 µL of the deuterated solvent. The monomer conversion was determined from the disappearance of the vinyl protons using the signal of DMF at 8.03 ppm as internal standard to normalize the signals of the vinyl protons. The molecular weights of the MAA copolymers were measured by Size Exclusion Chromatography (SEC) using a PL-GPC 50 integrated GPC system in DMF at 50 ºC with a flow rate of 1mL/min, a guard column Shodex KD-G 41 and a column GPC KD-806M. The molecular weights of the PEGMA (co)polymers were analyzed by Size Exclusion Chromatography Multi-Angle Light Scattering (SEC/MALS/RI) at 35 °C using a 0.1 M $NaNO_3$ aqueous solution as carrier at a flow rate of 0.6 mL/min. The pH of the eluent was adjusted to 10 adding NH_4OH. The equipment was composed by a LC20 pump (Shimadzu) coupled to a miniDAWN Treos multiangle (3 angles) light scattering laser photometer equipped with an He-Ne laser (l¼658 nm) and an Optilab T-Rex differential refractometer (658 nm) (all from Wyatt Technology Corp., USA). Separation was carried out using two columns in series (Ultra-hydrogel 250 and 120 with pore sizes of 250 and 120 Å, respectively)

The mechanical properties of the films were measured by tensile test. The internal morphology of the films was investigated by transmission electron microscopy (TEM). The films

were stained with RuO_4 to increase the contrast of the aromatic-rich areas. The water sensitivity of the polymer films was assessed by immersing the polymer films in water measuring water uptake and weight loss of the materials. The latex – MAA copolymer blends were immersed in water for 7 days and the latex – DMA_AMPS blends were immersed in water for 5 days. Detailed information these characterization methods is given in Section 1.2 of Appendix I.

7.3. Results and discussion

7.3.1. Synthesis of polymer dispersions

Stable polymer dispersions with 0 and 5 wt% NVP and solids content near 50 wt% were obtained in Latexes 1, 2, 13 and 14. The final conversion, particle size, gel content and molecular weight of the polymers are presented in Table 7.3. For the detailed analysis of the polymerization kinetics, the reader is referred to Chapter 2 for Latexes 1 and 2 and to Chapter 4 for Latexes 13 and 14.

Table 7.3. Main characteristics of the polymer dispersions produced in Latex 1, 2, 13 and 14. Latexes 13 and 14 marked with (*) were synthesized in BASF. Data determined by [a]gravimetry, [b]DLS, [c]HDC, [d]Soxhlet extractions in THF, [e]insoluble polymer fraction in MEK and [f]SEC in THF.

Run	Description	Final X_M[a] (%)	$dp_{z,seed}$[b,c] (nm)	$dp_{z,final}$[b,c] (nm)	Gel content[d,e] (%)	M_w[f] (kg/mol)
L1	Blank - 0% F.M.	96.9	54 ± 3[b]	111 ± 2[b]	< 1[d]	480
L2	5% NVP	96.5	58 ± 1[b]	135 ± 1[b]	< 1[d]	680
L13*	Blank - 0% F.M.	97.4	48 ± 13[c]	111 ± 17[c]	< 1[e]	606
L14*	5% NVP	96.7	42 ± 17[c]	121 ± 20[c]	< 1[e]	635

Monomer conversions higher than 96 % were achieved at the end of the polymerizations in the four reactions. Moreover, the incorporation of NVP into the polymer backbone using this polymerization procedure was verified by GC in Chapter 4. The polymer dispersions had final particle sizes between 111 and 135 nm. The polymers produced in the reactions presented gel contents near 0 % and weight average molar masses in the range of 480 and 680 kg/mol.

7.3.2. Synthesis of catechol-containing water-soluble copolymers

The catechol-containing copolymers were produced by batch solution polymerization. DMA was used as functional catechol monomer and three different hydrophilic monomers were copolymerized to make the polymer chains water-soluble: MAA, PEGMA and AMPS. In total 5 copolymers were prepared: In Runs 1 and 2, MAA was used as hydrophilic monomer and 0 and 10 wt% DMA was incorporated; in Runs 3 and 4, PEGMA was used as hydrophilic monomer and the DMA content was 0 and 15 wt%; and in Run 5, 80 wt% DMA was copolymerized with 20 wt% AMPS. The individual monomer conversions at the end of the reactions and the molecular weights of the copolymers are given in Table 7.4. In addition, the theoretical T_g of the copolymers were estimated using the Fox equation (Equation 7.1).[59] In Equation 7.1, w_1, w_2, $T_{g,1}$ and $T_{g,2}$ are the mass fraction and the glass transition temperatures of components 1 and 2. The T_g-s of the homopolymers used for the estimation of the T_g-s of the copolymers were: 105 °C for PMMA,[60] 227 °C for PMAA,[25] -22 °C for PolyPEGMA,[37] 124 °C for PAMPS[61] and 88 °C for PDMA.[62]

Table 7.4. Individual monomer conversions, molecular weights and estimated T_g-s for the catechol-containing copolymers.

Run	Copolymer	DMA (wt%)	DMA X_M (%)	Methacrylates X_M (%)	AMPS X_M (%)	M_n (g/mol)	*Đ*	$T_{g,Fox}$ (°C)
1	Blank_MAA	0	-	99	-	6 900	1.5	130
2	DMA_MAA	10	74	97	-	6 800	1.5	128
3	Blank_PEGMA	0	-	> 99	-	65 400	6.5	-22
4	DMA_PEGMA	15	79	> 99	-	-	-	-10
5	DMA_AMPS	80	94	-	96	-	-	95

$$\frac{1}{T_g} = \frac{W_1}{T_{g,1}} + \frac{W_2}{T_{g,2}} \qquad \text{(Equation 7.1)}$$

It is shown in Table 7.4 that in Runs 1 – 4 the conversion of the methacrylate monomers (MAA, MAA and PEGMA) was higher than 97 % and the conversion of DMA in Runs 2 and 4 was 74 and 79, respectively. The relatively low DMA conversions were attributed to the reactivity ratios of methacrylates with methacrylamides, which do not favor the incorporation of the methacrylamide type monomers into the polymer backbone (*e.g.* for copolymerization systems of methacrylamide "MA" and 2-hydroxyethylmethacrylate "HEMA" r_{MA} = 0.3 and r_{HEMA} = 1.53).[63] It must be taken into account, that due to the low DMA conversion, the real DMA wt% in Runs 2 and 4 was ≈ 7.5 wt% and ≈ 12 wt%, respectively. In Run 5, the monomer conversion of DMA was 96 % and the conversion of AMPS 94 %. It is remarkable that the polymerization proceeded to high conversions even at a DMA content as high as 80 wt%. As shown in Chapter 6, the use of polar H-bond acceptor solvents such as DMF and the selection of (meth)acrylate and (meth)acrylamide monomers reduces the chain transfer events to catechol and allows the successful polymerization of most systems.

Regarding the molecular weights, the MAA-copolymers synthesized in Runs 1 and 2 had very similar number average molar weights between 6800 and 6900 g/mol, indicating no influence of catechol on the molar masses. In these polymerizations, the addition of 1.25 % wbm BSH as CTA effectively reduced the molar mass of the copolymers. On the contrary, the addition of the same amount of CTA in Run 3 did not reduce efficiently the chain length of the PEGMA homopolymer, which showed a number average molar mass of 65 000 g/mol. From the monomer conversion and molar mass results (and assuming the MW of DMA_PEGMA was similar to the MW of the blank_PEGMA), it was estimated that there was an average of 2 catechol groups per DMA_MAA chain in Run 2 and an average of 22 catechol groups per DMA_PEGMA chain in Run 4.

The glass transition temperature (T_g) of the copolymers was also estimated using the Fox equation to facilitate the comprehension of the behavior of each copolymer in the latex – copolymer blends. The T_g and appearance of the copolymers varied depending on the monomers used for the synthesis. The MAA copolymers (Runs 1 – 2) had the highest T_g-s near 130 °C and they were glassy white solids. On the contrary, the PEGMA (co)polymers produced in Runs 3 – 4 were viscous and sticky liquids with a T_g around – 22 °C. The DMA_AMPS copolymer (Run 5) was also a glassy solid and had an intermediate T_g of around 95 °C.

7.3.3. Film appearance

After the synthesis, the blank (L1, L13) and 5 wt% NVP (L2, L14) latexes were combined with the catechol-containing water-soluble copolymers (Runs 1 – 5) to prepare materials with different copolymer contents. The appearance of the films prepared from the MAA, PEGMA and AMPS copolymers are shown in Figures 7.5, 7.6 and 7.7, respectively. It can be observed in Figures 7.5 - 7.7 that all the films prepared from the DMA copolymers showed a dark color. Since

the materials without catechol groups did not show a dark appearance, the dark color was ascribed to the catechol groups. Note that the Blank (L1) – blank_PEGMA blends were darker due to the aging of the blank dispersion stabilized with hydroquinone, which can be clearly seen looking at the film prepared from the neat latex.

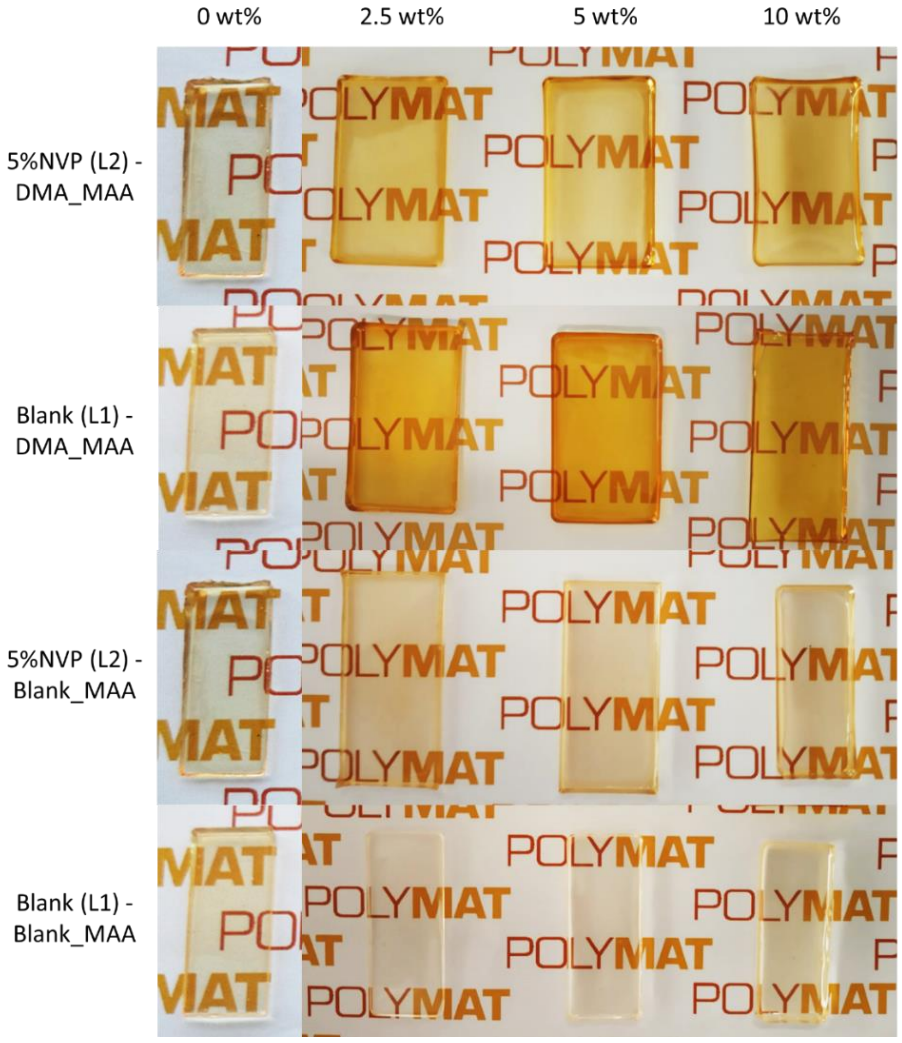

Figure 7.5. Physical appearance of the blends prepared from the blank (L1) and 5 wt% NVP (L2) latexes and DMA_MAA and blank_MAA copolymers.

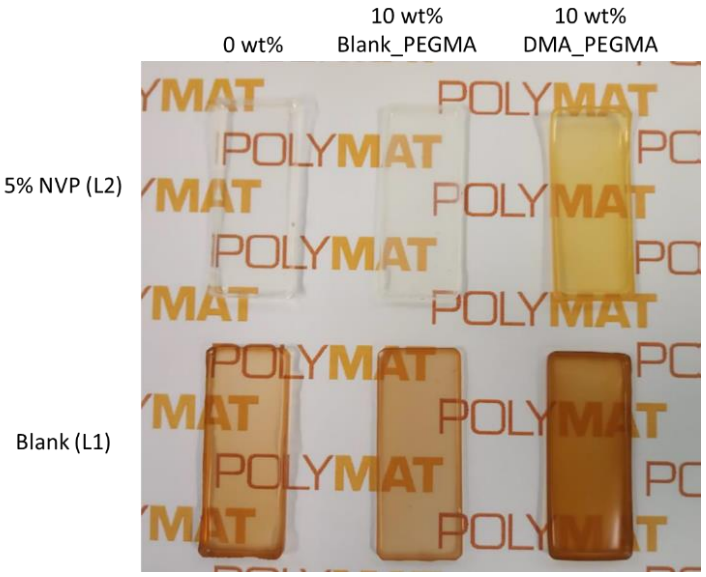

Figure 7.6. Physical appearance of the polymer films prepared from blank (L1) and 5 wt% NVP (L2) latexes with 10 wt% DMA_PEGMA and blank_PEGMA copolymers.

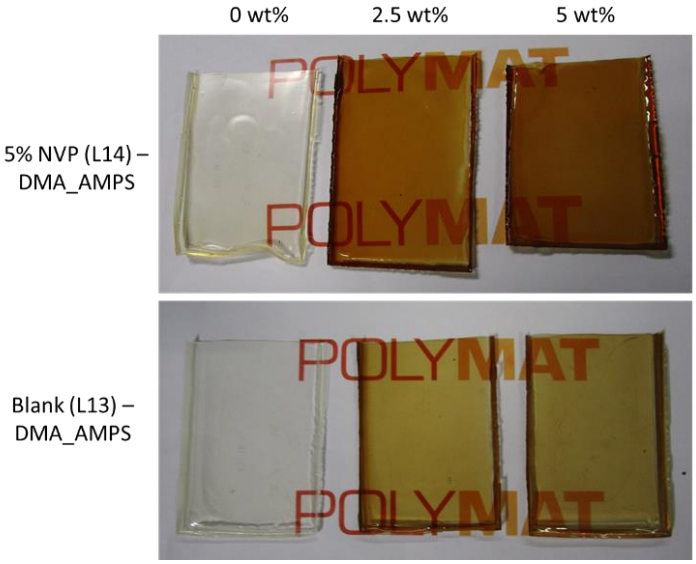

Figure 7.7. Physical appearance of the polymer films prepared from blank (L13) and 5 wt% NVP (L14) latexes with 0, 2.5 and 5 wt% DMA_AMPS.

7.3.4. Tensile properties and morphology of the films

The tensile properties of the films were measured to investigate the contribution of the pyrrolidone – catechol H-bonds to the mechanical strength of the materials. The stress-strain curves of the materials obtained blending blank (L1) and 5 wt% NVP latexes (L2) with different amounts of the MAA copolymers synthesized in Runs 1 and 2 are shown in Figure 7.8. The tensile parameters obtained from the stress-strain curves are presented in Table 7.4.

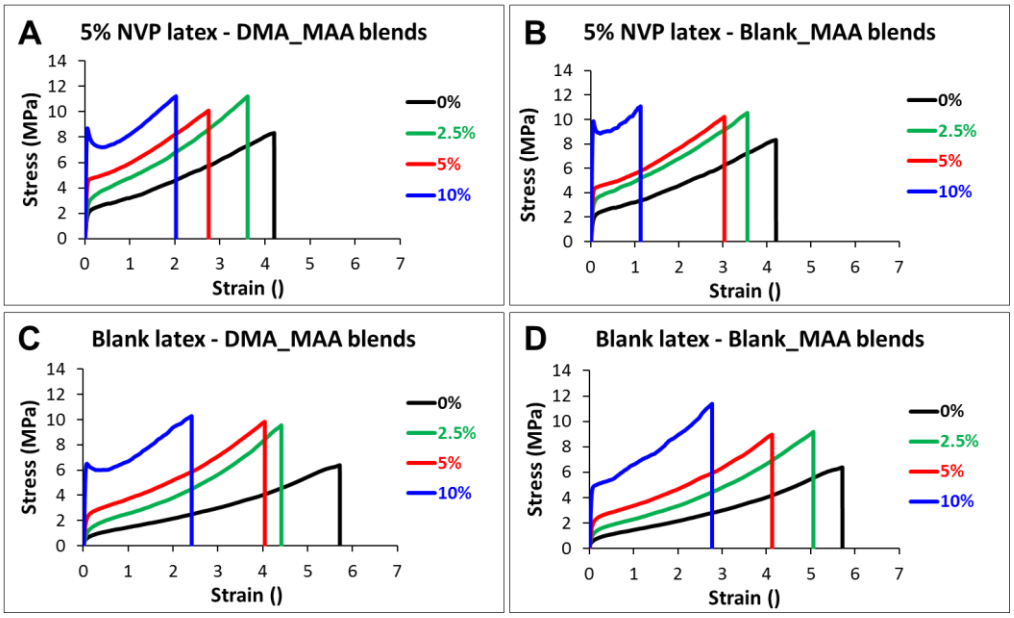

Figure 7.8. Stress-strain curves of the materials prepared from the blank / 5%NVP latex – MAA copolymers blends. The mechanical parameters related to these curves are summarized in Table 7.4.

Table 7.4. Mechanical properties related to the stress-strain curves shown in Figure 7.8.

Material	Copolymer wt%	Young's modulus E (MPa)	Yield stress σ_y (MPa)	Tensile strength σ_{max} (MPa)	Ultimate strain γ_{max} ()
5 % NVP (L1) - DMA_MAA	0	57 ± 4	2.1 ± 0.1	8.3 ± 0.03	4.18 ± 0.02
	2.5	75 ± 9	3.0 ± 0.3	11.2 ± 0.92	3.61 ± 0.02
	5	125 ± 13	4.6 ± 0.4	10.1 ± 0.32	2.74 ± 0.21
	10	271 ± 4	8.7 ± 0.2	11.2 ± 0.23	2.02 ± 0.11
5 % NVP (L1) - Blank_MAA	0	57 ± 4	2.1 ± 0.1	8.3 ± 0.1	4.2 ± 0.1
	2.5	88 ± 4	3.4 ± 0.3	10.5 ± 0.7	3.6 ± 0.1
	5	120 ± 6	4.4 ± 0.1	10.2 ± 0.1	3.0 ± 0.1
	10	323 ± 30	9.8 ± 0.3	11.1 ± 1.2	1.1 ± 0.8
Blank (L2) - DMA_MAA	0	21 ± 2	0.8 ± 0.1	6.5 ± 1.2	5.4 ± 0.7
	2.5	27 ± 9	1.3 ± 0.2	9.6 ± 1.3	4.4 ± 0.2
	5	58 ± 9	1.9 ± 0.1	9.8 ± 0.1	4.0 ± 0.1
	10	177 ± 4	6.5 ± 0.3	10.3 ± 0.6	2.4 ± 0.3
Blank (L2) - Blank_MAA	0	21 ± 2	0.8 ± 0.1	6.5 ± 1.2	5.4 ± 0.7
	2.5	40 ± 6	1.3 ± 0.2	9.2 ± 0.2	5.1 ± 0.1
	5	62 ± 3	2.3 ± 0.1	9.0 ± 0.1	4.1 ± 0.1
	10	113 ± 6	4.8 ± 0.1	11.4 ± 0.1	2.8 ± 0.1

The addition of the DMA_MAA and Blank_MAA copolymers to the blank and 5 wt% NVP latexes led to the formation of stiffer materials in all cases, which showed higher Young's modulus, yield stress and tensile strength and a loss in extensibility with the increase in MAA copolymer content. However, the stiffening observed in the four combinations was relatively similar without any notable contribution of the catechol groups. When comparing blank and NVP

containing latexes, there was a measurable increase in Young's modulus and yield stress which suggests that there is some benefit to enhancing interactions between the emulsion polymer and the water soluble polymer. Overall, the results indicate that similar to the NVP – TA system discussed in Chapter 4, the mechanical reinforcement of the materials arised primarily from the formation of a honeycomb microstructure of high T_g polymer around the polymer particles. In order to check that possibility, the microstructure of the 5 wt% NVP and blank materials with 10 wt% DMA_MAA was analyzed by transmission electron microscopy (TEM). The films were stained with RuO_4 to darken the catechol-rich areas. The TEM images of the stained films are shown in Figure 7.9.

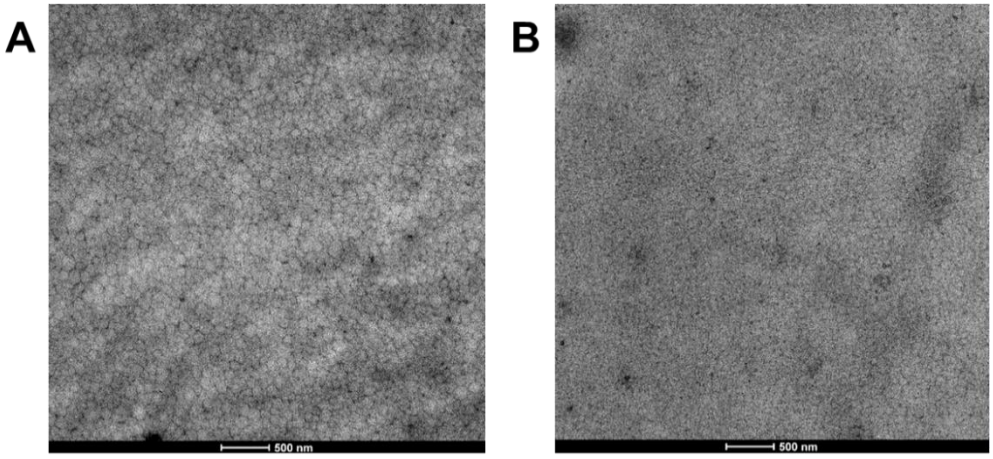

5% NVP (L2) – 10% DMA_MAA Blank (L1) – 10% DMA_MAA

Figure 7.9. TEM images of the stained (A) 5% NVP – 10% DMA_MAA and (B) blank – 10% DMA_MAA polymer films.

Figure 7.9 shows that the MAA copolymers distributed around the polymer particles in both cases. The distribution of the DMA_MAA copolymer in the film prepared from the 5 wt% NVP latex seemed more homogeneous but this did not have a major impact on the mechanical

performance of the material. Thus, from the TEM images it can be concluded that the stiffening observed in the tensile tests (see Figure 7.8) was caused by the formation of a connected hard MAA copolymer network around the polymer particles. However, unlike the NVP – TA system, in this latex – MAA copolymer blends the hydrogen bonds between the pyrrolidone and catechol were not necessary to drive the microstructuring of the materials. It is likely that the use of water-soluble H-bond donors with a methacrylic-type polymer backbone enhanced the compatibility between the polymer in the particles and the H-bond donors allowing the homogeneous distribution of the H-bond donors even in the absence of the pyrrolidone groups in the particles. In addition, compared to TA, the DMA_MAA copolymers utilized in this chapter are anionically charged, and since the electrostatic repulsion between two carboxylates is stronger than the attractive H-bonds between two catechol groups, it is likely that the copolymers remained soluble in water without forming aggregates. Therefore, during film formation they got trapped between the particles and formed a honeycomb structure.

In the second part of the work, soft copolymers with T_g-s near - 20 °C were used as water-soluble H-bond donors as an attempt to minimize the mechanical reinforcement coming from the hardness of the copolymer and emphasize the contribution of the H-bonds to the mechanical strength of the films. In Runs 3 and 4, a PEGMA macromonomer with a MW = 360 g/mol was used to synthesize water-soluble copolymers. This short chain PEGMA is not able to crystallize and it was chosen to avoid the contribution of the crystalline domains to the mechanical strength of the films. The tensile properties of the materials obtained by blending blank (L1) and 5 wt% NVP latexes (L2) with 10 wt% of the blank_PEGMA and DMA_PEGMA copolymers are shown in Figure 7.10 and the tensile parameters obtained from the stress-strain curves are presented in Table 7.5.

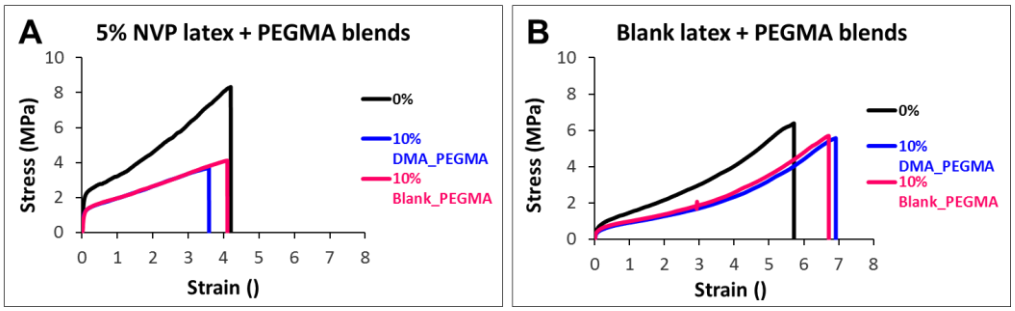

Figure 7.10. Stress-strain plots of the (A) 5%NVP (L2) – PEGMA and (B) blank (L1) – PEGMA copolymer blends.

Table 7.5. Mechanical parameters obtained from the stress-strain plots shown in Figure 7.10.

Latex	Copolymer wt%	Young's modulus E (MPa)	Yield stress σ_y (MPa)	Tensile strength σ_{max} (MPa)	Ultimate strain γ_{max} ()
5 % NVP (Latex 2)	0	57 ± 4	2.1 ± 0.1	8.3 ± 0.1	4.2 ± 0.1
	DMA_PEGMA 10 wt%	32 ± 2	1.2 ± 0.1	4.1 ± 0.1	4.2 ± 0.1
	Blank_PEGMA10 wt%	37 ± 8	1.2 ± 0.1	3.7 ± 0.1	3.7 ± 0.1
Blank (Latex 1)	0	21 ± 2	0.8 ± 0.1	6.5 ± 1.12	5.4 ± 0.8
	DMA_PEGMA 10 wt%	14 ± 2	0.4 ± 0.1	4.8 ± 0.8	7.0 ± 0.1
	Blank_PEGMA10 wt%	18 ± 6	0.6 ± 0.1	5.3 ± 0.4	7.1 ± 0.4

The addition of the PEGMA copolymers to the blank and 5 wt% NVP latexes had a plasticizing effect on the materials, very likely due to the low T_g of the PEGMA copolymers. However, similar to the materials prepared from the MAA copolymers, no effect of the pyrrolidone or catechol groups was observed. It is possible that the catechol concentration in the system was too low to efficiently reinforce the particle interfaces. Thus, in Run 5 the concentration of DMA was increased to 80 wt% and 20 wt% AMPS was used to provide the water-solubility. Among

the copolymers synthesized in this work, the chemical structure of DMA_AMPS was the closest one to the chemical structure of TA due to the high content catechol groups per molecule. The mechanical properties of the films prepared from the 5% NVP (L14) and blank (L13) latexes with 0, 2.5 and 5 wt% of DMA_AMPS are shown in Figure 7.11. The mechanical parameters related to the stress-strain curves are attached in Table 7.6.

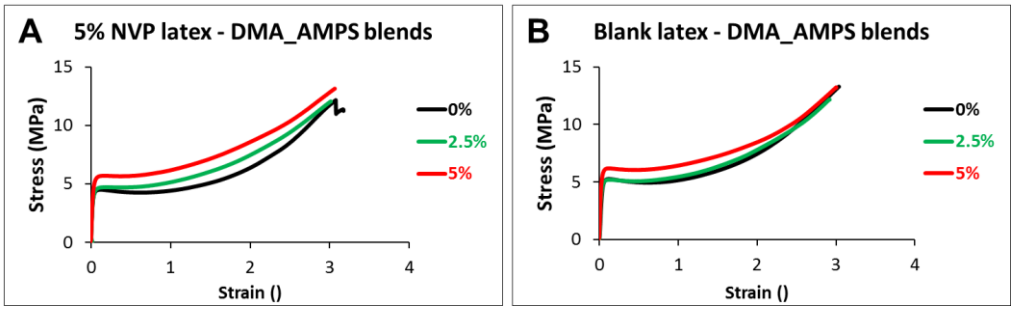

Figure 7.11. Stress-strain plots of the (A) 5 wt% NVP (L14) – DMA_AMPS and (B) blank (L13) – DMA_AMPS blends with 0, 2.5 and 5 wt% of water-soluble copolymer.

Table 7.6. Mechanical parameters obtained from the stress-strain plots shown in Figure 7.11.

Material	DMA_AMPS wt%	Young's modulus E (MPa)	Yield stress σ_y (MPa)	Tensile strength σ_{max} (MPa)	Ultimate strain γ_{max} ()
5 % NVP (Latex 14) – DMA_AMPS	0	173 ± 19	4.6 ± 0.1	11.6 ± 0.7	3.0 ± 0.2
	2.5	164 ± 16	4.8 ± 0.1	12.7 ± 0.4	3.1 ± 0.1
	5	188 ± 20	5.6 ± 0.1	13.3 ± 0.5	3.2 ± 0.1
Blank (Latex 13) – DMA_AMPS	0	169 ± 17	4.8 ± 0.3	12.7 ± 0.9	3.0 ± 0.1
	2.5	183 ± 17	5.3 ± 0.1	12.0 ± 0.8	3.0 ± 0.1
	5	250 ± 60	7.4 ± 0.5	13.5 ± 0.6	2.8 ± 0.4

Similar to the blends prepared from the MAA copolymers, the materials showed higher Young's modulus, yield stress and tensile strength with the copolymer content. However, the stiffening observed with the DMA_AMPS copolymer was moderate probably due to the lower T_g of the DMA_AMPS copolymer ($T_g \approx 95$ °C) compared to the MAA copolymers ($T_g \approx 130$ °C) and the greater extent of hydroplasticization of the AMPS copolymer. The materials cast from the blank and 5 wt% NVP latexes displayed very similar mechanical properties and no contribution of the pyrrolidone – catechol H-bonds on the mechanical strength was observed.

Overall, from the comparison of the tensile test plots presented in Figures 7.8, 7.10 and 7.11, it can be seen that the mechanical properties of the materials depended mainly on the T_g of the H-bond donor employed for the blend. This can be seen from the observation that the addition of the PEGMA copolymers with a $T_g \approx -20$ °C had a plasticizing effect on the polymer films while the addition of the high T_g copolymers prepared with MAA and AMPS caused a gradual stiffening in the materials with the copolymer content. Similar to the NVP – TA system discussed in Chapter 4, in these systems the reinforcement was attributed to homogeneous distribution of the hard water-soluble donor around polymer particles into a honeycomb microstructure. However, unlike the NVP – TA combination, with the use of copolymers the H-bonds between pyrrolidone and phenols were not necessary to drive the microstructuring of the films and no significant contribution of the pyrrolidone – catechol H-bonds on the mechanical strength of the films was observed. Possibly, the use of copolymers with a methacrylic-type polymer backbone enhanced the compatibility between the water-soluble H-bond donor and the polymer in the particles allowing the microstructuring of the films, even in the absence of H-bonds. In addition, in contrast to the system with TA, the presence of electrostatic repulsions between MAA and AMPS containing copolymers avoided the formation of aggregates in the

aqueous phase and favored the homogeneous distribution of the copolymers around the polymer particles during film formation.

7.3.5. Water sensitivity

The water sensitivity of the materials was analyzed by immersing the films in water and measuring the water wt% absorbed and the film wt% lost during the test. This analysis was carried out for the materials that showed a mechanical reinforcement in the tensile test, namely, the blends prepared from the blank_MAA, DMA_MAA and DMA_AMPS copolymers. The water uptake and weight loss of the blends prepared from the blank (L1) and 5%NVP (L2) latexes with 5 wt% of blank_MAA or DMA_MAA after 7 days of immersion in water are shown in Figures 12.A and 12.B, respectively. The water uptake and weight loss of the blank (L13) and 5 wt% NVP (L14) latexes with 0, 2.5 and 5 wt% DMA_AMPS copolymer after 5 days of immersion in water are shown in Figures 13.A and 13.B.

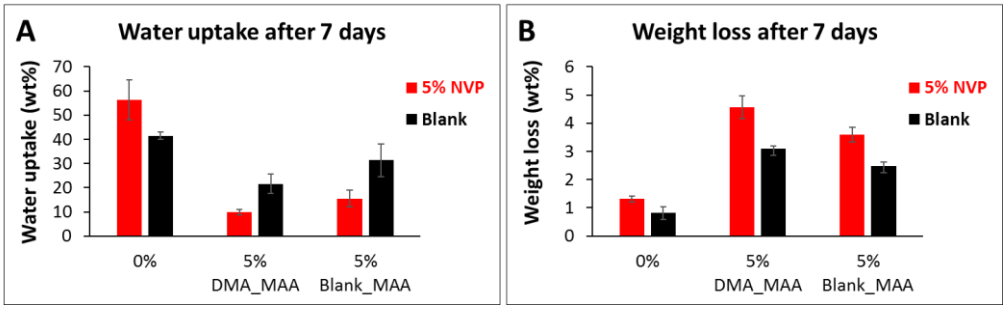

Figure 7.12. (A) Water uptake and (B) weight loss of the blends prepared from the blank (L1) and 5% NVP (L2) latexes and 5 wt% of the DMA_MAA and Blank_MAA copolymers.

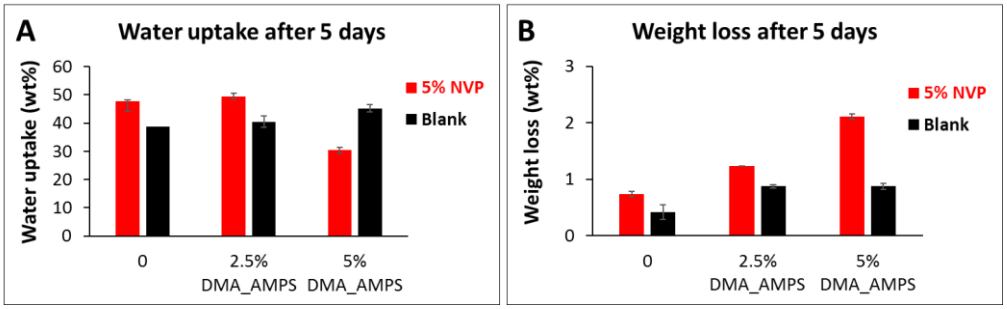

Figure 7.13. (A) Water uptake and (B) weight loss of the blends prepared from the blank (L13) and 5% NVP (L14) latexes with 0, 2.5 and 5 wt% DMA_AMPS.

First, the comparison of the materials prepared from the neat latexes shows that the addition of NVP slightly increased the water absorption and weight loss of the films due to the hydrophilic nature of NVP. Then, Figure 7.12.A shows that the blends prepared with of 5 wt% of the blank_MAA and DMA_MAA copolymers absorbed less water, especially in presence of 5 wt% NVP. This decrease in the water absorption of the films could be ascribed to the crosslinking of the polymer chains with H-bonds, or to the release of the water-soluble components from the films to the aqueous phase. Looking at 7.12.B, the high weight losses suggest that a high fraction of water-sensitive material was released to the aqueous phase during the tests, especially in presence of 5 wt% NVP. Similar behavior was observed for the latex – DMA_AMPS blends. Figure 7.13.B shows that the weight loss increased with the copolymer content for both blank and 5% NVP materials. In addition, the weight loss was greater in presence of NVP. In these blends, similar to the PVOH-containing films investigated in Chapter 3, the water-soluble copolymer and pyrrolidone hydrophilic corona around the polymer particles could have favored the penetration of water to the films and the release of water-sensitive material to the aqueous phase. In Chapters 4 and 5, the strong NVP-TA H-bonds retained TA in the films when the films were put in contact with water. In contrast, no contribution of the pyrrolidone-catechol or

pyrrolidone-carboxylic acid H-bonds was observed in the water-sensitivity of the materials when the copolymers were used. Very likely in these materials, the electrostatic repulsion between charged MAA and AMPS species overcame the strength of the H-bonds that held the catechol-containing copolymers into the films and favored the desorption of the donor molecules.

7.4. Conclusions

The aim of the work carried out in this chapter was the synthesis and utilization of catechol-containing water-soluble copolymers as synthetic substitutes of TA for the production of mechanically reinforced and less colored acrylic films.

First, using the knowledge gained in Chapter 6 on the free radical polymerizations (FRP) in presence of catechols, five copolymers with different T_g–s and catechol contents were successfully prepared using (meth)acrylamide- and (meth)acrylate-type monomers and DMF as solvent. Then, the catechol-containing copolymers were combined with polymer dispersions with 0 and 5 wt% NVP to prepare polymer films with different copolymer contents and investigate the effect of the H-bonds on film properties.

Unlike in previous chapters, the reference and H-bonded materials displayed very similar mechanical response, showing no influence of the pyrrolidone-catechol H-bonds on the mechanical performance of the films. Based on the film microstructure this can be explained because, unlike the NVP – TA system discussed in Chapter 4, even in the absence the of pyrrolidone groups a percolating network of the water soluble polymer could be observed in the dried films. In these materials the homogeneous distribution of the water-soluble copolymers around the polymer particles was ascribed to the better compatibility between the methacrylate-type copolymers and the acrylic particles and to the electrostatic repulsion between the water-

soluble copolymer chains which kept the donors soluble in water and prevented the formation of aggregates. Unlike the NVP – TA system discussed in Chapter 4, when the films were immersed in water, the pyrrolidone-catechol and pyrrolidone-carboxylic acid H-bonds did not lead to a significant improvement in the water-sensitivity of the material. Probably, the electrostatic repulsions between anionically charged MAA and AMPS species overcame the strength of the H-bonds holding them to the polymer films and promoted the desorption of the copolymers to the aqueous phase. Thus, while synthetic catechol-containing water soluble polymers can be synthesized using the knowledge gained in Chapter 6, further improvements in the design of these polymers will need to be performed to exceed the performance of the naturally occurring polyphenols used elsewhere in this thesis. Based on the experimental results in this chapter, future research would point to the synthesis of high T_g water-soluble non-ionic species containing high concentration of catechol groups.

7.5. References

(1) Erel-Unal, I.; Sukhishvili, S. A. Hydrogen-bonded multilayers of a neutral polymer and a polyphenol *Macromolecules* **2008**, *41*, 3962–3970.

(2) Tsukruk, V. V; Kozlovskaya, V.; Harbaugh, S.; Drachuk, I.; Shchepelina, O.; Kelley-loughnane, N.; Stone, M.; Tsukruk, V. V. Hydrogen-bonded LbL shells for living cell surface engineering *Soft Matter* **2011**, *7*, 2364–2372.

(3) Whittaker, J. L.; Subianto, S.; Dutta, N. K.; Choudhury, N. R. Induced insolubility of electrospun poly(N-vinylcaprolactam) fibres through hydrogen bonding with Tannic acid *Polymer* **2016**, *87*, 194–201.

(4) López, C. M.; Pich, A. Supramolecular Stimuli-Responsive Microgels Crosslinked by Tannic Acid *Macromol. Rapid Commun.* **2018**, *39*, 1700808.

(5) Nam, H. G.; Nam, M. G.; Yoo, P. J.; Kim, J. Hydrogen bonding-based strongly adhesive coacervate hydrogels synthesized using poly(N-vinylpyrrolidone) and tannic acid *Soft Matter* **2019**, *15*, 785–791.

(6) Jimenez, N.; Ballard, N.; Asua, J. M. Hydrogen Bond-Directed Formation of Stiff Polymer Films Using Naturally Occurring Polyphenols *Macromolecules* **2019**, *52*, 9724–9734.

(7) Narasimhan, B. N.; Dejis, G. S.; Ting, S. M. H.; Williams, M. A. K.; Malmström, J. A comparative study of tough hydrogen bonding dissipating hydrogels made with dirfferent network structures *Nanoscale Adv.* **2021**, *3*, 2934–2947.

(8) Jimenez, N.; Ballard, N.; Asua, J. M. Hydrogen-bond driven formation of microstructured pressure sensitive adhesives (PSAs) with enhanced shear resistance *Polymer* **2021**, *233*, 124210.

(9) Barton, J. M. Relation of glass transition temperature to molecular structure of addition copolymers *J. Polym. Sci. Part C Polym. Symp.* **1970**, *30*, 573–597.

(10) Schneider, H. A.; Rieger, J.; Penzel, E. The glass transition temperature of random copolymers: 2. Extension of the Gordon-Taylor equation for asymmetric Tg vs composition curves *Polymer* **1997**, *38*, 1323–1337.

(11) Lee, J. H.; Kopeckova, P.; Kopece, J.; Andrade, J. D. Surface properties of copolymers of alkyl methacrylates with methoxy(polyethylene oxide) methacrylates and their application as protein-resistant coatings *Biomaterials* **1990**, *11*, 455–464.

(12) Han, X.; Zhang, X.; Zhu, H.; Yin, Q.; Liu, H.; Hu, Y. Effect of Composition of PDMAEMA‐b‐PAA Block Copolymers on Their pH- and Temperature-Responsive Behaviors *Langmuir* **2013**, *29*, 1024–1034.

(13) Sato, T.; Okaya, T. Characterization and Physical Properties of Low Molecular Weight Poly(vinyl acetate) and Poly(vinyl alcohol) *Polym. J.* **1992**, *24*, 849–856.

(14) Oh, J. K.; Yang, J.; Tomba, J. P.; Rademacher, J.; Farwaha, R.; Winnik, M. A. Molar Mass Effect on the Rate of Polymer Diffusion in Poly(vinyl acetate-co-butyl acrylate) Latex Films *Macromolecules* **2003**, *36*, 8836–8845.

(15) Tomba, J. P.; Portinha, D.; Schroeder, W. F.; Winnik, M. A.; Lau, W. Polymer diffusion in high-M/low-M hard-soft latex blends *Colloid Polym. Sci.* **2009**, *287*, 367–378.

(16) Fasano, D. M.; Fitzwater, S. J.; Lau, W.; Sheppard, A. C. Diffusion of oligomers in latex systems — A route to low volatile organic compound (VOC) coatings *Can. J. Chem.* **2010**, *88*, 500–513.

(17) Williams, R.; Jencks, W.; Westheimer, F. *pKa Data Compiled by R. Williams*; 2011.

(18) Ceska, G. W. Carboxyl-Stabilized Emulsion Polymers *J. Appl. Polym. Sci.* **1974**, *18*, 2493–2499.

(19) Vorwerg, L.; Gilbert, R. G. Electrosteric Stabilization with Poly Acrylic)Acid in Emulsion Polymerization: Effect on Kinetics and Secondary Particle Formation *Macromolecules* **2000**, *33*, 6693–6703.

(20) Fritz, G.; Scha, V.; Willenbacher, N.; Wagner, N. J. Electrosteric Stabilization of Colloidal Dispersions *Langmuir* **2002**, *18*, 6381–6390.

(21) Reynhout, X. E. E.; Beckers, M.; Meuldijk, J. A. N.; Drinkenburg, B. A. H. Electrosteric Stability of Styrene / Acrylic Acid Copolymer Latices under Emulsion Polymerization Reaction Conditions *J. Polym. Sci. Part A Polym. Chem.* **2005**, *43*, 726–732.

(22) Pedraza, E. P.; Soucek, M. D. Effect of functional monomer on the stability and film properties of thermosetting core-shell latexes *Polymer* **2005**, *46*, 11174–11185.

(23) Benedek, I. *Pressure-Sensitive Adhesives and Applications*; New York, 2004.

(24) Wang, T.; Canetta, E.; Weerakkody, T. G.; Keddie, J. L.; Rivas, U. pH Dependence of the Properties of Waterborne Pressure-Sensitive Adhesives Containing Acrylic Acid *Appl. Mater. Interfaces* **2009**, *1*, 631–639.

(25) Kojima, T.; Tsuchiya, M.; Tago, K. Thermal analysis of polymer networks consisting of different homopolymers Poly(methacrylic acid)-net-poly(oxytetramethylene) *J. Therm. Anal.* **1997**, *49*, 149–154.

(26) Maurer, J. J.; Eustace, D. J.; Ratcliffe, C. T. Thermal Characterization of Poly(acrylic acid) *Macromolecules* **1987**, *20*, 196–202.

(27) Joanicot, M.; Wong, K.; Richard, J.; Maquet, J.; B., C. Ripening of Cellular Latex Films *Macromolecules* **1993**, *26*, 3168–3175.

(28) Zosel, A. Mechanical Properties of Films from Polymer Latices *Polym. Adv. Technol.* **1995**, *6*, 263–269.

(29) Richard, J. In *Film Formation in Waterborne Coatings*; Provder, T.; Winnik, M. A.; Urban, M. W., Eds.; 1996; pp. 118–153.

(30) Lee, D.; Kim, J. Preparation of Small-Sized Carboxylated Latexes by Emulsion Polymerization Using Alkali-Soluble Random Copolymer *J. Appl. Polym. Sci* **1998**, *69*, 543–550.

(31) do Amaral, M.; Asua, J. M. Synthesis of High Solid-Content Latex using Alkali-Soluble Resin as Sole Surfactant *Macromol. Rapid Commun.* **2004**, *25*, 1883–1888.

(32) Caballero, S.; De la Cal, J. C.; Asua, J. M. Radical entry mechanisms in alkali-soluble-resin-stabilized latexes *Macromolecules* **2009**, *42*, 1913–1919.

(33) Gonzalez, E.; Tollan, C.; Chuvilin, A.; Paulis, M.; Barandiaran, M. J. Effect of alkali-soluble resin emulsifiers on coalescence and interdiffusion between latex polymer particles *Colloid Polym. Sci.* **2015**, *293*, 2419–2427.

(34) Bandiera, M.; Balk, R.; Barandiaran, M. J. Grafting in polymeric dispersions stabilized with Alkali-Soluble Resins: Towards the production of leaching-free waterborne coatings *Eur. Polym. J.* **2017**, *97*, 77–83.

(35) Lopes Brito, E.; Ballard, N. Progress in Organic Coatings Film formation of Alkali Soluble Resin (ASR) stabilized latexes *Prog. Org. Coatings* **2021**, *159*, 106444.

(36) Ma, L.; Deng, L.; Chen, J. Applications of poly(ethylene oxide) in controlled release tablet systems: a review *Drug Dev. Ind. Pharm.* **2014**, *40*, 845–851.

(37) D'souza, A. A.; Shegokar, R. Polyethylene glycol (PEG): a versatile polymer for pharmaceutical applications *Expert Opin. Drug Deliv.* **2016**, *13*, 1257–1275.

(38) Peng, B.; Yao, Y.; Chen, Q.; Hu, B. Solid-State High-Resolution NMR Studies on PEO-Based Crystalline Solid Polymer Electrolytes for Lithium-Ion Battery *Annu. reports NMR Spectrosc.* **2015**, *85*, 67–92.

(39) Zhigang, X.; Dan, H.; Xiaolin, X. Poly(ethylene oxide)-based electrolytes for lithium-ion batteries *J. Mater. Chem. A* **2015**, *3*.

(40) Zhao, S.; Wu, Q.; Ma, W.; Yang, L. Polyethylene Oxide-Based Composites as Solid-State Polymer Electrolytes for Lithium Metal Batteries: A Mini Review *Front. Chem.* **2020**,

8, 1–7.

(41) Johnson, W. Final Report on the Safety Assessment of PEG-25 Propylene Glycol Stearate, PEG-75 Propylene Glycol Stearate, PEG-120 Propylene Glycol Stearate, PEG-10 Propylene Glycol, PEG-8 Propylene Glycol Cocoate, and PEG-55 Propylene Glycol Oleate *Int. J. Toxicol.* **2001**, *20*, 13.26.

(42) Jang, H.-J.; Shin, C. Y.; Kim, K. Safety Evaluation of Polyethylene Glycol (PEG) Compounds for Cosmetic Use *Toxicol. Res. (Camb).* **2015**, *31*, 105–136.

(43) Hombach, R.; Reiff, H.; Dollhausen, M. Polyisocianate preparation dispersible in water and their use as an additive for aqueous adhesives. US4663377A, 1987.

(44) Long, D. Water dispersible poly(urethane-ureas) prepared with diisocyanate blends. EP0369389A1, 1990.

(45) Thorne, S. J.; Backhouse, A. J. Polyisocianate mixture. US5202377A, 1993.

(46) Brown, W. T. Effect of Crosslinker Reaction Rate on Film Properties for Thermoset Coatings *J. Chem. Eng. Process Technol.* **2000**, *72*, 63–70.

(47) Flori, D. E. Low VOC, isocyanate based aqueous curable compositions. US 6316543 B1, 2001.

(48) Nabuurs, T.; Soer, W.-J.; Peters, R. Isocyanate crosslinking in two component waterborne coatings *Polym. Int.* **2018**, *68*.

(49) Tsaur, S.-L.; Fitch, R. M. Preparation and Properties of Polystyrene Model Colloids I. Preparation of Surface-Active Monomer and Model Colloids Derived Therefrom *J. Colloid Interface Sci.* **1986**, *115*, 450–462.

(50) Kim, J. H.; Chainey, M.; El-Aasser, M. S.; Vanderhoff, J. W. Emulsifier-Free Emulsion Copolymerization of Styrene and Sodium Styrene Sulfonate *J. Polym. Sci. Part A Polym. Chem.* **1992**, *30*, 171–183.

(51) Chang, W.; Liu, L.; Zhang, J.; Pan, Q.; Pei, M. Preparation and Characterization of Styrene/Butyl Acrylate Emulsifier-Free Latex with 2-Acrylamido-2- Methyl Propane Sulfonic Acid as a Reactive Emulsifier *J. Dispers. Sci. Technol.* **2009**, *30*, 639–642.

(52) Dai, M.; Zhang, Y.; He, P. Preparation and characterization of stable and high solid content St/BA emulsifier-free latexes in the presence of AMPS *Polym. Bull.* **2011**, *66*, 91–100.

(53) Bilgin, S.; Tomovska, R.; Asua, J. M. Effect of ionic monomer concentration on latex and film properties for surfactant-free high solids content polymer dispersions *Eur. Polym. J.*

2017, *93*, 480–494.

(54) Bilgin, S.; Tomovska, R.; Asua, J. M. Surfactant-free high solids content polymer dispersions *Polymer* **2017**, *117*, 65–75.

(55) Argaiz, M.; Ruip, F.; Aguirre, M.; Tomovska, R. Ionic Inter-Particle Complexation Effect on the Performance of Waterborne Coatings *Polymers* **2021**, *13*, 1–18.

(56) Sun, Q.; Farneth, W. E.; Harmer, M. A. Dimerization of α-Methylstyrene (AMS) Catalyzed by Sulfonic Acid Resins: A Quantitative Kinetic Study *J. Catal.* **1996**, *69*, 62–69.

(57) Xu, L. Q.; Jiang, H.; Neoh, K.-G.; Kang, E.-T.; Fu, G. D. Poly(dopamine acrylamide)-co-poly(propargyl acrylamide)-modified titanium surfaces for 'click' functionalization *Polym. Chem.* **2012**, *3*, 920–927.

(58) Haddock, T. H. Presure sensitive adhesive. EP 0130080 B1, 1988.

(59) Fox, T. G. Influence of diluents and copolymer composition on the glass transition temperature of a polymer system *Bull. Am. Phys. Soc. 1* **1956**, *123*.

(60) Mathiesen, D.; Vogtmann, D.; Dupaix, R. B. Mechanics of Materials Characterization and constitutive modeling of stress-relaxation behavior of Poly(methyl methacrylate) (PMMA) across the glass transition temperature *Mech. Mater.* **2014**, *71*, 74–84.

(61) Pal, S.; Mondal, R.; Guha, S.; Chatterjee, U.; Jewrajka, S. K. Homogeneous phase crosslinked poly(acrylonitrile-co-2-acrylamido-2- methyl-1-propanesulfonic acid) conetwork cation exchange membranes showing high electrochemical properties and electrodialysis performance *Polymer* **2019**, *180*, 121680.

(62) Meredith, H. J.; Wilker, J. J. The Interplay of Modulus, Strength, and Ductility in Adhesive Design Using Biomimetic Polymer Chemistry *Adv. Funct. Mater.* **2015**, *25*, 5057–5065.

(63) Kucharski, M.; Lubczak, R. Copolymerization of Hydroxyalkyl Methacrylates with Acrylamide and Methacrylamide I. Determination of Reactivity Ratios *J. Appl. Polym. Sci* **1996**, *64*, 1259–1265.

Chapter 8. Conclusions

With the aim of reducing VOC emissions and producing more sustainable coatings and adhesives, solventborne polymers are gradually being replaced by water-based alternatives. However, the mechanical properties of waterborne systems are typically not as good as those of solventborne products due to differences in the film formation process and this has limited the widespread use of waterborne polymers in some demanding applications that require high mechanical strength. Industrially, volatile plasticizing agents are commonly added to enable film formation of high T_g dispersions and produce mechanically resistant polymer films. However, the need for a volatile plasticizer brings back the environmental concerns related to the release of VOCs to the atmosphere. Another alternative is to crosslink the polymer chains after film formation to achieve mechanical resistance. Covalent chemistries have been widely utilized for the crosslinking of polymer chains and production of stiff polymer films. However, such chemistries often employ or release toxic chemicals, require annealing or present limited stability due to the high reactivity of the functional groups. As an alternative, the use of physical interactions offers the opportunity of creating network structures while avoiding the drawbacks related to covalent chemistries. The aim of this PhD thesis was to explore the use of hydrogen bonding for the physical crosslinking of waterborne polymer dispersions and the mechanical reinforcement of the materials cast from these systems. The work was targeted specifically towards the production of mechanically strong polymer films cast from non-toxic, stable and ambient curable waterborne dispersions.

In Chapter 2, the possibility of using pyrrolidone-hydroxyl and uracil-adenine to crosslink the polymer chains and reinforce mechanically the polymer films was investigated. First, functional polymer dispersions with pyrrolidone, hydroxyl, uracil and adenine were synthesized by emulsion

polymerization. Then, the polymer dispersions with complementary groups were combined and dried to prepare polymer films provided with pyrrolidone-hydroxyl and uracil-adenine H-bonds. However, all the materials showed very similar mechanical behavior, and no influence of the H-bonds on the mechanical properties of the films was observed. The fundamental examination of the systems revealed that the low association constant (K_a) of the pyrrolidone-hydroxyl pair around 1 M^{-1} leads to a limited number of H-bonds in the films and prevents the formation of a cohesive network. The uracil-adenine complex has a higher K_a around 100 M^{-1} which allows the buildup of a physical network. For this system, the lack of reinforcement was attributed to the low concentration of H-bonds (≈ 1 mol%) that can be reasonably incorporated coupled with the short lifetime of the interactions, which prevented their effective reinforcement of the mechanical properties. Thus, two approaches exist for the crosslinking of polymer dispersions with physical interactions. The first strategy consists in the use of high K_a complexes such as cytosine-guanine or Upy-Upy that ensure the efficient crosslinking of polymer chains and have complex lifetimes long enough to effectively contribute to the mechanical strength of the films. Nevertheless, preliminary experiments showed that the low solubility of such groups in water, common organic solvents and monomer mixtures limits the practical implementation of these systems. The second strategy, which was the focus for the rest of the thesis, relied on the use of the use of weakly associating units at much higher local concentrations and in blocky structures. In these circumstances, weak single H-bonds can work cooperatively to form junctions that present complex lifetimes higher than the individual H-bonds and can lead to crosslinked materials with enhanced mechanical strength.

The rest of the thesis was dedicated to investigate systems composed of functional polymer dispersions and water-soluble crosslinkers. In such systems, the interactions between the functional groups take place at the surface of the polymer particles during film formation

which results in high local concentrations of H-bonds in the particle boundaries and can potentially lead to physically crosslinked and reinforced particle interfaces. In Chapter 3, polyvinyl alcohol (PVOH) stabilized particles with hydroxyl groups were combined with polyvinyl pyrrolidone (PVP), gallic acid (GA) and tannic acid (TA) water-soluble species. The addition of the water-soluble species to the PVOH stabilized latex led to the formation of stiffer materials. However, the materials showed very poor water resistance due to the high fraction of hydrophilic compounds in the formulation. Despite the high H-bond density at the boundaries of the particles in these materials, when the films were exposed to water the H-bonds were disrupted by the water molecules and the hydrophilic components (PVOH free chains, PVP, TA and GA) were released to the aqueous phase. As result, the polymer films did not retain the mechanical strength after being exposed to water.

In Chapters 4 and 5, acrylic polymer dispersions with H-bond acceptor groups such as N-vinyl pyrrolidone (NVP) were combined with an aqueous solution of TA. Chapter 4 was dedicated to the development of stiff polymer films for coating applications and Chapter 5 was focused on the preparation of high shear resistance pressure sensitive adhesives (PSAs). As a result of the H-bonds between the pyrrolidone groups in the polymer particles and the hydroxyl groups of TA, TA distributed homogeneously around the polymer particles and arranged into a honeycomb microstructure. In the materials prepared in Chapter 4 for coatings applications, the microstructured materials showed improved Young's modulus and yield stress with the polyphenol content. In the absence of H-bonds, TA formed aggregates and the polymer films showed only a slight increase in Young's modulus and yield stress. In Chapter 5, the physically crosslinked and microstructured PSAs were developed using a similar approach. These PSAs showed enhanced shear resistance compared to systems where strong H-bonds were not present. In addition, while the increase in the cohesion was remarkable, the formation of the TA

microstructure only caused a moderate decrease in the work of adhesion and peel strength. Unlike the PVOH blends discussed in Chapter 3, the NVP-TA materials prepared in Chapters 4 and 5 showed water uptake values comparable to the blank materials due to the lower content of hydrophilic components in the films (10 wt% PVOH in Chapter 3 vs 5 and 4 wt% NVP in Chapters 4 and 5). In addition, in the polymers prepared in Chapters 4 and 5, the H-bonding groups were covalently attached to the polymer particles which prevented their free migration to the aqueous phase and reduced the weight loss of the polymer films after the immersion in water. Moreover, in the polymer films functionalized with pyrrolidone groups the leaching of TA was almost completely prevented by the strong H-bonds and the films retained the morphology and the mechanical strength even after extensive water exposure.

The reinforcing mechanism was applied to a variety of latexes (with different molecular weight polymers, variable H-bond acceptor monomer content, including AA in the formulation or employing NVC and UMA as alternative H-bond acceptors) proving the versatility of the approach for both coatings and PSA applications. The nature and molecular size of the crosslinker were shown to directly influence the final performance of the materials prepared for coating applications: less acidic OH groups (PVOH) were not able to form strong interactions and reinforce the materials, and smaller molecular size phenolic compounds (GA) were less efficient stiffening the materials.

Thus, the combination of acrylic polymer dispersions with H-bond acceptors and TA is a practical route for the preparation of microstructured materials with enhanced mechanical strength. However, the addition of TA provided an orange tint to the polymer films which was visible even in the white paints prepared with TiO_2 pigment in Chapter 4. Moreover, when used as formulated product the strong interactions between TA and the main coating components led to unstable products, which limits the potential application of TA in formulated products. As

alternative, the synthesis of copolymers containing catechol units in place of TA was proposed in this thesis. Similar to TA, the phenolic hydroxyl groups of catechols are strong H-bond donors, and H-bond interactions arising from catechols can be employed for the physical crosslinking of polymer chains. However, the direct incorporation of catechols is challenging in polymers produced by radical polymerization due to transfer and termination reactions that readily occur between catechols and radical species. Thus, before conducting the synthesis of the catechol copolymers in Chapter 7, the fundamental behavior of catechol groups in the radical polymerization of common monomers was explored in Chapter 6. The study revealed that while monosubstituted olefins such as styrene, methyl acrylate and acrylamide readily undergo chain transfer to phenolic hydrogens, methacrylate and methacrylamide monomers do not suffer any inhibitory activity and can be polymerized to high molecular weights without any influence of the catechol, even when the catechol is present in large amounts (50 wt % in the polymerization of MMA). These monomer-based effects are also applicable to the choice of the catechol-containing monomer, and therefore, the most suitable monomers are those such as dopamine methacrylamide/methacrylate which are less reactive toward the catechol moiety. In addition, it was demonstrated that even for the polymerization of monosubstituted olefins, the inhibitory activity of catechols can be substantially reduced by the selection of polar solvents with H-bond acceptor groups such as dimethyl formamide (DMF).

Using the synthetic guidelines provided by the experimental work in Chapter 6, five water-soluble copolymers with different T_g–s and catechol contents were successfully prepared in Chapter 7 using dopamine methacrylamide as catechol monomer, acrylamide- and methacrylate-type comonomers and DMF as solvent. Then, similar to the work carried out in Chapters 3-5, the catechol-containing copolymers were dissolved in water and combined with a polymer dispersion with 5 wt% NVP to prepare polymer films crosslinked with catechol-

pyrrolidone H-bonds. However, unlike in Chapters 3-5, a percolating network of the catechol-based copolymer around the polymer particles was formed even in the reference material without pyrrolidone groups and no influence of the pyrrolidone-catechol H-bonds on the mechanical performance of the films was observed. In addition, when the films were immersed in water, the pyrrolidone-catechol and pyrrolidone-carboxylic acid H-bonds did not lead to a significant improvement in the water-sensitivity of the material. Very likely, the electrostatic repulsions between anionically charged MAA and AMPS species overcame the strength of the H-bonds holding the water-soluble donors to the polymer films and promoted the desorption of the copolymers to the aqueous phase. Thus, while synthetic catechol-containing water-soluble polymers can be synthesized using the knowledge gained in Chapter 6, further improvements in the design of these polymers will need to be performed to exceed the performance of the naturally occurring polyphenols used in Chapters 3-5 of this thesis. For example, the use of high T_g water-soluble non-ionic species containing high concentration of catechol groups might lead to mechanically reinforced materials with good water sensitivity similar to TA, while keeping the versatility of using synthetic water-soluble copolymers.

Resumen y conclusiones

Con el objetivo de reducir las emisiones de compuestos orgánicos volátiles (COVs) y producir recubrimientos y adhesivos más sostenibles, los productos basados en disolventes están siendo gradualmente reemplazados por productos en agua. Sin embargo, las prestaciones mecánicas de los sistemas basados en agua son generalmente inferiores a las de sus análogos en base disolvente debido a diferencias en el proceso de formación de film, y esto ha limitado el uso de los sistemas basados en agua en algunas aplicaciones demandantes que requieren resistencia mecánica. Industrialmente, a menudo se añaden agentes plastificantes volátiles para favorecer la formación de film de dispersiones con alta T_g y preparar films poliméricos de alta resistencia mecánica. Sin embargo, la necesidad de un plastificante volátil vuelve a poner sobre la mesa las preocupaciones ambientales relacionadas con la liberación de COVs a la atmósfera. Otra alternativa es reticular las cadenas de polímero al final de la formación de film para aumentar la resistencia mecánica. Diferentes reacciones químicas en las que se forman nuevos enlaces covalentes han sido extensamente utilizadas para reticular las cadenas de polímero y producir materiales rígidos. Sin embargo, estas reacciones a menudo emplean o liberan productos químicos tóxicos, requieren altas temperaturas de curado o presentan una estabilidad limitada debido a la alta reactividad de los grupos funcionales. Como alternativa, el uso de interacciones físicas ofrece la oportunidad de entrecruzar las cadenas poliméricas y crear redes físicas mientras que evita los inconvenientes relacionados con las químicas covalentes. El objetivo de esta tesis doctoral era explorar el uso de puentes de hidrógeno para el entrecruzamiento físico de dispersiones poliméricas en base agua y el refuerzo mecánico de los films poliméricos formados a partir de las mismas. El trabajo estaba dirigido a la producción de

films poliméricos mecánicamente resistentes a partir de dispersiones acuosas no tóxicas, estables y curables a temperatura ambiente.

En el capítulo dos, se investigó la posibilidad de emplear los enlaces de hidrógeno pirrolidona-hidroxilo y uracilo-adenina para reticular las cadenas poliméricas y reforzar mecánicamente los materiales. Primero, se sintetizaron dispersiones poliméricas funcionales con grupos pirrolidona, hidroxilo, uracilo y adenina mediante polimerización en emulsión. A continuación, se combinaron las dispersiones poliméricas con grupos complementarios y se secaron para obtener films poliméricos provistos de enlaces de hidrógeno. Sin embargo, todos los materiales mostraron un comportamiento mecánico muy similar y no se observó ninguna influencia de los enlaces de hidrógeno en las propiedades mecánicas de los films. El análisis fundamental de los sistemas reveló que la baja constante de asociación del par pirrolidona-hidroxilo ($K_a \approx 1\ M^{-1}$) da lugar a un número limitado de enlaces de H en los films y evita la formación de una red física cohesiva. La combinación uracilo-adenina presenta una mayor K_a en torno a 100 M^{-1}, lo que permite la construcción de una red física. En este sistema, la falta de refuerzo se atribuyó a la baja concentración de enlaces de hidrógeno que pueden incorporarse razonablemente en los films (≈ 1 mol%) junto con el corto tiempo de asociación de los retículos físicos, lo que impidió que los enlaces de H reforzaran de manera efectiva las propiedades mecánicas. Por lo tanto, existen dos estrategias para el entrecruzamiento físico de las dispersiones poliméricas con enlaces de H. La primera estrategia consiste en el uso de complejos de alta K_a como las parejas citosina-guanina o Upy-Upy, que aseguran el entrecruzamiento eficiente de las cadenas poliméricas y tienen tiempos de asociación lo suficientemente largos para contribuir efectivamente a la resistencia mecánica de los films. Sin embargo, experimentos preliminares mostraron que la baja solubilidad de tales grupos en agua, disolventes orgánicos comunes y mezclas de monómeros limita la implementación práctica de

estos sistemas. La segunda estrategia, que fue el foco del resto de la tesis doctoral, consiste en el uso interacciones débiles pero en concentraciones locales mucho más altas. En estas circunstancias, los enlaces de H simples débiles pueden trabajar conjuntamente para formar uniones cooperativas que presentan tiempos de asociación más altos que los enlaces de H individuales de partida y pueden dar lugar a materiales entrecruzados con mayor resistencia mecánica.

El resto de la tesis fue dedicado a investigar sistemas compuestos por dispersiones poliméricas funcionales y agentes de cruzado solubles en la fase acuosa. En este tipo de sistemas, las interacciones entre los grupos funcionales ocurren en la superficie de las partículas poliméricas durante la formación de film, lo que da lugar a altas concentraciones de enlaces de H en los límites entre partículas y puede conducir a interfaces entre partículas reforzadas y reticuladas físicamente. En el capítulo 3, se combinaron partículas poliméricas estabilizadas con alcohol polivinílico (PVOH) con polivinil pirrolidona (PVP), ácido gálico (GA) y ácido tánico (TA) como agentes de cruzado solubles en agua. La adición de las especies solubles en agua al látex estabilizado con PVOH dio lugar a la formación de materiales más rígidos. Sin embargo, los materiales mostraron una baja resistencia al agua debido a la alta concentración de compuestos hidrófilos en la formulación. A pesar de la alta densidad de enlaces de H en las interfaces entre partículas, cuando los films fueron expuestos al agua, las moléculas de agua disrumpieron los enlaces de H y las especies hidrófilas (cadenas libres de PVOH, PVP, TA y GA) fueron liberadas a la fase acuosa. En consecuencia, los materiales no conservaron la resistencia mecánica tras ser expuestos al agua.

En los capítulos 4 y 5, se combinaron dispersiones acrílicas con grupos aceptores de enlaces de H como n-vinil pirrolidona (NVP) con una solución acuosa de TA. El capítulo 4 fue dedicado al desarrollo de films poliméricos rígidos para su aplicación como recubrimientos, y el

capítulo 5 se centró en la preparación de adhesivos sensibles a la presión (PSAs) con alta resistencia a la cizalla. Como resultado de los enlaces de H entre los grupos pirrolidona en las partículas de polímero y los grupos hidroxilo de TA disuelto en la fase acuosa, el TA se distribuyó homogéneamente alrededor de las partículas poliméricas formando una microestructura dodecaédrica. En los materiales preparados en el capítulo 4 para su uso como recubrimientos, los materiales microestructurados mostraron un módulo de Young y un límite de fluencia mayores con el contenido de TA. Por el contrario, en ausencia de los enlaces de H, el TA formó agregados en la matriz polimérica y los films mostraron solo un ligero aumento en el módulo de Young y en el límite de fluencia. En el capítulo 5, los PSA microestructurados y reticulados físicamente se prepararon utilizando una estrategia muy similar a la utilizada en el capítulo 4, combinando dispersiones acrílicas adhesivas con grupos aceptores de H y TA disuelto en la fase acuosa. Los PSAs reticulados físicamente mostraron una mayor resistencia a la cizalla en comparación con los materiales que no tenían enlaces de H. Además, mientras que el aumento en la cohesión de los PSAs fue remarcable, la formación de la microestructura de TA solo causó una moderada disminución en el trabajo de adhesión y resistencia al pelado de los adhesivos. A diferencia de las mezclas de PVOH descritas en el capítulo 3, los materiales NVP – TA preparados en los capítulos 4 y 5 mostraron valores de absorción de agua comparables al material de referencia debido al menor contenido de componentes hidrófilos en los films (10 % en peso de PVOH en el capítulo 3 frente a 5 y 4 % en peso NVP en los capítulos 4 y 5). Además, en los polímeros acrílicos preparados en los capítulos 4 y 5, los grupos aceptores de H estaban unidos covalentemente a las partículas de polímero, lo que impidió su libre migración a la fase acuosa y redujo la pérdida de peso de los films tras la inmersión en agua. Asimismo, en los films funcionalizados con grupos pirrolidona, los enlaces de H impidieron casi por completo la migración de TA a la fase acuosa y los materiales conservaron la morfología y la resistencia mecánica incluso después de una exposición prolongada al agua.

La estrategia descrita en líneas anteriores para obtener materiales microestructurados y reforzados mecánicamente fue aplicada a una amplia variedad de dispersiones poliméricas (con polímeros de diferente peso molecular, un contenido variable del monómero aceptor de enlaces de H, incluyendo AA en la formulación o empleando NVC y UMA como monómeros aceptores de enlaces de H alternativos) demostrando la eficacia y versatilidad del sistema para el refuerzo mecánico tanto de recubrimientos como de PSAs. Asimismo, se demostró que la naturaleza y el tamaño molecular del agente de cruzado soluble en agua influyen directamente en el rendimiento final de los recubrimientos: los grupos hidroxilo de PVOH son menos ácidos y no fueron capaces de formar interacciones fuertes con los grupos pirrolidona y reforzar los materiales, mientras que los compuestos fenólicos de menor tamaño molecular (GA) fueron menos eficientes aumentando la rigidez de los materiales.

Por lo tanto, la combinación de dispersiones poliméricas acrílicas con grupos aceptores de enlaces de H y TA es una ruta práctica para la preparación de materiales microestructurados con mayor resistencia mecánica. Sin embargo, la adición de TA proporcionó un color anaranjado a los materiales, que era visible incluso en las pinturas blancas preparadas usando TiO_2 como pigmento en el capítulo 4. Además, al emplear TA en productos formulados, las interacciones entre TA y los componentes principales de la formulación (pigmento, espesante) dieron lugar a productos inestables, lo que limita el uso de TA en productos formulados. Como alternativa, en esta tesis se propuso la síntesis de copolímeros con grupos catecol como sustitutos al TA. Al igual que en el TA, los grupos hidroxilo de los catecoles son fuertes aceptores de H y las interacciones con grupos catecol pueden utilizarse para el entrecruzamiento físico de las cadenas poliméricas. Sin embargo, la incorporación directa de catecoles a polímeros producidos mediante polimerización por radicales libres supone un reto, debido a las reacciones de transferencia y terminación que ocurren entre los radicales libres y los catecoles. Por lo tanto,

antes de llevar a cabo la síntesis de copolímeros con grupos catecol en el capítulo 7, se exploró la reactividad de los grupos catecol en la polimerización radicalaria de diferentes monómeros en el capítulo 6. El estudio reveló que mientras que las olefinas monosustituidas como estireno, el acrilato de metilo y acrilamida experimentan reacciones de transferencia de cadena a los hidrógenos fenólicos del catecol, los monómeros metacrilamida y metacrilato de metilo no sufren ninguna actividad inhibitoria y pueden polimerizarse hasta pesos moleculares elevados sin ninguna influencia del catecol, incluso cuando el catecol está presente en grandes cantidades (50 % en peso en la polimerización de MMA). Estos efectos también se aplican a los monómeros que tienen grupos catecol en su estructura, y por lo tanto, los monómeros funcionales con grupos catecol más adecuados para ser polimerizados por radicales libres son los de tipo metacrilato/metacrilamida, ya que son los menos reactivos con el grupo catecol. Además, se demostró que incluso para la polimerización de olefinas monosustituidas, la actividad inhibitoria de los catecoles puede reducirse sustancialmente mediante la selección de disolventes polares con grupos aceptores de enlaces de H como dimetilformamida (DMF).

Usando las pautas sintéticas proporcionadas por el trabajo experimental realizado en el capítulo 6, en el capítulo 7 se sintetizaron con éxito 5 copolímeros solubles en agua con diferentes T_g-s y contenidos en catecol utilizando metacrilamida de dopamina como monómero de catecol, comonómeros de tipo metacrilato y acrilamida y DMF como disolvente. A continuación, de acuerdo con el trabajo realizado en los capítulos 3-5, los copolímeros con catecol se disolvieron en agua y se combinaron con una dispersión polimérica con 5 % NVP para preparar films poliméricos entrecruzados con enlaces de H pirrolidona-catecol. Sin embargo, a diferencia de los resultados mostrados en los capítulos 3-5, los copolímeros de catecol formaron una microestructura dodecaédrica alrededor de las partículas de polímero incluso en el material de referencia sin grupos pirrolidona y no se observó ninguna influencia de

los enlaces de H pirrolidona-catecol en las propiedades mecánicas de los materiales. Además, cuando los films fueron sumergidos en agua, los enlaces de H pirrolidona-catecol y pirrolidona-ácido carboxílico no contribuyeron a una mejora significativa en la sensibilidad al agua de los materiales. Probablemente, las repulsiones electrostáticas entre las especies MAA y AMPS cargadas aniónicamente superaron la fuerza de los enlaces de H que mantienen a los copolímeros de catecol en los films y promovieron la desorción de los copolímeros a la fase acuosa. Por lo tanto, si bien se pueden se pueden sintetizar polímeros solubles en agua que contienen catecol utilizando el conocimiento adquirido en el capítulo 6, es necesario realizar mejoras en el diseño de estos copolímeros para superar el rendimiento de los polifenoles naturales utilizados en los capítulos 3-5 de esta tesis. Por ejemplo, el uso de especies no-iónicas de alta T_g solubles en agua y con una alta concentración de grupos catecol en la estructura podría dar lugar a materiales reforzados mecánicamente con una buena resistencia al agua, manteniendo las ventajas y versatilidad de usar copolímeros sintéticos.

Appendix I. General characterization methods

I.1. Latex characterization

I.1.1. Solids content and monomer conversion

The monomer conversion (X_M) is defined as the fraction of monomer that has been converted into polymer at any reaction time. The monomers employed for the synthesis of the polymer dispersions were volatile (MMA, BA, NVP, HEMA, etc.) and the resulting polymers were solid and non-volatile. Thus, the monomer conversion was determined gravimetrically, measuring the non-volatile fraction of the dispersion to follow the formation of polymer in the system. Experimentally, ≈ 2 mL latex samples were withdrawn from the reactor and the free radical polymerization was immediately quenched with the addition of ≈ 0.1 mL of a 1 wt % hydroquinone (HQ) solution in water. The samples were dried in aluminum caps at 65 °C until constant weight of the samples was achieved (≈ 2 days). The non-volatile fraction of the dispersions also called solids content (SC) was calculated from the weight ratio between the dry solid and the latex (Eq. I.1.)

$$SC = \frac{Dry\ solid\ (g)}{Latex\ (g)} \qquad \text{Equation I.1}$$

The monomer conversion was then calculated from the solids content of the dispersions according to Equation I.2, where NPF is the non-polymeric solid fraction of the sample (includes the initiator, surfactant and HQ), m_{latex} is the mass of the latex and m_{mon} is the amount of monomer. In semicontinuous polymerization processes two different conversions can be defined: the instantaneous conversion, which takes into account the monomer fed at each time to the

reactor; and the overall conversion, which considers the whole monomer amount that is going to be fed into the reactor. Both definitions are utilized in this work and the type of monomer conversion utilized (instantaneous vs overall) will be specified in each case.

$$X_M = \frac{m_{pol}}{m_{mon}} = \frac{SC * m_{latex} - NPF}{m_{mon}} \qquad \text{Equation I.2}$$

I.1.2. Particle size

I.1.2.1. Dynamic Light Scattering (DLS)

The particle size of the polymer dispersions synthesized in UPV/EHU was measured with Dynamic Light Scattering (DLS) using a Zetasizer Nano Z (Malvern Panalytical, UK). The diffusion coefficient (D) of a particle in a certain fluid depends on the temperature (T), viscosity of the medium (η) and hydrodynamic radius of the particle (R_H) according to the Stokes-Einstein law shown in Equation I.3 (k_B is the Boltzmann constant).

$$D = \frac{k_B\, T}{6\pi\, \eta\, R_H} \qquad \text{Equation I.3}$$

In the measurement, the sample is irradiated with a laser beam and the scattered light is recorded at one detection angle over time. The equipment measures the intensity fluctuations in the scattered light caused by Brownian motion, estimates the diffusion coefficient (D) and uses the Stokes-Einstein law to calculate the R_H. For the analysis, the latex was diluted with deionized water until a translucent dispersion was obtained to avoid multiple scattering.

In the figures that show the particle size time evolution, the theoretical growth of the particles was calculated by Equation I.4, where $D_{z,seed}$, $mass_{seed}$ and SC_{seed} are the z-average particle size, mass and solids content of the seed and $D_{z,t}$, $mass_t$ and SC_t are the z-average

particle size, mass and solids content of the latex at a given time. The calculations were made considering a seed of 55 nm and that there is no secondary nucleation such that all monomer added in the semi-batch stage is used to grow the particle.

$$D_{z,t} = D_{z,seed}\left(\frac{mass_t \cdot SC_t}{mass_{seed} \cdot SC_{seed}}\right)^{1/3} \qquad \text{Equation I.4}$$

I.1.2.2. Hydrodynamic capillary chromatography (HDC)

The particle sizes of the polymer dispersions synthesized in BASF (Latex 13, 14, 17-21) were determined by hydrodynamic capillary chromatography. In this analytical method, the polymer dispersion is injected into a capillary under laminar flow conditions. Larger particles will experience stronger exclusions from the capillary walls and they will tend to occupy the central part of the tube. Under parabolic flow profile, the flow velocity depends on the relative position in the tube, being the flow velocity minimum near the capillary walls and maximum in the center. Thus, particles of different sizes will cross the capillary at different velocities and will be separated depending on their size, being the large particles faster reaching the detector. The size of the particles is determined using a calibration that relates the size with the elution time.[1]

I.1.3. Gel content

I.1.3.1. Soxhlet extractions in THF

In the polymer dispersions synthesized in UPV/EHU, the gel content of the polymers (GC%) was determined by Soxhlet extraction using tetrahydrofuran (THF) as solvent and it was defined as the insoluble weight fraction of the polymer in THF. For the measurement, a few drops of the latex were deposited on glass fiber pads and the samples were dried for 2 days at room temperature. Then, the pads were inserted in the Soxhlet extractor and a continuous extraction

with THF under reflux was carried out for 24 hours. During the extraction, the un-crosslinked and soluble polymer chains dissolved in the THF and the insoluble polymer fraction (gel) remained in the pad. The pads were dried after the extractions and the gel content of the polymers was calculated using Equation I.5.

$$Gel\ content\ (GC\%) = \frac{Non\text{-}soluble\ polymer\ weight}{Total\ polymer\ weight} \qquad \text{Equation I.5}$$

I.1.3.1. Insoluble polymer fraction in MEK

For the polymer dispersions synthesized in BASF (Latex 13, 14, 17-21), the gel content was defined as the insoluble polymer fraction in methyl ethyl ketone (MEK). For the analysis, dry polymer films were immersed in MEK and after 24 hours of constant shaking, the insoluble polymer fraction was filtered, dried and weighted. The fraction of insoluble polymer was calculated according to Equation I.5.

I.1.4. Molecular weight distribution (MWD)

For the latexes produced in UPV/EHU, the molecular weight distributions of the soluble polymer fractions obtained after the Soxhlet extractions were measured using size exclusion chromatography (SEC) in THF at 35 °C with a THF flow rate of 1 mL min^{-1}. The SEC instrument consisted of an injector, a pump (Waters 510), three columns in series (Styragel HR2, HR4, and HR6), a differential refractometer detector (Waters 2410) and dual λ absorbance detector (Waters 2487, wavelength 265 nm). The equipment was calibrated using polystyrene standards and the molar masses reported related to polystyrene unless commented otherwise in the text.

The molecular weight distributions of the polymers synthesized in BASF were measured using Size Exclusion Chromatography (SEC) in THF at 35 °C with a THF flow rate of 1 mL/min. The samples were filtered prior to the analysis using 0.20 µm polytetrafluoroethylene (PTFE) filters. Separation was carried out using a guard column (Plgel 10 µm, length 5 cm, 7.5 mm inner diameter) and three Plgel 10 µm columns in series (length 30 cm, 7.5 mm inner diameter). A differential refractometer detector was used (DRI Agilent 1100).

I.2. Film properties

I.2.1. Glass transition temperature (T_g)

The glass-transition temperature (T_g) of the polymers and polymer blends were measured using a commercial differential scanning calorimeter, DSC (Q1000, TA Instruments). The procedure consisted of four scanning cycles: cooling, heating, cooling and heating. In Chapter 4 the temperature range employed for the analysis was (-50 °C) - 150 °C and in Chapter 5 the temperature range used for the analysis of the PSAs was (–80 °C) - 80 °C. The results from the second heating run are presented.

I.2.2. Morphology

The morphology of the films was investigated with transmission electron microscopy (TEM) using a Jeol TM-1400 Plus series 120 kV electron microscope. The polymer films were cut in a LEICA EM UC6 ultramicrotome at -25 °C in Chapters 4 and 7 and at -70 °C in Chapter 5. The films were stained with RuO_4 vapor for 20 min to increase the contrast of the phenolic rings. The ruthenium complexes with the aromatic rings and therefore the contrast of the image darkens the aromatic-rich areas.

I.2.3. Mechanical properties

The mechanical properties of the films prepared for coatings applications in Chapters 2, 3, 4 and 7 were evaluated by tensile test. The measurements were carried out in a TA.HD.plus Texture Analyser (Stable Micro Systems, UK) at 23 ± 2 °C, 50 ± 5% relative humidity and using a strain rate of 10 mm/min. Bone-shape probes were prepared by cutting the polymer films with a die cutter. The thickness of the test specimens varied in the range 400-800 μm. In order to check the reproducibility of the results, each material was analyzed at least 3 times. The most representative plot for each material is represented in the stress-strain graphs and the average Young's modulus, yield stress, tensile strength and ultimate strain values are given in the tables.

The mechanical properties of the L13,14 – Cat_AMPS materials prepared in BASF and discussed in Chapter 7 were measured by tensile test using probes with the dimensions specified in DIN 53504 S3A, at room temperature and a strain rate of 200 mm/min.

I.2.4. Water sensitivity

The water sensitivity of the polymer films was assessed by immersing the polymer films in water for a certain time and measuring water uptake, weight loss and release of tannic acid or gallic acid to the aqueous phase. In addition, the mechanical / adhesive properties were tested after the immersion.

In Chapter 3, the materials employed for the water absorption test were 1 mm thick and 2.5 cm diameter circular films and they were immersed in water for 5 days. In Chapter 4, 1 mm thick and 2.5 cm diameter circular films were immersed in water for 7 days. In Chapter 5, PSA circular films with a thickness of 1 mm and 1 cm diameter were immersed in water 7 days. In Chapter 7, rectangular films of 1 cm x 4 cm and ≈ 1 mm thickness were used for the test. The

latex – MAA copolymer blends were immersed in water for 7 days and the latex – DMA_AMPS blends for 5 days.

I.2.4.1. Water absorption

The water absorption was defined as the weight increase of the sample after the immersion in water for a given time, and was normalized by the initial weight of the specimen. The water absorption was calculated using Equation I.6 where m_{end} is the weight of the polymer film after the immersion and m_0 is the initial weight of the polymer film. In general, higher water absorption values indicate greater water sensitivity.

$$H_2O\ absorption\ (\%) = \frac{m_{end} - m_0}{m_{end}} 100 \qquad \text{Equation I.6}$$

I.2.4.2. Weight loss

After the immersion in water, the films were dried at 65 °C for two days and weighed to determine the weight lost during the immersion in water. The weight loss was normalized with the initial weight of the sample as expressed in Equation I.7 where m_d is the weight of the polymer film after drying and m_0 is the initial weight of the sample. Typically, the water-sensitive components of the formulation such as surfactants or water-soluble oligomers can migrate to the aqueous phase during the test decreasing the final weight of the polymer film. High weight loss values are usually related to high water sensitivity.

$$Weight\ loss\ (\%) = \frac{m_0 - m_d}{m_0} 100 \qquad \text{Equation. I.7}$$

I.2.4.3. Tannic acid and gallic acid release

In Chapters 3, 4 and 5 the tannic acid (TA) and gallic acid (GA) leached out from the films during the immersion in water was determined using UV-vis spectrophotometry. The absorption spectra were recorded on a S300 UV–vis spectrophotometer (Analytik Jena) and absorption-concentration calibration curves at 305 nm were employed to calculate the concentration of TA and GA in the aqueous phase. The TA / GA % released was calculated taking into account the TA / GA weight in each sample according to Equation I.8 where m_0 is the initial amount of TA / GA in the film and m_W is the amount of the phenol molecule in the aqueous phase. The calibration curves built for TA and GA are shown in Figures I.1 and I.2, respectively.

$$TA/GA\ release\ (\%) = \frac{m_0 - m_W}{m_0} 100 \qquad \text{Equation I.8}$$

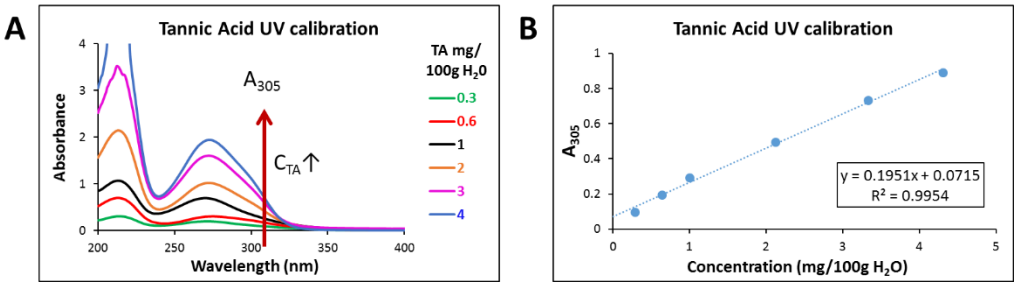

Figure I.1. UV-vis calibration curve of tannic acid in water. A) UV-vis absorption spectra of the TA water solutions used for the calibration and B) calibration curve.

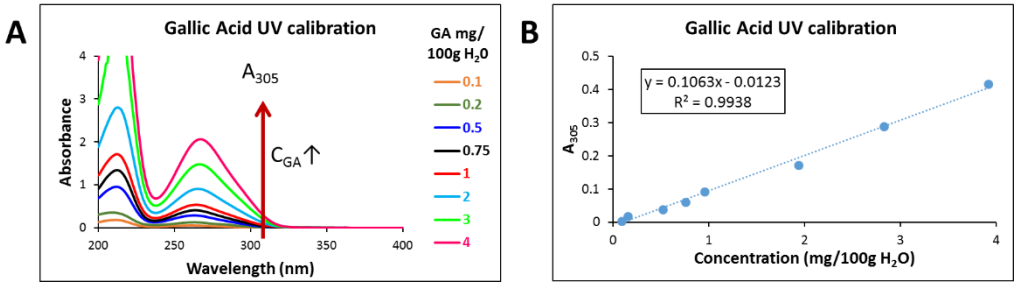

Figure I.2. UV-vis calibration curve of gallic acid in water. A) UV-vis absorption spectra of the GA water solutions used for the calibration and B) calibration curve.

I.2.4.4. Mechanical properties after immersion in H_2O

Bone-shape probes were immersed in water for the same time as in the water absorption test (5 days in Chapter 3 and 7 days in Chapter 4) and then the specimens were dried for 7 days at 23 ± 2 °C and 55 ± 5 % relative humidity. The mechanical properties were evaluated by tensile test with the conditions specified in Section I.2.3.

I.2.4.5. Adhesive properties after immersion in H_2O

For the determination of adhesive properties in humid conditions, the samples were immersed in water for 60 min, and they were wiped out with a paper cloth right before the probe tack test.

I.3. References

(1) Liu, L.; Veerappan, V.; Bian, Y.; Guo, G.; Wang, X. Influence of elution conditions on DNA transport behavior in free solution by hydrodynamic chromatography *Sci. China Chem.* **2015**, *58*, 1605–1611.

Appendix II. Supporting information for Chapter 6

II.1. Synthesis of dopamine methacrylamide (DMA)

II.1.1. Materials

Dopamine hydrochloride (99 %, Fischer Scientific) methacryloyl chloride (97 %, Alfa Aesar), ethyl acetate (ACS basic, Scharlau), tetrahydrofuran (THF, GPC grade, Scharlab), anhydrous methanol (99.8 %, Sigma Aldrich) sodium chloride (NaCl, synthesis grade, Scharlau), triethylamine (TEA, 99 %, Sigma Aldrich) and sodium sulfate (Na_2SO_4, anhydrous, Sigma Aldrich) were used as received.

II.1.2. Synthetic procedure

Dopamine methacrylamide was synthesized from methacryloyl chloride and dopamine dopamine and methacryloyl chloride based on a procedure reported by Xu *et al.*[1] The reaction pathway is shown in Scheme II.1.

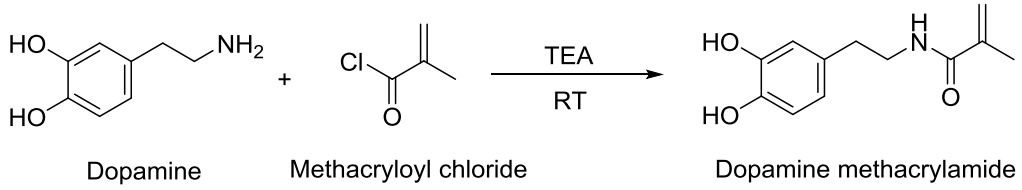

Scheme II.1 Synthesis of dopamine methacrylamide (DMA) from dopamine and methacryloyl chloride.

Dopamine hydrochloride (10 g, 52.7 mmol) was added to a 250 mL three neck round bottom flask equipped with two dropping funnels and it was degassed with nitrogen for 30 minutes. Anhydrous methanol (100 mL) and triethylamine (TEA, 7.35 mL, 1 eq.) were added to the round bottom flask under nitrogen. In the first funnel, trimethylamine (11 mL, 1.5 Eq.) and anhydrous methanol (11 mL) were added under nitrogen. A solution of methacryloyl chloride (6.18 mL, 1.2 eq.) in GPC grade THF (5 mL) was added in the second dropping funnel. The set up was placed in an ice bath and the content of both dropping funnels was slowly added simultaneously to keep the pH at 9. After the addition, the system was stirred overnight at room temperature. After the reaction, the volatiles were evaporated under reduced pressure. The resulting oil was redissolved in ethyl acetate (100 mL) and washed two times with a 1M HCl aqueous solution (2x100 mL) and two times with brine (2x100 mL). The organic layer was dried with Na_2SO_4 and the volatiles were removed under reduced pressure. The crude product was recrystallized from ethyl acetate.

II.1.3. Product characterization

The product was a beige powder. The ^{1}H-NMR spectrum of the monomer was recorded on a Bruker 400 MHz equipment using d_6-DMSO was used as solvent. The spectrum was acquired at room temperature with a relaxation decay time (D1) of 20 s and 16 scans. The ^{1}H-NMR spectrum of DMA is shown in Figure II.1. ^{1}H-NMR (400 MHz, DMSO-d_6) δ 8.69 ppm (2H, 2s, -C_6H_3(O**H**)$_2$), 7.94 ppm (1H, m, $C_6H_3(OH)_2$-CH_2-CH_2-N**H**-), 6.64 ppm (1H, d, -C_6H_2(**H**)$(OH)_2$, signal h), 6.58 ppm (1H, d, -C_6H_2(**H**)$(OH)_2$, signal g), 6.44 ppm (1H, d, -C_6H_2(**H**)$(OH)_2$, signal f), 5.63 ppm (1H, s, -C(=O)-C(CH_3)=CH(**H**), cis, signal b), 5.31 ppm (1H, s, -C(=O)-C(CH_3)=C(**H**)H, trans, signal c), 3.29 – 3.20 ppm (2H, q, $C_6H_3(OH)_2$-CH_2-C**H$_2$**-NH-, signal d) 2.64 – 2.48 ppm (2H, t, $C_6H_3(OH)_2$-C**H$_2$**-, signal e), 1.85 ppm (1H, s, -C(=O)-C(C**H$_3$**)=CH_2, signal a).

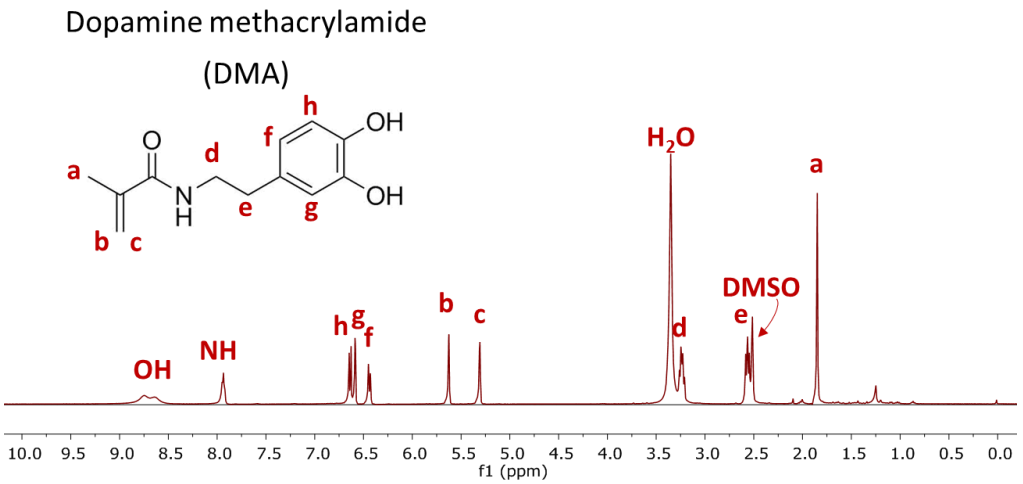

Figure II.1. ^{1}H-NMR spectrum of dopamine methacrylamide (DMA).

II.2. Synthesis of vinyl catechol (VC)

II.2.1. Materials

Caffeic acid (≥99.8 %, Sigma Aldrich), dimethyl formamide (DMF, ≥99.8 %, Sigma Aldrich), triethylamine (TEA, 99 %, Sigmal Aldrich), ethyl acetate (ACS basic, Scharlau), sodium chloride (NaCl, synthesis grade, Scharlau), and sodium sulfate (Na_2SO_4, anhydrous, Sigma Aldrich) were used as received.

II.2.2. Synthetic procedure

Vinyl catechol (VC) was synthesized from caffeic acid according to the procedure described by Takeshima *et al.*[2] The reaction pathway is shown in Scheme II.2.

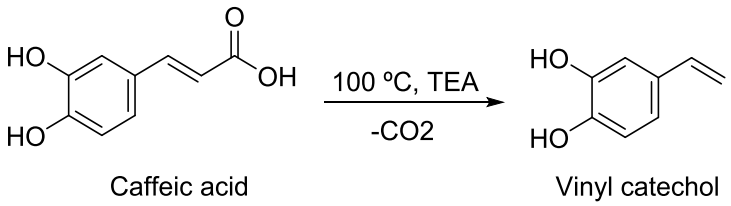

Scheme II.2. Synthesis of vinyl catechol starting from caffeic acid.

First, caffeic acid (3 g, 16.65 mmol) was dissolved in DMF (23 mL). Then, triethylamine (TEA, 6.9 mL, 3 eq.) was added to the solution and the mixture was heated to 100 °C under stirring employing an oil bath. After 1 hour, the reaction was cooled to room temperature. After the reaction, volatiles were evaporated under reduced pressure. The resulting oil was redissolved in ethyl acetate (100 mL) and washed two times with 1M HCl aqueous solution (2x50 mL) and two times with brine (2x100 mL). The organic layer was dried with Na_2SO_4 and the volatiles were removed under reduced pressure.

II.2.3. Product characterization

The ^{1}H-NMR spectrum of VC was recorded on a Bruker 400 MHz equipment using d_6-DMSO was used as solvent. The spectrum was acquired at room temperature with a relaxation decay time (D1) of 20 s and 16 scans. The 1H-NMR spectrum of vinyl catechol is shown in Figure II.2. 1H-NMR (400 MHz, DMSO-d6) δ 8.92 ppm (2H, s, -C_6H_3(O**H**)$_2$), 6.91 – 6.79 (1H, m, -C_6H_2(**H**)(OH)$_2$, signal d), 6.75 – 6.67 (2H, m, -C_6**H$_2$**(H)(OH)$_2$, signals d and f), 6.61 – 6.44 ppm (1H, dd, CH_2=C**H**-, signal a), 5.49 (1H, d, CH(**H**)=CH-, trans, signal c), 4.99 (1H, d, C**H**(H)=CH-, cis, signal b).

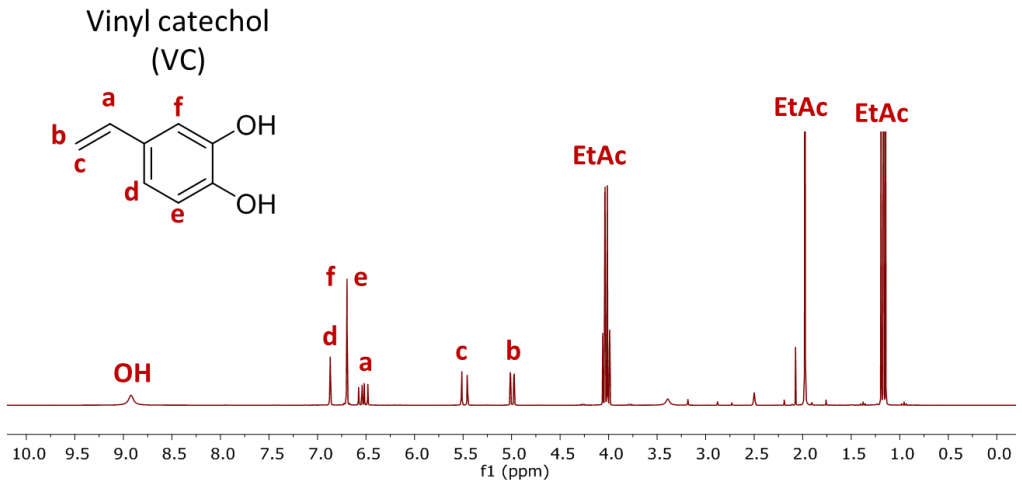

Figure II.2. ^{1}H-NMR spectrum of vinyl catechol (VC).

II.3 Reaction mechanism

The MALDI-TOF-MS spectra were interpreted on the basis of the proposed reaction mechanism presented in Scheme II.3. The formation mechanism of methacrylonitrile (MAN) from the termination by disproportionation of two tertiary radicals formed after the decomposition of AIBN[3] is shown in Scheme II.4.

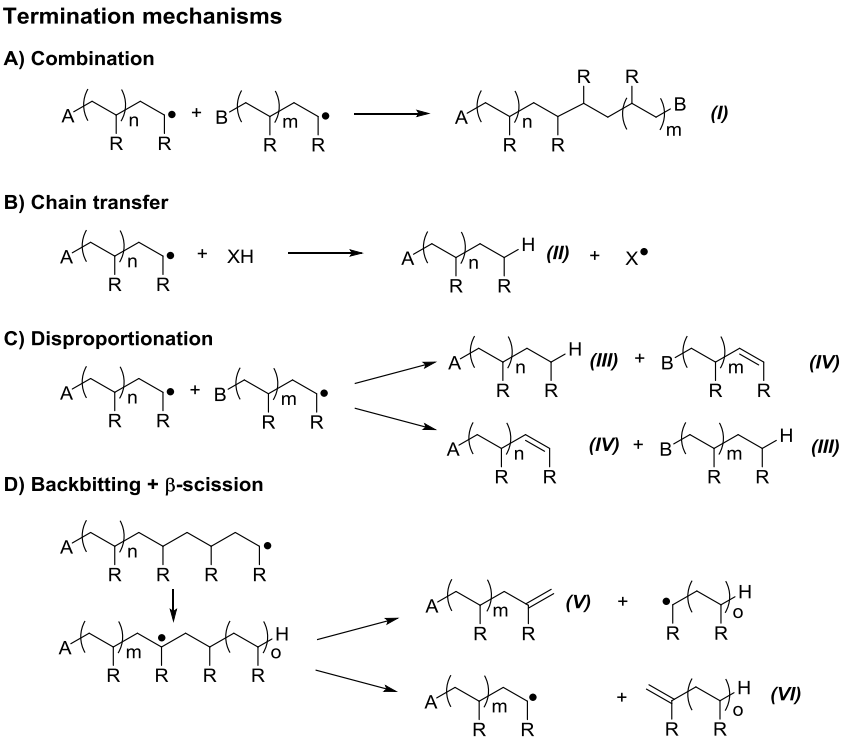

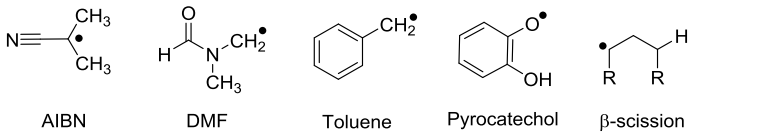

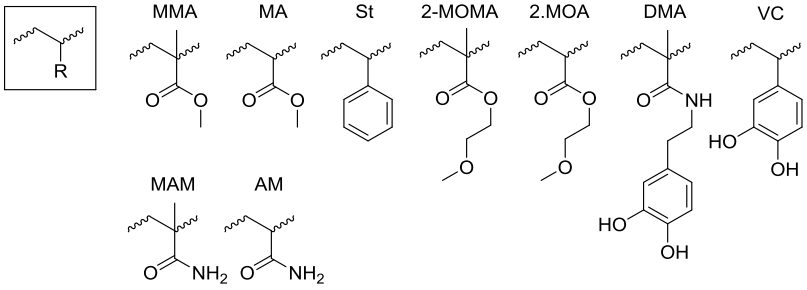

Scheme II.3. Termination mechanisms considered in this work.

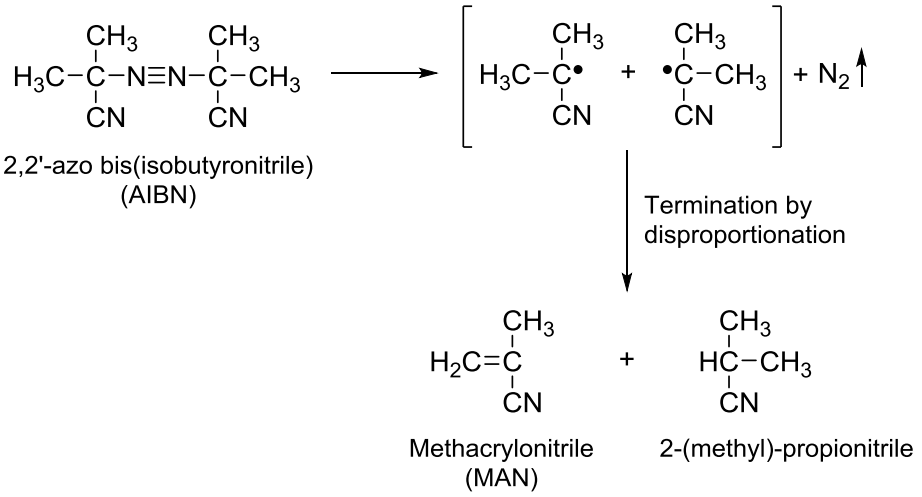

Scheme II.4. Methacrylonitrile formation mechanism from AIBN.[3]

II.4. MALDI-TOF-MS spectra

Whole range spectra of the PS and PMA polymers produced in set 1 of reactions are shown in Figures II.3 and II.4, respectively. The whole range spectra of the (co)polymers prepared in set 4 of reactions are presented in Figure II.5. The isotopic distribution of signals A and B in Run 1 (Figure 6.12.A) and the calculated isotopic distributions for the different termination mechanisms are compared in Figure II.6.

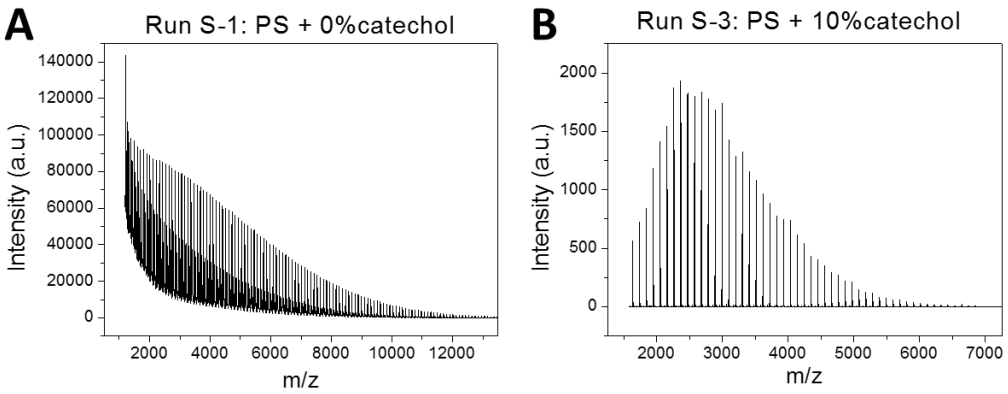

Figure II.3. MALDI-T-MS spectra of the PS polymers produced in Runs S-1 (part A) and S-3 (part B) in presence of 0 and 10 wt% pyrocatechol.

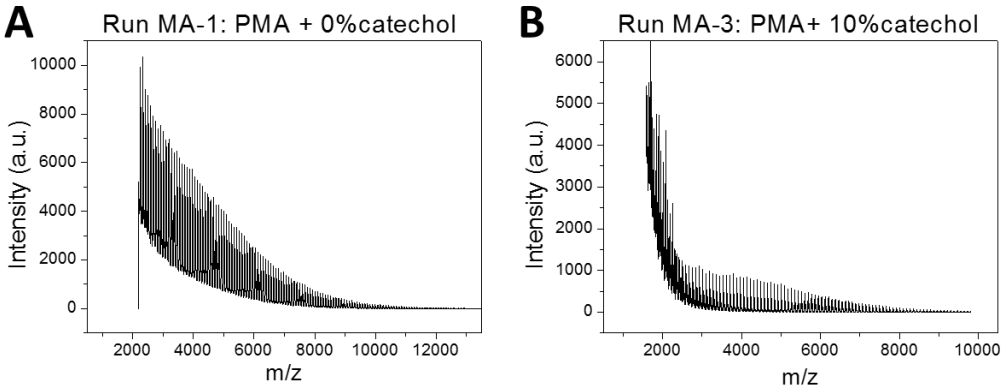

Figure II.4. MALDI-TOF-MS spectra of the PMA polymers produced in Runs MA-1 (part A) and MA-4 (part B) in presence of 0 and 50 wt% pyrocatechol.

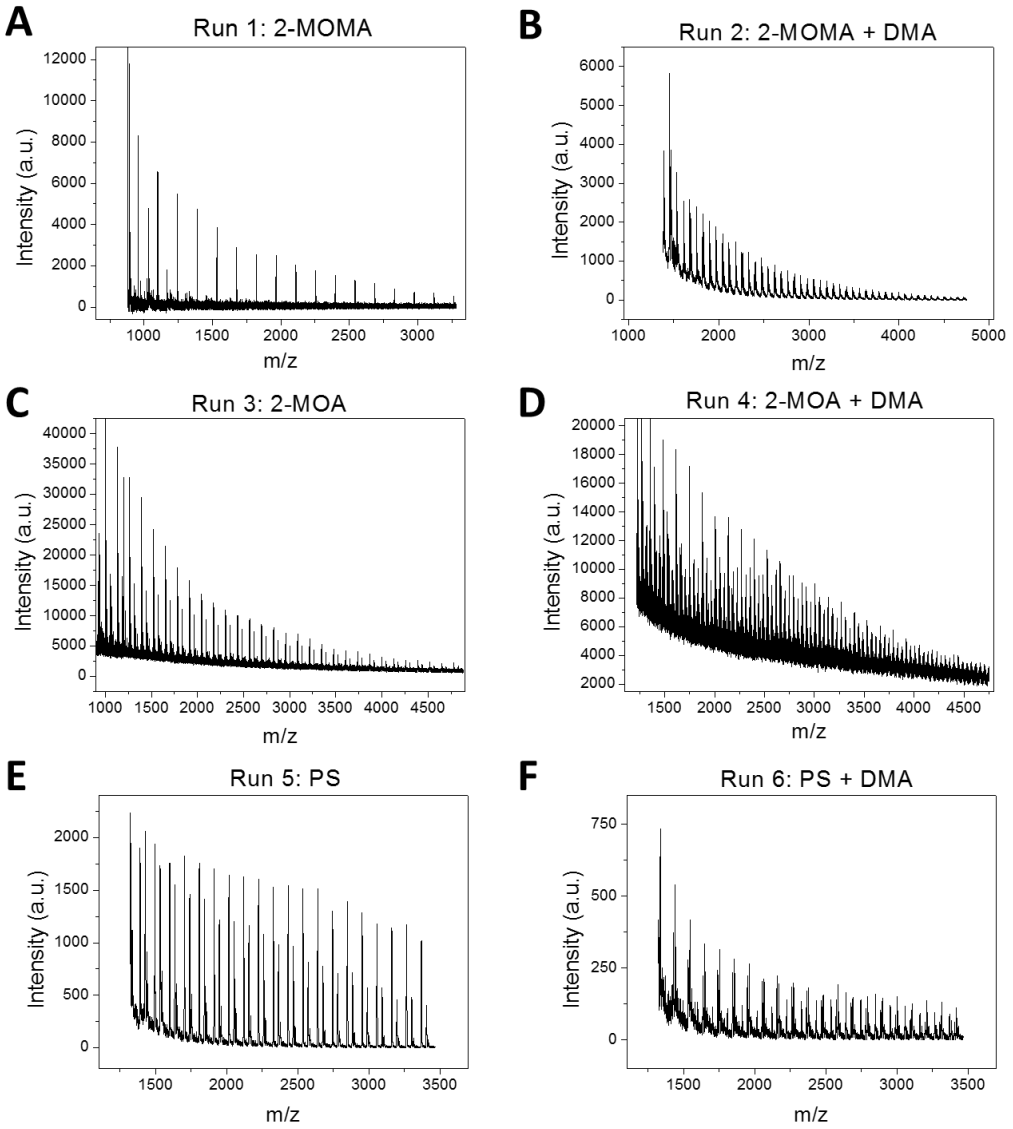
A
Run 1: 2-MOMA
Intensity (a.u.)
m/z
B
Run 2: 2-MOMA + DMA
Intensity (a.u.)
m/z
C
Run 3: 2-MOA
Intensity (a.u.)
m/z
D
Run 4: 2-MOA + DMA
Intensity (a.u.)
m/z
E
Run 5: PS
Intensity (a.u.)
m/z
F
Run 6: PS + DMA
Intensity (a.u.)
m/z

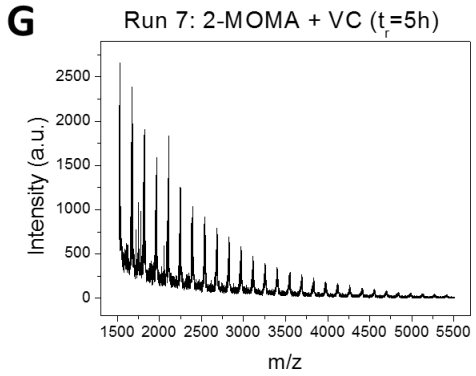

Figure II.5. MALDI-TOF spectra of the polymers produced in (A) Run 1 – 2-MOMA, (B) Run 2 - 2-MOMA + DMA, (C) Run 3 – 2-MOA, (D) Run 4 – 2-MOA + DMA, (E) Run 5 – S, (F) Run 6 – S + DMA and (G) Run 7 – 2-MOMA + VC.

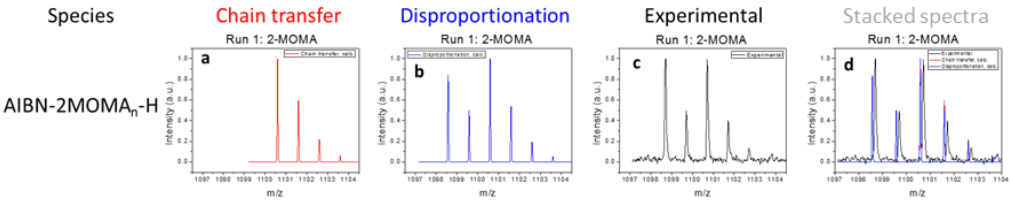

Figure II.6. MALDI-TOF-MS spectra (1097-1104 zoom) of the 2-MOMA polymer produced in Run 1: (A) Calculated isotopic distribution of the species terminated by chain transfer, (B) calculated isotopic distribution of the species terminated by disproportionation, (C) experimental isotopic distribution of the species in the 1097-1104 region and (D) overlapping of the previous three isotopic distributions.

II.5. Individual monomer conversions in Runs 1-11 of set 4 of experiments

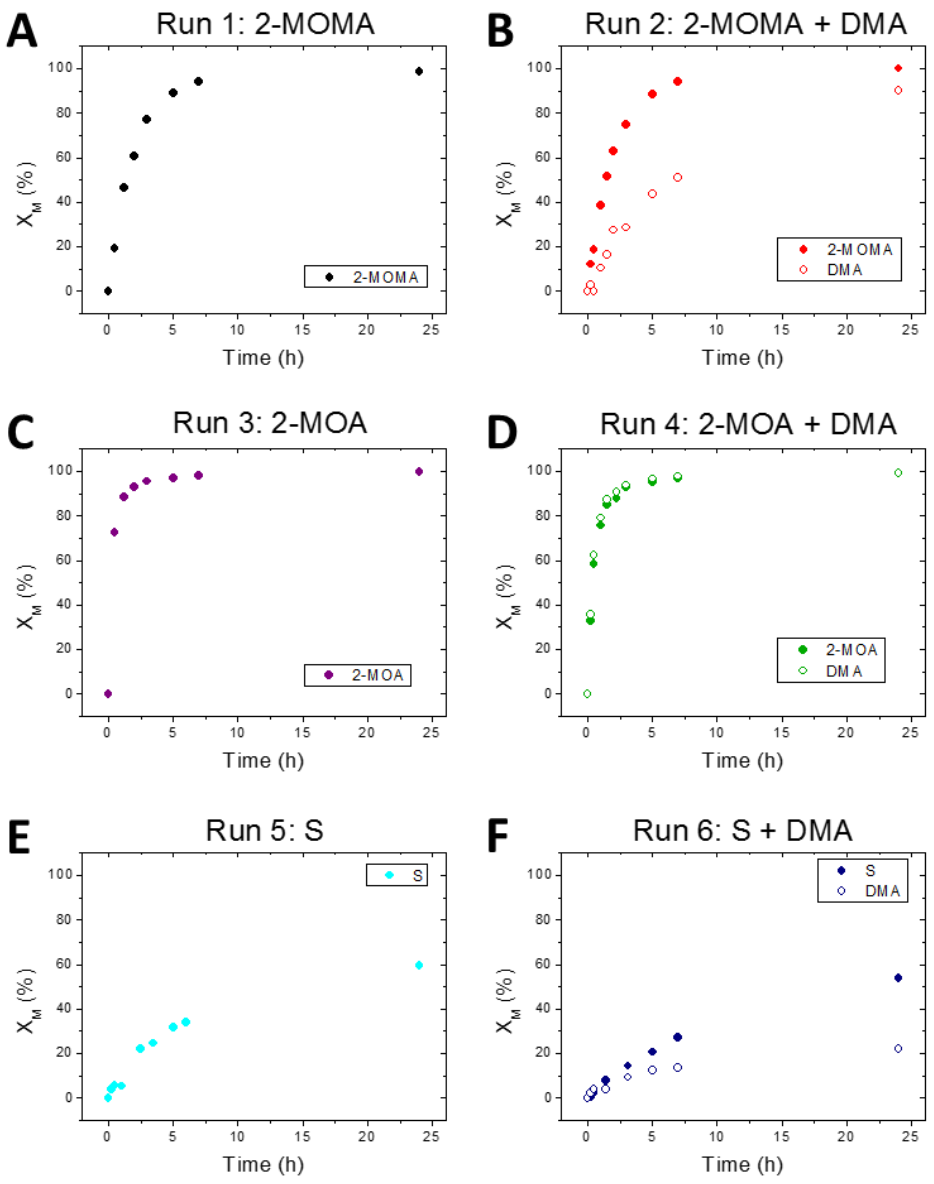

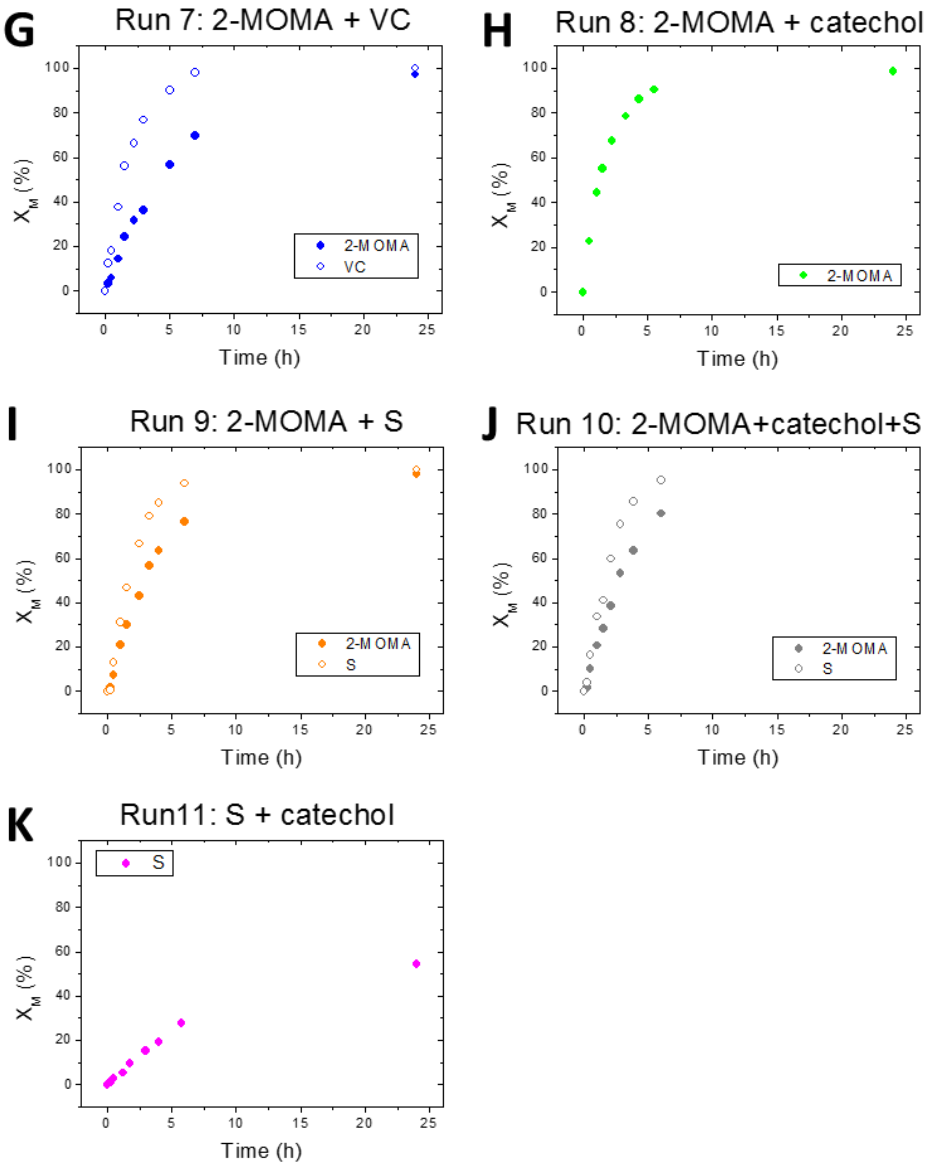

Figure II.7. Individual monomer conversions measured by ^{1}H-NMR in (A) Run 1 – 2-MOMA, (B) Run 2 - 2-MOMA + DMA, (C) Run 3 – 2-MOA, (D) Run 4 – 2-MOA + DMA, (E) Run 5 - S, (F) Run 6 – S + DMA, (G) Run 7 – 2-MOMA + VC, (H) Run 8 – 2-MOMA + catechol, (I) Run 9 – 2-MOMA + S, (J) Run 10 – 2-MOMA + catechol + S and (K) Run 11 – S + catechol.

II.6. Time evolution of the molecular weight distributions in Runs 1-7 of set 4 of experiments

The distributions obtained with the RI detector are presented in part 1 and the results obtained with the UV detector in part 2. The signal between 200 and 250 g/mol is given by the DMA and VC monomers.

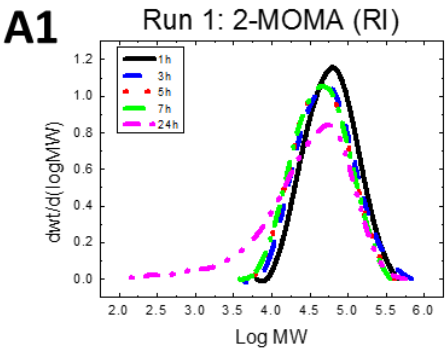
A1
Run 1: 2-MOMA (RI)
1h
3h
5h
7h
24h
dwt/d(logMW)
Log MW

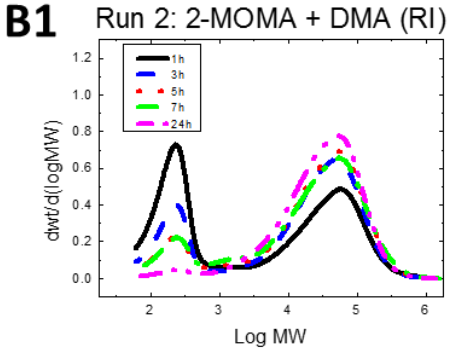
B1
Run 2: 2-MOMA + DMA (RI)
1h
3h
5h
7h
24h
dwt/d(logMW)
Log MW

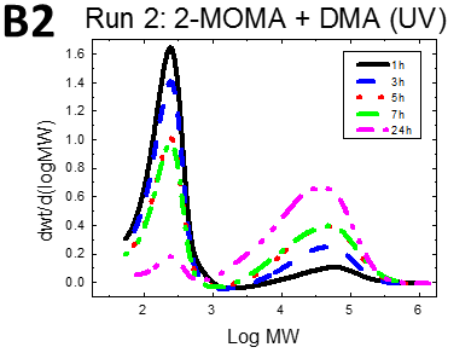
B2
Run 2: 2-MOMA + DMA (UV)
1h
3h
5h
7h
24h
dwt/d(logMW)
Log MW

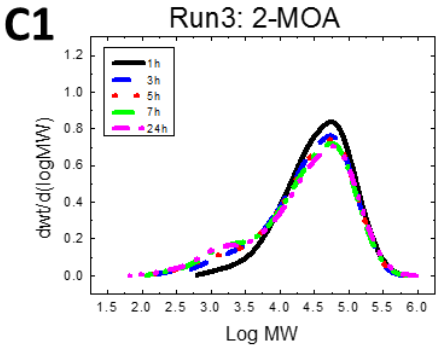
C1
Run3: 2-MOA
1h
3h
5h
7h
24h
dwt/d(logMW)
Log MW

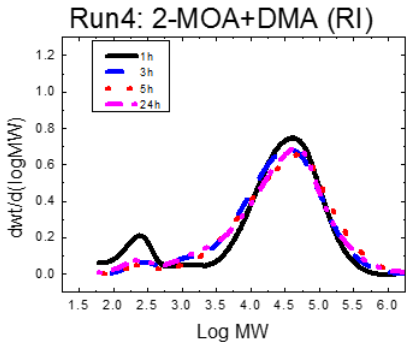
Run4: 2-MOA+DMA (RI)
1h
3h
5h
24h
dwt/d(logMW)
Log MW

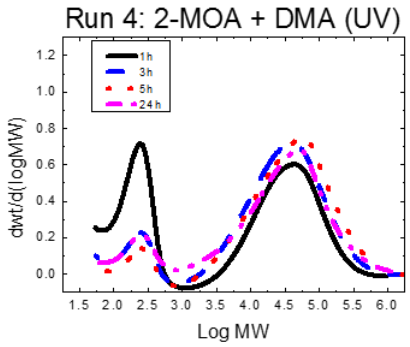
Run 4: 2-MOA + DMA (UV)
1h
3h
5h
24h
dwt/d(logMW)
Log MW

E1

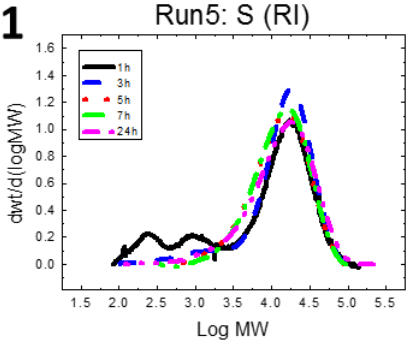
Run5: S (RI)
1h
3h
5h
7h
24h
dwt/d(logMW)
Log MW

E2

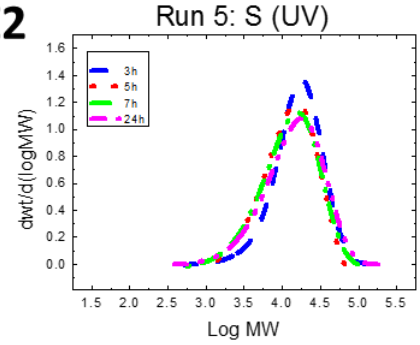
Run 5: S (UV)
3h
5h
7h
24h
dwt/d(logMW)
Log MW

F1

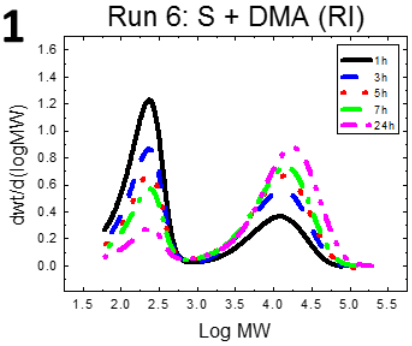
Run 6: S + DMA (RI)
1h
3h
5h
7h
24h
dwt/d(logMW)
Log MW

F2

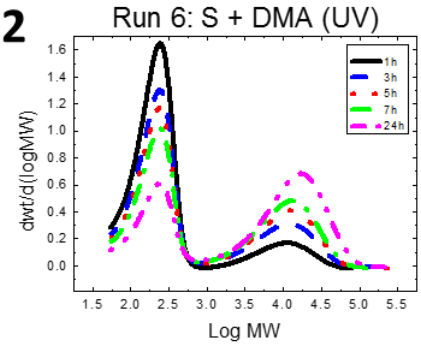
Run 6: S + DMA (UV)
1h
3h
5h
7h
24h
dwt/d(logMW)
Log MW

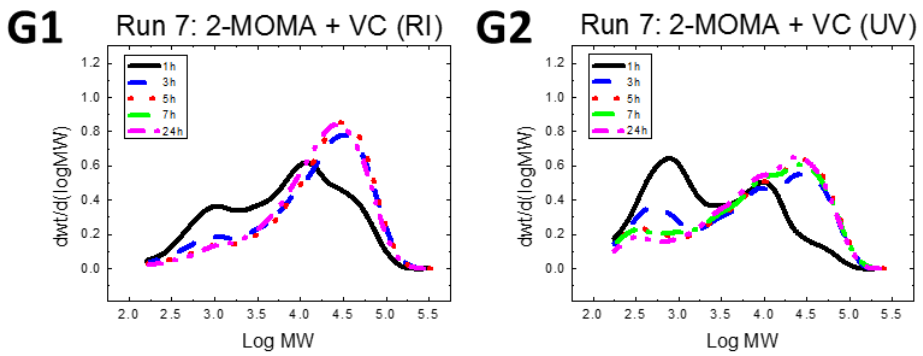

Figure II.8. Time evolution of the molecular weight distributions in (A) Run 1 – 2-MOMA, (B) Run 2 - 2-MOMA + DMA, (C) Run 3 – 2-MOA, (D) Run 4 – 2-MOA + DMA, (E) Run 5 – S, (F) Run 6 – S + DMA and (G) Run 7 – 2-MOMA + VC. The distributions obtained with the RI detector are presented in part 1 and the results obtained with the UV detector in part 2.

II.7. References

(1) Xu, H.; Nishida, J.; Ma, W.; Wu, H.; Kobayashi, M.; Otsuka, H.; Takahara, A. Competition between oxidation and coordination in cross-linking of polystyrene copolymer containing catechol groups *ACS Macro Lett.* **2012**, *1*, 457–460.

(2) Takeshima, H.; Satoh, K.; Kamigaito, M. Scalable Synthesis of Bio-Based Functional Styrene: Protected Vinyl Catechol from Caffeic Acid and Controlled Radical and Anionic Polymerizations Thereof *Sustain. Chem. Eng.* **2018**, *6*, 13681–13686.

(3) Moad, G.; Solomon, D. H.; Johns, S. R.; Willing, R. I. Fate of the Initiator in the Azobis (isobutyronitrile) -Initiated Polymerization of Styrene *Macromolecules* **1984**, *17*, 1094–1099.

Appendix III. List of acronyms, abbreviations and symbols

1H-NMR	Proton nuclear magnetic resonance
2-EHA	2-ethylhexyl acrylate
A	Hydrogen bond acceptor
AA	Acrylic acid
AAMA	Acetetoacetamido methacrylate
AdA	Adenine acrylate
AFM	Atomic force microscopy
AIBN	2,2'-azobis(2-methylpropionitrile)
ALMA	Allyl methacrylate
AM	Acrylamide
AMPS	2-acrylamido-2-methyl-1-propanesulfonic acid
AMS	4-azidomethyl styrene
AP	Acrylamidopyridine
APS	Amonium persulfate
ASR	Alkali soluble resin
a_T	Shift factor in frequency mastercurves
ATR	Attenuated total reflectance
BA	Butyl acrylate
BDDA	1,4-butanediol diacrylate
BHT	2,6-di-tert-butyl-4-methylphenol
BSH	n-butanethiol
C	Cytosine
CCEMA	Cyclohexylcarbodiimidoethyl methacrylate
$CDCl_3$	Deuterated chloroform
CDI	Carbodiimide
CEA	Carboxyethylacrylate
CMC	Critical micelle concentration
COV	Compuesto orgánico volátil
CTA	Chain transfer agent
C_{TR}	Chain transfer constant

D	Hydrogen bond donor
D	Diffusion coefficient
D1	Relaxation decay time
DAAM	Diacetone acrylamide
DBP	Dibenzyl peroxide
DCM	Dichloromethane
DFT	Density functional theory
DHPMA	2,3-dihydroxypropyl methacrylate
DLS	Dynamic light scattering
DMA	Dopamine methacrylamide
DMA	Dynamic mechanical analysis
DMF	Dimethyl formamide
DMSO	Dimethyl sulfoxide
DMTA	Dynamic mechanical thermal analysis
DP_n	Number average degree of polymerization
dp_z	z-average particle size
DSC	Differential scanning calorimetry
DSH	n-dodecanethiol
E	Young's modulus
EHTG	2-ethylhexyl thioglycolate
EPA	Environmental protection agency
F	Feeding stream
FM	Functional monomer
FRET	Fluorescence resonance emission transfer
FRP	Free radical polymerization
FTIR	Fourier transform infrared spectroscopy
G	Guanine
G'	Storage modulus
G''	Loss modulus
GA	Gallic acid
GC	Gas chromatography
GC	Gel content
GMA	Glycidyl methacrylate
HDC	Hydrodynamic capillary chromatography
HEMA	2-hydroxyethyl methacrylate
HMMA	Hexamethylol melamine

HPLC	High performance liquid chromatrography
HQ	Hydroquinone
IBMA	N-isobutoxy methacrylamide
K_a	Equillibrium association constant
k_B	Boltzmann constant
k_p	Propagation rate coefficient
KPS	Potassium persulfate
k_{tr}	Chain transfer rate coefficient
L	Latex
LPO	Lauryl peroxide
m	Mass
M, M_n	Number average molecular weight
MA	Methyl acrylate
MAA	Methacrylic acid
MALDI-TOF-MS	Matrix-assisted laser desorption/ionization time of flight mass spectrometry
MAM	Methacrylamide
MAN	Methacrylonitrile
M_c	Critical entanglement molecular weight
M_c	Average molecular weight between crosslinks
M_e	Average molecular weight between entanglements
MEK	Methyl ethyl ketone
MFFT	Minimum film formation temperature
MMA	Methyl methacrylate
M_s	Average molecular weight between associative groups
MW	Molecular weight
M_w	Weight average molecular weight
MWD	Molecular weight distribution
N	Average number of functional groups per polymer chain
NB	Nucleobase
NIPU	Non-isocyanate polyurethane
NMA	N-methylol acrylamide
NPF	Non-polymeric solid fraction
NVC	N-vinyl caprolactam
NVP	N-vinyl pyrrolidone
PAA	Poly(acrylic acid)
PBA	Poly(butyl acrylate)

PC	Pyrocatechol
PEG	Poly(ethylene glycol)
PEGMA	Poly(ethylene glycol) methacrylate
PEO	Poly(ethylene oxide)
PMMA	Poly(methyl methacrylate)
PrA	Propargyl acrylate
PS	Polystyrene
PSA	Pressure sensitive adhesive
PVOH	Polyvinyl alcohol
PVP	Polyvinyl pyrrolidone
R	Radius of polymer particles
R	Universal gas constant
r	Reactivity ratio
r_{CL}	Crosslinking rate
r_{Diff}	Diffusion rate
R_g	Radius of gyration
RH	Relative humidity
R_H	Hydrodynamic radius of the particle
rpm	Revolutions per minute
S	Styrene
S	Secondary interaction
SA	Stearyl acrylate
SANS	Small angle neutron scattering
SC	Solids content
SEC	Size exclusion chromatography
SEM	Scanning electron microscopy
T	Temperature
TA	Tannic acid
tanδ	Damping factor
tBCEMA	tert-butylcarbodiimidoethyl methacrylate
TEA	Triethylamine
TEM	Transmission electron microscopy
T_g	Glass transition temperature
THF	Tetrahydrofuran
T_M	Melting temperature
UMA	Ureido methacrylate

Upy	Ureido pyrimidinone
UrA	Uracil acrylate
UV-Vis	Ultraviolet-visible light
V-501	4,4-azobis(4-cianovaleric acid)
VAc	Vinyl acetate
VC	Vinyl catechol
VOC	Volatile organic compound
W	Work of adhesion
w	Weight fraction
wbm	Weight based on monomers
wt%	Weight percent
X_M	Monomer conversion
$X_{M,inst}$	Instantaneous monomer conversion
$X_{M,overall}$	Overall monomer conversion
ZPVE	Zero-point vibrational energy
ΔG	Association energy
ρ	Polymer density
σ	Stress
σ_{max}	Tensile strength
σ_N	Nominal stress
σ_R	Reduced stress
σ_y	Yield stress
τ_{rep}	Reptation time
τ_0	Monomer relaxation time
τ_s	Lifetime of the hydrogen bond
ω	Angular frequency
γ, λ	Strain
γ_{max}	Ultimate strain

List of publications, conference presentations and awards

Parts of this thesis have been published and presented in national and international conferences. The list of publications, presentations and awards related to this PhD work is as follows:

Publications

Jiménez, N.; Ballard, N.; Asua, J. M. Hydrogen bond-directed formation of stiff polymer films using naturally occurring polyphenols. *Macromolecules* **2019**, *52* (24), 9724–9734.

Jiménez, N.; Ballard, N.; Asua, J. M. Hydrogen-bond driven formation of microstructured pressure sensitive adhesives (PSAs) with enhanced shear resistance. *Polymer* **2021**, *233*, 124210.

Jiménez, N.; Ruipérez, F.; González de San Román, E.; Asua, J. M.; Ballard, N. Fundamental insights into free-radical polymerization in the presence of catechols and catechol-functionalized monomers. *Macromolecules* **2022**, 55 (1), 49-64.

Oral presentations

"Incorporation of hydrogen bonding for high performance waterborne coatings" N. Jiménez, N. Ballard, J. M. Asua. Industrial Liaison Program meeting 2017, Donostia-San Sebastián, Spain, September 2017.

“Hidrogeno loturen erabilpena errendimendu altuko estaldurak lortzeko” N. Jiménez, N. Ballard, J. M. Asua. Materialen Zientzia eta Teknologia IV. Kongresua, Donostia-San Sebastián, Spain, July 2018.

“Incorporation of hydrogen bonding for high performance waterborne coatings” N. Jiménez, N. Ballard, J. M. Asua. Industrial Liaison Program meeting 2018, Donostia-San Sebastián, Spain, September 2018.

“Incorporation of hydrogen bonding for high performance waterborne coatings” N. Jiménez, N. Ballard, J. M. Asua. XV reunion del Grupo Especializado de Polímeros (GEP) de la RSEQ y RSEF, Huelva, Spain, September 2018.

“Hydrogen bond directed formation of mechanically strong polymer films using naturally occurring polyphenols” N. Jiménez, N. Ballard, J. M. Asua. Graduate Research Seminar (GRS), Sentosa Island, Singapore, June 2019.

“Incorporation of hydrogen bonding for high performance waterborne coatings” N. Jiménez, N. Ballard, J. M. Asua. Industrial Liaison Program meeting 2019, Donostia-San Sebastián, Spain, September 2019.

“Incorporation of hydrogen bonding for high performance waterborne coatings” N. Jiménez, N. Ballard, J. M. Asua. Industrial Liaison Program meeting 2020, Donostia-San Sebastián, Spain, September 2020.

“Incorporation of hydrogen bonding for high performance waterborne coatings” N. Jiménez, N. Ballard, J. M. Asua. Industrial Liaison Program meeting 2021, Donostia-San Sebastián, Spain, September 2021.

"Hidrogeno loturen erabilpena errendimendu altuko estaldurak lortzeko" N. Jiménez, N. Ballard, J. M. Asua. Materialen Zientzia eta Teknologia V. Kongresua, Bilbao, Spain, November 2021.

Poster presentations

"Effect of chemical and physical crosslinking (hydrogen bonding) on the mechanical properties of P(MMA/BA) 50/50 films" N. Jiménez, N. Ballard, J. M. Asua. 6th PhD-Workshop on Polymer Reaction Engineering, Vienna, Austria, September 2017.

"Incorporation of hydrogen bonding for high performance waterborne coatings" N. Jiménez, N. Ballard, J. M. Asua. Functional Polymers, Donostia-San Sebastián, Spain, March 2018.

"Hydrogen bond directed formation of mechanically strong polymer films using naturally occurring polyphenols" N. Jiménez, N. Ballard, J. M. Asua. Graduate Research Seminar (GRS) and International Polymer Colloids Group Conference, Sentosa Island, Singapore, June 2019.

Awards

"Best Poster Award" in the International Polymer Colloids Group Conference, Sentosa Island, Singapore, June 2019.

"Scientific Photography Award" in 7th Scientific Photography Contest of Polymat, Donostia-San Sebastián, Spain, June 2020.